

KU Leuven

Biomedical Sciences Group

Faculty of Medicine

Department of Neurosciences

Research group Experimental Neurosurgery and Anatomy



**Sensitization of glioblastoma tumor micro-environment
to chemo- and immunotherapy by Galectin-1 reduction
after intranasal anti-Gal-1 siRNA administration**

Matthias VAN WOENSEL

Jury:

Promoter: Prof. Dr. Steven De Vleeschouwer

Promoter: Prof. Dr. Karim Amighi

Co-promoter: Prof. Dr. Stefaan Van Gool

Co-promoter: Dr. Nathalie Wauthoz

Chair: Prof. Dr. Rufin Vogels

Secretary: Prof. Dr. Paul Clement

Jury members:

Prof. Dr. Stefaan De Smedt

Prof. Dr. Clemens Dirven

Prof. Dr. Jean-François Baurain

Prof. Dr. Dominique Bullens

Dissertation presented in partial
fulfilment of the requirements for
the degree of Doctor in
Biomedical Sciences
(KULeuven) and Doctor in
Pharmaceutical Sciences (ULB)

Leuven, December 2016

Acknowledgements

Als de rook om je hoofd is verdwenen, dan is het tijd om je dankwoord te schrijven. Na een goede 4 jaar doctoreren, en bijna 10 jaar aan de KULeuven; komt ook hier een einde aan. In dit dankwoord zal ik me richten tot de personen die me hebben geholpen hier vandaag te staan. Elk van hun heeft op zijn of haar unieke manier zijn steentje bijgedragen aan dit thesis, en daarom wil ik ze graag hier even vermelden.

First of all, I would like to thank my promoter Steven De Vleeschouwer. Your ambition and vision to create new innovative drugs for patients with brain tumors has always inspired me. I remember I came to your office as a freshly graduated master student, to apply for this PhD position. We discussed the possibility of the nose-to-brain transport project, and I immediately understood that this project could become high-risk, high-gain. We started with full enthusiasm, which results today in this thesis. I would also like to thank you for the trust in me: you allowed me to explore new avenues and experiments by myself, which broadened my horizons. I am looking forward to the new endeavors that you will undertake. I would also like to thank my promoter at ULB: Karim Amighi. Given the multi-disciplinary approach of this project; a partner experienced in pharmaceutical development was mandatory for our project. From the first day, you welcomed me in the ULB-family, as if I had been around already for a long time. You provided me your experience, your facilities and the excellent guidance of Nathalie and Rémi. Your unique approach of combining academic research with industrial partners is highly inspiring. I wish you an exciting future with InhaTarget. Next, I would also like to thank my co-promoter Stefaan Van Gool. You introduced me into the field of immunoncology during my master thesis. Your dynamism motivated me to pursue a research project in this field. Although the last years haven't been easy, I would like to thank you for launching our project and guidance. Finally, I would like to thank also Nathalie, my co-promoter at ULB. You have an unlimited enthusiasm for research which is highly contagious. From the beginning, you provided me with a lot of guidance and help to make this project to what it is today. A special thanks for the last administrative hurdles the past months. I wish you and Cédric, and Margot a wonderful time ahead, and best of luck for your future academic career.

Innovatief onderzoek is kostelijk, en niet altijd rendabel. Daarom wil ik ook uitdrukkelijk onze financiële steun bedanken. De beschikbare middelen van het Herman Memorial Research Fund, Olivia Fund, Belgian Brain Tumor Support en het IWT (Agentschap voor Innovatie door Wetenschap en Technologie; nu Fonds Wetenschappelijke Onderzoek) en de dienst neurochirurgie; hebben ertoe bijgedragen dat ik me nooit moest zorgen maken over financiële limitaties, en dat de noodzakelijke kosten gedekt werden. De middelen in deze fondsen, zijn vaak verkregen door inspanningen van mensen, zoals Mevr. Ilse De Reze, die zich belangeloos willen inzetten om patiënten een betere toekomst te geven; waarvoor mijn oprechte dank.

I would also like to thank my jury members. They have read this thesis in detail, and provided excellent remarks and corrections, which increased the quality significantly. Moreover, I would like to thank you for being here today. Ik zou ook graag de professoren van het labo klinische immunologie bedanken: Prof. Ceuppens, Prof. Bullens, Prof. Schrijvers and Prof. Hellings. Vanaf de start met uitdagende IWT oefensessie's, en voorts met datasessie's op vrijdagochtend hebben jullie voor een constante evaluatie van mijn project gezorgd,

waarvoor dank. In het bijzonder bedank ik Prof. Ceuppens, om de gelegenheid te geven mijn experimenten in het labo klinische immunologie te kunnen uitvoeren.

Na 4 jaar en half doctoreren kom je met enorm veel mensen in aanraking. Collega's komen en gaan, en toch laat elk van hen een indruk achter die blijft. In een poging om niemand te vergeten: Christine, Lien, An, Isabel, Jeroen, Jochen, Zhe, Isabelle, Ellen, Jonathan, Lieve, Sven, Brecht S and Brecht C, Emilie, Valerie, Katleen, An-Charlotte, Joost, Lien S., Thais, Kasran, Matteo, Simone, Irina, Inge, Anais, Leen, Omer, Caroline, Abhi, Pavel, Petya en vele anderen: bedankt allemaal voor de leuke tijd en aangename babbels, hulp met experimenten en toffe labo-uitstapjes.

Enkele collega's wil ik ook in het bijzonder bedanken. Het is duidelijk dat ik met Jochen, Jeroen en Brecht een unieke tijd heb mogen beleven. 3 musketiers en 1 D'Artagnan (met dank aan Encarta 97 om erop te wijzen wie de 4^{de} muskietier was). Ik wil Jochen bedanken, om als stil water ook diepe gronden te hebben. De afgelopen jaren heb ik U leren kennen als de meest toegewijde collega die ik me kan indenken. Intussen weet ik het wel: elk labo heeft een Jochen nodig, iemand die elk protocol tot in de puntjes wil uitwerken, en koste noch moeite spaart om een collega uit de nood te helpen. De afgelopen jaren gingen niet altijd van een leie dakje, maar het einde is in zicht! Ik zal me vooral herinneren: "kruipt allemaal den boom in", "amai er is hier nog volk op de E314", en hoe je er toch in slaagt om elk trouwfeest op te vrolijken met stijlvolle dansspasjes. We komen elkaar nog wel tegen in de stille kempen! Brecht, blijf zoals je bent. Je levensenergie en optimisme zijn ongeëvenaard. Bedankt om de positieve noot erin te houden, alsook om de kasten vol te plakken met (schunnige) afbeeldingen. Ondertussen is het al Dr. Steelant, en de future is bright ... veel geluk met alles wat op je pad komt. Misschien moeten we nog maar eens naar de 'In den Rozenkrans' gaan? Jeroen, Dr. Pleasures, ook al ben je al enige tijd vertrokken uit het labo, de nagedachte aan sporza-man blijft! Bedankt voor de collegialiteit, de fijne babbels, de citytrips naar Rostock, en quizen. Voorts ben je ondertussen zorgvuldig in de vriendenkring geïnfiltreerd, dus we zien elkaar nog wel! Veel succes op de nieuwe job. Ik ben blij dat ik in jullie team zat!

Voorts wil ik ook Lieve, Ellen en Jonathan bedanken; vooreerst om me welkom te heten in hun bureau de eerste jaren. Lieve, je unieke manier om het labo te overzien heb ik altijd weten te appreciëren. Bedankt om mijn experimenten in goede banen te leiden, en assistentie te bieden waar nodig. Joost, veel succes met de laatste experimenten, en je verdere carrière in de neurochirurgie. Katleen (of was het nu met 'h'?), als nieuwe additie aan het neus-keel-oor team; veel geluk, en ook wat sterkte! Brecht C., laat maar weten als je die ILCs vindt, alsook de nieuwe cd van 'Oy Division'. Sven, veel geluk met de lancering van Euforea. Inge, het einde komt ook voor jouw stilaan nabij, veel geluk met de laatste experimenten. Lien S., succes met de nieuwe uitdagingen. Kasran, merci voor de goedlachse babbels! Karin, merci om mijn muizen te verzorgen, het toegewijde werk, en de gezellige babbels! Isabelle, ik bewonder je positivisme en wens je alle geluk bij de laatste experimenten! Omer, bedankt voor de Hagelandse wijn! Caroline, bedankt om allerhande praktische zaken te regelen! Anais, bedankt om raad en daad bij te staan met alle prille ouderschapszorgen! Louis is je ook dankbaar! Abhi, thanks for all the nice chats and insights on immune-oncology! I am sure a great research career is in front of you! Cheers ☺. Matteo, 'in bocca al lupo' for the next years! Everything will be alright! Thank you also Louis Boon, for providing sufficient amount of in vivo depleting antibodies. Bedankt aan Freya en Inne voor de western blots! Dean, bedankt voor de sequencing hulp!

Given the fact this thesis was obtained in joint agreement with ULB, I had also the privilege to meet colleagues at the center of Brussels. At first I would like to thank the team of the '4th floor'. Robert, Véronique and Florence: you have started this project, and provided me an excellent platform from which I could start my experiments. Next, I would like to thank Rémi; you guided me from the first day, and introduced me in the wonderful world of chitosan! Moreover, we became good friends, and like-minded spirits! I look forward to your developments! Antonio, when I am your age, I hope to have similar energy and spirit! Thank you for your enthusiasm. I also thank the team of Prof. Amighi for assisting me in the lab: Laurent, Julien, Jonathan, Cédric, Nancy, Federica, Vincent, Philippe, Romain, Max, Audrey and many others.

Next, a special thanks to the laboratory of vascular patterning at VIB is in place. Prof. Gerhardt, thank you for allowing me to use your facilities and microscopy unit. I also thank Pavel and Petya for the nice chats we had. This project would be nowhere near if I did not meet Thomas. Thomas, I thank you enormously! You have dedicated a great amount of time and efforts on my thesis; we spend so many hours/evenings at the microscope, trying to get the perfect picture! We had many philosophical discussions about life, research, and everything that keeps us going! I am confident you will have a great research career, starting in Paris. Besides the research, I wish you best of luck with Gabriel and Claire! I am pretty sure we will meet again!

Naast het onderzoek, wens ik ook mijn thuis omgeving te bedanken. Vooreerst mijn ouders, bedankt ma en pa om mij alle kansen te geven om mijn eigen interesses te ontwikkelen. Ik kon altijd op jullie steun en vertrouwen rekenen, wat er voor gezorgd heeft dat ik hier vandaag sta. Jullie hebben me geleerd om altijd nieuwsgierig te zijn, en te beseffen dat niets voor niets komt. Ik hoop dit ook aan onze Louis verder te kunnen geven. Merci! Jonas & Vika, bedankt om me bij te staan. Met plezier zal ik peter zijn van jullie dochtertje! Voorts wens ik ook mijn schoonouders te bedanken: Jan & Sonja. Bedankt om mij welkom te heten in jullie familie, en al de goede zorgen tijdens de afgelopen drukke jaren. Dit heeft er ook voor gezorgd dat ik mij volop in mijn thesis kon verdiepen. Bedankt. Voorts wens ik ook de vrienden te bedanken. Kwaliteitsvolle uitstapjes naar Schotland, tennismatchen, lange bbq avonden, mogelijks een kaaskroket-festijn af en toe, hielpen altijd om me te ontspannen; thanks!

Ine, zoals je destijds al voorspelde in jouw thesis, is het nu mijn beurt. Bedankt voor alle opofferingen, liefde en steun die je me geeft om hier vandaag te staan. Je weet als geen ander hoe me tot rust te brengen, en vult me perfect aan. De afgelopen jaren waren intens met bouwen en trouwen, en als kers op de taart is onze Louis er ook bij gekomen. Inmiddels al die events vond je toch de tijd en energie om mijn liefdevolle vrouw te zijn. Ik zie jullie doodgraag, en kijk uit naar onze toekomst samen.

Table of Contents

Acknowledgements	i
Table of contents	iv
List of abbreviations	vi
1. General Introduction	1
1.1 High Grade Glioma: an unmet medical need	1
1.1.1 Classification	1
1.1.2 Genomic background	1
1.1.3 Diagnosis and Standard of Care	2
1.2 Cancer immunology	3
1.2.1 Immune surveillance	3
1.2.2 Immune contexture for GBM: a battlefield between activation and suppression	4
1.2.2.1 Immune activation	4
1.2.2.2 Immune Suppression	5
1.2.2.3 Tumor derived factors for immune suppression	6
1.2.2.4 Immunotherapy	6
1.3 Galectin-1	7
1.3.1 Galectin-1 as a natural immune suppressive lectin	7
1.3.2 Non-immunological features of Gal-1 that drive tumor progression.	9
1.4 Local Administrations to treat GBM	11
1.5 Intranasal administration	12
1.5.1 Anatomy relevant for nose-to-brain transport	12
1.5.2 Macroscopical anatomy	12
1.5.2.1 Olfactory pathway/olfactory region	13
1.5.2.2 Trigeminal pathway/respiratory region	13
1.5.2.3 Other possible pathways	13
1.5.3 Microscopical anatomy	14
1.5.3.1 Nasal mucosa and mucus	14
1.5.3.2 Paracellular transport between nasal mucosa	15
1.5.3.3 Transcellular transport across nasal mucosa	15
1.5.3.4 Organization nerves/filia olfactoria	15
1.6 Pre-clinical and clinical evidence of nose-to-brain transport for GBM	16

1.6.1	Intranasal administration for GBM	16
1.6.1.1	Animal models	16
1.6.1.2	Clinical setting	18
1.6.1.3	Possible pitfalls	19
1.7	Improvement of the nose-to-brain pathway through formulations	20
1.7.1	Via Polymer-based nanoparticles	20
1.7.2	Lipid based nanosized formulations	23
1.7.2.1	Via (nano)emulsions	23
1.7.2.2	Via solid lipid nanoparticles	23
1.7.2.3	Via liposomes	23
1.7.3	Functionalization of the nanoparticle surface by ligands	24
1.7.4	Via gels	25
1.7.5	Via Indirect enhancers / devices	25
2.	Aims and Objectives	27
3.	RESULTS – PART 1: <i>Development of siRNA-loaded chitosan nanoparticles targeting Galectin-1 for the treatment of glioblastoma multiforme via intranasal administration</i>	29
4.	RESULTS – PART2: <i>Sensitization of glioblastoma tumor micro-environment to chemo- and immunotherapy by Galectin-1 intranasal knock-down strategy</i>	53
5.	RESULTS - PART 3: <i>PEGylated chitosan nanoparticles optimize nose-to-brain transport to target Galectin-1 in the treatment of glioblastoma</i>	73
6.	Addendum – Carrier development	83
7.	Final discussion and Perspectives	95
	Abstract	101
	Summary	103
	Samenvatting	105
	References	107
	Curriculum vitae	123
	Bibliography and awards	125
	Posters and presentations	127

List of Abbreviations

APC	Antigen Presenting Cell
AZA	Acetazolamide
BBB	Blood Brain Barrier
BFP	Blue Fluorescent Protein
BM	Basal Membrane
cDNA	copy DNA
CE	Columnar Epithelium
CED	Convection Enhanced Delivery
CNS	Central Nervous System
CS	Chitosan
CSF	Cerebrospinal Fluid
CTL	Cytotoxic Lymphocytes
CTLA-4	Cytotoxic T-lymphocyte-associated antigen
Da	Dalton
DAPI	4',6-Diamidino-2-phenylindole dihydrochloride
DC	Dendritic Cell
DD	Degree of Deacetylation
DQ	Degree of Quaternization
EGFR	Epidermal Growth Factor Receptor
FITC-FD4	Fluorescein Isothiocyanate-dextran 4 kDa
FNRS	Fonds National de la Recherche Scientifique
FSC	Forward Scatter
Gal-1	Galectin-1
GBM	Glioblastoma Multiforme
Gy	Gray
HMGB1	High mobility group box 1 protein
IFN- γ	Interferon - gamma
KO	Knock Out
LMWP	Low Molecular Weight Protamine
LOH	Loss of Heterozygosity
LP	Lamina Propria
M1	Macrophage-classically activated
M2	Macrophage-alternatively activated
mAb	Monoclonal Antibody
MDSCs	Myeloid Derived Suppressor Cells
MGMT	Methylguanine methyltransferase
MHC	Major Histocompatibility Complex
ML	Mucus Layer
MRI	Magnetic Resonance Imaging

mRNA	Messenger RNA
MW	Molecular Weight
NK	Natural Killer
NPSCs	Neural Stem and Progenitor Cells
PAMAM	Polyamidoamine
PBS	Phosphate buffered Saline
PCL	Poly-caprolactone
PD-1	Programmed Cell Death Protein Receptor
PDI	Poly Dispersity Index
PD-L1	Programmed Cell Death Protein Receptor Ligand
PEG	Poly-ethylene Glycol
PGE2	Prostaglandin E2
P-gp	P-glycoprotein
PLA	Poly Lactic Acid
PLGA	Poly lactic-co-glycolic acid
POH	Perillyl Alcohol
RDsiRNA	Red Dye labeled siRNA
RISC	RNA Interference Induced Silencing Complex
RNase	Ribonucleases
RPM	Rotations Per Minute
RT-qPCR	Real Time - quantitative Polymerase Chain Reaction
SDS	Sodium dodecyl sulfate
siGal1	Anti-Gal-1 siRNA
siRNA	small interfering RNA
SSC	Sideward Scatter
TAA	Tumor Associated Antigens
TCR	T Cell Receptor
TEER	Trans Epithelial Electrical Resistance
TEM	Transmission Electron Microscopy
Th1	Helper Tcell 1
TME	Tumor Micro Environment
TMZ	Temozolomide
TP53	Tumor Protein 53
TPP	Sodium tripolyphosphate
TRAIL	Tumor necrosis factor related apoptosis inducing ligand
Treg	Regulatory T cell
UPR	Unfolded Protein Response
VEGF	Vascular Endothelial Growth Factor
VIP	Vasoactive intestinal peptide
WGA	Wheat Germ Agglutinin

WHO World Health Organization
WT Wild Type
ZY Zombie Yellow

1. GENERAL INTRODUCTION

1.1. High Grade Glioma: an unmet medical need

1.1.1. Classification

Gliomas are by far the most common type of intrinsic brain tumor in adults, affecting about 5 individuals per 100 000 per year, and account for more than 50% of all intrinsic brain tumors. Gliomas can also occur in young children, in about 2 per million per year, resulting in the cumulative highest years of life lost amongst all cancer types. Histopathologically, gliomas can be subtyped according to the glial subtype from which they originate: astrocytomas (60-70%), oligodendroglial tumors (10-30%), ependymal tumors (<10%), and mixed gliomas (1, 2). Within the group of astrocytic tumors, high grade gliomas are most frequently observed. The World Health Organization classifies gliomas in several grades according to distinct histopathological criteria, such as presence of necrosis, proliferation of endothelium and abundance of mitosis. In more recent years, also molecular genetics are being considered to classify gliomas, as discussed later. Glioblastoma multiforme (GBM), a grade IV astrocytoma, is approximately four times more common than grade III anaplastic astrocytoma (3). GBM carries the hallmarks of grade IV neoplasms such as highly necrotic, hypoxic and mitotic areas (4).

1.1.2. Genomic background

At the genomic level, 'primary' GBMs are likely to develop due to a loss of heterozygosity (LOH) in large regions at chromosome 10 (5). These genetic alterations can lead to the amplification of Epidermal Growth Factor Receptor (*EGFR*) gene, *PTEN* mutation, *p16* deletions and *MDM2* amplification. Since *MDM2* functions as the counterpart of tumor protein 53 (TP53), the guardian of the genome, *MDM2* gene amplification will lead to a suppression of TP53. *PTEN* mutations will give rise to a lack of functional PTEN which normally exercises a phosphatase-type activity. Lack of functional PTEN will lead to the permanent phosphatidylinositol 3,4,5-triphosphate dependent-activation of the serine-threonine kinase Akt which is a proto-oncogene that makes cells resistant to apoptotic stimuli and promotes cell proliferation. Since mTOR is a direct target of the PI3/Akt pathway, this molecule can as well deregulate the cell cycle. Likewise, amplification or constitutively active mutant receptor EGFR can upregulate the proliferation rate of the tumor cells (6). Besides primary GBM, this tumor can also arise from a lower grade lesion. Interestingly, in recent years mutations in the genes isocitrate dehydrogenase 1 and 2 have been observed in these low grade gliomas. Growing data indicate that these mutations play a causal role in gliomagenesis, and lead to a secondary GBM.

Technical advances in gene expression profile analysis enabled a new classification scheme for GBM based on molecular characterization and signaling pathways that are important for GBM progression. Among the most important pathways are noted TP53, and receptor tyrosine kinase signaling. Based on gene expression the following GBM subtypes were proposed: classical, neural, proneural and mesenchymal (7). Classification systems according to shared signaling pathways, might pave the way

for a more personalized treatment schedule for the appropriate segment of patients. To this end, the WHO classification has entered the molecular era, and now classifies gliomas on both molecular and pathological observations (2). In this recent report, a simplified algorithm is presented where both the importance of isocitrate dehydrogenase 1 and 2, p53 alterations and 1p/19q deletions are taken into account.

1.1.3. Diagnosis and Standard of Care

Diagnosis of GBM is a multidisciplinary exercise for clinicians. Clinical symptoms can present as seizures, headaches and focal neurological deficits that correlate with the tumor-site such as aphasia, motor and sensibility deficits. Cognitive dysfunction is also extremely common in malignant gliomas. When a brain tumor is suspected, magnetic resonance imaging (MRI), with or without contrast infusion is preferred. By using image-guided stereotactic biopsy techniques, it is possible to obtain diagnostic tissue material with a low morbidity rate. Upon diagnosis, patients face a median survival outcome of just 14.6 months, and 88% of patients will die within 3 years (1, 8, 9). Relapse is universal and upon relapse, prognosis is even worse. Relapsed GBM patients have a median survival expectancy of only 9 months and almost all patients die within 18 months (10). The treatment failure is attributed to the diffuse infiltration of therapy-resistant tumor cells into surrounding healthy tissue. This results in recurrent tumor growth which, in 80% of the cases, develops very close to the resection cavity.

The multidisciplinary treatment of gliomas aims to improve neurological deficits and to increase survival, while maintaining the best possible quality of life. A first technique that is used is the neurosurgical removal of the tumor mass. Maximal resection is highly desirable since the absence of residual tumor mass positively correlate with the median tumor progression and survival time (11). In general, patients enter the so-called 'Stupp protocol', which consists of postoperative radiotherapy with concomitant temozolomide (TMZ) chemotherapy and continued use of adjuvant TMZ for 6 months after preferentially maximal safe surgical resection. As compared to patients treated with radiotherapy alone, this treatment protocol could prolong the median overall survival (OS) of over 500 newly diagnosed GBM patients by 2.5 months (from 12.1 to 14.6 months) and could improve the 2-year and 5-year survival rates (8, 9). Radiotherapy appears to be highly effective in transiently controlling the remaining tumor mass after resection. A total dose of 60 gray (Gy) has been proven to prolong the median survival of GBM patients (9). However, almost all patients relapse close to the targeted area of postoperative radiotherapy (12).

The success of TMZ in GBM is mainly attributed to its interesting properties to cross the blood-brain barrier; due to its low molecular weight, and appropriate lipophilicity. Its mechanism of action works via the formation of O6-methylguanine in the DNA. These DNA-methyl adducts will mispair with thymine during the next cycle of replication. The next futile cell cycles of DNA mismatch repair will lead to double strand breaks and subsequent apoptosis and/or autophagy (13). Recently, it was discovered that patients with a methylated O6-methylguanine-DNA methyltransferase (MGMT) promoter have better responses to chemotherapy with alkylating agents like TMZ (14). MGMT is a DNA repair enzyme that can remove alkyl groups from the DNA, supporting the prevention of DNA mismatch

during replication and transcription. Methylation of the genetic promoter of MGMT inhibits its biological activity. Therefore, MGMT promoter methylation is considered a very valuable predictive biomarker for therapy response to TMZ that can be tested for therapeutic decision making.

In previous years, several attempts have been undertaken to target the tumor proliferation rate by tackling either the growth signaling pathway (anti-EGFR therapy), or the blood supply (anti-VEGF therapy). In both cases, clinical trials have not succeeded to demonstrate a significant survival benefit. Acquired resistance such as secondary mutations in EGFR are often observed and limit the clinical efficacy (15). Of note, besides EGFR, also other tyrosine kinases are altered in GBM, and are clinically relevant targets: such as platelet-derived or hepatocyte growth factor receptor. In terms of anti-angiogenic therapy, GBM tumors seem to have an inherent resistance to these therapies in which tumors bypass angiogenic blockade (16). In this respect, the concept of targeting a single pathway, with a 'golden bullet' approach will most likely not lead to drastic survival improvement for GBM patients. Therefore, as later discussed, in this thesis multiple pathways were targeted, thereby challenging inherent tumor resistance mechanisms to a higher extent.

1.2. Cancer immunology

1.2.1. Immune surveillance

To define what makes that normal tissue can become cancer, it seems all cancer types share 6 common features that need to be fulfilled: resistance to cell death, sustained proliferation, evading growth suppressors, induction of angiogenesis, replication immortality and active metastasis (4). In the last decade, it became clear that cancer could be attributed with an additional feature: escape from immune surveillance (17, 18). It became evident that there is an inherent interplay between tumors and immunity. First of all, it was found that there was a higher incidence of certain types of tumors in immune-compromised patients. Moreover, if patients developed cancer, the amount of infiltrating lymphocytes could often be linked to a better survival. Likewise, also in animal models, carcinogenesis appears to be more successful in immune-compromised mice than in immune-competent mice.

How cancer and immunity are interconnected is often explained via the three E's of immune-editing: elimination, equilibrium and escape (Figure 1). In the first phase, a few cancer cells acquire a growth advantage and proliferate. However, innate and adaptive immunity are well equipped to deal with this abnormal cell growth. Due to genetic instability, cancer cells can acquire additional features to adapt this situation. They gain for instance tumor derived soluble factors that decrease immunity in the direct tumor micro-environment (TME). In this stage, cancer and immunity have come to equilibrium, where no tumor growth is taking place and a latent period exists. In more advanced stages, immunity is heavily affected by the tumor derived soluble factors, and becomes tolerant for tumor growth, and the cancer can escape the immune surveillance, which results in a clinical apparent tumor mass. The exact mediators as depicted in Figure 1 will be discussed in a later chapter.

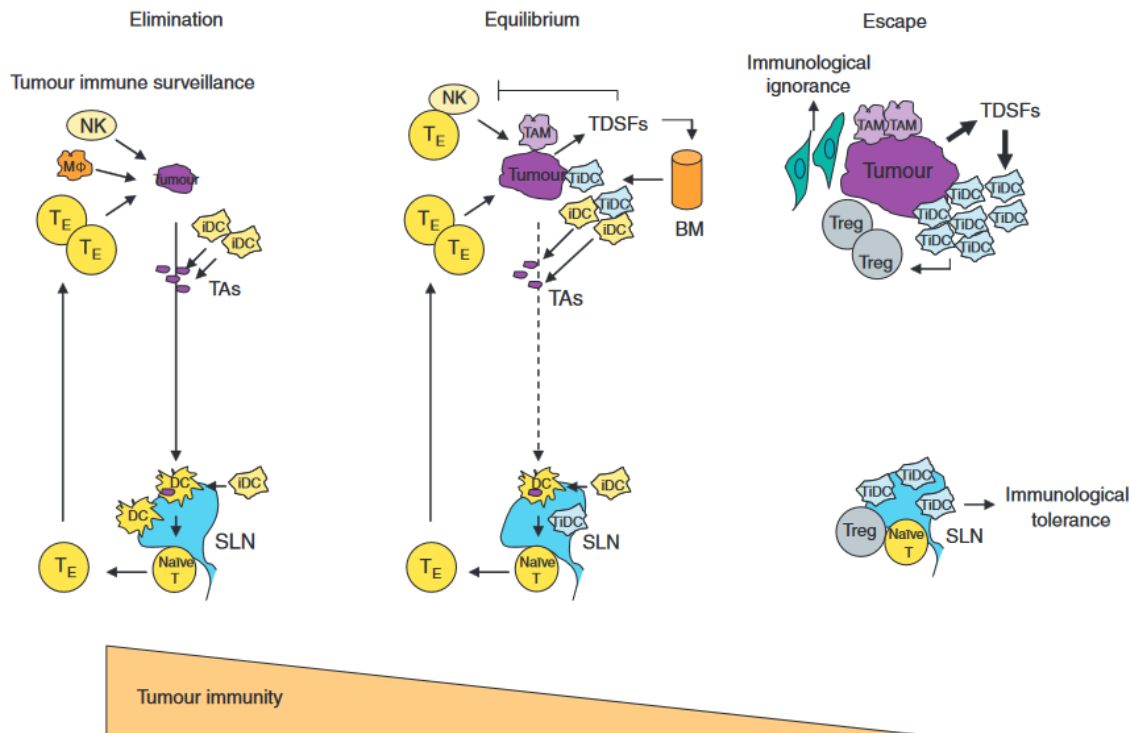


Figure 1. Cancer Immuno-editing. Modified adapted from Kim et al 2007: (17) A schematic process for understanding cancer immunoediting from immune surveillance to escape. When early tumor cells existed, these cells were easily eradicated by innate and adaptive immune responses. During growth, tumour cells are required for angiogenesis and stromal remodelling, which produce tumour cell variants that have low immunogenicity and are resistant to immune attack, and proceed to the equilibrium phase even though the elimination phase continues through immune selection pressure. Tumour progression leads to the release of tumour-derived soluble factors that are involved in several mechanisms of immune evasion in the escape phase. iDC, immature dendritic cell; Mφ, macrophage; NK, natural killer; TE, effector T cell; TAs, tumour antigens; SLN, sentinel lymph node; TiDC, tumour-associated iDC; TAM, tumour-associated macrophage; TDSFs, tumour-derived soluble factors; Tregs, regulatory T cells; BM, bone marrow.

1.2.2. Immune contexture for GBM: a battlefield between activation and suppression

1.2.2.1. Immune activation

In general, infiltration of lymphocytes in the CNS is a highly regulated process, which involves an activation stage of the endothelium, to allow passage towards the brain parenchyma, mediated by chemokines (CXCL12) and adhesion anchors on the endothelium (integrin $\alpha 4\beta 1$) (18). Especially CD8+, cytotoxic T cells (CTLs) are well equipped to kill tumor cells, with a high specificity (19). When antigen-presenting cells (APC) sample tumor associated antigens (TAAs), they will be presented in the lymph nodes, where selection of the most adequate CTLs will occur. CTLs can kill tumor cells via secretion of perforin and granzyme B upon interaction of T cell receptors (TCR) with the correct (tumor-associated) Ag, presented in Major Histocompatibility Complex I (MHCI). Infiltration of such CTLs are associated with an improved survival in many cancer types. As for CD4+ lymphocytes, T helper 1 (Th1) cells are in general thought to further stimulate the CTL response, and support the overall anti-tumor inflammation via Interferon-gamma (IFN- γ) secretion. IFN- γ can facilitate the development of tumor specific CTL, stimulate and recruit dendritic cells (DCs) and Natural Killer cells

(NKs). Moreover, IFN- γ can also upregulate MHC I molecules on tumor cells, which increases the susceptibility for CTL and NK cell lysis. NK cells can recognize cells with a high density of MHC I and eliminate them via perforin and granzyme cytolysis, tumor necrosis factor related apoptosis inducing ligand (TRAIL), and reactive oxygen species (20). NKG2D is a receptor on NK cells that can recognize and detect transformed cells, which express NKG2D ligands, independently from the MHC class I context. Besides NK cells, also other cells of the innate immune system can infiltrate GBM such as DCs and Tumor Associated Macrophages. These APC are equipped to sample and process TAAs in the MHC context. Especially DCs are potent CD8 stimulators, as they can crosspresent exogenous Ag in the MHC I context (21). Intratumoral accumulation of DCs has been shown to increase survival (18). The presence of macrophages is an ambiguous prognostic factor for GBM. In fact, many literature reports reveal that there are at least two distinct macrophage subpopulations, according to their activation stimulus (22). Either, they report about classically activated macrophages (M1), or alternatively activated macrophages (M2). These M1 macrophages are activated by an IFN- γ driven inflammation, as described above, which results in a spontaneous release of pro-inflammatory cytokines such as TNF- α and IL-1 β . On the other hand, M2 macrophages are activated by Th2 cytokines as IL-4, or even anti-inflammatory stimuli as IL-10 and TGF- β , which results in a reciprocal release of these anti-inflammatory cytokines, and activation of the arginase metabolism. In many diseases such as stroke, experimental auto-immune encephalomyelitis, and more recently also GBM, M1 macrophages are responsible for the initial wave of inflammation, at the early onset of disease. On later time points, the balance seems to switch from immune activation by M1, to immune suppression by M2. What causes the switch, or even differential recruitment of distinct macrophage types, is unknown. In recent reports, it became clear that these tumor infiltrating macrophages are a class of highly dynamic cell types, which can respond to different stimuli from different sources, with different receptors and even lead to similar responses. Consensus is arising that the Th1-M1 and Th2-M2 paradigm is probably not satisfactory in part by increasing knowledge about co-receptor, secreted factors and further subtyping being the focus of ongoing research (22-24).

1.2.2.2. Immune Suppression

Not only M2 (-like) macrophages can exert immune suppression in the TME, but also other distinct cell populations. Within the myeloid cell fraction, we can also distinguish Myeloid Derived Suppressor Cells (MDSCs). These suppressor cells are characterized by their myeloid lineage CD11b and Gr-1 expression. More in detail, they can be divided in Ly6C⁺ for monocytic MDSCs and Ly6G⁺ for granulocytic MDSCs. They can exert an inhibitory effect on T cells by many features, among which the production of reactive oxygen species and NO, L-arginine and cysteine deprivation and even the expansion of Treg. In glioma patients, both monocytic and granulocytic MDSCs are increased in the circulation, and have been shown to suppress IFN- γ production in T cells (25, 26).

The main drivers in cell-mediated immune suppression in glioma are often believed to be the Treg population. Under non-pathological conditions, Tregs mediate homeostatic peripheral tolerance by suppressing autoreactive T cells. This particular population has been demonstrated to infiltrate abundantly the glioma TME, and several studies find a strong correlation between increasing amounts

of Tregs, and worse prognosis for glioma (27-29). Similar to the MDSCs, Tregs in the circulation of GBM patients have demonstrated anti-proliferative properties on their T cells (30). Moreover, the frequency of Tregs in TME of GBM is even more pronounced than the Tregs in circulation (27). Tregs are suggested to be recruited to the site of inflammation via CCL2/22 chemokines, which can be either secreted by glioma cells themselves (31), or also MDSCs (32). Once they enter the GBM site, they release immune suppressive factors such as IL-10 and TGF- β , which directly inhibits T cell proliferation or impairs APC function. Cell-cell contact with APCs can also induce indoleamine 2-3 dioxygenase secretion via Cytotoxic T-lymphocyte-associated antigen (CTLA-4) inhibitory molecule/b7 interaction, which reduces tryptophan in T cells, thereby rendering them anergic (33).

1.2.2.3. Tumor derived factors for immune suppression

As discussed previously, in the equilibrium phase of immune-editing, the GBM tumor cells learn how our immune system works, and more importantly, how they can evade their recognition. Tumor cells secrete numerous soluble factors in the extracellular matrix of the TME that affect all immune cells present. For instance, high secretion loads of VEGF, Prostaglandin E2 (PGE2), CCL2, IL-10 and TGF- β can attract MDSCs and Tregs (34). Besides the recruitment of immune suppressors, other factors can induce anergy in the present CTLs, such as programmed cell death-1 receptor ligand (PD-L1, also known as B7-H1). This strong suppressor signal can interact with PD-1 present on both CD4+ and CD8+ infiltrating (activated) lymphocytes. A last category of factors are directed to induce apoptosis in activated lymphocytes, such as Galectin-1 (Gal-1). Several publications pinpoint Gal-1 as an ideal target to increase the efficiency of immunotherapy. In a later section we will further elaborate on Gal-1 and elucidate how it became a validated target for GBM.

1.2.2.4. Immunotherapy

In the previous section, the main protagonists and antagonists were discussed that orchestrate the immunity in GBM TME. Given the dismal prognosis of patients, the aggressiveness of the tumor and the high morbidity, it is clear the balance is tilted in favor of immune suppression. Over the past decades, immunotherapy gained a lot of momentum, with the aim to become a complementary standard therapy for cancer, next to surgery and chemo-radiotherapy. Immunotherapy has multiple advantages over classical treatment modalities. Immunotherapy can work highly specific, with a theoretical minimum of off-target toxicity. Moreover, once a patient's immune system is orchestrated to attack a tumor mass, memory can be induced, thereby protecting the patient from recurrence for a long time period. The potential of immunotherapy as 4th pillar of cancer therapy was recognized by awarding it in 2013 by Science as the breakthrough of the year (35). Several interesting approaches on immunotherapy are discussed here, with relevance to the work that will be presented later on in the manuscript.

A first immune stimulatory approach is DC vaccination (36). Monocytes are isolated from the patient, and differentiated towards immature DCs, since these are the most potent APCs, demonstrated by their ability for crosspresentation, high levels of co-stimulation (CD80/86) and potency to migrate to lymph nodes (via CCR7). Subsequently, TAA are provided to the DCs, and a maturation stimulus,

which results in APC that contains TAA, presented in the MHCII context. When injecting this final product back into the patient, these cells can elicit a potent CD4+ and CD8+ T cell response, selectively directed to the tumor mass (37). Although many clinical trials were initiated, there is currently no standard product, with many variations in cultivation of DCs, and source of Ag (either well-defined such as peptides, or undefined such as whole tumor lysate), which makes the interpretation of efficacy over big patient cohorts a challenging task (36). In melanoma and especially metastatic prostate cancer (Sipuleucel-T, Provenge®), DC vaccines were used, with clinically improved outcome (38). A recent meta-analysis suggests a modest long term benefit of DC vaccination in GBM patients' as well and could detect objective responses such as increased IFN- γ production in vaccinated patients (39). Of note, this meta-analysis has some inherent limitations that can bias the outcome. Despite this promising approach, the clinical benefit is still considered to be sub-optimal, mainly due to the enormous burden of immune suppression as presented earlier. Therefore, consensus is arising that merely stimulating the immune system is not sufficient, and alleviation of the breaks on the immune system should be combined together. In this area of research, many advances have been made in checkpoint blockage, in particular regarding CTLA-4 and PD-1 inhibition, which are the natural brakes on the immune reaction during respectively the priming and the effector phase. APC can touch CTLA-4 on T cells and render them anergic. Ipilimumab (anti-CTLA4) has obtained FDA approval for brain metastases of melanoma. As explained before, PD-1 receptor is present at many CD4+ and CD8+ infiltrating lymphocytes. GBM tumors are equipped with PD-L1 and upon contact with PD-1 they can render these lymphocytes anergic in proliferation and effector function. Monoclonal antibodies blocking CTLA-4 and PD-1 or their ligands PD-L1/2 have been developed and widely used in various cancers, and in combination. After the approval of anti-CTLA-4 in 2011, anti-PD-1 (nivolumab and pembrolizumab, for metastatic squamous non-small cell lung cancer and relapsed melanoma) recently obtained FDA approval and several anti-PD-1 ligands are also entering the market (MEDI4736, MDX-1105). Combination of nivolumab and ipilimumab has been explored in advanced melanoma, renal cell cancer and non-small cell lung cancer, with clear improved outcome (40). Some toxicity issues were observed as diarrhea, hepatitis, colitis and pneumonitis, which could be managed by standard compensatory therapy of immune suppressors. Interestingly, management of these adverse events with corticosteroids, or tumor necrosis alpha antagonists, did not seem to affect the efficacy of ipilimumab (41). If adverse events appear, they were more often attributed to ipilimumab than nivolumab, which could indicate that anti-PD-1 blocking is more applicable, since the PD-1/PD-L1 axis is predominantly active at the tumor site, whereas CTLA-4 is constitutively expressed amongst all T cells that interact with APCs as the natural inhibitory signal.

1.3. Galectin-1

1.3.1. Galectin-1 as a natural immune suppressive lectin

As mentioned before, Gal-1 is secreted by glioma cells and can actively suppress the immune system by inducing apoptosis in activated T cells. Gal-1 was first discovered as a ~14-kDa subunit protein originally found in electric eels by Teichberg et al. and subsequently in bovine heart and other tissues by De Waard et al.(1976) and Nowak et al.(1976) (42). Nowadays, Gal-1 is considered as a natural

occurring immune regulator, as indicated by its upregulation in the uterus during pregnancy (43). Furthermore *gal-1* expression can be found in cardiac, skeletal and smooth muscle tissue, but also in hematopoietic cells (44). As suggested by the upregulation during pregnancy, under physiological conditions Gal-1 plays a role during pregnancy and developmental stages, rather than at later life. Therefore also, *gal-1* knock-out mice are viable and reproductive, with minor abnormalities such as defective outgrowth of bulbus olfactorius and defective B cell response. As the name suggest, Gal-1 is a glycan binding lectin with affinity for β -galactoside containing glycoproteins and lipids. Galectins have a conserved carbohydrate recognition domain responsible for the β -galactoside binding (45). Although galectins families do not have the signal sequence needed for protein secretion through the usual secretory pathway, some galectins are secreted in the extracellular space (46). A first clue that Gal-1 could be implicated in glioma biology was given when a positive correlation was demonstrated between *gal-1* expression and malignancy state of astrocytomas (47). The average expression level was only slightly increased in low-grade astrocytoma but was markedly increased in anaplastic astrocytoma and glioblastoma, which was later confirmed in two independent studies (48, 49).

Most relevant for our research, is the active immune regulation that is attributed to Gal-1. As mentioned earlier, Gal-1 has the potential to recognize and bind activated lymphocytes (via CD45, CD43, CD3...) (50, 51). Resting T cells can also bind Gal-1, but interestingly only the activated T cells undergo apoptosis. Both caspase dependent and independent apoptosis mechanisms have been reported, but the exact mechanism is to be determined, which likely depends on both the concentration of Gal-1, and whether Gal-1 is present as a monomer or dimer (50). Importantly, Gal-1 is not exclusively produced by GBM tumor cells, but also by the activated TME vasculature. Also here, endothelial cells that express Gal-1 induce apoptosis in bound T cells (50). Gal-1 can react quickly and at very low concentration (0.01 to 0.1 μ M), which makes it an excellent regulator to maintain homeostasis, and an adequate adaptive immune response under non-pathological conditions (52). This feature was also demonstrated when mice received recombinant Gal-1 to inhibit collagen induced arthritis (52).

Beside the direct effect of Gal-1 on T cell survival, many other effects of Gal-1 on the immune system are suggested. Another example includes the modulation of T cell proliferation. Gal-1 was demonstrated to inhibit antigen-induced proliferation of naive and antigen-experienced CD8+ T cells (53, 54). Thus, these data indicate a role of Gal-1 as an autocrine negative growth factor for CD8+ T cells.

On another crucial interface, Gal-1 has been demonstrated to inhibit T cell receptor (TCR) signaling. Gal-1 antagonizes TCR responses known to require costimulation and processive protein tyrosine phosphorylation, such as IL-2 production, but is permissive for TCR responses that only require partial TCR signals, such as IFN- γ production (55). This suggests that Gal-1 facilitates Ag-specific tolerance induction and blocks TCR activation. To further support tolerance induction, Gal-1 was also demonstrated to increase the amount of IL-10 secretion in unpolarized Th cells, with functional resemblance to Treg cells which actively suppress T cell proliferation.

Before T cells can be active at the tumor site, or any site of inflammation, they have to extravasate the systemic circulation. To this respect, Gal-1 was demonstrated as a negative regulator of T-cell recruitment to the endothelium via limiting T-cell capture, rolling, and adhesion to activated endothelial cells under flow (56).

As noted earlier, Gal-1 can stimulate unpolarized T cells to produce IL-10 and mimic Treg function. Furthermore, it has recently been observed that Gal-1 is also upregulated in Treg, and the expression is crucial for the suppressive nature of Tregs, as demonstrated by the decreased regulatory activity of Tregs isolated from Gal-1 K.O. mice (57). Moreover, in classical Hodgkin lymphoma, Gal-1 was demonstrated to favor the secretion of Th2 cytokines and the expansion of CD4+CD25^{high} FOXP3+ Treg cells.

Whereas the past mechanisms were mainly focused on the effect of Gal-1 on the lymphoid compartment, there is also a limited amount of literature discussing the role of Gal-1 on the myeloid counterpart. At first, Gal-1 was demonstrated to induce tolerogenic DCs. Tumor lysate-prepared DCs fail to produce an effective anti-tumor response in the presence of Gal-1. Besides DCs, also macrophages can be affected by Gal-1, which can induce the M2 macrophage phenotype (arginine metabolism driven) (58). As demonstrated in a stroke model, addition of Gal-1 can promote M2, and prevent M1 phenotype, thereby decreasing inflammation, leading to reduced stroke-associated damage (59).

1.3.2. Non-immunological features of Gal-1 that drive tumor progression.

As described before, TMZ is the chemotherapeutic drug that GBM patients receive in the standard protocol. However, it has been demonstrated that Gal-1 can be used by GBM tumor cells to induce resistance towards TMZ. Genomic damage induced by TMZ, can result in increased cellular stress, with many abnormalities on the proteome. Therefore, the endoplasmic reticulum can adequately respond to this TMZ-induced stress by inducing the unfolded protein response (UPR), which involves the reduction of protein synthesis and increasing chaperones, thereby alleviating the stress of misfolded proteins (60). Gal-1 was demonstrated to drive this UPR phenomenon, with sustained gene expression of e.g. ORP150, HERP genes that are known to be involved in chemo-resistance. Decrease of Gal-1 in Hs683 human GBM cells, could increase the sensitivity to TMZ, and increase the survival of tumor bearing mice, especially in combination with TMZ (61). In the standard Stupp protocol, patients receive also radiotherapy. Recently, it has been demonstrated that radiation of Lewis lung carcinoma models could increase Gal-1 expression (62), which is thought to attribute the lymphopenia during radiotherapy. In other reports, Gal-1 is even noted to drive radiotherapy-resistance through activation of pi3/Akt pathway. Together, these findings underline that Gal-1 maintains a TME that is well designed to abrogate cytotoxic agents, such as chemo- and radiotherapy.

On another level, Gal-1 was found to be highly upregulated in hypoxic regions, as part of the answer to unsatisfactory oxygen supply (63). Gal-1 was demonstrated to be a direct target of hypoxia-inducible-factor-1-alpha, a transcription factor that responds in situation where oxygen is insufficiently available, and adapted responses like vascular endothelial growth factor (VEGF) production are

evoked. In the TME, it was demonstrated that Gal-1 was not only tumor-derived, but also the tumor associated vasculature could produce Gal-1. Decreasing Gal-1 could markedly impair the endothelial cell proliferation and migration, resulting in a less pronounced tumor vasculature (64). In a recent report Croci et al, demonstrated that Gal-1 could take over VEGF signaling when this pathway was blocked (65). Anti-VEGF therapy is nowadays widely tested in clinical setting, to block the aberrant tumor related angiogenesis. However, patients often do not respond to this treatment, and Gal-1 might be responsible for inducing this parallel signaling to continue angiogenesis in TME, to maintain oxygen and nutrients supply for tumor progression. Besides compensatory signaling to VEGF, Gal-1 is also directly involved in the molecular processing of VEGF, via chaperone regulation (66). As a result, Gal-1 decrease in HS683 human GBM cells could decrease the secretion of VEGF, and overall vessel count in TME (61).

Beside an increased expression in hypoxic areas of TME, Gal-1 was also preferentially expressed at the tumor border. In addition, Gal-1 expression was increased in biopsies taken from the invasive tumor periphery, than biopsies from the tumor bulk mass. These findings support the idea that Gal-1 is involved in micro-metastasis in the CNS. In vitro scratch assays, revealed indeed a role for Gal-1 in tumor cell motility (67). Furthermore, also an effect on proliferation of GBM cells has been attributed to Gal-1. It was demonstrated that Gal-1 could anchor RAS protein in the inner plasmatic membrane, which enables continuous activation and increased cell division (68).

In conclusion, Gal-1 is a versatile protein, upregulated in the TME of GBM, and it can support immune-suppression, chemo resistance, migration, proliferation and angiogenesis, which all attribute to the malignancy of GBM and drive tumor progression. This pivotal role, makes Gal-1 an attractive target to tackle in GBM. However, to block Gal-1 in a selective (i.e. not interfering with other galectines) and multimodal (i.e. blocking both the intracellular and extracellular Gal-1) fashion, is challenging. Both monoclonal antibodies (Ab), and small molecules (Davanat, Anginex) have been tested, but none can fulfill all the prerequisites as described above (69, 70). Therefore, in this project we intended to use small interfering RNA (siRNA) to target *gal-1* mRNA (Figure 2). siRNA molecules are a duplex of 21-25 bp RNA strands and use the endogenous RNA interference pathway to specifically degrade mRNA, and preventing translation. In this pathway, siRNA molecules need to enter the cytoplasm of the cell where Dicer cuts siRNA into smaller fragments. These fragments can then be loaded into the RNAi-induced Silencing Complex (RISC), where one strand is randomly chosen (71). This complex, is complementary to the right mRNA fragment (i.e. *gal-1* mRNA), which can be degraded and no protein will be formed. Importantly, this technique does not induce genomic alterations (in contrast to e.g. CRISPR, a novel highly interesting tool to alter gene expression). Therefore, the decrease of the protein-of-interest is only temporary, until the siRNA is degraded, or diluted throughout cell divisions, in a sub-optimal siRNA concentration.

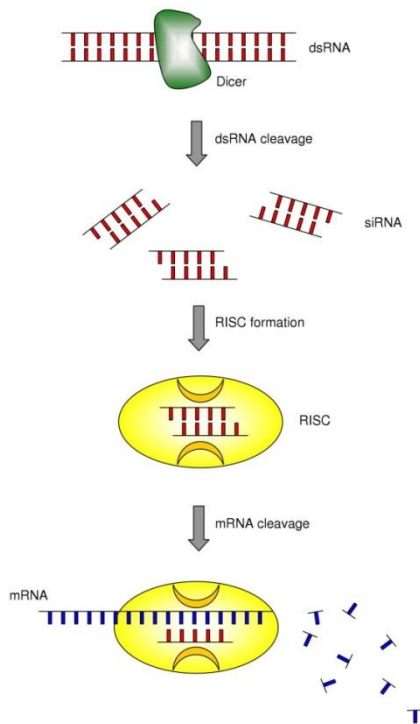


Figure 2. RNAi pathway. siRNA molecules are present in the cytoplasm and are recognized by the RISC complex, which produces complementary RNA strands that can directly target mRNA encoding the transcript of interest. Degradation of mRNA prevents protein translation, and consequently both the intra and extracellular protein content.

As mentioned before, Gal-1 is mainly produced in the TME of GBM via endothelial cells, and tumor cells. In order to tackle Gal-1 in these cells, we have to transport siRNA molecules in the CNS, and more in particular into the TME. To deliver active therapeutic agents to the GBM, many approaches were already described, and are briefly discussed here below. *The following paragraphs were obtained from Van Woensel et al. and modified or updated if necessary (72).*

1.4. Local Administrations to treat GBM

As the brain is well-protected by the blood-brain barrier (BBB), administering pharmacological agents with intracerebral biological activity is a challenging task (73). Even when drugs are permeable through the BBB, it is often difficult to reach therapeutic intratumoral concentrations. To overcome this problem, local administrations can be used, such as convection enhanced delivery (CED), intracerebral infusion, and wafers at the resection site. CED is a continuous infusion that uses a convective flow to drive the pharmacological agent into a large tissue area. One or more catheters are placed in the tumor mass, around the tumor or the resection cavity. Even with the use of well-developed catheters as reflux-preventing, hollow-fiber and balloon-tipped catheters, the leakage of infusates is nearly always detected (74). This leakage is a waste of therapeutic agent, and can, moreover, exert possible adverse effects on the healthy surrounding tissue and complicates the ability to estimate reliable iso-distribution volumes. Also, for CED, encouraging clinical data have been obtained, for example in the field of cytotoxin administration via CED (75). Cytotoxins are recombinantly produced proteins that consist of a vector/ligand/receptor and a bacterial toxin. A first example was DT.CRM107–Tf, a conjugate between transferrin and a diphtheria toxin derivative. Several clinical responses were observed but in phase III, toxicity was observed and the trial was stopped (76). CED administration of IL13-PE38QQR, a cytotoxin that consists of IL-13 and

Pseudomonas exotoxin A, was evaluated in a randomized phase III trial with recurrent GBM patients. It showed a median overall survival of 42.7 weeks and even up to 55.6 weeks for patients with an optimally positioned catheter (77). The local administration of chemotherapeutic drugs via CED, for example taxol, has also been explored in brain tumor patients and seems to have modest beneficial effects (78). We refer to an excellent review by Debinski et al. for additional information on the topic of CED in the context of brain tumors (79). Despite these positive clinical outcomes, complications are unfortunately inherent to CED. Surgical installation of one or more catheters, and the convective inward flow, often lead to complications such as infection, wound healing problems, inflammation, edema, and seizures (80, 81). In particular, CED is unlikely to be practical for drugs which need to be administered chronically. In more recent years, the intranasal pathway is being discovered as a non-invasive alternative to the invasive CED treatment modality.

1.5. Intranasal administration

Intranasal transport is the direct transport of therapeutic agents from the nasal cavity to the brain. This is a mainly extracellular and transcellular transport, involving the olfactory and respiratory regions of the nasal cavity. Intranasal administration has already been used for many years in the clinic to administer substances that cannot be given orally. These substances will reach the systemic circulation through intranasal instillation. Only a few decades ago, the potential of intranasal administration to reach the CNS gained interest (82, 83). Pharmacological agents can bypass the BBB during this transport and enter the CNS. The BBB is normally only permeable to lipophilic molecules, with a molecular weight (Mw) less than 600 Dalton (Da) (84). The LogP, the partition coefficient between solubility in octanol versus water, is estimated to be 1.5 – 2.7 for an efficient transport over the BBB (85). The very low permeability of the BBB is associated with low levels of pinocytosis and the presence of tight-junctions (TJs), which is critical for the CNS to maintain homeostasis (86). Furthermore the BBB is also equipped with a high number of drug transporters, such as P-glycoprotein (P-gp), which further prevents the entry of pharmacological drugs to the CNS (87). By circumventing the BBB via intranasal transport, the repertoire of possible therapeutic agents can be expanded to proteins, cells, nucleotides, viral vectors, and chemotherapeutics. Moreover, advantages of nose-to-brain transport include the avoidance of the systemic circulation, reducing the risk of systemic side effects and hepatic/renal clearing, and the possibility of chronic administration. Its non-invasiveness, the self-administration by patients with high patient compliance, and the rapid onset of action represent an attractive option to further explore this route of administration to ultimately improve the prognosis for GBM patients.

1.5.1. Anatomy relevant for nose-to-brain transport

In the next paragraph the anatomical organization of the nasal cavity will be discussed, in particular the structures that are necessary for understanding nose-to-brain transport. This topic has already been the subject of several excellent reviews (84, 88, 89). Therefore only a summary is present here, underlining the key-points in the anatomical organization in the nasal cavity relevant for intranasal transport to the CNS. First, the possible pathways that are responsible for an effective nose-to-brain

transport will be discussed. Next, a closer look will be provided into the anatomical structures that decide whether the applied substance can undergo nose-to-brain transport.

1.5.2. Macroscopical anatomy

1.5.2.1. Olfactory pathway/olfactory region

The exact mechanisms underlying nose-to-brain transport are not yet fully understood, but the olfactory pathway seems to play a pronounced role (Figure 3). The olfactory region in humans accounts for <10 % of the nasal cavity. Pharmaceutical agents can gain fast access to the CNS along the olfactory nerve fibers of the olfactory bulb, which is the only anatomical structure of the CNS that is in direct physical contact with the extracranial environment. This was well-illustrated by Jansson et al. by intranasal administration of a fluorescent dye and subsequently monitoring of the route of transport along the olfactory nerves (90). The olfactory pathway starts at the olfactory receptor neurons, located at the olfactory mucosa. These cells pick up olfactants and transmit the information to the CNS, mediating the sense of smell (91). The olfactory receptor neurons are surrounded by basal cells, microvillar cells, and supporting cells, all connected by TJs. These basal cells act as neural progenitor cells which can replace the olfactory receptor neurons during their continuous turn-over. The constant replacement of olfactory receptor neurons, make the olfactory mucosa 'leaky' and thereby improve the nose-to-brain transport (92). From these olfactory receptor neurons, axons project through the cribriform plate which separates the nasal and cranial cavities, on to mitral cells in the olfactory bulbs. Subsequently the olfactory bulbs will project on to different brain regions including the olfactory tract, the anterior olfactory nucleus, the piriform cortex, the entorhinal cortex, the amygdala, and the hypothalamus (93, 94). Upon intranasal administration, intra- and perineural transport is possible along these projections.

1.5.2.2. Trigeminal pathway/respiratory region

Another major player in nose-to-brain transport is the respiratory region in the nasal cavity (Figure 3). This area can reach up to 80-90% of the nasal cavity in humans. This epithelium layer is necessary for warming and humidifying the inspired air, and for removing particles, allergens, and microorganisms. The layer consists of ciliated and non-ciliated columnar cells, goblet cells, and basal cells (95). The goblet cells secrete mucus, which is propelled by the ciliated cells, towards the nasopharynx, where it is swallowed or expectorated. Interestingly, the respiratory region is innervated by projections of the trigeminal nerves. Also these nerves contribute to the nose-to-brain transport (96). The trigeminal nerve (or fifth V cranial nerve) has three main branches: the ophthalmic nerve (V1), the maxillary nerve (V2), and the mandibular nerve (V3). Only V1 and V2 will innervate the nasal passages via the ethmoidal branch (V1), nasopalatine branch (V2), and nasal branch (V2) (97). From the respiratory epithelium, these branches will enter the brain at two sites, which is quite peculiar: the foramen rotundum and the superior orbital fissure thereby creating two entry sides into both the caudal and the rostral brain regions. In summary: when a pharmacological agent is administered intranasally, the agent can travel along the olfactory and trigeminal pathways, projecting towards the more rostral and

more caudal regions, respectively. Transport along the nerves, either olfactory, or trigeminal, is believed to be perineuronal and intraneuronal, as discussed later.

1.5.2.3. Other possible pathways

Perineural transport along the olfactory and trigeminal nerves is probably the major determinant of the nose-to-brain pathway. However, other connections between the nasal cavity and the CNS are also possible candidates. It is not unlikely that, for instance, the facial nerve or the Grueneberg ganglion is also an entry point towards the CNS (98). Beside the neural pathways, the vasculature pathways are also gaining interest. The olfactory region's vascularization originates from small branches of the ophthalmic artery, while the respiratory region receives blood supply from branches of the maxillary artery (99). Intranasally administered drugs can reach the systemic circulation via this vascularization and pass the BBB to enter the brain, especially if the applied drugs are small and lipophilic. More likely, molecules can also travel perivascular along the channels associated with blood vessels, located between the outermost layer of blood vessels and the basement membrane of surrounding tissue [38]. Perivascular transport is not only driven by diffusion but also by bulk flow and arterial pulsation, which might explain the rapid distribution in the CNS of intranasally administered drugs (100). Direct transport from the nasal cavity to the cerebrospinal fluid (CSF) has been reported, but is a rather unclear mechanism (101, 102). Absorption of the applied substance in the lymphatic vessels, located just under the basal lamina and draining the deep cervical lymph nodes of the neck, has also been reported (103).

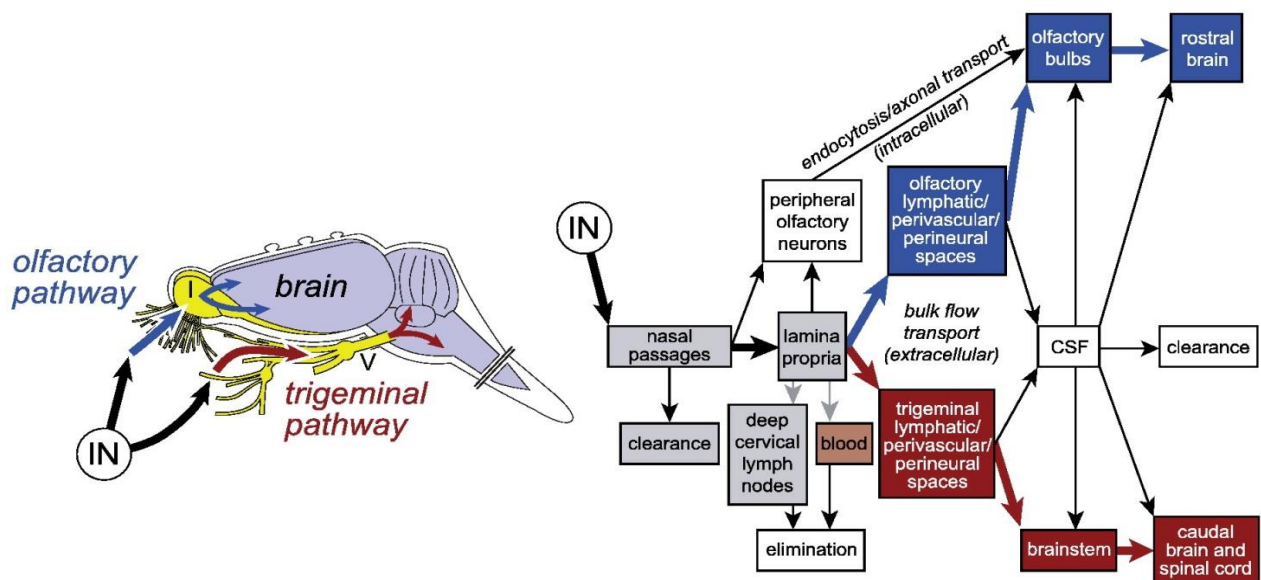


Figure 3. Nose to brain Transport. Modified adapted from Lochhead et al 2012 (88): A schematic representation of the transport from the nasal cavity towards the CNS. Molecules can travel mainly via two pathways, the olfactory and trigeminal pathway, which respectively project into the rostral brain and caudal brain areas. The presumed mode of transport is mainly perineural in the gaps between the bundles of nerves, projecting to the appointed areas.

1.5.3. Microscopical anatomy

In this paragraph, the hurdles and entry points that need to be overcome for an intranasally applied substance, to travel along the proposed routes to the CNS will be discussed.

1.5.3.1. Nasal mucosa and mucus

The first barrier that a pharmacological agent will encounter upon intranasal administration is the mucus layer covering the olfactory and respiratory mucosa. Mucus is a complex mixture secreted by the goblet cells in the mucosa, and consists out of 95% water, 2% mucin, 1% salt, 1% albumin, lysozymes, lactoferrin, immunoglobulins, and lipids (104). The resulting pH of mucus in the nasal cavity is close to neutral or slightly acidic (pH 5.5-6.5) (105). The mucus layer is propelled towards the pharynx by the cilia. It should be noted that only the cilia on the respiratory mucosa can move the mucus because the cilia on the olfactory mucosa lack the dynein arms which are necessary for motion (106). These cilia can beat with a frequency of 1 000 beats per minute, and propel the mucus 5 mm per minute (107). If a pharmacological agent successfully reaches the nasal cavity, this is the first barrier to cross. Next, the drug can travel between cells, paracellular or through cells, i.e. transcellular.

1.5.3.2. Paracellular transport between nasal mucosa

When the applied substance needs to travel between epithelial cells, it will have to cross several barriers. Two epithelial cells can be in close approximation with each other using several junctions: TJs, adhering junctions, desmosomes, and gap-junctions (108). The intactness of these junctions will determine the success of the paracellular transport. There is also a size limitation: the hydrophilic channel between two epithelial cells is about 8 Å (108). Questions about the integrity of these junctions remain, due to the constant renewal of the olfactory receptor cells, and the integrity of the entire mucosa (109). Certain formulations can temporarily open these junctions and therefore promote nose-to-brain transport, as discussed later. This transport route is rapid and can occur within 30 minutes after application.

1.5.3.3. Transcellular transport across nasal mucosa

An applied substance larger than 20 nm is believed to travel transcellular. Many possible mechanisms are described in the literature and depend on the nature of the substance: clathrin-dependent or independent, caveolae-dependent or independent, macropinocytosis or phagocytosis (110). It is reported that substances smaller than 200 nm prefer caveolae-mediated endocytosis, while substances in a range of 200-1000 nm prefer clathrin-mediated endocytosis. Transcellular transport is generally rather slow, ranging from hours to several days. Substances entering an olfactory receptor neuron will undergo intraneuronal transport in the anterograde direction towards the olfactory bulb (111).

1.5.3.4. Organization nerves/filia olfactoria

In the lamina propria, just underneath the olfactory mucosal layer, the different axons of olfactory receptor neurons conjoin and are ensheathed by Schwann cells. These structural organizations are called filia olfactoria, and were first described by de Lorenzo et al. (112). Typically 20 axons are bundled together in fascicles. One Schwann cell can easily contain 5-10 fascicles, and thereby contain > 100 axons. Perineuronal channels of 10-15 nm are present here and act as ionic reservoirs. Mesaxons are also present within the filia olfactoria and are pores that allow the passage of extracellular fluids. Transneuronal transport is dependent of the diameter of the axons, which in human ranges from 100 nm to 700 nm (113).

1.6. Pre-clinical and clinical evidence of nose-to-brain transport for GBM

In this paragraph, an overview is provided of the intranasally applied non-formulated substances relevant for the treatment of GBM (Table 1). Other non-formulated substances that have been already extensively reviewed fall beyond the scope of this manuscript (88, 114). Next, the enhancement by means of formulations for the intranasal transport will be discussed.

1.6.1. Intranasal administration for GBM

1.6.1.1. Animal models

Given the advantages of nose-to-brain transport, reports have been made on treating GBM with intranasally applied substances. The most evident choice of substances is probably the intranasal administration of chemotherapy. Wang et al. reported the uptake of methotrexate into the CSF upon intranasal administration (115). After intranasal or IV administration of methotrexate, the CSF and plasma were collected. They reported that intranasal administration delivered more methotrexate to the CSF and less to the plasma than IV administration. Methotrexate is a folic acid antagonist and is being used for a variety of systemic malignancies. Intravenous injections of methotrexate were attempted to treat malignancies of the CNS. Methotrexate is poorly lipophilic, highly bound to proteins in the serum, and can therefore barely pass the BBB (116). Nevertheless, methotrexate is a very potent treatment modality and can also be used for CNS lymphoma via intrathecal injections (117). Adverse events such as progressive paraplegia, anemia, and cerebral metabolite changes are not rare following intrathecal injections. Based on the positive findings intranasal delivery of methotrexate was further investigated (118). This group inoculated 9L rat glioma cells in the right frontal cortex of rats, followed by intranasal administration of methotrexate. They observed a significant antitumor response to intranasal methotrexate delivery. After 10 days and 3 administrations, the tumor weight was significantly lower in the rats that received intranasal methotrexate. The group that received intraperitoneal injections of methotrexate displayed only a small decrease in tumor weight.

Nose-to-brain transport of another chemotherapeutic agent, 5-fluorouracil, was also reported (119). Comparing the plasma and CSF upon intravenous or intranasal administration brought them to the conclusion that the delivery of 5-fluorouracil in the CSF is augmented by nasal drug application. 5-Fluorouracil is a chemotherapeutic agent that is clinically used to treat breast cancers, melanomas,

and pancreatic cancers. It is a pyrimidine analog, and will irreversibly inhibit the thymidylate synthase enzyme (120). Side effects of systemic administration include myelosuppression, diarrhea and dermatitis. A similar study in rats was performed with raltitrexed, which is clinically used in the treatment of advanced colorectal cancer and also inhibits the thymidylate synthase (121). After intranasal administration they found different concentrations of raltitrexed in the brain, with rank order: olfactory bulb > olfactory tract > cerebrum > cerebellum. Intranasal administration delivered significantly more raltitrexed into the CNS than intravenous administration. These results are encouraging, and suggest that some chemotherapeutics that were put aside due to poor BBB permeability might have to be reconsidered using intranasal administration.

Not only are chemotherapeutics intranasally applied in the context of GBM, but also antisense oligonucleotides. An excellent study by Hashizume et al. provided evidence that antisense oligonucleotides can also travel from nose-to-brain and have therapeutic effects in a rat glioma model (122). The compound, GRN163, is an antisense oligonucleotide targeting telomerase, which is expressed in a majority of GBM (123). U-251 MG tumor cell bearing rats were treated with intranasal administration of GRN163. After only 30 minutes, they tracked the compound in the trigeminal nerves and the brain stem, suggesting rapid distribution. Treatment for 12 consecutive days, starting when a 20 mg tumor was already present, resulted in a highly significant improvement of survival. Another interesting finding is the tumor specificity. They reported a preferential distribution of the compound in the tumor cells, which are positive for telomerase, whereas the normal tissue does not express telomerase. The preferential distribution seemed to be even more pronounced after intranasal administration than with CED administration (124).

Whereas chemotherapeutic agents cannot distinguish between GBM and healthy CNS, compounds as the GRN163 can be specific. Another example of tumor-tropism is the use of oncolytic viruses. These viruses preferentially proliferate in tumor cells and cause a lethal infection of these cells (125). Özduman et al. provided evidence for the ability of the vesicular stomatitis virus VSVrp30a to destroy several human and mouse tumors implanted in the mouse brain, after intravenous injection of the virus (126). Normally, the BBB will not permit the VSVrp30 to cross, and therefore, the intravenous injection would have no effect. However, they observed that upon tumor engraftment, the BBB becomes leaky and the virus can reach the CNS. Interestingly, Özduman also reported that when U87 glioma cells were stereotactically unilaterally engrafted on the olfactory bulbs of SCID mice, an olfactory bulb glioma was established. When the VSVrp30 was administered intranasally, the olfactory bulb gliomas were selectively infected and killed.

Nose-to-brain transport does not seem exclusively reserved for small molecules and viruses: a study by Reitz et al. showed the potential of cells to travel along the proposed route of transport (127). In this research they managed to intranasally administer neural stem and progenitor cells (NSPCs). When mice were challenged with intracranial injections of U87, NCE-G55T2 or GL261 glioblastoma tumor cells, the intranasally administered NSPCs travelled specifically towards the tumor environment. The restorative potential and inherent pathotropism, in combination with guidance of danger signals, should explain the specific homing of the NSPCs towards the tumor environment. These NSPCs are a

good candidate for the targeted delivery of biologically active gene products, both after intracerebral injection and after intranasal administration (128). Therefore a clinical study (NCT01172964) has started with the intracerebral injection of the HB1.F3 neural stem cell line that was genetically modified and carries the prodrug-converting enzyme cytosine deaminase, which can convert the non-toxic prodrug 5-fluorocytosine to 5-fluorouracil. Given the new insights that neural stem cells can also be delivered intranasally, a non-invasive alternative is established.

1.6.1.2. Clinical setting

To our knowledge, there is only one clinical study concerning intranasal administration of chemotherapeutics in GBM patients. Da Fonseca et al. established a phase I/II study with the intranasal administration of monoterpene perillyl alcohol (POH), a Ras-protein inhibitor, in patients with a recurrent GBM (129, 130). At first, this study was initiated with an oral delivery of POH. However, serious adverse events of nausea, vomiting and diarrhea were reported. Upon reconsideration, an intranasal formulation was created, suited for nose-to-brain transport. In a small cohort of patients, they observed that the compound POH is well tolerated and that in some patients tumor regression is noticeable, suggestive of the antitumor activity of POH (131). In the phase I/II study, they observed a significant increase in survival of recurrent primary GBM patients, from 2.3 to 5.9 months, compared to historically matched controls. A better response to treatment was noticed in patients with recurrent primary GBM in a deep location than in a lobar location. Next, a larger increase in survival was noticed in patients with a recurrent secondary GBM, progressing from a lower grade lesion, than in recurrent primary GBM patients. This means that patients evolving from a lower grade malignancy respond better to the intranasal POH, although secondary GBMs might have a slightly better natural prognosis as compared to primary GBMs. Moreover, an additional large scale clinical trial (phase 1/2) with this approach has been launched (GDCT0257383).

Table 1. Intranasal administration of pharmacological agents for the treatment of GBM, both in animals and in humans. (+AZA: addition of acetazolamide for reducing CSF turnover)

Compound	Intranasal dose	Plasma concentration	CSF concentration	GBM model	Efficacy	Ref.
<i>Animals</i>						
Methotrexate	3.2 mg/kg	345 ± 58 ng/ml	1278 ± 393 ng/ml	-	-	(115)
Methotrexate	2.5 mg	1 µg/ml	12.54 ± 1.54 µg/ml (+AZA)	9L rat glioma	Decreased tumor weight	(118)
5-fluorouracil	26.7 nmol	2.4 fmol/ml	6 fmol/ml (+AZA)	-	-	(132)
GRN163	0.65 µmol	-	-	U-521 MG rat glioma	Increased median survival from 35 days to 75.5 days	(122)

Vascular Stomatitis Virus	2.5 x 10 ⁷ PFU	-	-	U87 MG glioma	Selective infection and killing of olfactory bulb tumor	(126)
Neural Stem and Progenitor cells	3 x 10 ⁵ cells	-	-	U87 MG, NCE-G55T2, GL261	Rapid, targeted migration of cells towards intracerebral glioma	(127)

Human

Monoterpene perillyl alcohol	440 mg/day	-	-	Recurrent GBM patients with at least 3 relapses	Increased median survival from 2.3 to 5.9 months	(130)
------------------------------	------------	---	---	---	--	-------

1.6.1.3. Possible pitfalls

Despite all the promising accumulating (pre-) clinical data about the challenging nose-to-brain pathway, pitfalls are present and should be considered before attempting to validate this approach. Firstly, nose-to-brain transport is for now restricted to potent molecules. These molecules could be dissolved or dispersed in a small volume of liquid: the maximal delivery in mice is 24 µl, in rats 40-100 µl, and in humans 0.4 ml or formulated as a powder with a limited mass/volume. Next, the applied substances have to resist the mucociliary clearing on the nasal mucosa, which transports the mucus at a rate of 5 mm/minute. Although intranasal delivery can bypass the first pass effect in the liver, nasal cytochrome P450, as well as proteases and peptidases, are also present in the nasal mucosa, and can induce a pseudo-first-pass-effect. The cytochrome P450 can even have up to a fourfold higher NADPH-cytochrome P-450 reductase content than in the liver (133). Furthermore, the translation of animal data to humans should be handled with caution. The anatomical differences between animal models and human are distinct. Rodent are obligatory nasal breathers, while primates are oronasal breathers. The nasal passage in rat is more complex than in humans, and has a larger surface-to-volume ratio. Nasal cavities in mice, rat and human present a volume of 0.032, 0.26, and 25 cm³, respectively (95). The differences in anatomy and physiology can also be beneficial: CSF replacement in humans takes about 5 h, while in mice only 1.5 h. The slow CSF replacement is even more pronounced in older humans, which represent the dominant GBM patient population (95).

For these reasons, and to further increase the efficacy and potential of nose-to-brain transport, formulations can be developed. Pharmaceutical formulations can offer the active compound stability in its environment of administration, protection against possible destruction, and even specificity for the targeted tissue. These features should result in an increased half-life time, and concentration in the CSF, of the active compound and therefore an increased pharmacological effect.

1.7. Improvement of the nose-to-brain pathway through formulations

Many types of formulations can be developed according to the requirements of their application. In the case of formulations for intranasal administration, the uptake of active molecules in the brain is mainly formulated as nanoparticles. Nanoparticles are defined as having a size smaller than 1 μm . They are designed to protect the drug, and promote transcellular or paracellular transport to the CNS, depending on their properties. In the first paragraph of this section, the potential of nano-technology with different polymers and lipids will be underlined. Next, the application of ligand-specific lectins, emulsions and gels, which are used to increase the nose-to-brain transport, will also be discussed. Finally, several indirect enhancers of the intranasal pathway will be discussed.

1.7.1. Via Polymer-based nanoparticles

Chitosan (CS) is a β -(1–4)-linked D-glucosamine and N-acetyl-D-glucosamine co-molecule, which represents a linear backbone structure linked through glycosidic bonds. CS is obtained upon the deacetylation of chitin, derived from crustacean shells. This molecule contains primary amines which can be protonated, and are positively charged in most physiological fluids. CS is in many aspects an interesting polymer in which active molecules can be encapsulated, and is therefore one of the most studied polymers in the field of transmucosal drug delivery (134, 135). This excipient is known as a polycationic, biocompatible, and biodegradable polymer, which presents mucoadhesive and permeation-enhancing properties and which presents non toxicity and low immunogenicity (136). In intranasal delivery, it improves the nasal residence time of the formulation by decreasing the mucociliary clearance due to its bioadhesive properties (137, 138). This excipient could be used to elaborate different types of intranasal formulations including solution, dispersion, and powder formulation. CS based intranasal powder has been shown to possess a higher residence time than a solution (139). Moreover, CS has the property to transiently open the tight junction of the mucosal epithelium, which increases the permeability of very polar compounds such as peptides, proteins or nucleic acids (140). CS nanoparticles can be prepared according to several methods, as reported in the excellent review of Amidi et al. (140). The most popular method for intranasal administration is ionic gelation, in which an anionic solution is added drop wise to the polycationic CS and crosslinks, i.e. performs gelation, to form nanoparticles (141). A characteristic of the CS nanoparticles is their positive charges in acidic to neutral pH, resulting from the primary amines ($\text{pK}_a \sim 6.5$). In physiological pH, the sialic acids and ester sulfates ($\text{pK}_a \sim 1.0\text{-}2.6$) in the mucus layer are strongly negatively charged, thereby the CS nanoparticles and the sialic acids and ester sulfates can form strong electrostatic interactions (105).

A first illustrative study was performed by Wang et al. who prepared estradiol containing CS nanoparticles with a mean size of 269.3 ± 31.6 nm and a zeta potential of +25.4 mV (142). The charge of the particles is important in terms of stability: particles that display a charge $> +20$ mV are more likely to remain stable in solution. Achieving high concentrations of estradiol in the CNS could be beneficial in treating Alzheimer's disease (143). CS nanoparticles were obtained by ionic gelation with tripolyphosphate anions. Estradiol was administered in a dose of 0.48 mg/kg either intranasally or

intravenously. The CSF concentration was increased after intranasal administration from 29.5 ± 7.4 ng/ml for intravenous administration to 76.4 ± 14 ng/ml. A similar experiment was performed by Al-Ghananeem et al. (144). In this study didanosine was incorporated into the CS nanoparticles. Here they also observed an increase of the didanosine, both in the CSF and in the brain, after intranasal administration of the formulated drug. Another study incorporated thymoquinone into nanoparticles with a mean size of minimum 172.4 ± 7.4 nm, and a charge of $+30.3 \pm 2.15$ mV (145). This molecule has been proven to ameliorate cognitive deficits and neurodegeneration and therefore it might be of value in treating Alzheimer's disease (146). With a 18-fold increase of the brain-targeting efficiency and two-fold increase of the brain drug direct transport percentage as compared to thymoquinone in solution, i.e. without CS nanoparticle formulation, they concluded that the formulated thymoquinone had better brain targeting efficiency. Another study, encapsulated another Alzheimer's disease drug, rivastigmine, in CS nanoparticles, with an average size of 185.4 ± 8.4 nm and charge of $+38.40 \pm 2.85$ mV (147). They coupled the particles with ROD-123, fluorescent rodamine dye, and observed a higher intensity of fluorescence in the brain upon intranasal administration compared to intravenous administration. Consequently, the concentrations of rivastigmine delivered by the formulated nanoparticles were significantly higher compared to intranasal or intravenous administration of rivastigmine in solution. The area under the curve (AUC) of intranasally administered rivastigmine CS particles in the brain was 3.11 times higher than intravenously administered rivastigmine in solution, and 1.92 times higher than intranasally administered rivastigmine in solution. These results suggest that after intranasal administration, the CS-rivastigmine particles reach the brain through both a direct nose-to-brain pathway, and the systemic circulation. Another example was published by Md et al. and provides supplementary evidence that chitosan nanoparticle formulations can improve nose-to-brain transport (148). In this publication, bromocriptine was loaded into CS nanoparticles, resulting in particles with a mean size of 161.3 ± 4.7 nm, and a zeta potential of $+40.3 \pm 2.7$ mV. Bromocriptine acts as a protector of dopaminergic cells and is therefore a well-known drug in Parkinson's disease (149). Bromocriptine was labeled with technetium, a radio-active substance, to measure the distribution. The brain/blood ratio was 0.47 ± 0.04 for intranasal administration of bromocriptine in solution, 0.69 ± 0.031 for intranasal administration of bromocriptine-CS nanoparticles and 0.05 ± 0.01 for intravenous administration of bromocriptine-CS nanoparticles. Interestingly, the increased concentration of bromocriptine in the brain was also reflected in clinical responses. Mice were administered haloperidol, which elicits typical Parkinson symptoms such as catalepsy and akinesia. These symptoms were reversible after bromocriptine-loaded CS nanoparticles administration. Rather than using chitosan to form nanoparticles, other nanoparticles can also be covered by CS chains, and thereby benefit from the advantages of CS. CS surface modifications of polystyrene particles resulted in an increased transmucosal transport (150). With respect to this thesis, we have chosen chitosan nanoparticles as an optimal platform to answer our research questions. We refer to chapter 6 in this thesis, to find a detailed characterization of the production process of the siRNA loaded chitosan nanoparticles as used in our research.

Not only CS nanoparticles are studied for nose-to-brain transport, but also other polymers. For instance, maltodextrin has been used (151). When these 60 nm nanoparticles (Biovector) were

applied together with morphine, the duration of the antinociceptive activity was increased. With co-administration of the nanoparticles, no increase in morphine concentration in the blood was observed, and the effects of morphine were reversible by naloxone. Another extensively studied polymer is polyethylene glycol (PEG). This well tolerated, polyether structure has been shown to be very versatile in many applications, and is typically used to improve hydrophilicity, and increase the circulation time in the blood stream. The addition of PEG onto the surface of nanoparticles, thereby improving the diffusion across the mucus, can improve their uptake (152). Methoxy PEG-poly(lactic acid) (PLA) nanoparticles were used to improve the uptake of encapsulated nimodipine (153). These PEG-PLA particles have a mean size of 76.5 ± 7.4 nm and a negative charge. The olfactory bulb/plasma and CSF/plasma nimodipine concentrations were significantly higher after nanoparticle formulation than for intranasal administration of nimodipine solution. Also in other reports, they used the properties of PEG to slip molecules across the mucus barrier (154). Indeed low molecular weight PEG, with a hydrophilic and almost neutrally-charged surface, has a minimized mucoadhesion. In this way, particles can rapidly slip through the mucus. They observed that polystyrene nanoparticles covered with low molecular weight PEG could slip faster through the mucus layer. This new insight results in an apparent paradox: should nanoparticles be strongly mucoadhesive (e.g. with chitosan), or should they slip across the mucus layer (e.g. with PEG coating)? Next, the potential use of poly(lactic-co-glycolic acid) (PLGA) polymer for the nose-to-brain pathway was explored. PLGA, like PEG, PLA and chitosan, is a biocompatible, biodegradable polymer and improves drug stability and release (155, 156). PLGA nanoparticles, with a size of 91.2 ± 5.2 nm, were loaded with olanzapine, an antipsychotic drug. Their poor bioavailability, due to the hepatic first-pass metabolism, and the poor brain uptake due to P-gp - efflux pumps, stimulated the search for an alternative administration route (157). Formulating olanzapine in the PLGA nanoparticles increased the uptake into the brain by 6.35-fold after intravenous administration, and even 10.86-fold after intranasal administration. A last kind of polymer which draws attention for nose-to-brain targeting is the poly(amidoamine) (PAMAM) dendrimer. These polymers are repetitive branches that grow from a core. Many versatile molecules can be attached to their surface. Kim et al. connected an arginine onto the surface of a PAMAM dendrimer (158). This resulted in nanoparticles with a size of 188.7 ± 1.9 nm and a charge of +22.3 mV. Small interference RNA (siRNA) targeting against the high mobility group box 1 protein (HMGB1) was electrostatically attached onto the nanoparticles. HMGB1 is released by dying cells and acts as a danger signal, thereby aggravating the damage of a stroke or other neurotoxic insults. Upon intranasal administration, they observed a wide distribution of the construct into the brain, including the hypothalamus, the amygdala, the cerebral cortex, and the striatum. Moreover, the localization of the PAMAM dendrimer and the siRNA was associated with an efficient knock-down of the protein of interest: HMGB1. When a stroke was induced into animals, the group that received the intranasal administration of the construct had a remarkably decreased infarction volume. Also using several behavioral tests, they could demonstrate that the treated group had a clear therapeutically response to the treatment.

1.7.2.Lipid based nanosized formulations

1.7.2.1. Via (nano)emulsions

In literature, lipids are used as another possible method of formulating active compounds, more specifically lipophilic ones, in nanoparticles and further enhancing the nose-to-brain transport. Emulsions are a mixture of two or more liquids that are normally immiscible, such as oil-in-water. For intranasal transport, which requires small sizes, nanoemulsion, which contains droplets smaller than 100 nm, are a rising field of interest. Kumar et al. formulated risperidone, an antipsychotic drug, into a nanoemulsion (159). The mucoadhesivity of the risperidone nanoemulsion was increased with the addition of 0.5 % CS (w/w) onto the droplet surface, which resulted in a globule size of 16.7 ± 1.21 nm. The superiority of the CS- coated nanoemulsion, in terms of brain/blood concentration ratio and more rapid transport, was demonstrated in comparison to the nanoemulsion without CS and in comparison to a simple risperidone solution, all after intranasal administration. Kumar et al. further studied this mucoadhesive nanoemulsion, with the incorporation of olanzapine, which is also an antipsychotic drug (160). Here too, the mucoadhesive nanoemulsion seemed superior in terms of a higher drug targeting efficiency and direct nose-to-brain transport. Jogani et al. prepared a mucoadhesive microemulsion with tacrine, a reversible cholinesterase inhibitor used in Alzheimer's disease (161). The more rapid and more extensive transport of tacrine towards the brain showed the superiority of the mucoadhesive emulsion. Furthermore, mice were administered with scopolamine to induce amnesia. The mucoadhesive tacrine emulsion resulted in a faster regain of the memory loss.

1.7.2.2. Via solid lipid nanoparticles

Besides polymeric nanoparticles, lipid nanoparticles are also interesting candidates for brain targeting due to their rapid uptake by the brain, biocompatibility, biodegradability and weak toxicity. In this aspect, Eskandari et al. formulated valproic acid in nanostructured lipid carriers based on palmitate. These lipid nanoparticles were prepared by solvent diffusion method followed by ultrasonication (162). The brain/plasma ratio of valproic acid was 8.4 ± 0.32 after intranasal instillation, as compared to 1.65 ± 0.29 after intraperitoneal injection. Moreover, rats were better protected from seizures after intranasal administration. Joshi et al. formulated ondansetron HCl in solid lipid nanoparticles based on glycerol monostearate, which were also created by solvent diffusion (163). Radiolabelling of these lipid nanoparticles showed a rapid uptake of these complexes in the brain of rabbits.

1.7.2.3. Via liposomes

Another classic drug delivery systems are liposomes. These structures consist of a lipid double layer that contains a hydrophilic core. Hydrophobic molecules can be integrated into the lipid layer and hydrophilic molecules can be encapsulated in the core. The use of liposomes is also feasible for intranasal administration, and nose-to-brain transport. Rivastigmine was formulated in liposomes (164). When compared to rivastigmine in solution, the formulated rivastigmine-liposomes increased the rivastigmine concentration in the brain from 0.33 ± 0.29 $\mu\text{g/ml}$ to 0.98 ± 0.74 $\mu\text{g/ml}$. The use of cationic liposomes was also explored when formulating ovalbumin with these liposomes (165). Liposomes were prepared by combination of dioleoylphosphatidylcholine, cholesterol, and

stearylamine. After intranasal administration, they observed a rapid distribution in the brain of the fluorescent labeled ovalbumin, with the highest concentration after 1 hour. Priprem et al. also used liposomes for nose-to-brain transport. They formulated quercetin in liposomes, which consists of egg phosphatidylcholine and cholesterol followed by dispersion in 50% polyethylene glycol in water (166). Rather than a quantitative approach, they observed an anxiolytic effect of intranasally administered formulated quercetin that was more rapid and at a lower dose as compared to oral administration.

1.7.3. Functionalization of the nanoparticle surface by ligands

The previous paragraphs clearly demonstrated the potential of nanoparticles to improve and enhance nose-to-brain transport. Given good biological knowledge, skilled pharmaceuticals, and an optimal control of the preparation process of these nanoparticles, a further improvement could be made by addition of lectins onto the surface of the nanoparticles. These lectins can recognize carbohydrate structures and thereby improve attachment to the mucus, cilia etc. This technique was well studied with the conjugation of wheat germ agglutinin (WGA) onto PEG-PLA particles (167). WGA has a specific binding to N-acetyl-D-glucosamine and sialic acids, both of which structures are abundantly present in the mucosa of the nasal cavity (168). As a fluorescent marker, they included 6-coumarin into these particles and after intranasal administration they observed a two-fold increase in the brain of the WGA-conjugated particles, as compared to unmodified ones. In a next report, vasoactive intestinal peptide (VIP) was incorporated into the WGA-PEG-PLA nanoparticles (169). Compared to intranasal administration of VIP in solution, the unmodified PEG-PLA particles increased the AUC in the brain 3.5-4.7-fold, and the WGA-modified PEG-PLA 5.6-7.7-fold. Another report studied the toxicity and immunogenicity of the WGA-PEG-PLA construct and demonstrated its safety profile (170). In a similar setting, Ulex europeus agglutinin 1 (171) and low molecular weight protamine (LMWP) to PEG-PLA nanoparticles (172) were prepared. Recently, lactoferrin was identified as an interesting protein. Lactoferrin is a natural binding iron protein, and its receptor is abundantly present on the respiratory epithelial cells and neurons (173). This property was demonstrated by the enhanced nose-to-brain delivery of NAP, a neuroprotective peptide, when conjugating lactoferrin with PEG-co-poly(ϵ -caprolactone) (PCL) nanoparticles (174). By injection of β -amyloid, rats developed a model for Alzheimer's disease, which was significantly delayed by intranasal administration of lactoferrin-conjugated nanoparticles. A last approach in ligand-specific enhancement of the nose-to-brain pathway is the phage display method. This high-throughput screening method, allows the study of protein-protein interactions which identified nose-to-brain homing peptides (175). The isolated phage reached the brain, after intranasal administration, at a rate 50-fold higher than a control phage. This is the first report that such a short peptide sequence can enhance nose-to-brain transport. Liposomes and nanoparticles can also be functionalized with cell penetrating peptides. Yang et al. described a formulation of rivastigmine in liposomes functionalized with a cell-penetrating peptide (176). They observed higher concentrations of rivastigmine in the brain after intranasal administration of the cell-penetrating peptide-liposomes than with the liposomes or rivastigmine in solution. Closely related to our project, Kanzawa et al, recently published a report where PEG-PCL particles were functionalized

with cell penetrating peptides, and enloaded with siRNA targeting Raf-1, an important tumor promoting protein. Intranasal administration could increase the survival in combination with camptothecin (177).

1.7.4. Via gels

From all the different polymers described in the previous sections, it is not only possible to make nanoparticles, but also mucoadhesive gels. Gels are three dimensional networks with a high viscosity, containing the active molecule. Charlton et al. demonstrated the gelling properties of chitosan and two low methylated pectins: LM-5 and LM-12 (178). In a subsequent article, they published that the gel with 1% chitosan had a retention time on the human nasal mucosa that increased from 1.33 minutes to 12.58 minutes (179). The potential of mucoadhesive gel formulations was also displayed in another report (180). They coupled radioactive siRNA to PAMAM dendrimers to form dendriplexes, and formulated these particles into mucoadhesive gels containing either 1% (w/w) chitosan or 0.25% (w/w) carbopol 974P NPTM. These gels were prepared by blending the chitosan or carbopol with 23% (w/w) of thermosensible poloxamer to obtain in-situ gelation. Such a thermosetting gel has a phase transition below the temperature in the nasal cavity (32°C to 35°C) and above room temperature. Therefore it can be administered as a liquid. Different concentrations of the different gels were tested and no toxicity was observed. Two intranasal doses were necessary to achieve higher brain concentrations of radioactivity than achieved by intravenous administration of dendriplexes or intranasal administration of naked siRNA. Khan et al. prepared a gel with chitosan and hydroxylpropyl methylcellulose and incorporated ropinirole, a dopamine D2 agonist (181). Upon intranasal administration of the formulated ropinirole, concentrations in the brain were 8.5 times higher than after intravenous administration, and 3 times higher than after intranasal administration of non-formulated ropinirole. PEG, another popular polymer used for intranasal administration with or without mucoadhesive CS, was used, to prepare a thermosetting gel with poloxamer conjugated with metoclopramide hydrochloride to enhance drug release (182). Intranasal administration of the gel increased the bioavailability from 51.7%, for oral drug solution, to 69.1%. With similar gels, using carbopol, carboxymethyl cellulose and PEG, Babu et al. found an increased delivery of melatonin in the olfactory bulb (183). Upon intranasal administrations of these gels, the increased delivery in the CSF was respectively 9.22-, 6.77- and 4.04-fold, as measured by microdialysis.

1.7.5. Via Indirect enhancers / devices

There are also different approaches increasing the efficiency of nose-to-brain transport without using formulations. The route of transport is challenging, and not every obstacle can be overcome by the galenic formulations discussed in the paragraphs above. Therefore several indirect enhancers can be applied to further increase and optimize the transport to the brain. For instance, the inhibition of P-gp at the BBB can increase uptake in the brain. A portion of the intranasally applied substance can travel through the systemic circulation, into the brain. Graff et al. observed that co-administration of a P-gp inhibitor, rifampin, and an active substance, increased the brain concentration after nasal instillation (184). Another possible method was proposed by Charlton et al. (185). By applying a local vasoconstrictor, one could eliminate the uptake into the systemic circulation and thereby favor the

nose-to-brain route. However, when applying ephedrine, no increased uptake was observed. This was in contrast with the results of Dhuria et al. (186, 187). They observed a significant increase in the brain, and decrease in the systemic circulation of hypocretin-1 after intranasal administration, in combination with phenylephrine administration. A possible explanation for this discrepancy suggested by Mistry et al., is that the rapid onset of action by phenylephrine is more advantageous than the long on-set of action of the ephedrine as used by Charlton et al. (114). When an intranasally applied substance achieves high concentrations in the brain, a part will be rapidly transported and cleared by the turnover of the CSF. As suggested already in previous sections, the slower the CSF turnover is, the longer the active substance can remain in the CSF and be transported towards distinct brain regions. Therefore, Shingaki et al. tested the use of acetazolamide in combination with intranasal administration of 5-fluorouracil, given the previously demonstrated successes of 5-fluorouracil after intranasal administration (132). Acetazolamide is a carbonic anhydrase inhibitor that can inhibit the secretion of the CSF in the choroid plexus and is clinically used to treat idiopathic intracranial hypertension (188). They observed that the intravenous administration of acetazolamide can increase the brain distribution of intranasally applied 5-fluorouracil by 200-300%.

The potential of nose-to-brain transport is now generally accepted and a number of non-formulated proteins and peptides, such as insulin and oxytocin are already being tested in humans (189, 190). The experiences from these trials, together with the classical trials that use the nose for e.g. vaccination, have stimulated private companies to develop several devices. These devices target powder or droplet substances specifically to the nasal cavity. In the study by Charlton et al., the superiority of drops over sprays was demonstrated (179). Many interesting devices are entering the clinic and can serve as useful tools to implement nose-to-brain transport clinically in the healthcare industry. One example is the ViaNase™ (Kurve technologies, Bothell, Washington, US). In a clinical study, insulin was administered to Alzheimer's disease patients to improve their cognitive functions, given the neuroprotective properties of insulin (190). The ViaNase™ is a liquid based drug delivery device based on controlled particle dispersion. Other interesting devices are the UNI-dose (Aptar, France), OptiMist™ (OptiNose, Oslo, Norway) and DirectHaler™ (Lyngby, Denmark), which are devices that target liquid or powder nasal formulations to the nasal cavity, including the olfactory region, without deposition in the lungs or oesophagus. The OptiMist™ is a breath actuated device and has been proven to result in more deposition in the nasal cavity than a spray pump (191, 192). With respect to clinical application, not only will the device be of importance but also the position of the head as it is likely that active substances might come loose from the nasal mucosa by gravity (193). In the majority of the articles discussed, animals were placed in the supine position. Van den Berg et al. found that the supine position with the head at 70° and 90° was the most favorable (194). In non-human primates, the most favorable position is the 'praying to Mecca', with the head down and forward (89).

2. AIMS AND OBJECTIVES

As described above, many novel therapies are emerging to contribute to cure, or at least treatment of GBM patients. However, over the past decades, no major breakthroughs were observed and for the majority of patients, their ultimate prognosis remains unchanged. Also in our research group, we have tried to set up a clinical approach by treating GBM patients with DC vaccinations. Despite a fraction of long-term surviving patients, the majority of patients responded insufficiently to this elaborative treatment modality. Objective immunologic responses, such as IFN- γ producing CTLs could often be observed, but without convincing clinical benefit. These observations made us believe that the TME should be well equipped to withstand this immune mediated attack. Active immune suppression in the TME context of GBM patients is now believed to be the major hurdle why immunotherapy cannot work to its full extend.

In this project, the general aim was to modulate the TME in order to decrease the immune suppression environment. Therefore, we chose to target Gal-1 which is a well-validated target in GBM and known to be a potent suppressor of immunity. In particular, we aimed to modulate the TME in a patient-friendly and non-invasive way. GBM by itself, and the current treatment modalities are already weighing heavily on the quality of life of most patients. Therefore, modulating the TME by using the nose-to-brain transport would be an ideal scenario. Intranasal transport could be administered by the patient themselves, with reduced systemic exposure (and toxicity) and needle-free.

To test our hypothesis, we evaluated the nose-to-brain transport in a murine GBM model, GL261 model, which is the most validated syngeneic, immune-competent model available. In particular the following aims we wished to achieve:

- I. To develop a nanocarrier formulation that can protect anti-Gal-1 siRNA molecules, and also transport them from the nasal cavity to the CNS, in particular the TME of GBM;
- II. To set-up an experimental chain (screening platform) which could identify the best potential candidate formulation to continue working with;
- III. To identify the in vivo nose-to-brain transport and assess the decrease of Gal-1 in situ;
- IV. To combine the anti-Gal-1 therapy with the most clinically relevant therapies such as TMZ, DC vaccination and PD-1 blocking;
- V. To initiate the optimization of the selected formulation;

3. RESULTS – PART 1 – PAPER 1

Development of siRNA-loaded chitosan nanoparticles targeting Galectin-1 for the treatment of glioblastoma multiforme via intranasal administration

As described above, many pharmaceutical formulations can be prepared that promote the direct nose-to-brain transport. Each of these formulations has its own properties and specifics which are adapted to the cargo that is loaded into these nanocarriers. In our project, we wanted to load hydrophilic siRNA molecules, which are known to be very sensitive to degradation. Therefore, our carrier complex should have properties as protection from RNase enzymes, able to complexate with hydrophilic molecules, achieve complexes that are in the nano-range, and able to deliver siRNA into the cytoplasm of the target cells. We refer to our addendum in this thesis, where the rationale is discussed why we chose chitosan nanoparticles to continue working with. In brief, chitosan nanoparticles are broadly used as transfection tool, to deliver all kinds of nucleic acids (plasmid DNA, siRNA...) into cytoplasm. Moreover, chitosan is also an interesting pharmaceutical excipient that possesses muco-adhesive and epithelial barrier modulation properties, thereby promoting a direct nose-to-brain transport.

With this background in mind, we prepared a study with the following aims

- I. To evaluate the ability of chitosan nanoparticles to protect siRNA molecules from degradation by RNase enzymes, during different time periods;
- II. To determine if chitosan nanoparticles can induce a selective mRNA degradation of Gal-1 in vitro, which will be evaluated both on mRNA, as on protein level, both in murine and human cell cultures;
- III. To measure how GL261 cells are affected in terms of in vitro mobility when Gal-1 is reduced, therefore a scratch assay will determine the invasiveness;
- IV. To define the epithelial modulation properties of chitosan nanoparticles in vitro, where the chitosan nanoparticles will be incubated with epithelial cells, both human lung and nasal derived;
- V. To evaluate the aforementioned nose-to-brain transport in vivo, with a focus on transport through the olfactory bulb, and transport into the TME
- VI. Lastly, to determine the in vivo functionality of the siRNA molecules and, if siRNA molecules reach the TME target, to quantify the amount of Gal-1 mRNA degradation.

The research paper discussing the results of this section is presented on the following pages

Development of siRNA-loaded chitosan nanoparticles targeting Galectin-1 for the treatment of glioblastoma multiforme via intranasal administration

Journal of Controlled Release, Volume 227, 10 April 2016, Pages 71–81

doi:10.1016/j.jconrel.2016.02.032

Matthias Van Woensele^(1,a,b), Nathalie Wauthoz^(b), Rémi Rosière^(b), Véronique Mathieu^(c), Robert Kiss^(c), Florence Lefranc^(d), Brecht Steelant^(e), Ellen Dilissen^(e), Stefaan W. Van Gool^(f), Thomas Mathivet^(g), Holger Gerhardt^(g), Karim Amighi^(b) and Steven De Vleeschouwer^(a,h)

^(a) Research Group Experimental Neurosurgery and Neuroanatomy, KU Leuven, Herestraat 49, Leuven 3000, Belgium;

^(b) Laboratory of Pharmaceutics and Biopharmaceutics, Faculté de Pharmacie, Université Libre de Bruxelles (ULB), Bvd du triomphe CP207 Brussels 1050, Belgium;

^(c) Laboratoire de Cancérologie et de Toxicologie Expérimentale, Faculté de Pharmacie, ULB, Bvd du triomphe CP207 Brussels 1050, Belgium;

^(d) Department of Neurosurgery, Erasmus University Hospitals, Brussels 1050, Belgium;

^(e) Laboratory of Clinical Immunology, KU Leuven, Herestraat 49 box 811 Leuven 3000, Belgium;

^(f) Laboratory of Pediatric Immunology, KU Leuven, Herestraat 49 box 811 Leuven 3000, Belgium;

^(g) Vascular Patterning Laboratory (Vesalius Research Center), VIB, Leuven 3000, Belgium;

^(h) Department of Neurosurgery, University Hospitals Leuven, Herestraat 49 Leuven 3000, Belgium.

Abstract

Galectin-1 (Gal-1) is a naturally occurring galactose-binding lectin, which is overexpressed in glioblastoma multiforme (GBM). Gal-1 is associated with tumor progression, and is a potent immune suppressor in the tumor micro-environment. To inhibit Gal-1 in GBM, an effective therapy is required that reaches the central nervous system tumor, with limited systemic effects. In this study, we report for the first time that concentrated chitosan nanoparticle suspensions can deliver small interfering RNA (siRNA) into the central nervous system tumor within hours after intranasal administration. These nanoparticles are able to complex siRNA targeting Gal-1 to a high percentage, and protect them from RNase degradation. Moreover, a successful intracellular delivery of anti-Gal-1 siRNA resulted in a decreased expression of Gal-1 in both murine and human GBM cells. Sequence specific RNA interference, resulted in more than 50 % Gal-1 reduction in tumor bearing mice. This study indicates that the intranasal pathway is an underexplored transport route for delivering siRNA-based therapies targeting Gal-1 in the treatment of GBM.

Keywords:

Chitosan, nanoparticles, siRNA, Galectin-1, Glioblastoma, intranasal

Text Manuscript

1. Introduction

Gliomas are the most common types of intrinsic brain tumor, affecting 5-10 people/100 000/year. Glioblastoma (GBM) is the most frequent glioma of astrocytic origin, categorized by the World Health Organization (WHO) as a grade 4 tumor (3). Current treatment modalities fail to save GBM patients. The optimal treatment regimen consists of maximal surgical resection, followed by chemo- and radiation therapy. This multimodal treatment results in a median overall survival of only 14.6 months, and a two-year survival rate of maximal 30% (8). The poor prognosis has provoked a search for many novel treatments over the past years. However, very few have proven clinical efficacy (1, 195, 196).

In our research facilities, the potential of immunotherapy as novel approach has been explored to further improve the survival of GBM patients (197, 198). Immunotherapy will harness the patient's own immune system against the GBM (199). In relapsed malignant glioma patients, a modest number of long-term survivors is reported. These are defined as surviving more than 24 months after reoperation and dendritic cell vaccination (200, 201). In newly-diagnosed GBM patients, a median survival of 18.3 months is reported in the case of an integrated postoperative radiochemoimmunotherapy approach (202), and a promising two-year survival rate, according to long-term analysis data (unpublished data). Despite the possibility of inducing long-term survival, the final outcome for many patients remains unchanged with immunotherapy (203). Consensus is arising that GBM tumors are very potent immune-evasive tumors, pre-disposed to circumventing immune-targeting therapies (204, 205). Therefore, the rational combination of new and conventional therapies will be necessary to overcome this devastating disease.

Currently, the mediators that create this immune-evasive tumor micro-environment are under intensive investigation. Our research group and others have identified Galectine-1 (Gal-1) as a potent naturally-occurring immune-suppressive protein, preferentially upregulated in GBM (63, 206). Gal-1 can induce apoptosis in activated CD8+ T cells, antagonize T cell signaling and block pro-inflammatory cytokine secretion (51, 57). It was previously demonstrated in the murine GBM GL261 model that depletion of Gal-1 increased the efficacy of dendritic cell-based immunotherapy (207). From these data, Gal-1 is considered a potent immune regulator in GBM. Gal-1 is not only involved in immune suppression for GBM progression, but also several other key features have been attributed to this lectin (44). Upregulation of Gal-1 is correlated with an increased motility of GBM cells (206). Via rearrangement of the actin skeleton, Gal-1 can introduce a migratory phenotype in GBM cells (208). Moreover, Gal-1 has been proven to promote angiogenesis in the tumor-micro environment (61, 209). Not only GBM cells can over-express Gal-1, but also the endothelial cells associated with the tumor (64). Functioning as a modulator for vascular endothelial growth factor maturation, Gal-1 can promote vessel growth (61). Furthermore, Gal-1 has been discovered to be a mediator in the chemo-resistance of GBM cells towards temozolomide, the most commonly used chemotherapeutic agent against GBM (210). Gal-1 can regulate endoplasmatic reticulum stress to promote cell survival under temozolomide treatment

(61, 65, 210). In summary, Gal-1 is a crucial mediator at the interface of many GBM-promoting phenomena, and therefore an ideal target candidate for combating GBM.

Many strategies have been used to target Gal-1, such as small-chemical molecules (Davanat®, Anginex and derivatives such as OTX-008). RNA interference has also been developed, with proven effectiveness (61, 211). Short double-stranded small interfering RNA (siRNA) can be loaded into the RNA-induced silencing complex (RISC) and selectively destroy the mRNA encoding for the protein (212), in this case Gal-1. Reaching a critical concentration at the tumor site is a major point of concern. The most effective but invasive method mentioned in literature to reach the GBM tumor is deemed to be via intraventricular injection, where the siRNA are infused using an osmotic mini-pump (213).

A mounting body of evidence seems to reveal that the intranasal pathway might represent a non-invasive alternative administration method (84, 114). Intranasal transport has been described as a direct pathway from the nasal cavity towards the central nervous system via the olfactory and trigeminal nerves, delivering therapeutics to the rostral and caudal brain regions respectively (88). Recently, the pharmaceutical aspects of further enhancing nose-to-brain transport have been reviewed for brain diseases (214). In this study, the design was focused on pharmaceutical formulations that improve transport through the nasal mucosal, nasal epithelium and cells, protect the siRNA from degradation (e.g. RNase) and thereby increase overall bio-availability in the central nervous system (CNS) of the active compound. Therefore, chitosan was chosen as the excipient for constituting nanoparticles because: (i) chitosan is a biodegradable and biocompatible polymer based on β -(1–4)-linked D-glucosamine and N-acetyl-D-glucosamine subunits, which are linked via glycosidic bonds (134) which have positive charges at physiologic pH allowing a high payload of negatively charged molecules such as siRNA; (ii) this interesting excipient possesses mucoadhesive and permeation-enhancing properties, which seem ideal for further enhancing nose-to-brain transport (137, 215, 216); and (iii) chitosan nanoparticles have also been widely investigated for their transfection potential, in particular for siRNA delivery in the cytosol due to endosomal escape (217).

Considering the pivotal role of Gal-1 in glioma biology, and the possibility to block Gal-1 in the tumor micro-environment using a non-invasive administration method, this study aims to: (i) develop chitosan nanoparticles that complex and protect siRNA specific for Gal-1 targeting; (ii) evaluate the transfection potential on both murine and human GBM cell lines; (iii) investigate its permeation-enhancing properties on an epithelial layer; (iv) assess the *in vivo* distribution of fluorophore-tagged siRNA-formulation in the CNS tumor after intranasal instillation; and (v) to verify if the presence of anti-Gal-1 siRNA corresponds with intratumoral reduction of Gal-1 via sequence specific mRNA degradation.

2. Materials and Methods

2.1. Materials

Chitosan (Heppe Medical Chitosan, Germany) was obtained that had a well-defined molecular weight of 50 kDa, giving a viscosity of 10 mPa.s for a 1% w/v solution in 1% acetic acid at 20°C. The degree of de-acetylation amounted to 85.2%. Sodium tripolyphosphate (TPP), sucrose, sodium dodecyl sulfate (SDS) and Fluorescein Isothiocyanate-dextran (FITC-FD4) were purchased from Sigma-Aldrich. Anti-Gal-1 (human: 5'GCUGCCAGAUGGAUACGAAdTdT3', mouse:

5'ACCUGUGCCUACACUUCAAdTdT3') and scrambled siRNA (5'GGAAAUCCCCAACAGUGAdTdT3') were purchased from GE Dharmacon, and, if necessary, labeled with fluorescein or 5'-dye 547 (custom design, Lafayette, USA).

Methylcholanthrene-induced murine C57BL/6J syngeneic GL261 glioma cells were kindly provided by Dr. Eyupoglu (University of Erlangen, Germany) and were cultured as previously described (218). Primary glioblastoma cultures were obtained from resection specimens from patients after informed consent (UZ Leuven Medical Ethics Committee approval S57028). In brief, tumor specimens were dissociated via 30 min incubation with collagenase D and DNase at 37°C. Subsequently, mononuclear cells were isolated on a Ficoll density gradient (Lymphoprep, AxisShield, Norway), and cells were seeded in RPMI medium under 20% fetal calf serum conditions. The *Calu-3* cell line was purchased from the American Type Culture Collection, ATCC HTB-55, and cultivated under the same conditions as described elsewhere (219).

Eight-to-ten week-old female C57BL/6J mice were purchased from Harlan (Horst, The Netherlands). The mice were maintained under conventional pathogen-free conditions. All experiments were approved by the bioethics committee of KU Leuven, which follows international guidelines.

2.2. Preparation of nanoparticles

Nanoparticles were obtained by ionic gelation. Chitosan polymers were positively charged by dissolution in 0.1 M acetic acid buffer pH 4.5. TPP was chosen as an ionic crosslinker to interconnect the chitosan polymers. Due to the negative charge of both TPP and the phosphates in siRNA, chitosan nanoparticles formed spontaneously (217). TPP (1 mg/ml) was added to chitosan (0.7 mg/ml) under constant stirring (1300 RPM, 25°C), with a chitosan to TPP weight ratio of 2.625/1. Encapsulation of siRNA molecules was achieved by pre-incubation of siRNA and TPP before nanoparticle formation, with a total amount of 24 µg siRNA for 1 ml of nanoparticles (1.4% of theoretical payload). The nanoparticles were stirred for 30 min at room temperature. Subsequently, particles were collected via ultracentrifugation at 40 000 x g for 20 min. The sediment was redispersed in 0.075 M acetic acid buffer pH 4.5, and the supernatant was centrifuged again twice. The three sediments were pooled and freeze-dried in the presence of sucrose as a lyoprotectant, with a nanoparticle/lyoprotectant weight ratio of 1/8.

2.3. Characterization of nanoparticles

2.3.1. Size, charge and stability

The hydrodynamic diameter (Z-average), and the polydispersity index (PDI) of the nano-sized formulations were determined by dynamic laser scattering and the zeta potential via laser Doppler electrophoresis using a Zetasizer Nano ZS (Malvern Instruments, UK). The measurements were made in triplicate after a dilution of 1:10 v/v in 0.075 M acetic acid buffer pH 4.5 at 37°C. The stability of the freeze-dried nanoparticles at 4°C in a desiccator was assessed after their reconstitution in Milli-Q water. For transmission electron microscopy (TEM), anti-Gal-1 siRNA loaded chitosan nanoparticles (reconstituted from freeze-dried powder) were set onto a carbon-coated EM grid and allowed to settle

for 30 seconds. Grids were then blotted on filter paper and stained for 30 seconds with uranyl acetate (2%). After further blotting and drying, samples were directly observed on a Tecnai 10 TEM (FEI). Images were captured with a Veleta camera and processed with iTEM and Adobe Photoshop softwares.

2.3.2. siRNA encapsulation efficiency

The percentage of encapsulated siRNA was determined using the SYBR green assay (73). This selective dye can only emit fluorescence upon binding into the helix of siRNA molecules. The nanoparticles were prepared and stirred for 30 min. Subsequently, the particles were incubated with SYBR green for 30 min. Free siRNA was used to prepare a standard curve and was detected by a fluorescence plate reader in a black 96-well plate (Nunc) at 480 nm (ex) and 520 nm (em). As a positive control, 0.1% SDS was added to break ionic complexations. In parallel, the percentage of unencapsulated siRNA was evaluated in the supernatant after ultracentrifugation by measuring the fluorescent unencapsulated siRNA. The following equation was used to determine the encapsulation efficiency:

$$EE (\%) = 100 \times \frac{C_{\text{total siRNA}} - C_{\text{uncomplexed siRNA}}}{C_{\text{total siRNA}}}$$

2.3.3. Protection against siRNA degradation

Protection against siRNA degradation from ribonucleases (RNases) was assessed by a gel retardation assay. In brief, the chitosan nanoparticles were incubated with 0.07% recombinant RNaseA (Life Technologies) at 37°C. Then, the particles were loaded onto a 4% agarose gel that was prepared with Tris/borate/EDTA buffer (10 x Ultrapure TBE, Life Technologies). For better visualization, particles were dissociated using 0.1% SDS before loading them onto the gel. An equal amount of free siRNA was also incubated with RNaseA, and loaded onto the gel. Migration of siRNA was forced by applying 55 V for 2 h. Visualization was achieved by staining the gel with ethidium bromide for 30 min.

2.4. Interaction with glioma cells

Both murine GL261 glioma cells and human primary culture glioblastoma cells were grown on a glass cover slip. Next, particles loaded with fluorescein-tagged siRNA were incubated with the cells. At regular time intervals, the glass cover slips were washed and fixed in 4% paraformaldehyde for 10 min. For the human primary cultures, an additional immunofluorescence staining was performed, which stained their nuclei with 4',6-Diamidino-2-phenylindole dihydrochloride (DAPI, Sigma).

2.5. Transfection assay

Both murine GL261 glioma cells and human primary glioblastoma cells were cultivated up to a density of maximum 60% full confluence. Chitosan nanoparticles were added in serum-free culture conditions overnight up to a final siRNA concentration of 20 nM. The cells were washed extensively with

phosphate buffered saline (PBS) and put back into serum condition media. From this cell population, glioblastoma cells were seeded for the assessment of the transfection efficiency over time.

2.5.1.mRNA

Treated cells were harvested at different days post-transfection, and RNA was isolated (Miniprep, Qiagen) and quality-controlled via spectrophotometer (Nanodrop, Thermo scientific). Subsequently, a cDNA template was created via a reverse polymerase reaction (Superscript II, Invitrogen) and a real-time quantitative polymerase chain reaction (RT-qPCR) was performed on these samples. Following this, primer pairs were used to detect Gal-1 and GAPDH as a housekeeping gene (Supplementary Table 1 M&M). The ratio of Gal-1/GAPDH in untreated cells was used as the 100% baseline.

Supplementary Table 1 M&M. Primer pairs and probes for RT-qPCR Sequences for Gal-1 and GAPDH to quantify the amount of murine mRNA encoding for Gal-1

Gene	Primer/probe	Sequence
Galectin-1	forward	caa tca tgg cct gtg gtc tg
	Reverse	gtg tag gca cag gtt gtt gct g
	Taqmanprobe	tcg cca gca acc tga atc tca aac ct
GAPDH	Forward	tca cca cca tgg aga agg c
	Reverse	gct aag cag ttg gtg gtg ca
	Taqmanprobe	atg ccc cca tgt ttg tga tgg gtg t

2.5.2.Protein

Treated cells were harvested at different days post-transfection, and proteins were isolated (Tissue Protein Extraction Reagent, Life Technologies). Protein concentration was determined via a colorimetric assay (BCA kit, Life Technologies). Equal amounts of total protein were separated by sodium dodecyl sulfate/polyacrylamide gel electrophoresis and transferred to a polyvinylidene difluoride membrane. Membranes were incubated overnight with a primary antibody: rabbit anti-Galectin-1 (1:1000; Peprtech, Quebec, Canada) or Galectin-3 (1:1000, Abcam). As a protein-loading control, all blots were stained with rabbit anti- β -Actin (1:5000; Abcam). The secondary antibody used was peroxidase-conjugated goat anti-rabbit IgG (1:5000; Dako). Visualization was performed using chemi-luminescence (Western Lightning, Perkin Elmer). Quantification of the bands was performed using ImageJ software.

2.5.3. Migration assay

Four days after transfection, GL261 cells were plated into 6-well plates. Cells were allowed to attach overnight, and grown to a monolayer. With a 200 µl pipet tip, a scratch was introduced without affecting the plate coating. Three independent pictures were taken of this scratch, and the experiment was performed in quadruplet. Pictures were taken at 12, 23 and 48 h after introducing the scratch. The surface area was calculated using ImageJ software and calculated as a percentage of the baseline surface area.

2.6. Epithelial barrier integrity

Calu-3 cells were seeded on 12-well Transwell inserts at a density of 500 000 cells/ml (0.4 µm translucent polyester, Greiner). After 14 days, a confluent monolayer was formed that displayed a stable transepithelial electrical resistance (TEER), measured using an EVOM/Endohm (WPI Inc, Sarasota, USA). To confirm the formation of a confluent monolayer, and the adherence of the formulation onto the monolayer, immunofluorescence staining was performed. After fixation, the cells were blocked in TNB buffer (0.1 M Tris pH 7.4; NaCl 150 mM; 0.5% blocking reagent Perkin Elmer, Boston) for 2 h and rabbit anti-tubulin (1/100, Abcam) primary antibody was added, diluted in TNB (2 h, 25°C). Cells were washed thoroughly with TNT (0.1 M Tris pH 7.4; NaCl, 150 mM; 0.2% Triton X-100) and Alexa fluor 555 donkey anti-rabbit IgG was added (1/200, Life Technologies). Afterwards DAPI was added for nuclei staining. In the case of tight-junction assessment, anti Zona Occludens-1 (ZO-1) antibody was used as the primary antibody (1/100, Life Technologies). To evaluate the capacity of chitosan nanoparticles to disturb the epithelial barrier integrity transiently, the chitosan nanoparticles were incubated on a monolayer of Calu-3 cells for 2 h at a concentration of 0.06% and 0.03% (w/v). TEER was measured in function of time, and baseline TEER measurements were expressed as 100%. In addition, macromolecular permeability was measured as an alternative parameter for evaluating the integrity of the epithelial barrier. Fluorescent Dextran 4kDa (FD4) was used as a hydrophilic model drug, a surrogate for the paracellular transport route (219). In case of primary nasal epithelium, cells were isolated and seeded as published in previous report (220) .

2.7. *In vivo* experiments

2.7.1. CNS distribution

For *in vivo* distribution studies, mice were anesthetized with isoflurane 3% during the administration period. Each mouse was administered with 8 times 3 µl drops with a time interval of 3 min between each drop, delivered with a micro-pipet and non-adhesive tips (Eppendorf, Belgium). Administrations were performed and from 4 h after the last administration, mice were sacrificed by intraperitoneal injection of Nembutal, and perfused with cold PBS followed by perfusion with 4% formaldehyde. Nasal mucosa and brains were carefully isolated, and fixed for an additional 12 h with 4% formaldehyde. The nasal mucosa was prepared for sectioning using scalpels and classical paraffin-microtome sectioning at 5 µm. Brain specimens were prepared for sectioning by embedding in 4% agarose then cut into 200 µm sections using a vibratome. Sections were preserved in PBS containing 0.01% sodium azide until staining and visualization. All specimens were stained with DAPI for nuclei as background

architecture. To visualize vessels, two staining techniques were used. For *in vivo* vessel staining, 50 µg isolectin-488 (I21411, Life Technologies) was injected by IV 2 h before sacrifice. To stain blood vessels on vibratome sections, they were blocked with TNB for 2 h, and incubated overnight with rabbit anti-GLUT-1 primary antibody (1/100, 07-1401, Merck Millipore) or anti-fluorescein (1/100, ANZ0109, Life Technologies) diluted in TNB. After extensive washing with TNT, donkey anti-rabbit IgG – Alexa fluor 555 – was added overnight (1/200, A31572, Life Technologies), and sections were mounted (Dako mounting medium). Visualization of the slides was performed using confocal microscopy (SP8, Leica), with magnification at 25x. Images were processed using ImageJ software.

2.7.2. GL261 tumor inoculation

The mice were intracranially injected with GL261-WT or GL261-BFP tumor cells as previously described (221). Briefly, 0.5×10^6 tumor cells were injected at 2 mm lateral and 2 mm posterior from bregma at a depth of 3 mm below the dura mater by using a stereotactic frame (Kopf Instruments, Tujunga, CA). Stereotactic inoculation was performed under sterile conditions. Intracranial tumors develop within 3 weeks, and mice were monitored three times a week for weight and neurological deficit scale scoring as described earlier (221). All animal experiments were performed with permission of the Ethical Committee of the KULeuven on laboratory animal welfare (ethical committee p135/2013).

2.7.3. Gal-1 quantification

Mice received 4 intranasal administered anti-Gal-1 siRNA loaded nanoparticles at day 5, 8, 12 and 15 after tumor inoculation. At day 20, or earlier if mice developed clinical signs of massive tumor burden, mice were sacrificed and perfused with PBS. Whole brains were isolated and homogenized in 2ml tissue protein extraction buffer (78510, Thermo Scientific). Debris was removed, and supernatant was used for colorimetric protein analysis (BCA kit, Pierce, Life Technologies) and western blot analysis, similar as described above. Also for immunofluorescence a similar protocol was used as for e.g. GLUT-1 staining, with anti-Gal-1 as primary antibody (1/100, R&D).

2.7.4. GeneRACE-PCR

GeneRACE-PCR protocol was used to prove mRNA cleavage, as described elsewhere (222), with minor modifications (L1502-01, Thermo Scientific). In brief, tumor bearing mice were treated intranasally with anti-Gal-1 siRNA loaded nanoparticles at day 5, 8, 12 and 15; and sacrificed at day 20 at which a small piece of tumor was harvested and RNA was isolated with the RNeasy Mini kit (QIAGEN), and the GeneRACE oligo was ligated to the mRNA fragments (Thermo Scientific), both following the manufacturer guidelines. Gal-1 specific cDNA synthesis was performed with gtggccttgagtgaagcca as Gal-1 cDNA synthesis primer. PCR amplification was performed with cgacuggagcagcaggacacugac as cDNA specific primer for mGal-1, and atggaggccatcaactacatggcg to the Gal-1 cDNA sequence. PCR products were ligated into pCR-4 TOPO vectors and cloned into one-shot competent E.Coli cells. Upon overnight incubation at 37 °C, positive colonies were picked,

incubated an additional overnight at 37°C and selected for miniprep to isolate the plasmids. T3 and T7prom sites were used for sequencing provided by the manufacturer (LGC genomics).

3. Results

3.1. Particle characterization

To select the optimal formulation, a thorough assessment process was prepared for several parameters of paramount importance (i.e. composition of the formulation and experimental parameters used for the preparation of the nanoparticles). An initial selection criterion was the size of the nanoparticles. Therefore, the influence of the chitosan polymer's molecular weight, the stirring speed and the concentration of chitosan on the hydrodynamic size (Z-average) of the nanoparticles was assessed and reported in Table 1.

Table 1. Critical parameters that affect the ionic gelation of nanoparticles Evaluation of the critical parameters that affect the size distribution of the nanoparticles produced by ionic gelation: molecular weight of the chitosan, magnetic stirring speed during the process, chitosan concentration. Evaluation of the size distribution before and after the freeze-drying process, with sucrose as lyoprotectant in an 8/1 weight ratio. Measurements are expressed as the mean \pm SD, $n \geq 3$. * Mann-Whitney test, # linear regression analysis.

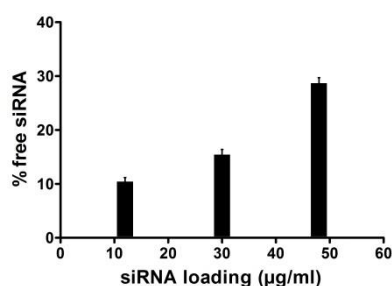
Variable		Size (nm, \pm SD)	Effect (p-value)
Molecular weight	50 kDa	163 \pm 7	Yes, p = 0.01*
	90 kDa	181 \pm 10	
Stirring speed	700 RPM	178 \pm 2	Yes, p = 0.009*
	1300 RPM	137 \pm 5	
Concentration of chitosan	0.7 mg / ml	129 \pm 5	Yes, p = 0.003 [#]
	2 mg / ml	306 \pm 11	
Freeze drying process	Before	139 \pm 4	No, p = 1*
	After	141 \pm 5	

A lower molecular weight up to 50kDa, higher stirring speed up to 1300 RPM and lower concentration of chitosan up to 0.7 mg/mL resulted in the smallest particles. These were characterized by a Z-average of 141 \pm 5 nm and a PDI of 0.27 (i.e. a monomodal and monodispersed distribution), as reported in Table 2.

Table 2. Particle characteristics Formulation particle size and polydispersity index from dynamic light scattering, zeta potential from laser Doppler electrophoresis, siRNA encapsulation in the formulation with or without SDS and encapsulation efficiency. Measurements are expressed as the mean \pm SD (n=3).

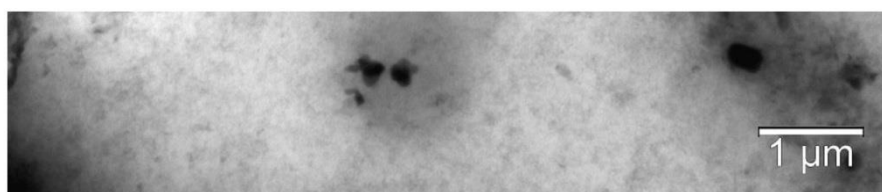
Zeta average (nm, \pm SD)	Poly-dispersity index	Zeta potential (mV)	siRNA payload (μ g/ml)	siRNA encapsulation (% \pm SD)	siRNA encapsulation with SDS (% \pm SD)
141 \pm 5	0.3	+ 32mV	24	81 \pm 3	4 \pm 2

A total of 24 μ g/ml siRNA was formulated, as a higher amount resulted in a higher loss of siRNA (Supplementary Figure 1). Further dilution of chitosan (< 0.7 mg/ml) did not result in formation of particles (data not shown). The smallest nanoparticles were obtained by producing them using 50 kDa chitosan, stirred at 1300 RPM, and dissolved at 0.7 mg/ml. These were selected for further work. All the characteristics of these are described in Table 2. After production, the particles were collected by ultracentrifugation, and freeze dried without modification of size or zeta potential of the particles, as reported in Table 1.



Supplementary Figure 1. Loading capacity of chitosan nanoparticles. siRNA molecules were loaded into chitosan nanoparticles at a dose of 12, 30 or 48 μ g/ml, and free siRNA was detected using the sybr green assay.

Moreover, these freeze-dried particles stored at 4°C in a dessicator remained stable for at least 8 weeks in terms of size and charge after reconstitution (data not shown). The final product after reconstitution was also subjected to TEM, which confirmed the submicron size of the nanoparticles (Supplementary Figure 2). TEM pictures were difficult to obtain due to sucrose deposition as used for lyoprotective properties.



Supplementary Figure 2. Transmission electron microscopy of siRNA-loaded chitosan nanoparticles after reconstitution

3.2. siRNA encapsulation and protection from degradation

The siRNA loading capacity of chitosan nanoparticles was evaluated using SYBR green assay. To avoid loss of siRNA, a maximal loading capacity of 24 µg/ml siRNA was chosen for further studies. In this condition, $81 \pm 3\%$ of siRNA was complexed and encapsulated into the nanoparticles. The formulated siRNA was instantaneously released upon incubation with 0.1% SDS, as indicated by a loss of encapsulation efficiency (Table 2). Moreover, the high encapsulation efficiency was confirmed via the ultracentrifugation concentration process, where after three centrifugal cycles, 85% of the fluorescent siRNA was measured inside the sediment (data not shown).

Furthermore, the siRNA protection from RNase degradation was evaluated (Figure 1). To allow migration and therefore optimized visualization, chitosan nanoparticles were immediately destroyed by adding SDS just before loading on the gel. No degradation of siRNA was observed when the siRNA-loaded nanoparticles were incubated with RNases at 37°C for several time periods. In contrast, free siRNA rapidly degraded and could not be observed after 30 min (or longer) incubation with RNases. These results confirmed that a high percentage of the siRNA was complexed and encapsulated into the nanoparticles, and that these nanoparticles provided an excellent protection from degradation.

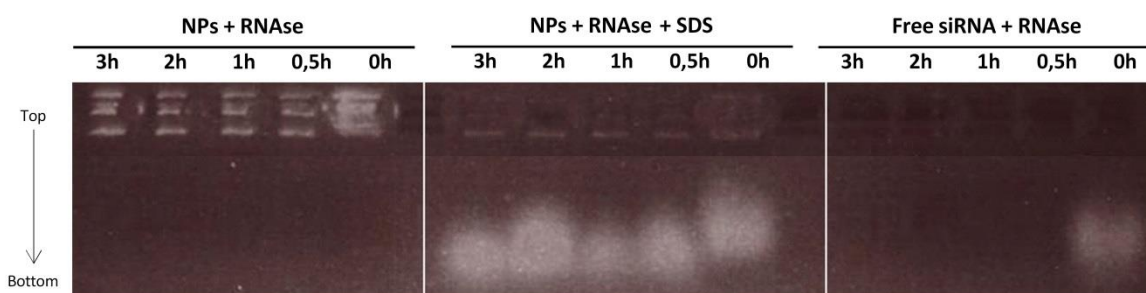


Figure 1. Loading capacity and protection from RNases siRNA loading and protection from RNase degradation at different times (0, 0.5, 1, 2 and 3 h) using a gel retardation assay. siRNA-loaded chitosan nanoparticles (CS NPs) or free siRNA were incubated with RNases and then exposed to sodium dodecyl sulfate (SDS) (NPS+RNase+SDS) or not (NPS + Rnases and free siRNA+RNase) before being loaded onto the agarose gel and applying 55 V for 2 h and then staining the gel with ethidium bromide.

3.3. Nanoparticle behavior on tumoral cells

Cell attachment of the chitosan nanoparticles was tested on both a murine GBM cell line, GL261, as well as on human primary GBM cultures. In both cases, 2 h after co-incubation in serum free media, a rapid attachment on the tumoral cells was observed (Figure 2 A + D). To evaluate whether the attachment of the nanoparticles on the GL261 tumor cells also induced a decrease of Gal-1 expression, mRNA and protein analysis were performed (Figure 2 B + C). For the GL261 cells, strong and specific Gal-1 mRNA degradation was observed rapidly after transfection. After 1 week, the Gal-1 mRNA level was recovered. In contrast, scrambled siRNA-loaded chitosan nanoparticles had no influence on the Gal-1 expression. Regarding the protein level, a strong decrease was observed starting from day 4 after transfection until at least day 7. The specificity of anti-Gal-1 siRNA was

demonstrated by immunoblotting for Galectine-3, which was not affected (Supplementary Figure 3). In parallel, the Gal-1 degradation in primary GBM tumor cell cultures was also analyzed (Figure 2 E + F). In six independent primary GBM cultures, a strong decrease in Gal-1 expression was notable from day 4 to day 7 post transfection (Fig 2 E + F).

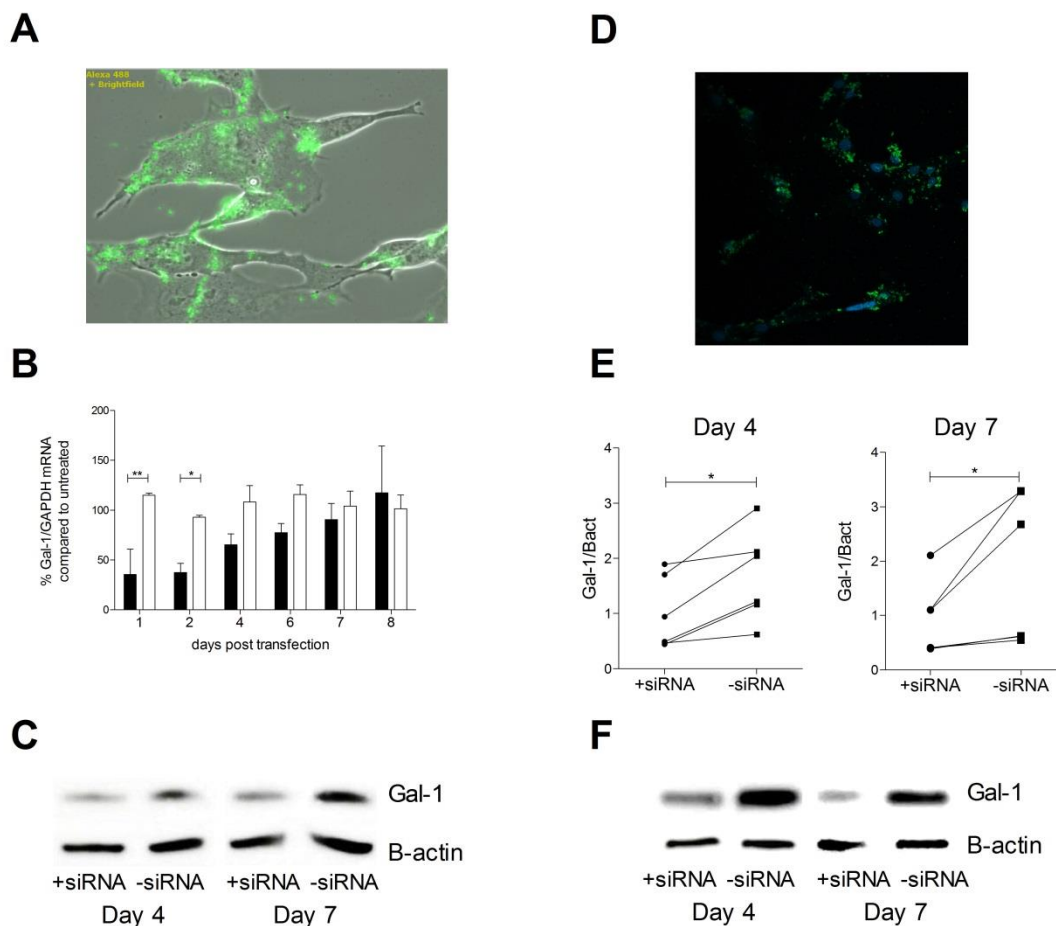
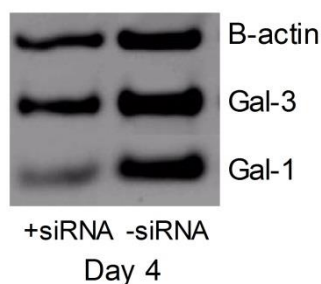


Figure 2. Interaction of chitosan nanoparticles loaded with fluorescein-tagged siRNA with murine (GL261) and human glioblastoma cells (primary cultures from patient tumors) Analysis on (A, B and C) murine or (D, E, F) human glioblastoma cell culture. Immunofluorescence pictures of (A) murine GL261 GBM cells and (D) cells from human primary GBM culture, with a brightfield or DAPI background respectively, 2 h after incubation with green fluorescein-tagged siRNA-loaded chitosan nanoparticles. (B) Relative Gal-1 mRNA expression in comparison to GAPDH mRNA on murine GL261 GBM cells evaluated at different days by RT-qPCR (black bar: cells incubated with siRNA-loaded nanoparticles; white bar: cells incubated with scrambled siRNA-loaded nanoparticles, expressed as the mean \pm SD, n=3; two-way ANOVA). (C) Protein level of Gal-1 determined by western blot on murine GL261 GBM cells incubated with chitosan nanoparticles loaded with (+siRNA) or without (-siRNA) siRNA at day 4 and 7 after the incubation. (E) Protein level of Gal-1 determined by western blot on six independent primary human GBM cultures at day 4 and 7 after incubation of nanoparticles loaded with (+siRNA) or without (-siRNA) (n=6, paired t-test, one-tailed) (F) Representative Western blot of a human primary GBM at day 4 and 7 after incubation of nanoparticles with (+siRNA) or without siRNA (-siRNA). * p < 0.05 and ** p < 0.01.



Supplementary Figure 3. Specific knockdown of Gal-1. GL261 cells were transfected with anti-Gal-1 siRNA-loaded chitosan nanoparticles. Four days later, Gal-1 and Gal-3 protein levels were determined via western blot.

To investigate further the biological significance of Gal-1 suppression, an assessment of the cell motility was performed via a scratch wound assay. Forty-eight hours after introducing the scratch, this assay revealed a significantly lower motility profile for the GL261 cells when Gal-1 expression was reduced (Figure 3). Twenty-three hours after introducing the scratch, a similar pattern was observed, although without significant difference (data not shown).

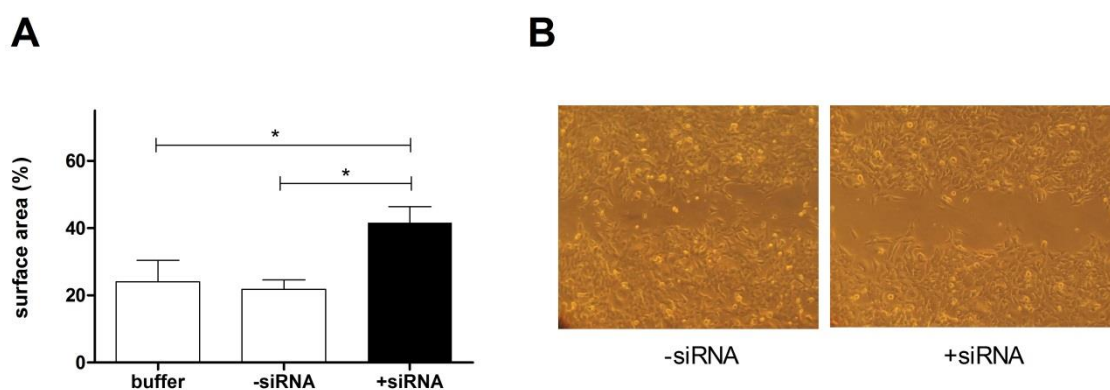


Figure 3. Scratch wound assay for migration analysis on murine GBM GL261 cells (A) Quantification and **(B)** morphological illustration of scratch area 48 h after introducing the scratch on murine GL261 GBM cells incubated with chitosan nanoparticles loaded with (+siRNA) or without (-siRNA) siRNA. The surface area was calculated as a percentage from time 0. Measurements are expressed as the mean + SEM (n=12); one-way ANOVA with Bonferroni's multiple comparison test, * $p < 0.05$.

3.4. Formulation-mediated epithelial modulation

The modulation of tight-junctions by chitosan-based formulations was evaluated using the bronchial epithelial Calu-3 cell line. First, the homogeneous distribution of the chitosan nanoparticles was visualized on the apical side of a Calu-3 monolayer (Fig 4 A). A significant reduction in TEER was found 2 h after adding chitosan nanoparticles (0.06% w/v) (Fig 4 B + Supplementary Figure 4 A). Moreover, we could confirm the TEER reduction on primary nasal epithelium cells (Supplementary Figure 4 B). This decrease in TEER was transient and recovered, at the latest, 24 h after particle incubation (Supplementary Figure 4 A + B). Together with a decreased TEER, a trend towards a higher permeability of FD4 was found (Figure 4 B + C). A disturbed ZO-1 protein expression was

found, indicating the loss of ZO-1 in between the cell-cell contact (Figure 4 D). Upon chitosan administration, this decrease in ZO-1 suggested the internalization of tight junctions.

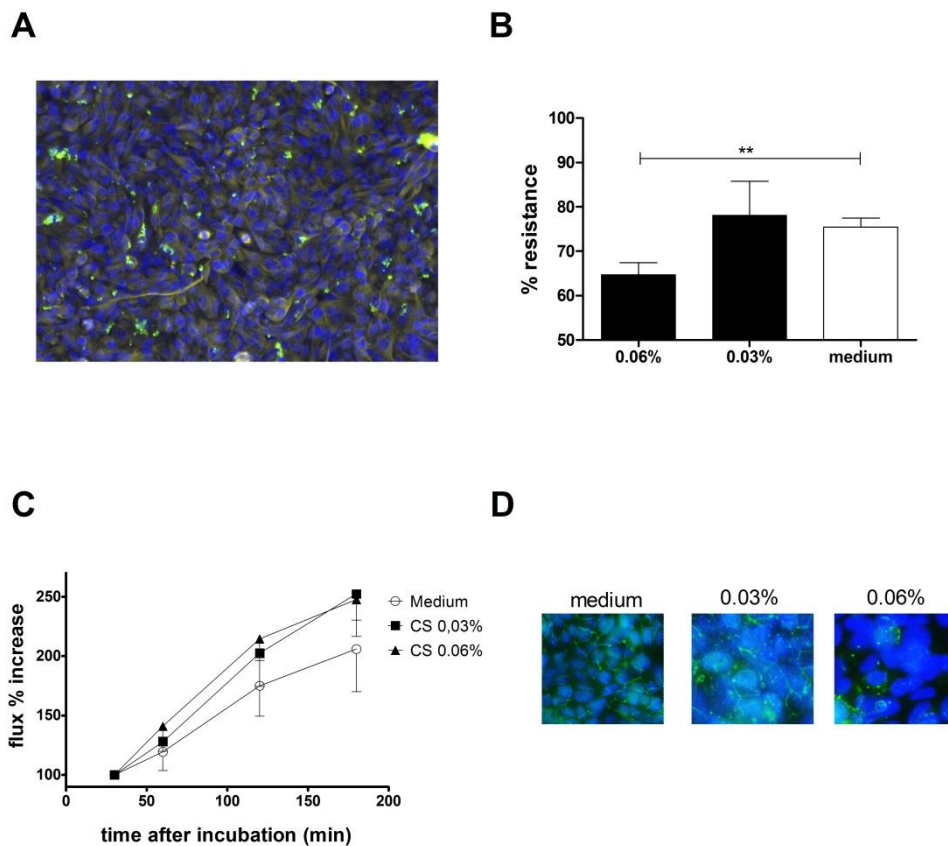
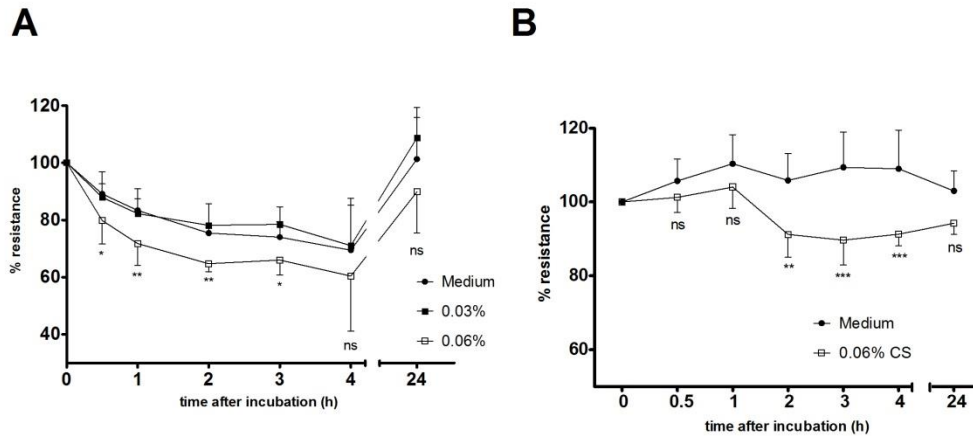


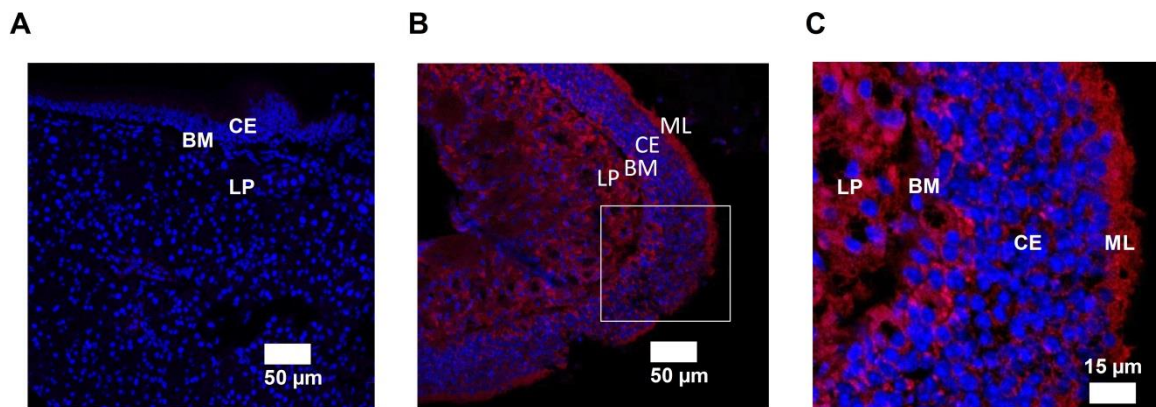
Figure 4. Interaction of siRNA-loaded chitosan nanoparticles with a Calu-3 monolayer airway epithelium (A) Representative immunofluorescence staining of a Calu-3 monolayer airway epithelium 2 h after incubation of green-fluorescein-tagged siRNA-loaded chitosan nanoparticles (blue = nuclei, yellow = tubuline, green = nanoparticles). **(B)** TEER measurement at 2 h after incubation with siRNA-loaded chitosan nanoparticles relative to the baseline TEER at time = 0. The measurements are expressed as mean + SD (n=9); one way ANOVA with Dunn's multiple comparison test with ** p < 0.01. **(C)** FD4 passage over a Calu-3 monolayer airway epithelium expressed as a percentage of flux increase over time, after incubation of siRNA-loaded chitosan nanoparticles at 0.03% or 0.06% w/v. The measurements are expressed as the mean ± SEM (n=6) **(D)** Representative Immunofluorescence staining for localization of ZO-1 tagged by green fluorescein antibody 2 h after incubation with siRNA-loaded chitosan nanoparticles (green: ZO-1, blue: nuclei).



Supplementary Figure 4. Trans epithelial electrical resistance measurements on (A) Calu-3 cells and (B) primary nasal epithelium, derived from freshly isolated nasal mucosal biopsy. Chitosan nanoparticles were incubated at 0.03% (A) and 0.06% (A+B). Measurements are expressed as the mean \pm SD, $n \geq 3$. * $p < 0.05$, ** $p < 0.01$ and * $p < 0.001$ via two way ANOVA. (ns: non-significant)**

3.5. Transport to the central nervous system

As a first barrier to entrance, the nasal mucosa of the treated animals were assessed. In control untreated mice, no presence of red dye-547 fluorophore-tagged anti-Gal-1 siRNA (RDsiRNA) was observed (Figure 5 A). After injection of non-formulated naked siRNA, only mild adherence on the mucus layer was noticed (Figure 5B), in contrast with RDsiRNA chitosan nanoparticles treated mice, where RDsiRNA were observed in the nasal mucosa 8 h after administration (Figure 5 C). To further delineate in detail the passage through the epithelial layer, mice were intranasally administered with RDsiRNA chitosan nanoparticles for 3 consecutive days and sacrificed 4 h after the last administration for processing to classical paraffin sections. A strong presence of RDsiRNA was detected in the nasal mucosa (Supplementary Figure 5 B). In particular, a strong concentration of RDsiRNA was present on the mucus layer (ML; Supplementary Figure 5 C). Moreover, the transport of RDsiRNA was revealed by their presence over the columnar epithelium (CE) into the lamina propria (LP).



Supplementary Figure 5. Detailed morphology on the nasal mucosa. Paraffin processed picture (A) of control untreated mouse; (B) mouse treated intranasally for 3 consecutive days, and sacrificed

4 h after the last administration of red dye-547 siRNA-loaded chitosan nanoparticles; with a box around the area of interest; **(C)** magnification of the mucosal layer. Red = dye 547-labeled siRNA, blue = nuclei, ML = mucosal layer, CE = columnar epithelium, BM = basal membrane, LP = lamina propria.

To further assess the transport towards the CNS, the olfactory bulb and the hindbrain were assessed for the presence of RDsiRNA (Figure 5 + Supplementary Figure 6). A thorough assessment of the olfactory bulb indicated no presence of red fluorescence in control untreated mice (Figure 5 D) and in naked-siRNA treated mice (Figure 5 E). However, in mice treated with RDsiRNA-loaded nanoparticles, a red fluorescent signal (RDsiRNA) was observed at the tip of the olfactory bulb 4 h after administration (Figure 5 F). A more diffuse distribution of the RDsiRNA was observed at 8 h post-administration (Figure 5 G).

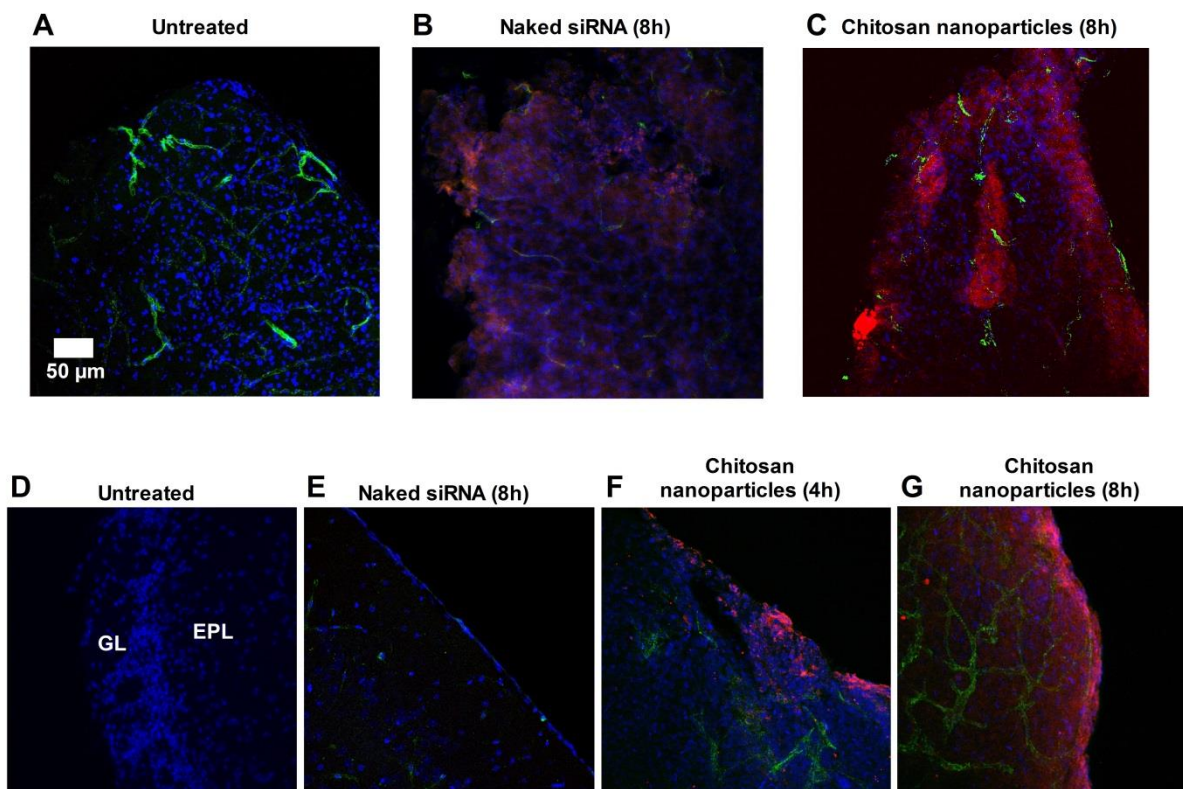
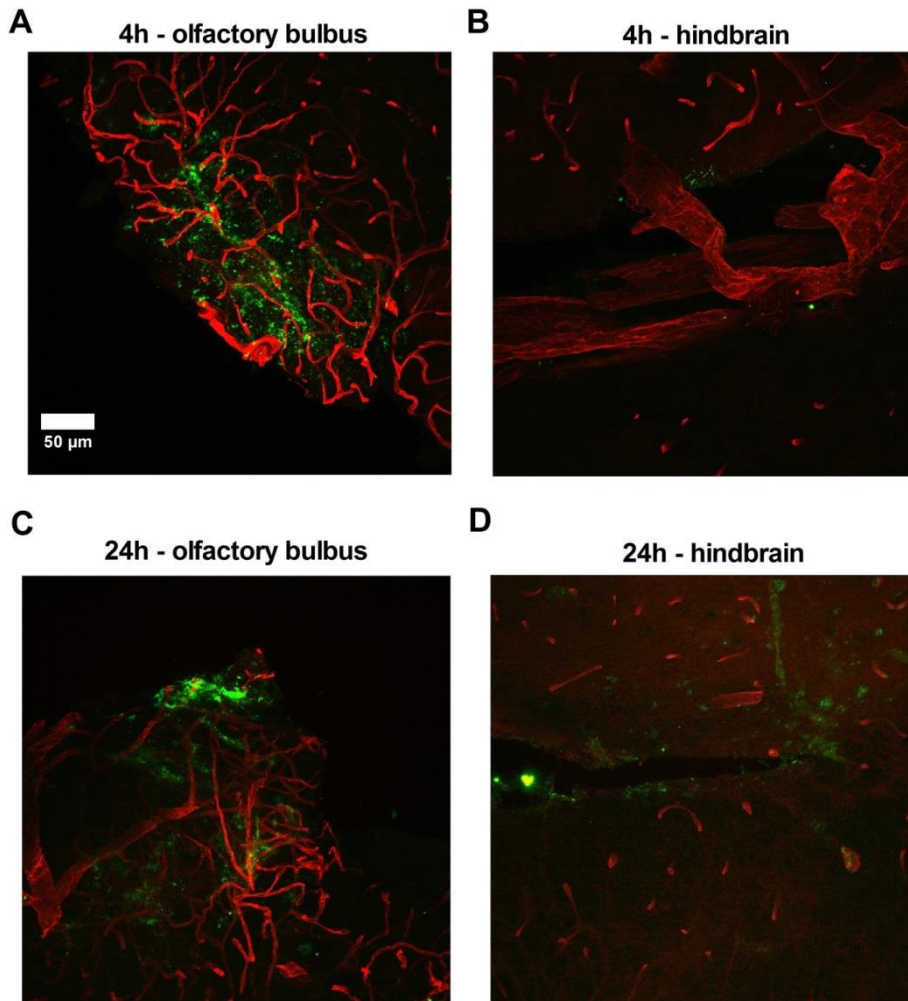


Figure 5. Fluorescent microscopy of the nasal mucosa and olfactory bulb. Confocal picture of nasal mucosa of **(A)** control untreated mouse, **(B)** mouse treated with naked RDsiRNA, 8h post administration and **(C)** mouse treated RDsiRNA-loaded chitosan nanoparticles, 8h post administration. Transport in the olfactory bulb was revealed with confocal picture of **(D)** control untreated mouse, which received no treatment and **(E)** mouse treated with naked RDsiRNA treated mouse, 8 h post administration, **(F)** mouse treated with RD siRNA-loaded chitosan nanoparticles 4 h after and **(G)** 8 h post administration of red dye-547 siRNA-loaded chitosan nanoparticles; Red = dye 547-labeled siRNA, blue = nuclei, green (except D) = vessels. GL = glomerular layer, EPL = external plexiform layer.

Furthermore, the transport of siRNA-loaded chitosan nanoparticles to the hindbrain was also assessed via a parallel technique. This technique involved the amplification of the green fluorescein-labeled siRNA with an anti FITC-FITC conjugated antibody (Supplementary Figure 6). Moreover, the presence of anti-Gal-1 siRNA was not only at the side of the olfactory bulb (Supplementary Figure 6 A), but also in the hindbrain (Supplementary Figure 6 B). Both loci are suggestive of the aforementioned

pathways. Trigeminal nerves were also examined, but no clear presence of fluorescent siRNA was observed (data not shown).



Supplementary Figure 6. Fluorescent microscopy of the olfactory bulb and hindbrain
Confocal picture of the olfactory bulb in a treated mouse, 4 h (A) and 24 h (B) after administration of green-fluorescein siRNA-loaded chitosan nanoparticles. Confocal picture of the hindbrain in a treated mouse 4 h (C) and 24 h (D) after administration of green-fluorescein siRNA-loaded chitosan nanoparticles. Red = GLUT-1 staining (vessels), green = anti-fluorescein Ab-FITC, targeting fluorescein siRNA-loaded nanoparticles.

3.6. Transport to an intracranial glioma

As we demonstrated above, the anti-Gal-1 siRNA loaded chitosan nanoparticles can efficiently reach the central nervous system. To address the question whether a central nervous system tumor can be reached, GL261 cells were inoculated, and allowed to grow tumors for 14 days, until a solid mass is present (Figure 6). Tumor area on the section was defined via the isolectin-green staining for tumor-associated blood vessels. Vessels were dilated and seemed to lack an organized structure, suggestive for impaired blood flow and oxygen supply. In untreated control mice, no RDsiRNA could be detected (Figure 6 A). In the experimental group, mice received intranasally with RDsiRNA anti-Gal-1 siRNA loaded chitosan nanoparticles. After a single administration, an abundant RDsiRNA signal was notable

in the tumor micro environment. After 4 h this signal seemed more particulated (Figure 6 B), and after 8 h more diffuse (Figure 6 C). This figure clearly demonstrated the feasibility of reaching the tumor micro-environment via the intranasal route. Question remained if the anti-Gal-1 siRNA could reach also the tumor cells, which are besides blood vessels and macrophages, the major cell populations that produce Gal-1 in the glioma. Therefore, GL261-BFP positive tumor cells (blue) were injected. Both in the tumor center (Figure 6 D) as in the tumor border (Figure 6 E), fluorescein-siRNA signal, which corresponds to the green color could be found. Moreover, we could observe also a strong green signal associated with some vessels, despite perfusion, suggestive for presence in endothelial cells.

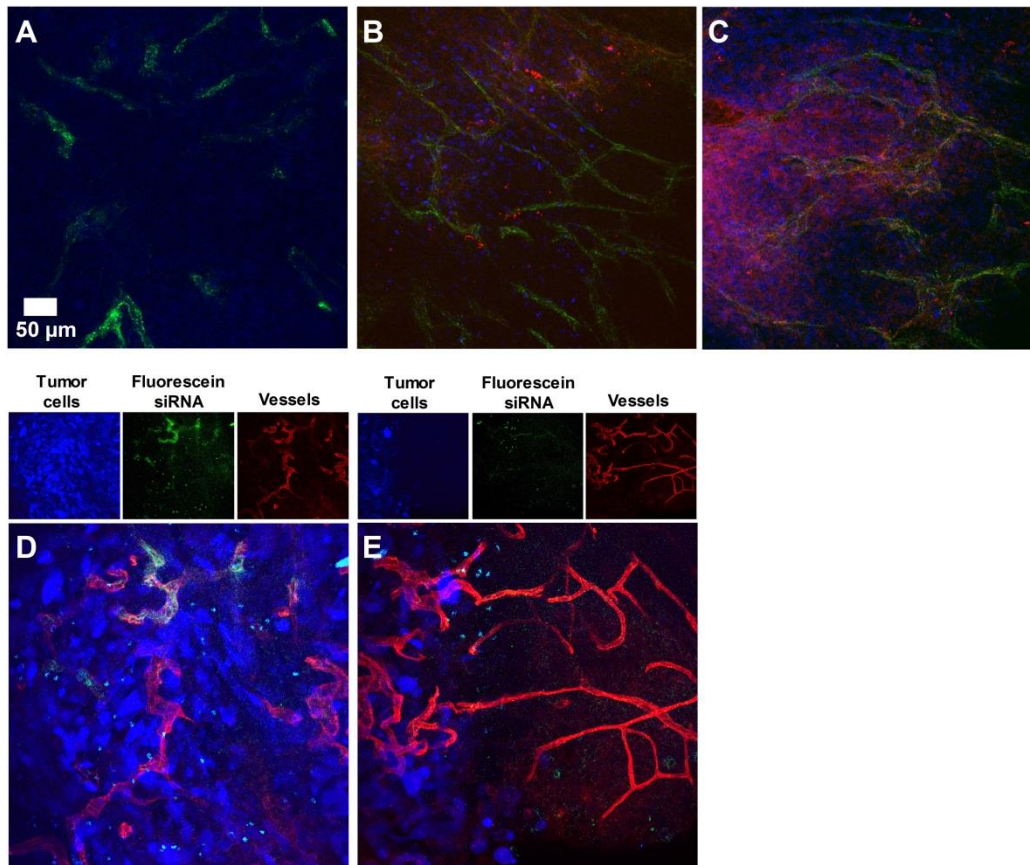


Figure 6. Rapid occurrence in the tumor micro environment. Confocal picture of (A) control untreated mouse, (B) RD-siRNA loaded chitosan nanoparticles treated mouse 4h, and after 8h (C); Red = RDsiRNA, blue = nuclei, green = vessels. Distribution/local tropism in the tumor micro environment was demonstrated by confocal picture of treated mouse 4h after the last administration fluorescein siRNA loaded chitosan nanoparticles at the tumor center (D) or border (E) of BFP-GL261 tumors; Red = vessels, blue = tumor cells, green = fluorescein-siRNA.

3.7. Intratumoral reduction of Gal-1

Next, the presence of the anti-Gal-1 siRNA in the tumor micro-environment was correlated with the functionality of the RNA interference molecules. In previous *in vitro* results, a strong decrease of Gal-1 was observed 4 to 7 days post transfection (Figure 2). This biological Gal-1 turnover was also observed in tumors after intra-tumoral injection (data not shown) of anti-Gal-1 siRNA loaded chitosan nanoparticles. Therefore, anti-Gal-1 siRNA enloaded nanoparticles were intranasally administered

until day 15 post tumor inoculation. Mice were then sacrificed at day 20 post tumor inoculation. In two independent experiments, a strong decrease of Gal-1 in the tumor micro-environment of treated mice was observed compared to control and untreated mice (Figure 7 A). Quantification of the bands, revealed a significant reduction of Gal-1 in the tumor bearing brains of mice (Figure 7 B). In a parallel experiment, mice were treated and sacrificed at day 20 post tumor inoculation for immunofluorescence staining which confirmed Gal-1 reduction (Figure 7 C + D).

3.8. In vivo evidence of RNAi in the tumor microenvironment

GeneRACE-PCR technique allows the amplification of sequence specific nucleotide-fragments via oligo-ligation. As a positive control, *in vitro* transfected RNA GL261 sample was used, 3 days after transfection (Lane 5, Figure 7 E). Two fragments were amplified, one at 481 bp (representing the intact mRNA fragment of Gal-1) and one around 280 bp (representing a cleft mRNA fragment of Gal-1). In untreated mice, this PCR resulted in 1 fragment of 481 bp (Lane 2 and 4, Figure 7 E) and in treated mice (lane 1 and 3), this PCR resulted in 2 fragments, as in the positive control, which indicates the sequence specific cleavage of Gal-1 mRNA due to the anti-Gal-1 siRNA. This finding was further supported by sequencing of the amplified fragment which revealed splicing at the siRNA binding site of the Gal-1 mRNA (Figure 7 F).

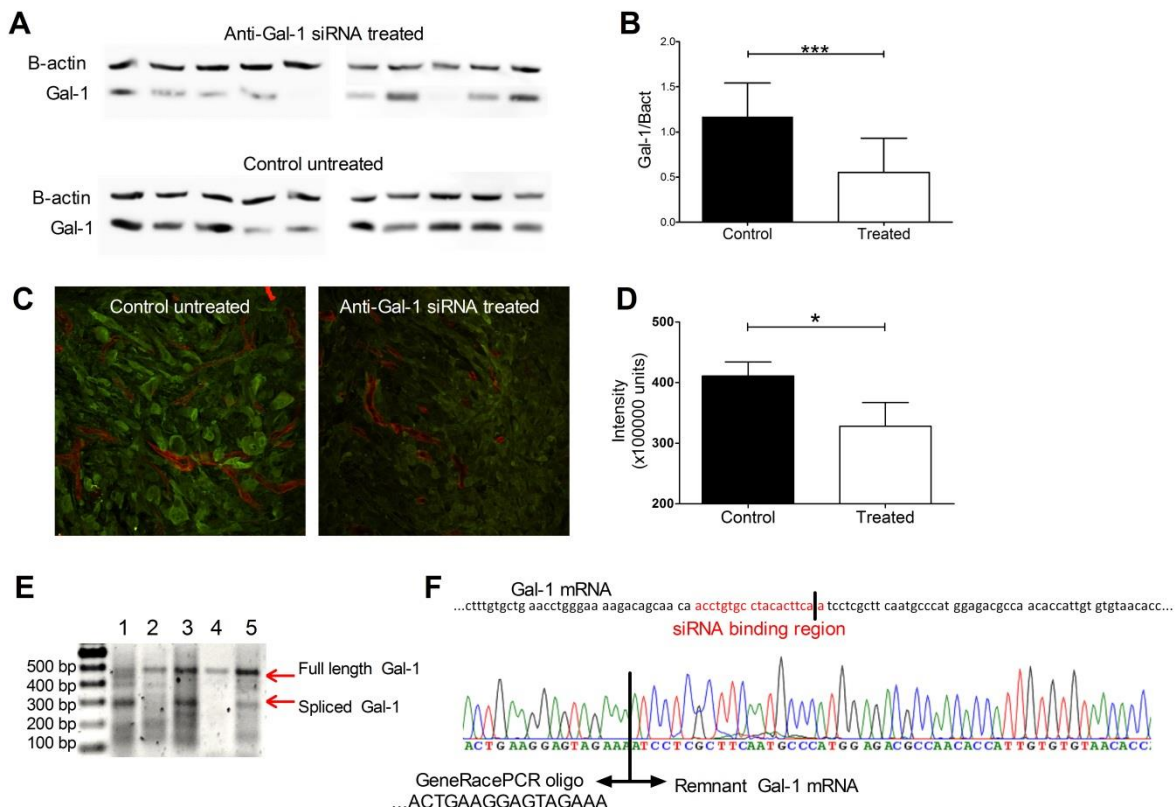


Figure 7. Specific knockdown of Gal-1. Western blot (A) and quantification (B) of mice untreated or treated with anti-Gal-1 loaded chitosan nanoparticles. (unpaired one tailed t-test; n=10/group; *** p < 0.001, blots belong to two independent experiments, and each lane is a unique mouse). Immunofluorescence illustration of tumor area (C) and quantification of picture intensity (D) of control untreated mice or of mice treated intranasally with anti-Gal-1 siRNA loaded chitosan nanoparticles,

sacrificed at day 20 after tumor inoculation. Green = Gal-1, red = Glut-1. (unpaired t-test; n=5/group; * p < 0.05). Intratumoral specific cleavage of Gal-1 mRNA revealed by **(E)** GeneRacePCR which resulted in a PCR product that corresponds to cleft Gal-1 fragment at 256-287 bp in anti Gal-1 siRNA treated mice (lane 1 and 3), while in control untreated mice (lane 2 and 4) no band was observed but the full length Gal-1 mRNA (481 bp), in lane 5 a positive control can be observed which represents mRNA of *in vitro* treated GL261 cells at day 3 post transfection. **(F)** the cleft fragment of lane 3 was subcloned, and sequenced, which indicated the mRNA fragment was cleft by sequence specific binding of anti-Gal siRNA

4. Discussion

In this study, we describe the development of anti-Gal-1 siRNA-loaded chitosan nanoparticles by ionic gelation that can: (i) protect siRNA from RNase *in vitro*; (ii) transiently open tight-junctions on an epithelial monolayer *in vitro*, with an increased macromolecule permeability across the barrier; (iii) transiently decrease the Gal-1 protein level and its expression *in vitro* on murine and human GBM cells as well as a decrease of the tumor cell motility; (iv) increase siRNA transport from the nasal cavity into the CNS, and (v) decrease Gal-1 in the tumor micro environment of glioma bearing mice.

Nanoparticles were prepared under mild conditions, which prevent degradation of the siRNA during production processes. The parameters that were critical for the nanoparticle size were polymer chain length, stirring speed and chitosan concentration. In previous reports, lower-molecular-weight chitosan has been proven to have a higher transfection potential (223). Therefore, we selected the smallest size of nanoparticles (sub 200 nm), prepared with low molecular weight chitosan, for further work. This was due to their higher bioavailability and because they are less prone to opsonisation by macrophages and dendritic cells and so display a lower risk for embolization when entering the bloodstream (224). In the literature, nanoparticles are concentrated using centrifugal filters to obtain 0.5 mg/kg as the best results (225). By using ultracentrifugation and lyophilization, we concentrated the nanoparticles to a higher degree (i.e. 1.92mg/kg), with a minimal loss of siRNA. Afterwards, we evaluated the best conditions for freeze-drying the nanoparticles. For this, we used different concentrations of different lyoprotectants (i.e. sucrose, trehalose, mannitol), and based conditions on solubility and protection of the nanoparticles. The optimal conditions were to use sucrose as the lyoprotectant at 500 mg/mL. In terms of protection from degradation, the stability of siRNA in contact with RNases was equal to literature reports (217).

When applying siRNA-loaded chitosan particles to GBM cells, a rapid attachment to the cells was observed, in conformity with literature reports (134, 226). This was in strong contrast to non-formulated siRNA, which failed to attach to the cells, and most likely was degraded by the cell culture medium. However, the localization of the siRNA-loaded chitosan nanoparticles on the cells does not necessarily result in an uptake (227). To evaluate whether the particles are also taken up by the GBM cells, Gal-1 mRNA and protein levels were assessed in the murine cell line, and the protein level was assessed for six individual primary tumor cell cultures. In this study, we described for the first time the ability of chitosan nanoparticles to decrease Gal-1 for several days in both murine and human glioblastoma cells. As a control, the specificity of the siRNA via Galectin-3 western blot analysis was checked, and no significant decrease of Gal-3 was observed. Other Gal-1 targeting strategies, such as Davanat, did show affinity to Gal-3, although binding occurred at another side than the beta-galactoside domain of

Gal-3 (69). The mechanism of the siRNA release from the chitosan polymer is most likely to rely on the proton sponge effect, creating lysosomal damage by scavenging of H⁺ by the primary amines of the chitosan polymer (228). Furthermore, we were able to confirm the effect on migration of GBM cells when Gal-1 was reduced (208).

For the purpose of intranasal administration, and reaching the CNS, it will be mandatory to transiently disturb the epithelial layer (216). Under physiological conditions, the olfactory and respiratory epithelia in the nasal mucosa form an impermeable barrier for exogenous substances. This barrier is firmly interconnected via tight-junctions (229, 230). Chitosan has already been widely described as a permeation enhancer, and the results of this study confirm these reports (114, 219, 231). In line with these findings, we confirmed its ability to decrease the TEER over these monolayers and increase the flux of macromolecules. More importantly, we observed similar results in lung epithelium cells (Calu-3) as in primary nasal epithelium cells, underlining the common mechanistic effects of chitosan on epithelial barriers. These effects were most likely caused by the internalization of tight junction complexes (231). Remarkably, we found that the chitosan formulation can increase the flux of FD4 without affecting the TEER, underlining the complex organization in the paracellular spaces.

For *in vivo* assessment, transport across the nasal mucosa and into the central nervous system was demonstrated. In this study, a rapid spread of the formulation was observed in the nasal mucosa, while in control untreated mice, no fluorophore was observed. As depicted in Figure 5 and supplementary Figure 5, the accumulation of nanoparticles was observed on the mucosa, with a particle-shape presence. There was also a clear passage through the epithelial cells and into the lamina propria. To evaluate the distribution into the CNS, we first focused on the olfactory bulb, as this is the main entry route. Via DAPI nuclei staining, we could clearly distinguish the glomerular layer, characterized by profound round-shaped organizations, if the bulb was dissected to its full extent. These pictures were in line with previous reports of intranasal delivery, although the latter were based on other formulations or no formulations (232, 233). We observed a strong and increasing signal from the dye-547 siRNA 4 h and 8 h after a single administration. These pictures clearly underline the importance and feasibility of direct transport from the nasal cavity to the CNS via the olfactory pathway. Next, we were also interested to find the presence of siRNA in the hindbrain, as an alternative pathway to the CNS via the trigeminal nerves. To further amplify our signal, we stained the fluorescein-labeled siRNA with an FITC-coupled anti-fluorescein antibody. In these experiments, we confirmed siRNA's presence in the olfactory region, but we also found a profound signal from the siRNA in the hindbrain, 4 h and 24 h after a single administration. The question remains whether the signal we observed is siRNA formulated into particles, or released siRNA that travels as single molecules. Previous research with intraventricular osmotic mini-pump infusion revealed that non-formulated siRNA can induce a specific knockdown in the CNS (213).

In the presented work, monitoring the influx of anti-Gal-1 siRNA inside the tumor micro-environment was shown to be feasible. Vast presence of the fluorophore-tagged siRNA was demonstrated 4 h after intranasal administration. To explain this rapid distribution in the central nervous system after intranasal administrations multiple pathways are likely to be contributing (84, 114). A major

determinant is the direct transport via the olfactory, and to a lesser extent the trigeminal pathway. Local accumulation at these sides was demonstrated, suggestive for a direct, paracellular transport. From there, a rapid spread can occur via the cerebro-spinal fluid circulation. On the other hand, parenchymal diffusion might also explain distribution into surrounding brain areas. For delivery of intranasal administered stem cells for the treatment of glioma, chemo-attractants will be of key importance (127). Besides this direct route, transport can occur via the systemic distribution. The nasal mucosa is well vascularized and chitosan is considered a potent absorption and permeation enhancer (216). So besides promoting the direct transport towards the olfactory bulb, there can also be leakage into the systemic vasculature. This systemic circulation can explain the vessel-associated signal of siRNA we observed. In GBM biology it becomes more evident that the integrity of the blood brain barrier is no longer intact, and that this can increase the delivery of anti-Gal-1 siRNA (234). Whether the passage of anti-Gal-1 siRNA via this pathway, is cell-mediated, or rather happens as sole molecules and particles, still remains a question. We also noticed that at a later time point (8h), the dotted like structure is less apparent, and the fluorophore tagged anti-Gal-1 siRNA is more diffusely spread out. This can be explained by the disassembly of the particles under physiological pH-values, or the de-aggregation of multiple nanoparticles clotted by blood components. In more detail, the intense fluorophore-tagged siRNA signal was observed which is localized in the tumor micro-environment that correlates with the presence of tumor cells. For these experiments, we used GL261-BFP cells, and the blue signal of the tumor cells did co-localize with the green fluorescent signal of fluorescein-tagged anti-Gal-1 siRNA. Moreover, in these pictures strong presence was to be noted in the vasculature of the tumor associated vessels. As described, these mice were perfused prior to fixation, so the signal is either firmly attached to the endothelial cells, or inside the endothelial cells. This un-anticipated localization can be beneficial, due to the vast expression of Gal-1 by the tumor associated vessels (209). Several stimuli such as hypoxia, or secretion of IL-1beta, TNFalpha can lead to endothelial cell activation (64). Moreover, Gal-1 is considered an angiogenic factor as recently demonstrated by Croci et al (65).

In terms of bio-activity of the construct, we already demonstrated that *in vitro* the anti-Gal-1 siRNA loaded chitosan nanoparticles can reduce Gal-1 in GL261 cells in low quantities up to 20 nM. From previous research, GL261 model is known to grow tumors as fast as 20 days post tumor inoculation, so the timeframe to interfere with tumor-growth is only limited (221). Therefore, we chose to administer the anti-Gal-1 siRNA loaded chitosan nanoparticles at day 5, 8, 12 and 15 after tumor inoculation. Moreover, from our *in vitro* data, it takes 4 to 7 days post transfection before Gal-1 is notably decreased on the protein level. So in our experimental design, the mice were sacrificed at day 20 post tumor inoculation (and 5 days after the last intranasal administration). We observed a strong significant decrease of Gal-1 in treated mice, suggesting a specific knockdown. Furthermore, Gal-1 protein reduction was confirmed via immunofluorescence on vibratome sections. On mRNA level, we found that there was less Gal-1 mRNA in the treated group, however this was not significant. This might be due to the timing of sampling, as described in our *in vitro* data; mRNA is degraded especially the first 48h after transfection, and recuperates in the following days. Moreover, we noticed that in some *in vitro* experiments there can be a rebound expression during the recuperation phase. Despite

no significant *in vivo* Gal-1 reduction could be found on mRNA level (for the dose and frequency of administration used in these experiments), we were able to demonstrate the sequence specific cleavage of the Gal-1 mRNA via GeneRACE PCR technology. Sequencing of the remnant Gal-1 mRNA fragment, revealed cleavage nearby the anti-Gal-1 siRNA binding sequence. In previous reports, the exact site of degradation was mentioned as 10 bp upstream the siRNA binding region (222). Subcloning of our GeneRACEPCR product revealed many different cleavage sites, all close to the siRNA binding sequence. In part, this might represent also partially degraded mRNA fragments as a result of the siRNA induced degradation of Gal-1 mRNA.

5. Conclusion

In this study, we describe for the first time that a highly concentrated suspension of siRNA-loaded chitosan nanoparticles is an excellent formulation for delivering anti-Gal-1 RNA interference technology into the central nervous system. The ease of chitosan nanoparticle manufacturing does not affect the effectiveness of siRNA molecules and delivers siRNA rapidly into murine and human GBM cells, leading to a reduced migration of the tumor cells. On the epithelial cells monolayer, we observed a modulation of the tight junctions, and higher passage through the monolayer. These behaviors were most likely due to internalization of ZO-1. After intranasal administration in healthy mice, we observed a rapid spread into the nasal mucosa, and furthermore into the olfactory bulb and the hindbrain. Most striking was the substantial amount of labeled formulation that could be observed 4 h after administration. Moreover, we were able to show the intratumoral distribution of anti-Gal-1 siRNA into orthotopic GBM grafted tumor-bearing mice, where Gal-1 was selectively reduced as monitored by several techniques. These results underline the feasibility of the intranasal pathway to deliver biological active agents to central nervous system neoplasms such as glioblastoma.

6. Acknowledgements

The authors wish to thank IWT Flanders (SBO; Strategisch Basis Onderzoek – research grant 121206), BBTS (Belgian Brain Tumor Support), Olivia Hendrickx research fund (www.olivia.be), the Herman Memorial Research fund and the James E. Kearney Foundation for their funding of this study. RK is a Director of Research with the Fonds National de la Recherche Scientifique (FRS-FNRS; Belgium).

4. RESULTS – PART2 – PAPER2

Sensitization of glioblastoma tumor micro-environment to chemo- and immunotherapy by Galectin-1 intranasal knock-down strategy

In our previous work, we have shown that it is feasible to reach the central nervous system and more in particular the TME, via intranasal administration in a murine GBM model. Moreover, we could demonstrate a sequence specific cleavage of Gal-1 mRNA, which provides additional evidence that siRNA molecules reach their target and are fully active. This pivotal achievement, strengthened our belief in this project, and we pursued to look further into the TME modulation caused by Gal-1 decrease. In this regard, we concentrated on the immune compartment where Gal-1 is known to be of high relevance. Whereas a large pool of data exists on Gal-1 and the lymphoid (adaptive) arm of immunity, little is known about the effects on the myeloid (innate) counterpart. We focused on the M1/M2 axis, as these cell populations are gaining momentum in GBM biology as respectively pro-inflammatory and anti-inflammatory cell types. Furthermore, we highlighted also the possibility of treating GBM with checkpoint inhibition such as anti-PD-1, which is nowadays by far the most popular immunotherapeutic intervention in solid-tumor oncology.

With this background in mind, we prepared a study with the following aims

- I. To study in a detailed manner the myeloid landscape after decreasing Gal-1, more importantly with a focus on M1 and M2 balance;
- II. To determine if there are also changes to be observed on the lymphoid counterpart, both on the suppressive side (Treg, FoxP3+), as on the activation side Th1 (CD4, IFN- γ) and CTL (CD8, IFN- γ);
- III. To evaluate if these changes in the immune contexture of TME are relevant enough to alter the survival curve of tumor bearing mice, this can be in monotherapy, or in combination therapy with either TMZ, DC vaccination and PD-1 blocking;
- IV. To elucidate the underlining mechanisms by which possible synergistic effects between decreasing Gal-1 and chemo-immunotherapy can be caused

The research paper discussing the results of this section is presented on the following pages and the supplementary figures are depicted afterwards – at the moment of writing, this manuscript was under revision at OncoImmunology

Sensitization of glioblastoma tumor micro-environment to chemo- and immunotherapy by Galectin-1 intranasal knock-down strategy

Matthias Van Woensele (1,2,*) & Thomas Mathivet (3,4,*), Nathalie Wauthoz (2), Rémi Rosière (2), Véronique Mathieu (5), Robert Kiss (5), Florence Lefranc (6), Louis Boon (7), Jochen Belmans (8), Stefaan W. Van Gool (9), Holger Gerhardt (3,4), Karim Amighi (2), Steven De Vleeschouwer (1,10)

Affiliations

- (1) Research Group Experimental Neurosurgery and Neuroanatomy, KU Leuven, Herestraat 49, Leuven 3000, Belgium;
- (2) Laboratoire de Pharmacie Galénique et de Biopharmacie, Université libre de Bruxelles (ULB), Boulevard du triomphe CP207, Brussels 1050, Belgium;
- (3) Vascular Patterning Unit, VRC, VIB, Herestraat 49 box 912, Leuven 3000, Belgium
- (4) Vascular Patterning Laboratory (Vesalius Research Center), Department of Oncology, KU Leuven, Herestraat 49 box 912, Leuven 3000, Belgium
- (5) Laboratoire de Cancérologie et de Toxicologie Expérimentale, Université libre de Bruxelles (ULB), Boulevard du triomphe CP205/01, Brussels 1050, Belgium;
- (6) Department of Neurosurgery, Erasmus University Hospitals, Route de Lennik 808-1070, Brussels 1050, Belgium;
- (7) EPIRUS Biopharmaceuticals, BV, Yalelaan 46, Utrecht 3584, The Netherlands;
- (8) Laboratory of Pediatric Immunology, KU Leuven, Herestraat 49 box 811, Leuven 3000, Belgium;
- (9) Medizinische Leitung der Translationalen Onkologie, Immunologisches Onkologisches Zentrum, Köln, Germany;
- (10) Department of Neurosurgery, University Hospitals Leuven, Herestraat 49 box 7003, Leuven 3000, Belgium.

* Authors share first authorship; equal contribution

Acknowledgments & Grant Support

The authors wish to thank IWT Flanders (SBO; Strategisch Basis Onderzoek – research grant 121206), BBTS Belgian Brain Tumor Support), The Olivia fund (www.olivia.be), the Herman Memorial Research fund (HMRF) and the James E. Kearney Foundation for their funding of this study. RK is a Director of Research with the Fonds National de la Recherche Scientifique (FRS-FNRS; Belgium). HG and TM are supported by Stichting Tegen Kanker (STK) and an ERC consolidator grant (REshape 311719).

TEXT MANUSCRIPT

ABSTRACT

The glioblastoma (GBM) tumor micro environment (TME) overexpresses Galectin-1 (Gal-1) which drives chemo- and immunotherapy resistance. We designed siRNA targeting *gal-1* (siGal-1) loaded chitosan nanoparticles that promote a direct nose-to-brain transport, and successfully silence *gal-1* in the brain TME. This reduction induces a remarkable switch in the TME contexture where myeloid suppressor cells and regulatory T cells were reduced, while CD4+ and CD8+ T cells were increased. *gal-1* knock-down seems to reduce macrophages' polarization switch from M1 to M2 during GBM progression. These changes result in a tumor vasculature normalization and modest increase in survival for tumor bearing mice. The rational combination of intranasal siGal-1 treatment with temozolomide and immunotherapy such as dendritic cell vaccination or PD-1 blocking results in synergistic effects and drastically increases the survival of tumor bearing mice. These findings provide evidence that Gal-1 could be a valuable adjuvant clinical target to further increase the efficiency of checkpoint blockade and chemotherapy.

INTRODUCTION

Central nervous neoplasms are subtyped in either primary or secondary brain tumors. Within the primary tumors, glioblastoma multiforme (GBM) is the most prevalent high grade glioma (1, 2). GBM carries the hallmark of a high grade neoplasm with highly necrotic, hypoxic and mitotic areas (4). Current therapy consists of debulking, followed by chemoradiotherapy, and results in a median survival of 14.6 months (8). Novel treatment regimens have entered the clinical arena, but none has shown drastic impact on GBM patient survival (196). Especially the field of immunotherapy seems to offer a promising avenue. Dendritic cell (DC) vaccinations have been explored, in many centers including ours, and a recent meta-analysis suggests a small, long-term beneficial impact of DC mediated immunotherapy (36, 39, 201). Recently, numerous clinical trials are recruiting patients for checkpoint inhibition in GBM such as Programmed Cell Death protein-1 (PD-1) blocking (ClinicalTrials.gov identifier: NCT02335918, NCT02529072).

Despite the high numbers of clinical trials, and novel biological compounds, patients' prognosis remains unchanged. In order to have new biological therapies active at the tumor site, more research is needed to understand the peculiar dynamics which are created in the tumor micro environment (TME) of a GBM. Consensus is arising that the GBM TME is a highly tumor-promoting and immune-evasive locus in the central nervous system. In particular, intensive research has been done about Galectin-1 (Gal-1) in the TME of GBM (44, 235). Gal-1 is a 14 kDa lactose binding lectin, which has been proven to play a pivotal role in the promotion of GBM. Increasing the migration and resistance against chemotherapy (i.e. temozolomide, TMZ) of GBM cells are well accepted key features of Gal-1 (61, 206, 210). Moreover, the immunosuppressive and angiogenic properties of Gal-1 in the context of GBM have been well documented (61, 207).

As a non-invasive alternative route to deliver therapeutic agents into the central nervous system, and more specifically into the TME of GBM, we proposed the nose-to-brain transport via intranasal administration (214). Previously we described that chitosan nanoparticles are able to transport siGal-1 to the GBM TME where we observed a sequence specific reduction of *gal-1* expression (236).

This study aimed to investigate the consequences of reducing Gal-1 in the TME during the GBM progression on both myeloid and lymphoid compartments of the immune system. Moreover, we evaluated the effect on survival for tumor bearing mice, either in siGal-1 monotherapy or in combination with temozolomide and immunotherapy as DC vaccination and PD-1 blocking. Our findings identify Gal-1 as a key-hub regulator of the TME that drives resistance towards conventional chemotherapy and explorative immunotherapy. Nose-to-brain delivery to modulate the TME is an underexplored treatment modality and beholds great promise for GBM patients, especially when combined with chemo- and immunotherapy.

RESULTS

To investigate the role of *gal-1* expression in GBM tumorigenesis, we first assessed whether its presence is linked to changes in the myeloid compartment of TME infiltrating leukocytes. Via flow cytometry, a reduction in CD11b+ leukocytes from 37 to 28% was detected when mice were treated with intranasal siGal-1 (Fig. 1A; gating strategy Supp Fig1). Further subtyping revealed that this reduction was mainly caused by a reduction in immune suppressive monocytic myeloid derived suppressor cells (MDSCs) defined as Ly6C+CD11b+ leukocytes from 26 to 20% (Fig. 1B). In granulocytic MDSCs (Ly6G+CD11b+) no major alterations were noticed. Besides MDSCs in the TME, also macrophages can exert immune suppressive functions. In particular, macrophages can be subtyped in M1 (MHCII^{high}, MRC-) or M2 (MHCII^{low}, MRC+) from which the latter are known to reduce inflammation and worsen the prognosis in GBM. Via flow cytometry, we found that reduction of Gal-1 promotes the M1 phenotype, and prevents the M2 phenotype (Fig 1C + 1D). Also in immunofluorescence staining, we found that Gal-1 plays a role in M1 to M2 macrophages switch (Fig 1E). Reducing *gal-1* expression resulted in abundantly more M1 macrophages than M2. This effect was most pronounced during the late stage of GBM in our murine model. Quantification revealed that the total pool of F4/80+ macrophages is not affected, whereas the M1 vs. M2 polarity is greatly altered at late stage GBM (Fig 1F). Moreover, as an extra control, we could not detect any effect of scrambled siRNA loaded chitosan nanoparticles.

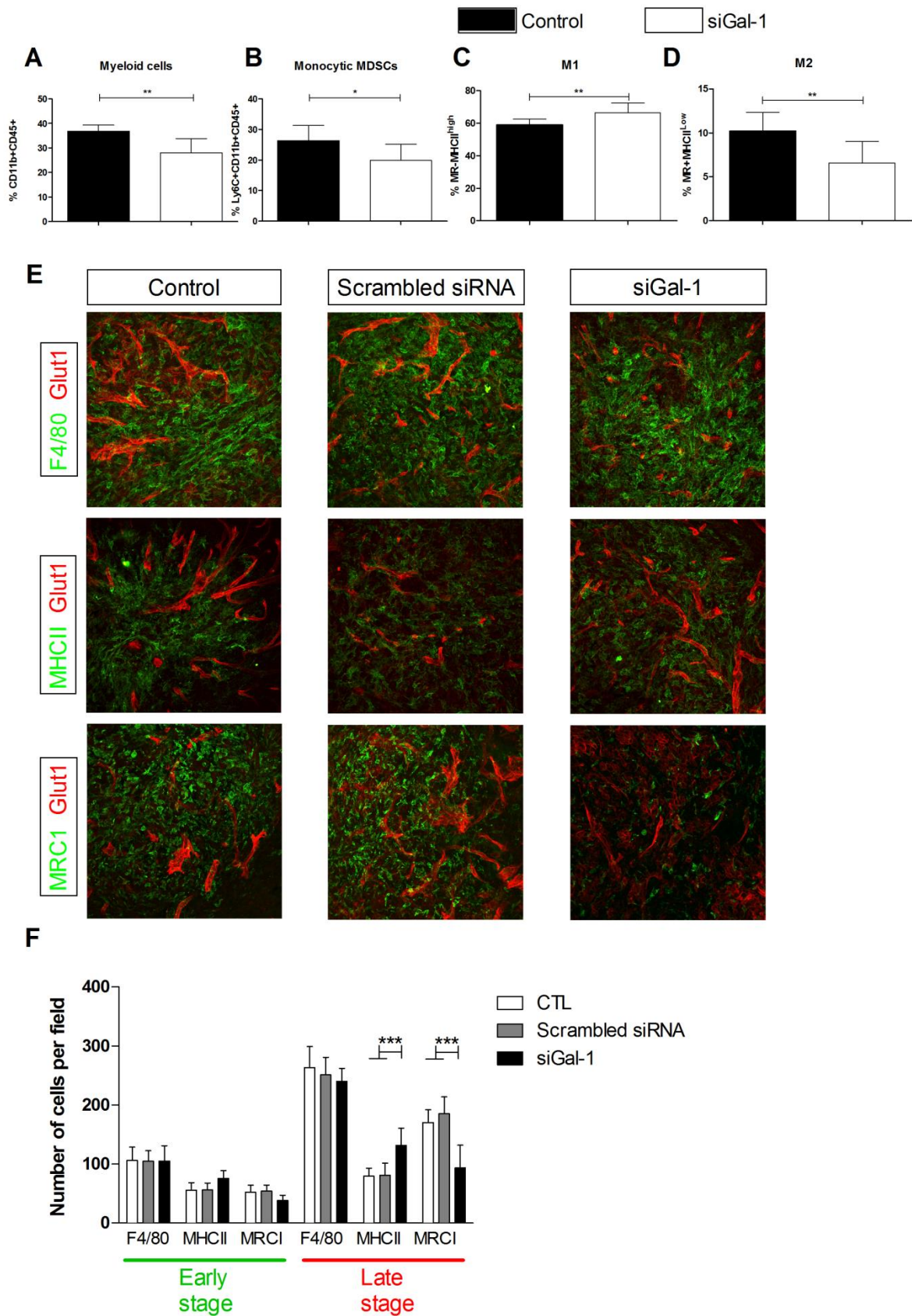


Figure 1 : Effect of *gal-1* knock-down the myeloid cell population during GBM progression. Flow cytometry was performed on isolated mononuclear brain infiltrating cells of mice that were left untreated, or treated with siGal-1 on day 4, 8, 12 and 15 after tumor inoculation, and brains were

isolated at day 20. Different stainings assess several cell populations with (A) the myeloid cells, as gated by ZY-, CD45+, CD11b+; (B) monocytic MDSCs as ZY-, CD45+, CD11b+, Ly6C+; (C) M1 macrophage phenotype as CD45+, CD11b+, ZY-, MRC-, MHCII^{high}; as % of CD11b+ (D) M2 macrophage phenotype as CD45+, CD11b+, ZY-, MRC+, MHCII^{low}: as % of CD11b+. In panel A-D, white bars represent the treated mice, and groups were compared with unpaired t-test (* = $p < 0.05$, ** = $p < 0.01$). (E) Confirmation of the panel C and D via immunofluorescence, which indicates that the total amount of macrophages in the TME is not affected, but merely the polarization of M1 to M2 polarization. MRC1+ M2 macrophages are reduced with siGal-1 therapy, as compared to untreated or scrambled siRNA treated mice (F) Quantification of multiple sections of several mice ($n = 4$ /group), indicates the effect is most pronounced at late stage GBM (day 20 after tumor inoculation, with 4 administrations at day 4, 8, 12 and 15), whereas in early stage (day 12 after tumor inoculation; 2 administrations, at day 4 and 8) these differences were less pronounced. Black bars represent treated mice, white bars are untreated controls, and gray bars are treated with scrambled siRNA; groups were compared via two way ANOVA, with Bonferroni post test as compared to control and scrambled siRNA (***) = $p < 0.001$).

Given the previously mentioned alterations in the immune suppressive myeloid cells, we subsequently looked into the lymphoid counterpart and monitored the regulatory T cell population (Treg). Both on mRNA as on protein level, we detected a decrease of FoxP3+ cells, which is a transcription factor for Treg (Fig 2A + 2B; gating strategy Supp Fig 2). Conclusively, these data indicate a general reduction of immunosuppression in GBM, in both the innate and adaptive arm of immunity, when *gal-1* expression is reduced.

On the other side of the spectrum, we have investigated the immune stimulatory mediators in GBM. Overall, we found a decrease in leukocytes (CD45+ viable cells; Fig 2C; gating strategy Supp Fig 3), which we mainly attribute to the decrease in overall myeloid MDSCs and M2 macrophages. Further co-staining revealed a significant increase in CD3+ lymphocytes (Fig 2D). In detail, we found a general increase in helper T (Th, CD4+CD3+ lymphocytes), and cytotoxic T cells (CTL, CD8+CD3+ lymphocytes) (Fig 2E + 2G). These cells were not only increased as percentage, but also in functional gain, as measured by their interferon- γ (IFN γ) production, indicated as Th1 (CD4+) and CTL (CD8+) lymphocytes relative to the total amount of leukocytes (Fig 2F + 2H). A major limitation of flow cytometry being the absence of absolute cell number information, the calculation of ratios strongly indicate relevant qualitative changes in the TME. Hence, we calculated the percentage of Th1 to Treg, and CTL to Treg, as an indication of how the balance between immune activation and immune suppression is situated (Fig 2I + 2J). For both categories we observed a significant shift towards immune activation, underlining the role of Gal-1 as a potent immune-suppressor.

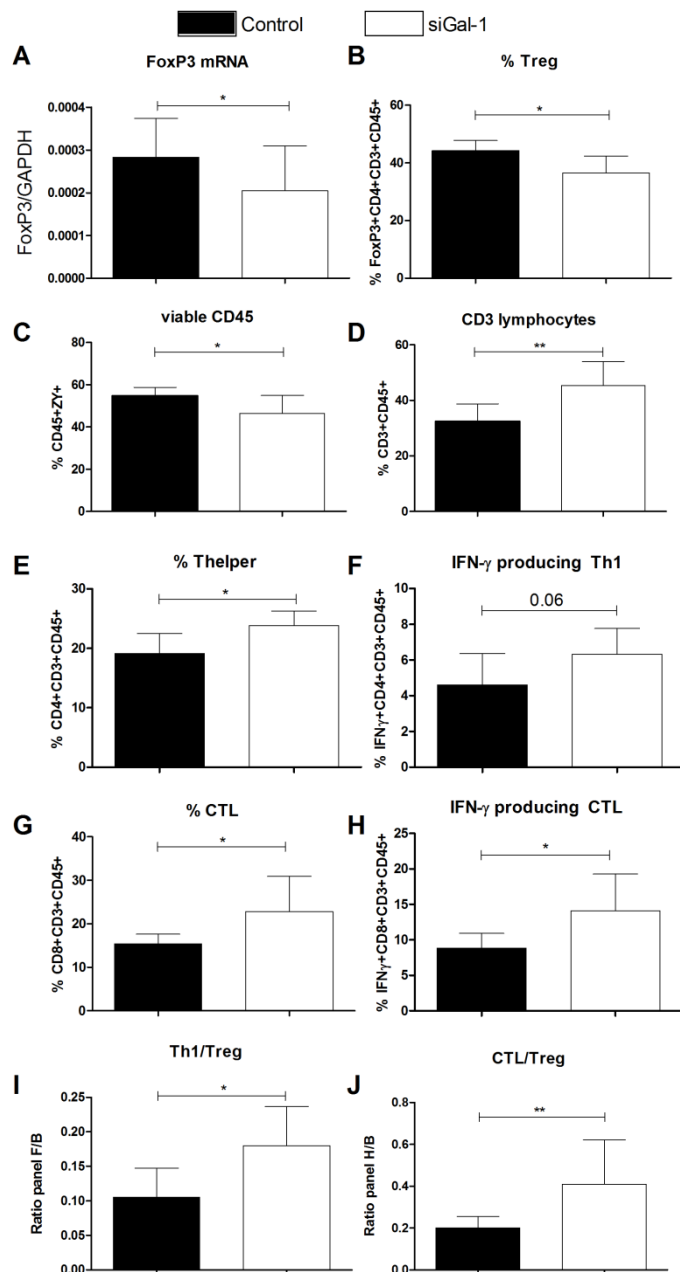


Figure 2 : Effect of *gal-1* knock-down on the lymphoid cell population during GBM progression. RT-qPCR was performed on isolated GBM specimen of mice that were left untreated, or treated with siGal-1 on day 4, 8, 12 and 15 after tumor inoculation, and brains were isolated at day 20 (A) , which revealed a significant reduction for *foxP3* transcription factor expression (n = 10/group, * = p < 0.05). Flow cytometry was performed on isolated mononuclear brain infiltrating cells of mice that were left untreated, or treated with siGal-1 on day 4, 8, 12 and 15 after tumor inoculation, and brains were isolated at day 20. Different stainings assess several cell populations with (B) Tregs, as gated by single cells, ZY-, CD45+, CD3+, CD4+, FoxP3+; (C) Leukocytes, as single cells, ZY-, CD45+ (D) Lymphocytes as single cells, ZY-, CD45+, CD3+; (E) Thelper as single cells, ZY-, CD45+, CD3+, CD4+; (F) Th1 as single cells, ZY-, CD45+, CD3+, CD4+, IFN γ + gated to CD45+; (G) CTL as single cells, ZY-, CD45+, CD3+, CD8+; (H) CTL as single cells, ZY-, CD45+, CD3+, CD8+, IFN γ + gated to CD45+. To evaluate the relative presence of immune activation vs. suppression, ratios were calculated that reveal a significant shift for (I) Th1 vs. Treg and (J) CTL vs. Treg. White bars represent the treated mice, and groups were compared with unpaired t-test (n = 5/10/group, * = p < 0.05, ** = p < 0.01).

We observed in previously published results that reducing *gal-1* expression can inhibit the migration and/or proliferation pattern of GL261 murine GBM cells *in vitro* (236). In combination with the remarkable changes in TME contexture as observed above, we assessed the possible survival benefit in GL261 tumor bearing mice. First, we asked whether intranasal siGal-1 as monotherapy could induce a survival benefit (+siRNA, Fig 3A). We observed a significant shift in survival when siGal-1 loaded chitosan nanoparticles were administered during GBM progression. A small shift in median survival was induced of 2.5 days, and more importantly, about 20% long-term survival was induced. As a negative control, empty chitosan nanoparticles were also administered (-siRNA, Fig 3A), and failed to induce a survival benefit.

As mentioned earlier, reducing *gal-1* expression has been shown to improve the efficacy of chemotherapeutic drugs such as TMZ. After three administrations of 40 mg/kg we observed a significant median survival shift for glioma bearing mice, from 19 days in untreated mice, to 32 days in TMZ treated mice (Fig 3B). Combining the intranasal siGal-1 administration and per os TMZ administration resulted in synergistic survival benefit. In the combination therapy, median survival increased from 32 days in TMZ treated mice, to 53 days in siGal-1 and TMZ treated mice. We also observed in this experiment a long-term survival of 40% whereas in monotherapy we could only observe about 20% long-term survival. These results indicate that reducing *gal-1* expression could apply as an adjuvant treatment modality to TMZ administration.

As indicated above, monotherapy that reduces *gal-1* expression could clearly shift the balance from immune suppression to activation; resulting in a modest survival benefit (Fig 3A). Rational combination of this siGal-1 sensitization technique with other immunotherapies seemed appealing. Therefore we started with a prophylactic vaccination model established in our facilities (221). Mice were vaccinated two weeks before tumor inoculation with lysate pulsed DC vaccines which results in strong anti-tumoral immunity as indicated by the survival benefit of 20.5 days in untreated mice, to 42 days in DC vaccine treated mice (Fig 3C). We observed that combining DC vaccine with siGal-1 could further push the significance level, and increase median survival to 53 days with about 30% long-term survival. Statistical difference could not be observed between DC vaccine and the combination therapy, largely attributed to the heterogeneous effect of DC vaccine. As a second immunotherapy approach, we tested checkpoint blockade by means of PD-1 blocking in established brain tumors. Intraperitoneal injection of anti-PD-1 antibody could increase the survival from 17.5 days in untreated mice, to 30 days in anti-PD-1 treated mice (Fig 3D). Concomitant intranasal administration of siGal-1 drastically improved the therapeutic effect of anti-PD-1 administration, resulting in a median survival of 51.5 days and about 20% long term survival. We conclude from these data that siGal-1 therapy is effective in rational combination with immunotherapy.

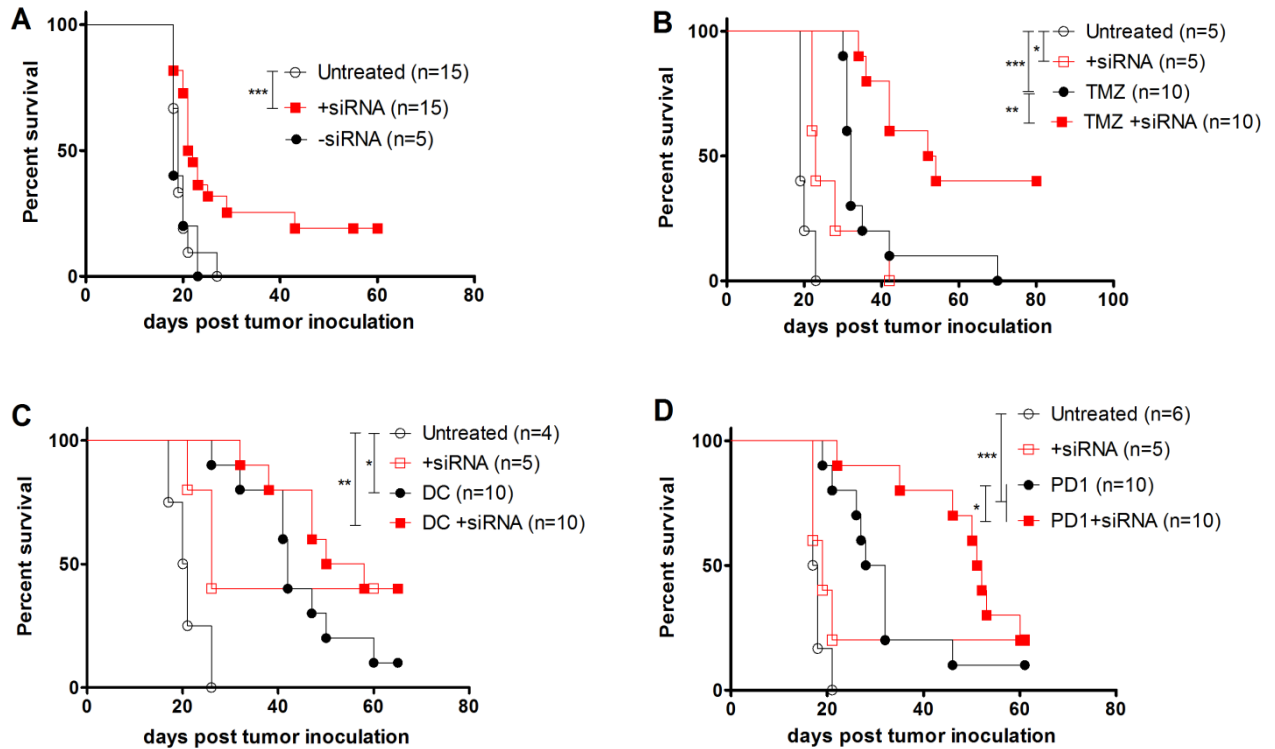
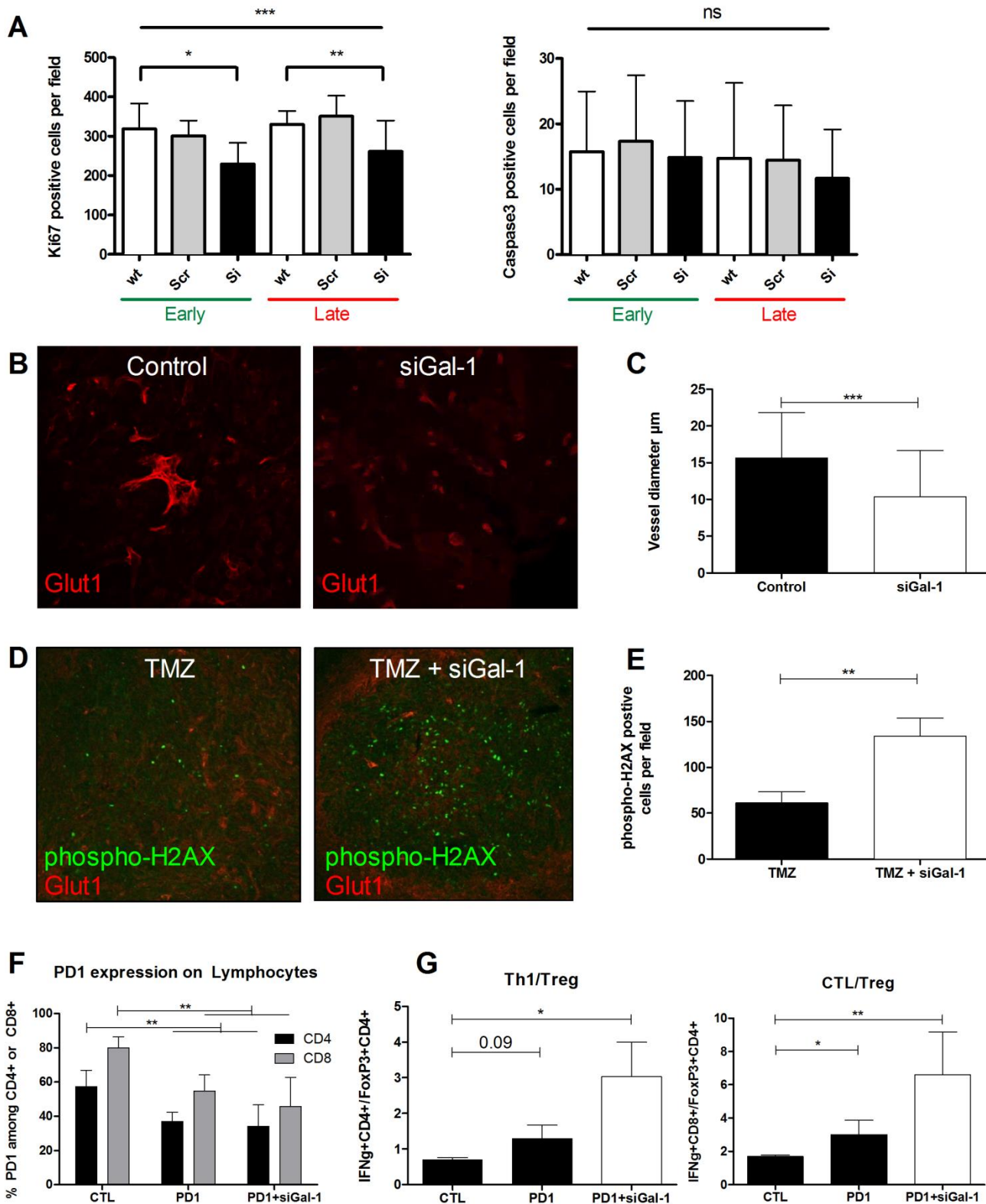


Figure 3 : Survival benefit of siGal-1 monotherapy, or in combination with chemo- and immunotherapy. Mice were inoculated with 0.5×10^6 GL261 cells which induce a lethal GBM after 15-20 days. (A) Mice were left untreated (clear dots), treated with siGal-1 on day 4, 8, 12 and 15 after tumor inoculation (red squares), or treated with empty nanoparticles (without siRNA, black dots). Combination strategy with (B) TMZ was organized by siGal-1 administration at day 2, 4, 7 and 11 after tumor inoculation prior to TMZ administration at day 8, 11 and 15, at a dose of 40 mg/kg. For combination with immunotherapy, DC vaccination (C) and PD-1 blocking (D) were included. In (C), mice received monotherapy siGal-1 as described in panel A (open red squares), prophylactic DC vaccination at day -14 and -7 before tumor inoculation (200 μ g lysate/million DCs, IP, black dots), or the combination of DC vaccination and siGal-1 (closed red squares). In (D), mice received anti-PD-1 mAb at day 7 and 12 after tumor inoculation (100 μ g/day, IP, black dots) or the combination of PD-1 blocking and siGal-1 (closed red squares). Curves were compared by Log-Rank survival analysis. (n = as indicated, * = $p < 0.05$, ** = $p < 0.01$ and *** = $p < 0.001$).

Above, we observed a small survival benefit for mice that received monotherapy siGal-1 (Fig 3A). We therefore measured the proliferation of GL261 tumors when untreated (CTL) or treated with scrambled (Scr) or siGal-1 (Si), via Ki67+ proliferation stainings on early and late stage GBM, as explained in Figure 1F (Fig 4A left; pictures Supp Fig 4). Here we noticed that siGal-1 therapy inhibits proliferation already after day 12 post tumor inoculation. Furthermore, no changes in apoptosis were observed, via Caspase3 staining (Fig 4A, right; pictures Supp Fig 5). Moreover, we observed a strong synergistic effect of reducing *gal-1* expression in combination with chemo and immunotherapy. To this end, we tried to elucidate the underlying attributing factors that drive this synergy. To explain the synergy with chemotherapy, we noticed that TME associated vessels in the tumor bearing mice that were treated with siGal-1 were healthier than in untreated mice (Fig 4B). In untreated control mice, tumor vasculature present typical features of dilated and leaky vessels whereas *gal-1* targeting therapy significantly reduces vessels caliber (Fig 4C). This phenotype could also be observed in the

experiment mentioned in Fig 1E. Large TME blood vessels are typically poorly perfused, and induce vascular shunts, and therefore we hypothesized that TMZ could reach a larger tumor volume if vessels showed a normalized appearance. To observe the distribution pattern of TMZ, we prepared immunofluorescence staining for DNA damage via co-staining for phospho-H2aX, which stains double strand break repair mechanisms (Fig 4D and E). As indicated by the green dots, equal dose of TMZ could affect a larger tumor area, and induce aggravated DNA damage, when pre-treated with siGal-1, causing a healthier vasculature.

To elucidate the contributing factors that explain the synergy between siGal-1 therapy and anti-PD1 therapy, we performed flow cytometry analysis of tumor infiltrating lymphocytes. We observed that anti-PD1 therapy can effectively reduce the expression of PD-1 on CD4+ and CD8+ lymphocytes (Fig 4F). Next, we observed that the ratio between Th1 response and Treg, or CTL and Treg, was increased upon anti-PD-1 therapy, and even more pronounced after the combination therapy (Fig 4G). These data indicate that anti-PD1 therapy by itself can stimulate the immune activation, as also indicated by the survival benefit in Figure 3D and that the combination of siGal-1 therapy and anti-PD1 therapy can further increase the immune stimulation.



inoculation (right panel), and stained for GLUT-1 (red), which stains vasculature. (C) Quantification revealed significantly enlarged vasculature in untreated mice. (n = 5/group, ** = p < 0.01) (D) TMZ induced DNA damage was measured by phospho-H2AX staining (green), which (E) indicated a significant higher DNA damage pattern if mice were pre-treated with siGal-1. (n = 3/4/group, ** = p < 0.01) (F) Analysis of brain infiltrating lymphocytes during anti-PD-1 therapy (at day 7 and 12 after tumor inoculation, 100µg/day), at day 18 post tumor inoculation, revealed a significant decrease of PD-1 expression on CD4+ (black bars) and CD8+ (gray bars) lymphocytes. In (G) the ratio immune activation to immune suppression was calculated for Th1 and CTL respectively (IFNγ+CD4+CD3+CD45+ZY-) and (IFNγ+CD8+CD3+CD45+ZY-), as compared to Treg (FoxP3+CD4+CD3+CD45+). (n = 5/group, * = p < 0.05 and ** = p < 0.01).

DISCUSSION

Understanding the peculiar cellular and molecular dynamics in the TME of malignancies such as GBM is a prerequisite for the development of effective non-invasive therapies. Our current work is focused on Gal-1 as an important driver in GBM biology to inherent resistance against chemo- and immunotherapy. Specifically, we demonstrate that, by using the nose-to-brain transport, we are able to suppress *gal-1* expression in the TME, which results in a shift from immune suppression to immune activation. The intranasal construct to block *gal-1* expression in GBM that is presented here reaffirms previous findings obtained by much more invasive approaches or by approaches not transposable at the clinical level. Moreover, we could demonstrate synergistic effects with novel immunotherapeutic agents as anti-PD-1 blocking, which gives additional arguments why nose-to-brain transport to reduce *gal-1* expression could represent a valuable adjuvant therapy.

In a syngeneic, orthotopic murine model for GBM, we provide evidence that reducing *gal-1* expression prevents the polarization from M1 macrophages to M2 macrophages during GBM progression. Activation of the M2 phenotype has been shown to worsen the prognosis and aggravate disease through secretion of vascular promoting factors as VEGF-A, and immune suppressive factors such TGF-β and IL-10. In earlier work, we have demonstrated that this macrophage population relocates around TME associated vessels to form perivascular cuffs and further drives vascular abnormalities as observed in GBM progression (Mathivet T. et al.; Dynamic stroma reorganization drives blood vessel dysmorphia during glioma progression; under revisions). Therefore, a decrease in M2, but also in CD11b monocytes, and more in particular the monocytic MDSCs, can already relieve a major fraction of the immune suppressive counterweight present in the TME (237). In recent years, it became more likely that there is an intensive crosstalk between the immune suppressive actors of the myeloid side and of the lymphoid arm of the immune system. We also find a decrease in FoxP3+ Treg cells in the TME when Gal-1 is reduced. Whether this effect is, a myeloid-lymphoid interaction, potentially mediated by CCL22, or a direct effect of Gal-1, remains unclear (32). The presence of Gal-1 and the recruitment of FoxP3+ cells is already established in previous reports (238). Not only do we find evidence for alleviation of immune suppression, but also for promoting immune activation. CD3+ lymphocytes are increased within the TME upon Gal-1 reduction, and more specifically, both Th1 and CTL are infiltrating the GBM. It was demonstrated that GL261 cells upon IFN-γ stimulus, can up regulate MHC I molecules, and thereby are more susceptible to CD8+ mediated destruction

(239). These findings are in line with the proposed role of Gal-1 that drives apoptosis in activated T cells when reaching the TME (50).

In further functional testing of our intranasal siGal-1 construct, we observe that mice have small, but significant survival benefit when treated in monotherapy siGal-1. We observe a 2.5 days shift in median survival, and a long term survival induction of 20%, explained by a decreased Ki67 proliferation of treated GL261 gliomas. In a previous report, we demonstrated that we are able to decrease *gal-1* expression in the TME by 50% as measured by western blot analysis (236). Despite this robust decrease of Gal-1, the survival benefit in monotherapy is only modest. To our understanding, we do not consider siGal-1 therapy as a monotherapy, but rather as an adjuvant therapy, which can be combined with chemo- and immunotherapy. Combination therapy of intranasal siGal-1 (at a dose of 1 unit at day 2, 4, 7 and 11) and per os temozolomide (at a dose of 40 mg/kg at day 8, 11 and 15) elicits a significant synergistic survival benefit. The shift in median survival was similar as described previously, with intratumoral and intraventricular siGal-1 injections (61), although no long-term survivors were observed, most likely due to the use of nude-mice, and therefore lacking an immune component. This underlines the bio-equivalence of the non-invasive intranasal pathway, in comparison with aggressive, invasive therapies. We observed that treatment with siGal-1 can reduce the vascular diameter in the TME from 15 μm to 10 μm . Previous reports, describe how tumor derived Gal-1 can enhance endothelial function in migration and proliferation potential (240), or even complement VEGF signaling (65). This reduction can be either attributed to the reduction in M2 (and lack of VEGF-A secreted in the perivascular spaces), or the direct anti-angiogenic effects of siGal-1. Therefore, the pre-treatment with siGal-1 can make that TMZ can be better perfused in the entire TME, and reach more tumor mass *in toto*. On the other hand, the reduction of Gal-1 obtained with siGal-1 pre-treatment alters the unfolded protein response to endoplasmic reticulum stress, increasing thereby the inherent sensitivity of GBM cells to TMZ delivered afterwards (61). Accordingly, in other, non-reported, experiments we did not observe this synergy when siGal-1 therapy is administered concomitantly or later in the dosing schedule. Assessment of the aggravated DNA damage induced by alkylating chemotherapy in the combination demonstrates that more tumor tissue is affected by administration of TMZ, as pointed out by upregulation of phospho-H2aX histone complexes which try to repair double strand breaks. This impairment results in G2/M arrest (241). Other possible treatment combinations can be found in the field of immunotherapy. In a first approach, we tested DC vaccination strategy, as developed in our laboratory as a potent prophylactic immunotherapy in the murine GL261 model. In this dosing schedule, we can only demonstrate non-significant, additive survival benefit upon Gal-1 reduction. However, with immune checkpoint inhibition via PD-1 blocking, combination therapy leads to synergistic survival benefits in mice with established brain tumors. We also find an increased immune stimulation of lymphocytes in the TME in the combination treatment, as compared to PD-1 blocking alone. Of note, aberrant vasculature in tumors is suggested as a substantial barrier for extravasation of T cells (237). As siGal-1 could efficiently reduce the vasculature abnormalities, this could also explain the influx of Th1 and CTL. According to Robert Clark Equations, we observed a synergistic effect of combining anti-PD-1 therapy and TMZ therapy with siGal-1, whereas an additive effect of DC mediated immunotherapy in combination with

siGal-1 (Supp Fig 6). Adjuvant therapies such as siGal-1 therapy might represent valuable methodologies to further increase the efficiency of anti-PD-1 and TMZ therapy.

In our research, we have elaborated on several key features of GBM tumor progression that are driven by Gal-1 biology. We have addressed proliferation, angiogenic, immunological, and TMZ-resistance properties in a manner where we targeted *gal-1* expression via intranasal transport. This research paves the way for the development of a clinical implementation of the nose-to-brain transport in the current treatment schedule of GBM patients. To our knowledge, this is the first report in literature where the aforementioned pathway was validated from pharmaceutical development, to biological efficacy in a GBM tumor model.

MATERIALS & METHODS

Animals and treatments

International ethical guidelines were followed and approved by the bioethics committee at KU Leuven. Tumor inoculations were performed as described previously (236). In brief, 0.5×10^6 GL261 cells were stereotactically injected in the striatum of 8-10 weeks old C57Bl/6 mice (C57BL/6J01aHsd, Harlan, The Netherlands). GL261 cells were received as a gift from Dr. Eyupoglu, University of Erlangen, Germany. Long term survival was defined as exceeding 3 x median survival of untreated control mice. Intranasal siGal-1 administrations were administered as 8 droplets of 3 μ l with a non-adhesive micropipette tip (Eppendorf). Total amount of 1 administration was defined by 48 μ g siRNA/dose and chitosan nanoparticles composition as described before (236). In brief, chitosan nanoparticles were prepared by ionic gelation of tripolyphosphate and chitosan, while adding siRNA. Consequently, particles were collected by ultracentrifugation at 40000 x *g* during 3 cycles of 20 min, and freeze-dried with sucrose as lyoprotectant. At the indicated time points, chitosan nanoparticles were administered intranasally, under 3 % isoflurane anesthesia.

TMZ administrations were performed as described previously (239). In brief, Temodal capsules were opened and dissolved in a phosphate buffer, with an equal amount of L-Histidine, and administered in a total volume of 200 μ l by gavage (Schering-Plough, Belgium). For survival experiments mice received 40 mg/kg TMZ at day 8, 11 and 15 post tumor inoculation. For phospho-H2AX assessments, mice received 80 mg/kg TMZ at day 13 and 14 post tumor inoculations, and were sacrificed for immunostainings 4 h after the last administration.

DC vaccinations were performed as described previously (221). In brief, 200 μ g irradiated lysate was loaded per 1×10^6 immature DCs. Subsequently DCs were pulsed towards mature DCs with LPS, settled for 24 h, and intraperitoneal administered at day 14 and day 7 prior to tumor inoculation. Anti-PD-1 antibodies (RMP1-14) and isotype controls (Rat IgG) were dissolved in saline (Braun, The Netherlands) and intraperitoneal administered at day 7 and 12 post tumor inoculation (100 μ g/administration, Epirus Biopharmaceuticals).

Flow cytometry

Flow cytometric analysis was performed as described earlier (239). In brief, animals were sacrificed by lethal injection of Nembutal at the indicated time points, and perfused with PBS (Lonza, Belgium). Single cell suspensions were obtained after mincing with scalpels and 30' incubation with DNase (Invitrogen) and CollagenaseD (Roche). Mononuclear cells were separated from debris via Percoll gradient centrifugation (Sigma), and the intermittent layer was washed twice with PBS. Surface stainings were performed with antibodies as mentioned in Table M&M 1.

Table M&M 1: Flow cytometry antibodies

Antigen	Fluorochrome	Origin
CD45	AF700	Ebioscience
CD11b	BV421	BD
Ly6C	AF647	Biorad
Ly6G	FITC	BD
MHCII	PerCP Cy5.5	Biolegend
Mannose Receptor	PE	Biolegend
Isotype Rat IgG2a,k	PE	Biolegend
Live/dead	Zombie Yellow	Biolegend
CD3	FITC / PE	Ebioscience
CD4	PerCP Cy5.5 / APC-eF780	Ebioscience
CD8	BV421	BD
NKp46	APC	Biolegend
FoxP3	PE	Ebioscience
PD-1	PE	BD
IFN- γ	PerCP Cy5.5	BD

The intracellular detection of FoxP3 was performed using a FoxP3 staining kit (eBioscience, San Diego, CA) according to the manufacturer's protocols. For intracellular IFN- γ staining, cells were stimulated for 4 h with 100 ng/ml phorbol myristate acetate, 1 μ g/ml ionomycin and 0.7 μ g/ml monensin. Cells were fixed in 1% PFA for 15 min. and resuspend in 0.5% PBS/BSA until acquiring by cytometer (LSRFortessa, BD). Cell population analysis was performed with FlowJo.

Immunofluorescence staining

Immunofluorescence staining was performed on mouse brain vibratome sections as described earlier (236). Following primary and secondary antibodies are summarized in Table M&M 2.

Table M&M 2: Immunofluorescence staining:

Antigen/ Primary Antibody	Origin	Secondary Antibody	Origin
GLUT-1	Millipore	Donkey Anti-rabbit Alexa 555	Life Technologies
GLUT-1	Abcam	Donkey Anti-mouse Alexa 555	Life Technologies
GLUT-1	Santa Cruz	Donkey Anti-goat Alexa 555	Life Technologies
F4/80	Life Technologies	Donkey Anti-rat Alexa 488	Life Technologies
MHCII	Thermo Scientific	Donkey Anti-rat Alexa 488	Life Technologies
Ki67	Abcam	Donkey Anti-rabbit Alexa 647	Life Technologies
MRC-1	R&D Systems	Donkey Anti-goat Alexa 488	Life Technologies
γ -H2AX	Cell Signaling Technology	Donkey Anti-rabbit Alexa 555	Life Technologies
Caspase-3	Abcam	Donkey Anti-rabbit Alexa 555	Life Technologies

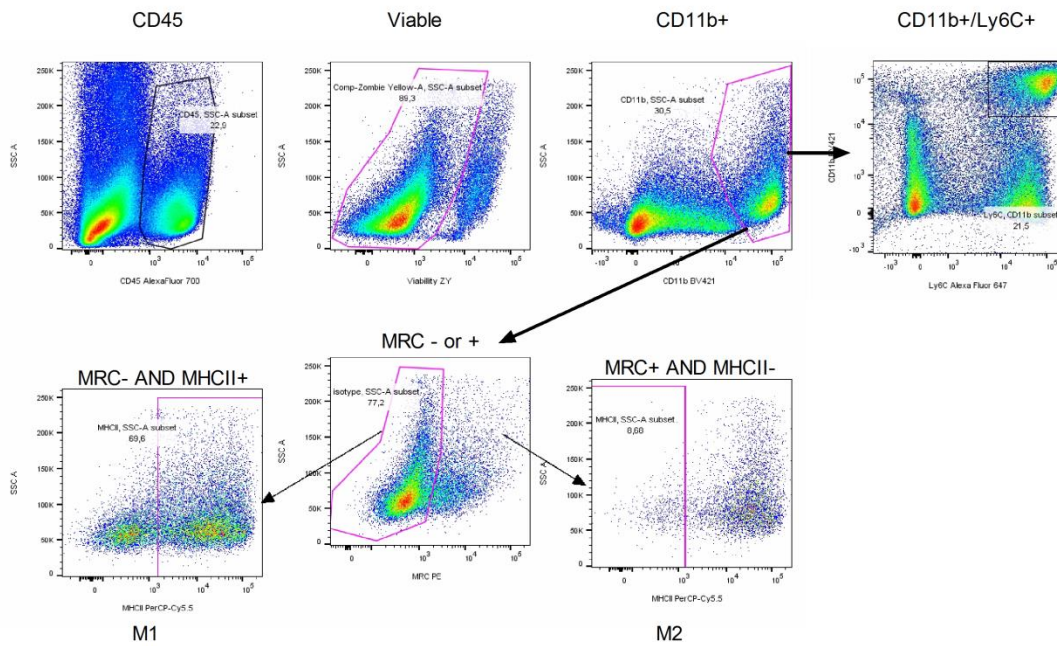
Acquisition was performed on Leica SP8 confocal microscope and analyzed via Adobe Photoshop and ImageJ Using a 25x water immersion objective.

Quantitative assessment of vessel diameter was performed by measuring at least 12 vessel diameters in 3 independent pictures per mouse.

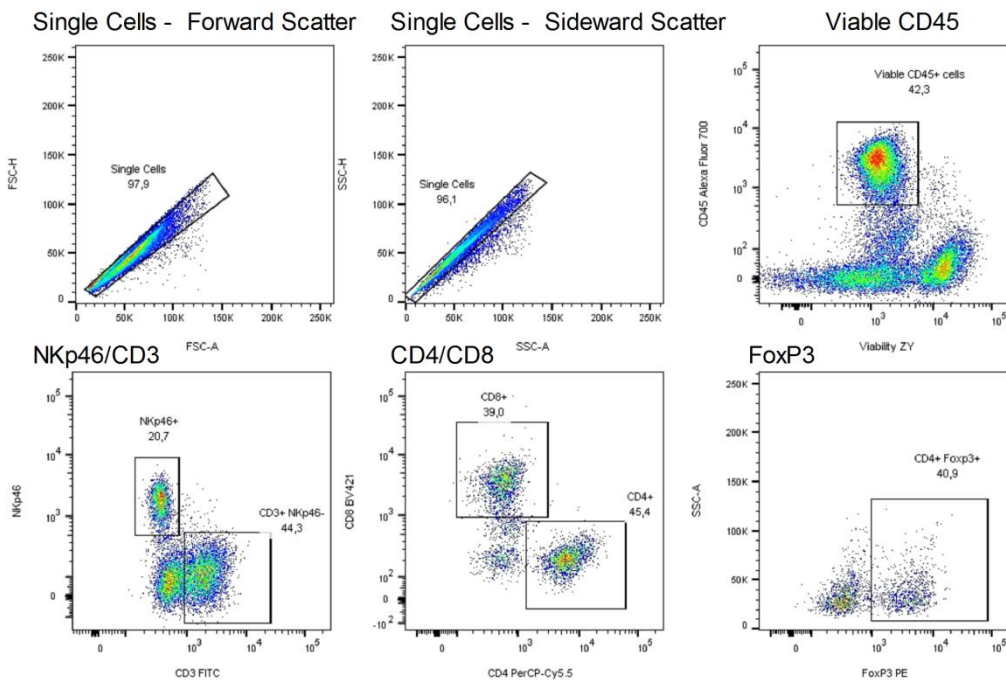
RT-qPCR

mRNA analysis on siRNA treated tumor biopsies were processed as described earlier (236). Total RNA was isolated, and PCR reaction was prepared for GAPDH as housekeeping gene, and *foxP3* as gene of interest (Forward: ccc agg aaa gac agc aac ctt , Reverse: ttc tca caa cca ggc cac ttg, Taqman Probe: atc cta ccc act gct ggc aaa tgg agt c).

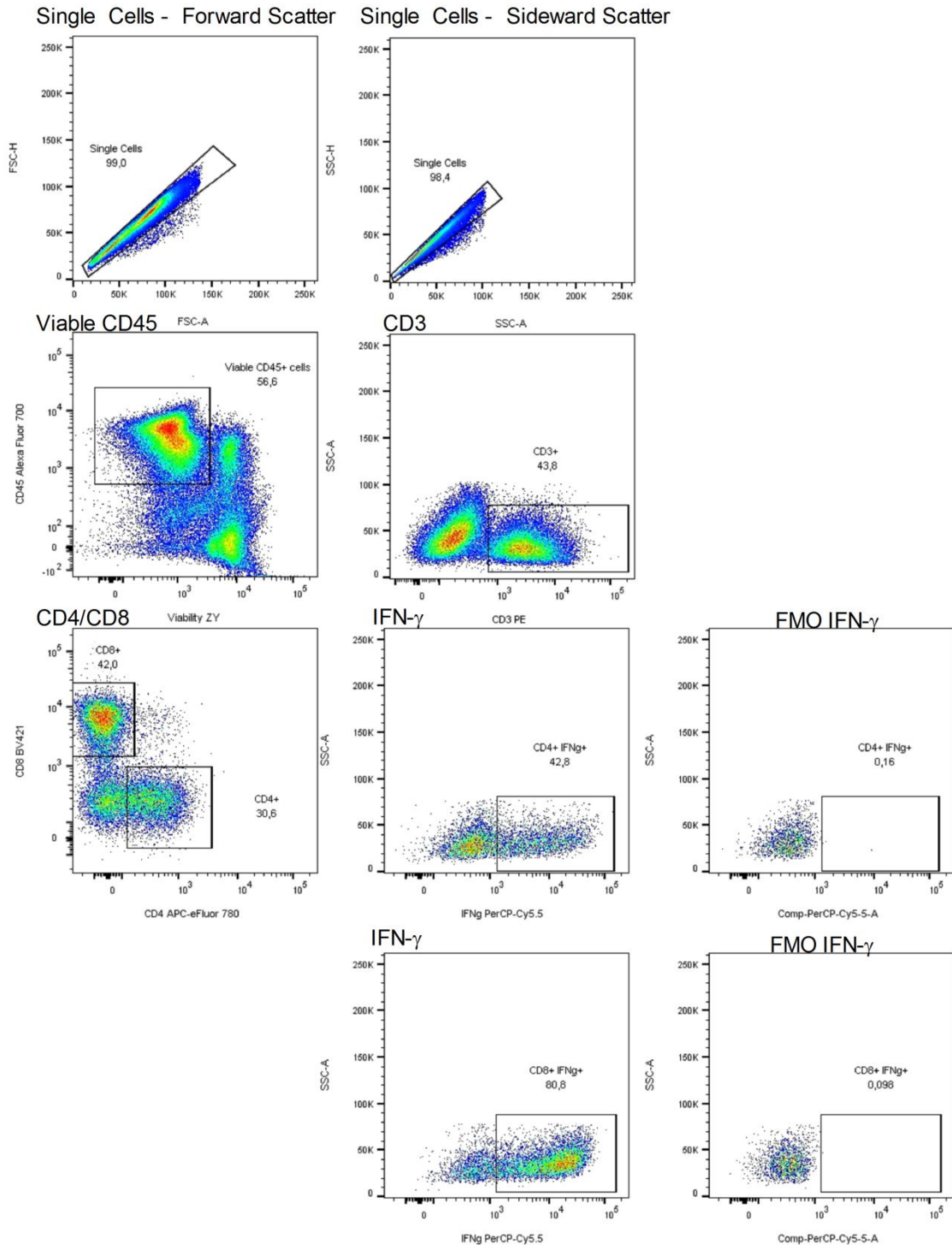
SUPPLEMENTARY FIGURES LEGENDS



Supplementary Figure 1 : Gating strategy for myeloid cell population. Flow cytometry was performed on isolated mononuclear brain infiltrating cells of mice and gated for CD45 positive (leukocytes), viable cells (ZY negative), and CD11b positive (myeloid). Subsequently, we looked either into Ly6C for monocytic MDSCs and Ly6G for granulocytic MDSCs. Furthermore, we also analyzed the CD11b positive cells for MRC1 expression (middle, down row), and we monitored for MRC1 negative cells for MHCII positive (M1 macrophage phenotype), on the other side, we monitored the MRC1 positive cells for MHCII negative (M2 macrophage phenotype).

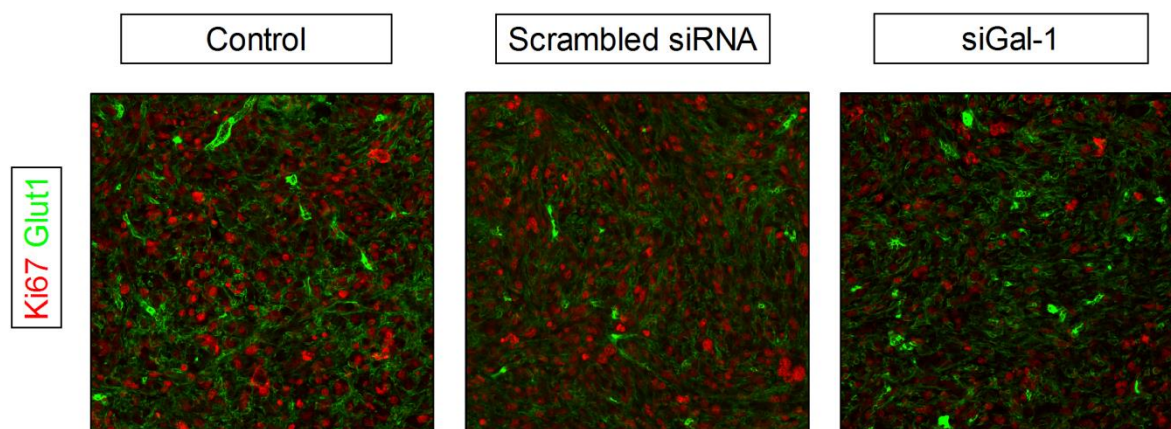


Supplementary Figure 2 : Gating strategy for Treg. Flow cytometry was performed on isolated mononuclear brain infiltrating cells of mice and gated for single cells (via SSC and FSC), CD45 positive (leukocytes), viable cells (ZY negative), and CD3 positive (lymphoid). Subsequently, we looked into CD4 and CD8 for T cells, and within the CD4 gate, we monitored the expression of FoxP3 expression.

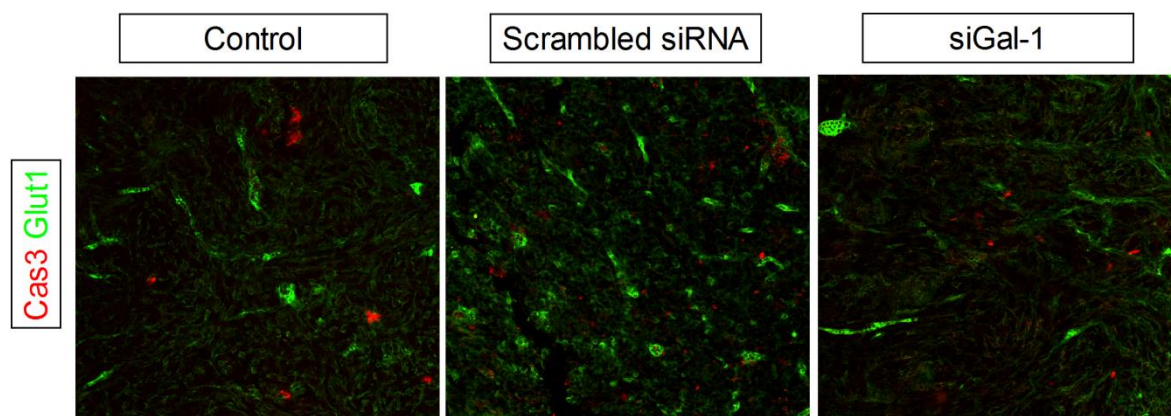


Supplementary Figure 3 : Gating strategy for Lymphoid cell populations. Flow cytometry was performed on isolated mononuclear brain infiltrating cells of mice and gated for single cells (via SSC and FSC), CD45 positive (leukocytes), viable cells (ZY negative), and CD3 positive (lymphoid). Subsequently, we looked into CD4 and CD8 for T cells, and for both cell populations, we monitored

the expression of IFN- γ expression, as guided by Fluorescence Minus One, to determine the proper gating strategy.



Supplementary Figure 4: Ki67 staining pictures. Mice were inoculated with 0.5×10^6 GL261 cells which induces a lethal GBM after 15-20 days. Representative pictures of late stage tumors are shown for control, untreated mice; mice treated with scrambled siRNA loaded chitosan nanoparticles, or mice treated with siGal-1.



Supplementary Figure 5: Cas3 staining pictures. Mice were inoculated with 0.5×10^6 GL261 cells which induces a lethal GBM after 15-20 days. Representative pictures of late stage tumors are shown for control, untreated mice; mice treated with scrambled siRNA loaded chitosan nanoparticles, or mice treated with siGal-1.

Nature of interaction	Formula
Antagonistic	$(AB/C) < (A/C) \times (B/C)$
Additive	$(AB/C) = (A/C) \times (B/C)$
Synergistic	$(AB/C) > (A/C) \times (B/C)$

	(AB/C)	>, =, < ?	(A/C) x (B/C)	Effect
TMZ exp	2,789473684	>	2,038781163	SYNERGY
DCvacc exp	2,634146341	=	2,598453302	ADDITIVE
PD-1 exp	2,942857143	>	1,86122449	SYNERGY

Supplementary Figure 6: Calculations for interactions. Based on median survival data (from Figure 3B, 3C and 3D), the calculations for antagonistic effect, additive effect and synergistic effect were carried out based on the Robert Clark Equations (R Clarke, 1997, Breast Cancer Research and

Treatment, 46:225-278); where A = response to treatment 1 (= siGal-1), B = response to treatment 2 (= TMZ, DCvacc or anti-PD-1) and C = response to no treatment (= control)

5. RESULTS - PART 3 - PAPER 3

PEGylated chitosan nanoparticles optimize nose-to-brain transport to target Galectin-1 in the treatment of glioblastoma

In our previous work, we have demonstrated how a relative simple formulation can induce major changes in the TME of GBM progression. We could demonstrate that reduction of Gal-1 clearly alters the immune suppressive nature of this TME, and becomes more susceptible to immunotherapy. All the previous results were obtained with a nano-sized formulation prepared of native chitosan polymers. Whereas this was an ideal candidate to conduct this proof-of-concept study, there's a fair chance that more potent formulations for in vivo application could be prepared. With lower concentrations of siRNA, we should be able to still reach the CNS, and the TME. To this end, we attempted to alter the formulation in favor of the nose-to-brain transport, by adding a PEG polymer on the native chitosan. As explained in the introduction, PEGylation could potentially decrease the reactivity of chitosan polymers, and reduce the ability to adhere mucosal layers, while promoting passage through the mucosa.

With this background in mind, we prepared a study with the following aims

- I. To conjugate and characterize a co-polymer, consisting of PEG and chitosan, preferably with a low Mw PEG, in a low % of engraftment;
- II. To determine if the most important properties of chitosan nanoparticles were altered i.e. transfection of GL261, reduction of Gal-1, and modulation of the epithelial barrier
- III. To evaluate if on any level we can demonstrate a superiority of PEGylated chitosan nanoparticles in comparison to native chitosan nanoparticles;
- IV. To elucidate if also these PEGylated chitosan nanoparticles, can be able to pass the nasal mucosa, and enter into the TME of a murine GBM model

The research paper discussing the results of this section is presented on the following pages and the supplementary figures are depicted afterwards – at the moment of writing, this manuscript was in preparation and further experiments were ongoing.

PEGylated chitosan nanoparticles optimize nose-to-brain transport to target Galectin-1 in the treatment of glioblastoma

Matthias Van Woensele (1,2) & Thomas Mathivet (3,4), Nathalie Wauthoz (2), Rémi Rosière (2), Véronique Mathieu (5), Robert Kiss (5), Florence Lefranc (6), Louis Boon (7), Jochen Belmans (8), Brecht Steelant (9), Stefaan W. Van Gool (10), Holger Gerhardt (3,4), Karim Amighi (2), Steven De Vleeschouwer (1,11)

Affiliations

- (1) Research Group Experimental Neurosurgery and Neuroanatomy, KU Leuven, Herestraat 49, Leuven 3000, Belgium;
- (2) Laboratoire de Pharmacie Galénique et de Biopharmacie, Université libre de Bruxelles (ULB), Boulevard du triomphe CP207, Brussels 1050, Belgium;
- (3) Vascular Patterning Unit, VRC, VIB, Herestraat 49 box 912, Leuven 3000, Belgium
- (4) Vascular Patterning Laboratory (Vesalius Research Center), Department of Oncology, KU Leuven, Herestraat 49 box 912, Leuven 3000, Belgium
- (5) Laboratoire de Cancérologie et de Toxicologie Expérimentale, Université libre de Bruxelles (ULB), Boulevard du triomphe CP205/01, Brussels 1050, Belgium;
- (6) Department of Neurosurgery, Erasmus University Hospitals, Route de Lennik 808-1070, Brussels 1050, Belgium;
- (7) EPIRUS Biopharmaceuticals, BV, Yalelaan 46, Utrecht 3584, The Netherlands;
- (8) Laboratory of Pediatric Immunology, KU Leuven, Herestraat 49 box 811, Leuven 3000, Belgium;
- (9) Laboratory of Clinical Immunology, KU Leuven, Herestraat 49 box 811 Leuven 3000, Belgium;
- (10) Medizinische Leitung der Translationalen Onkologie, Immunologisches Onkologisches Zentrum, Köln, Germany;
- (11) Department of Neurosurgery, University Hospitals Leuven, Herestraat 49 box 7003, Leuven 3000, Belgium.

Abstract

Glioblastoma is until today, one of the most aggressive and lethal tumors. Recent advances in surgery, chemo-and radiotherapy were not able to induce a significant shift in prognosis for these patients, and therefore this disease clearly presents an unmet medical need. Much evidence is arising that therapeutic delivery of biologicals can be accomplished by using the nose-to-brain transport. In the present work, we have developed PEGylated chitosan nanoparticles intended for intranasal transport, to deliver Galectin-1 targeting siRNA molecules from the nasal cavity towards the central nervous system. Successful cytoplasmatic delivery was demonstrated by efficient Gal-1 reduction on GL261. Superior nasal epithelial barrier modulation was demonstrated in comparison to native

chitosan. Moreover, we could demonstrate an efficient delivery into the tumor micro-environment of an orthotopic murine glioblastoma model.

Introduction

Despite recent advances in the treatment schedules of glioblastoma (GBM), the prognosis for patients remains unchanged. Upon diagnosis, patients face a median survival of 14,6 months with the standard treatment of surgery, radio and chemotherapy (8). Also young children and often young adults are struck by this devastating disease, and therefore the cumulative years of life lost, are the highest in GBM (242). For this unmet medical need, many novel therapies have been developed. Especially in the field of immunotherapy for oncology, major advances have been made. Releasing the breaks on the immune system can result in potent anti-tumor immunity. In detail, the use of checkpoint inhibition via anti-CTLA-4 and anti-PD-1, has demonstrated high efficacy in metastatic melanoma (40). Also for GBM, immunotherapy is an attractive approach. To this end, in our research facilities, we explored in the past, a clinical grade protocol to treat patients with dendritic cell vaccination, in order to increase immunity towards GBM (36, 201). With a subpopulation of long term survivors, modest successes were achieved. However, consensus is arising that the tumor micro environment (TME), is adequately equipped to withstand the immune attack (18). As described in our earlier publications, Galectin-1 (Gal-1), is a potent immune-suppressive molecule secreted in the TME (243). Gal-1 can swiftly drive activated T-cells into apoptosis, recruit regulatory T cells (Tregs) and blunt T cell receptors, thereby decreasing the chance that GBM will be eradicated by immunity (50, 51).

In previous work, we have demonstrated that it is feasible to modulate the TME contexture via the intranasal transport (236). In detail, we have shown that chitosan nanoparticles can deliver anti-Gal-1 siRNA (siGal-1) molecules from the nasal cavity towards the TME. Delivery of siGal-1 could turn around the TME from immune-suppression to immune-activation, resulting in synergistic survival benefits with PD-1 blocking. The use of chitosan is attractive because of the ease of complexation with siRNA molecules, and moreover chitosan is known to be biocompatible and biodegradable (134). A major drawback in using native chitosan nanoparticles is that chitosan polymers have to be protonated to become water soluble. Protonation of primary amines is usually achieved in slightly acidic media. Moreover, native chitosan is known to aggregate in physiological media. Therefore, in recent years, many approaches have been tested to increase the hydrophilicity of chitosan (223). Interestingly, recent reports have indicated that PEGylation i.e. the addition of PEG, could increase the nose-to-brain transport, since particles can rather slip through the mucus layer, than sticking on it (154, 232). To this end, Kanazawa et al. manufactured an interesting co-polymer of PEG and polycaprolactone which delivers siRNA through the intranasal route (177, 232). A popular method seems to engraft polyethylene-glycol (PEG) on chitosan in order to increase the hydrophilicity of the polymer and also the stability. PEG is a biological inert polymer, which is mainly used to increase circulation time of biologicals in physiological fluids. It is demonstrated as non-toxic and biodegradable. To construct this co-polymer, several chemical reactions have been proposed, among which the carbodiimide crosslinker chemistry (244).

In this study, we aimed to prepare a block copolymer consisting of PEG and chitosan, which could result in particle formation that encapsulate and protect siRNA molecules. Furthermore, we attempted to set up a parallel study to our previous research, to evaluate the nose-to-brain transport of PEGylated chitosan nanoparticles in comparison to native chitosan particles. In detail, these particles were evaluated for their potential to transfect GBM cells in vitro, and the distribution in the TME.

Results

Carboxydiimide crosslinker chemistry can link between carboxylic acids and primary amines. Since chitosan has multiple units containing primary amines, carboxylated PEG was selected. Reagents were added in excess (EDC and NHS), and we calculated to produce a yield of PEGylated chitosan of 5%. Via ^1H NMR, the conjugation of PEG and chitosan was confirmed (Figure 1). The peak at 3.6-3.7 ppm reflects the repetitive units of PEG; other peaks were generated by chitosan and deuterium. Calculations of the integrals of the different peaks corresponding to this copolymer, revealed an engraftment ratio of about 3.3%. siRNA containing particles were obtained with a theoretical N/P ratio of 2.625, with a size of about 180 nm, and a charge of +15.3 mV.

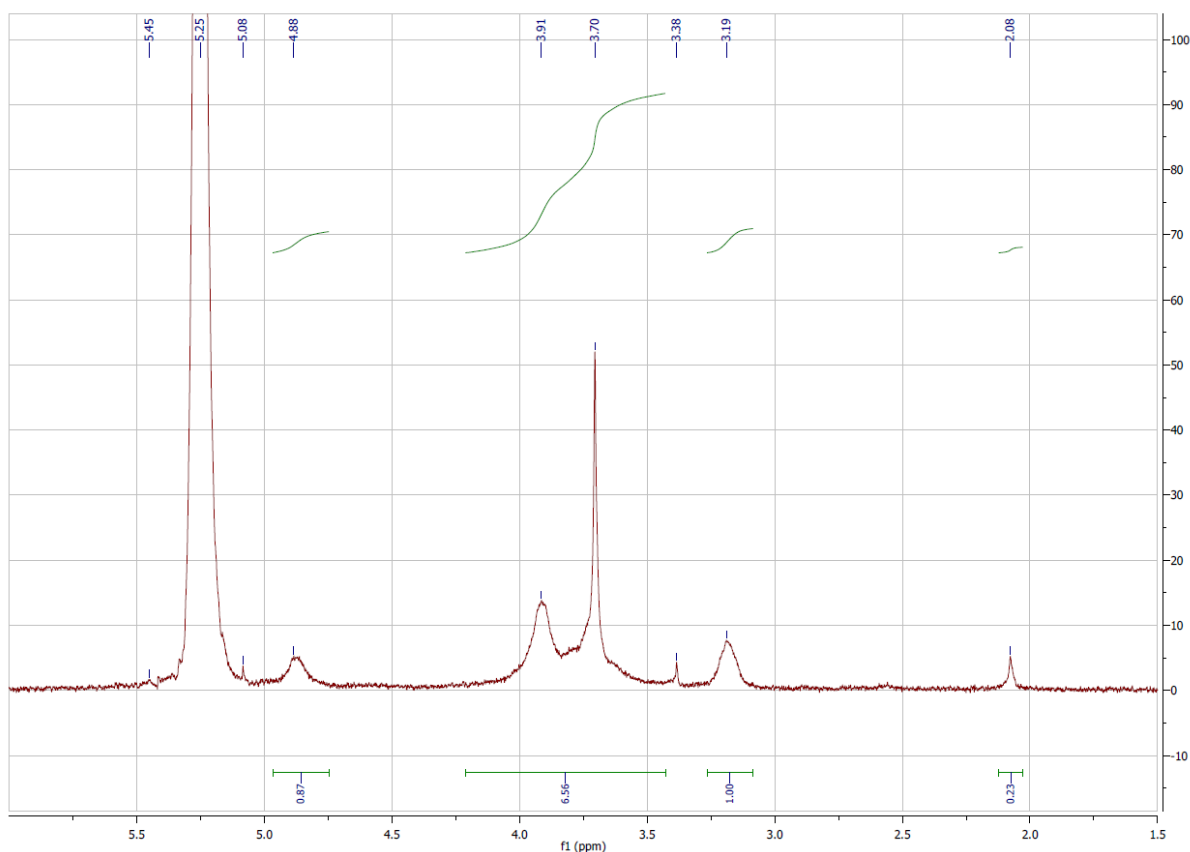


Figure 1. PEGylated chitosan ^1H NMR spectrum. The peak at 3.6-3.7 ppm corresponds to CH₂ by PEG.

An important parameter to assess the functionality of PEGylated chitosan nanoparticles is the protection from degradation. To this end, siGal-1 loaded particles were co-incubated with RNase

enzymes, and loaded onto an agarose gel (gel retardation assay). As observed here, particles could protect siGal-1 for at least 2h at 37 °C, underlining the strong complexation between PEGylated chitosan and siRNA. We also notice that free siRNA was rapidly degraded upon co-incubation with RNase enzymes.

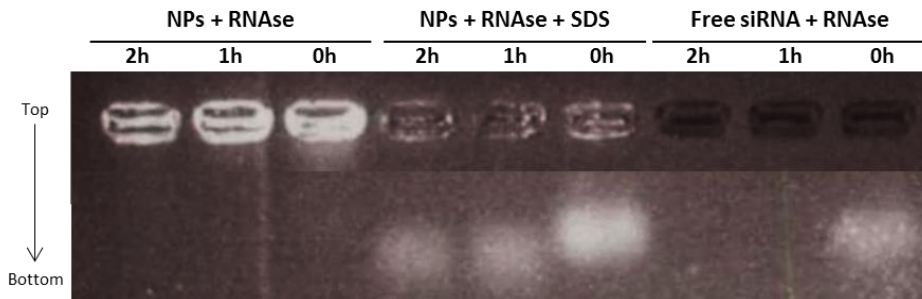


Figure 2. Protection from RNases. siRNA loading and protection from RNase degradation at different times (0, 1, and 2 h) using a gel retardation assay. siRNA-loaded PEGylated chitosan nanoparticles (NPs) or free siRNA were incubated with RNases and then exposed to sodium dodecyl sulfate (SDS) (NPs+RNase+SDS) or not (NPS + Rnases and free siRNA+Rnase) before being loaded onto the agarose gel and applying 55 V for 2 h and then staining the gel with ethidium bromide.

Next to protection from degradation, PEGylated chitosan nanoparticles need to be able to enter GBM cells, and deliver siGal-1 in the cytosol. In order to assess the transfection potential, we evaluated the possibility for adherence by means of fluorescence microscopy. Here, green fluorescein-labeled siGal-1 PEGylated chitosan nanoparticles can be observed on GL261 cells. These particles adhered already 6h after transfection (Figure 3A). More importantly, particles need to escape endo-lysosomal degradation. Therefore we assessed the functionality of siGal-1 by measuring the decrease of Gal-1 in GL261 cell culture. In accordance with previous experiments, the decrease of Gal-1 is strongest at day 4 to day 7 post transfection. Also here, we noticed a strong decrease of Gal-1 during this period, indicating the cytoplasmatic delivery of siGal-1 in GL261 cells (Figure 3B).

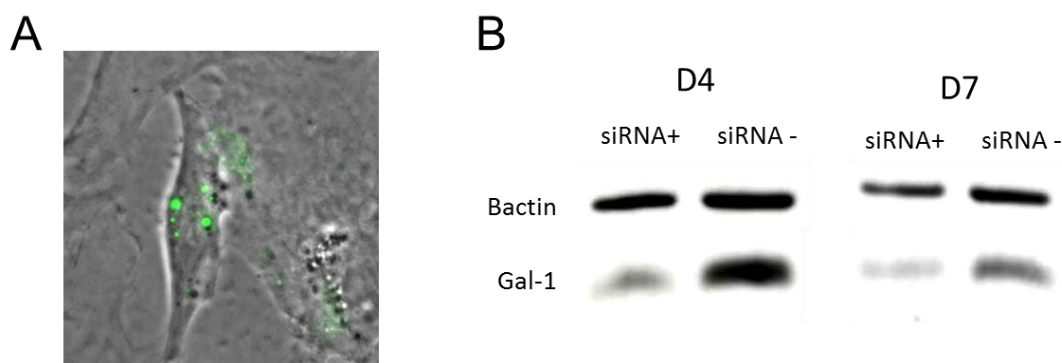


Figure 3. Interaction with GL261 cells. (A) after 6h, fluorescein loaded - PEGylated chitosan nanoparticles are able to attach to GL261 cells; moreover in (B) immunoblotting confirmed that siGal-1 is delivered into the cytosol, and that Gal-1 is efficiently reduced from day 4 to day 7, as monitored by loading equal amounts of protein. (Bactin = B actine, Gal-1 = Galectin-1; at D4 or D7 = day 4 and day 7 post transfection; cells were treated with anti-Gal-1 siRNA loaded particles (siRNA+), or without siRNA (siRNA-))

In order to evaluate the epithelial barrier modulation, PEGylated chitosan nanoparticles were incubated with epithelial monolayers, either Calu-3 (lung adenocarcinoma, Figure 4 A) or derived from nasal biopsies (Figure 4 C and D). At a concentration of 0.03 % on Calu-3 cells, we observed a decrease in transepithelial electrical resistance (TEER), which was reduced by almost 50 % at 2 h post incubation (Figure 4 A). Decreasing the resistance, as a measurement for the intactness of the monolayer, could also permeate macromolecules to travel over the monolayer. We found an increase in flux of FITC labeled 4 kDa Dextran, although not significant. Interestingly, and most relevant for nose-to-brain in a clinical setting, PEGylated chitosan could also modulate epithelial intactness on human nasal epithelial cells. In two human nasal derived cell cultures, we found a decrease of resistance in PEGylated chitosan treated monolayers. Interestingly, in the first cell culture (Figure 4 C), this decrease was exclusively present with PEGylated chitosan, and not with native chitosan. In contrast, in the second cell culture, native chitosan seemed superior to the PEGylated chitosan, which was still able to modulate the barrier.

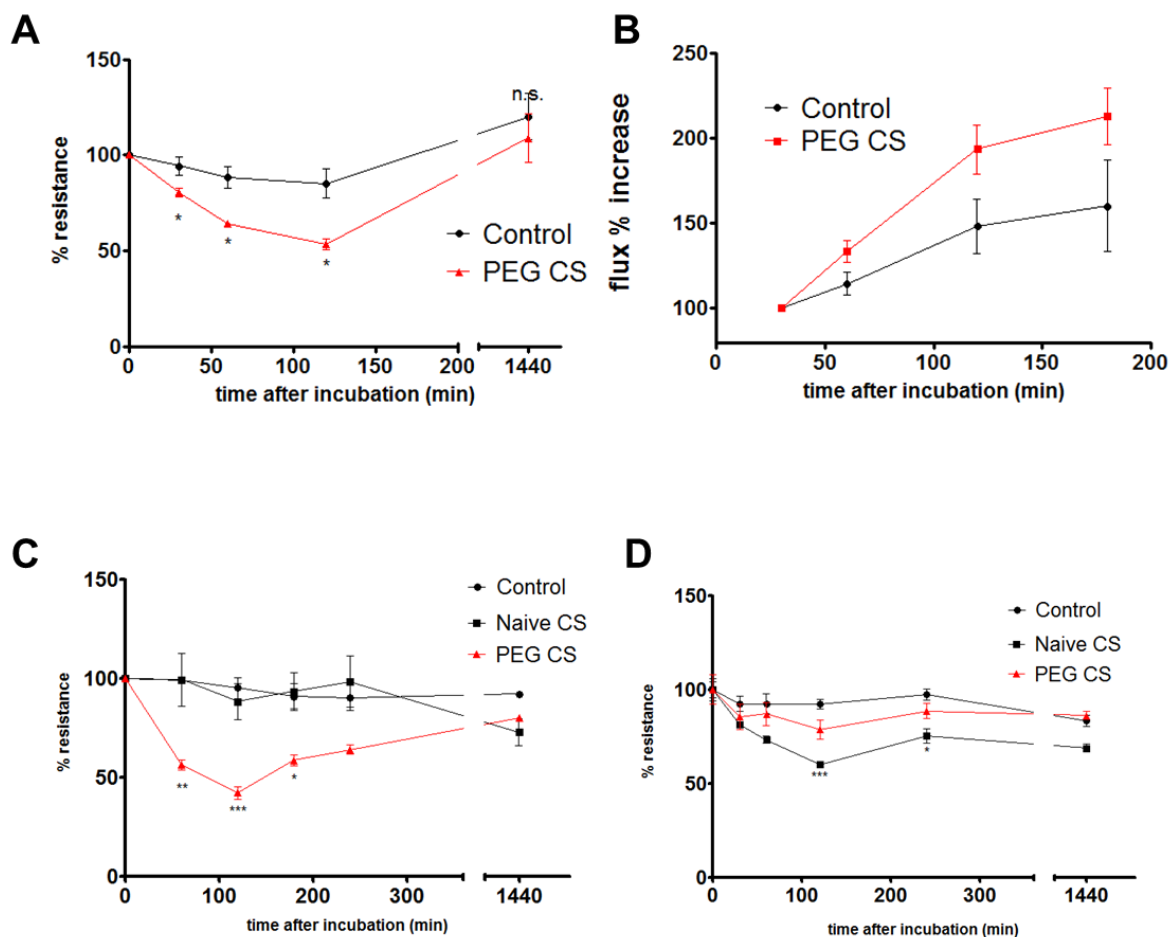


Figure 4. Interaction of siRNA-loaded chitosan nanoparticles with a Calu-3 monolayer airway epithelium (A) TEER measurement after incubation with PEGylated chitosan nanoparticles relative to the baseline TEER. The measurements are expressed as mean \pm SEM, unpaired t-test (* $p < 0.05$, and *** $p < 0.001$ ($n=4$); **(B)** FD4 passage over a Calu-3 monolayer airway epithelium expressed as a percentage of flux increase over time, after incubation of siRNA-loaded PEGylated chitosan nanoparticles at 0.03% w/v. The measurements are expressed as the mean \pm SEM ($n=4$). **(C+D)** TEER measurements on primary nasal epithelium, derived from freshly isolated nasal mucosal biopsy.

PEGylated and native chitosan nanoparticles were incubated at 0.03% . Measurements are expressed as the mean \pm SD, $n \geq 3$. * $p < 0.05$, ** $p < 0.01$ and *** $p < 0.001$ via two way ANOVA. (C: Patient 1; D: Patient 2).

To evaluate the potential for nose-to-brain transport, a primary requisite is nasal passage. Therefore we administered intranasal Red dye siRNA loaded PEGylated chitosan nanoparticles. Similar to our previous results, the nasal mucosa was removed for read-out, and two parallel visualization techniques were used, either through paraffin processing (Figure 5 A and B), or for vibratome sectioning (Figure 5 C). In previous work, we have demonstrated the absence of red fluorophore (corresponding to siRNA) in untreated control mice; the treated mice presented here were processed in identical conditions. We observed a strong adherence of siRNA onto the mucus layer after 4h (Figure 5 A), but also passage through the individual epithelial columnar layer (detail in Figure 5 B). These finding were also confirmed on vibratome sections, which demonstrates a very homogenous spread of siRNA (Figure 5 C). More importantly, we also found the presence of red siRNA already 4 h after single administration in the TME. The clear diffuse pattern distribution demonstrates a swift transport from the nasal cavity towards the TME (Figure 5 D).

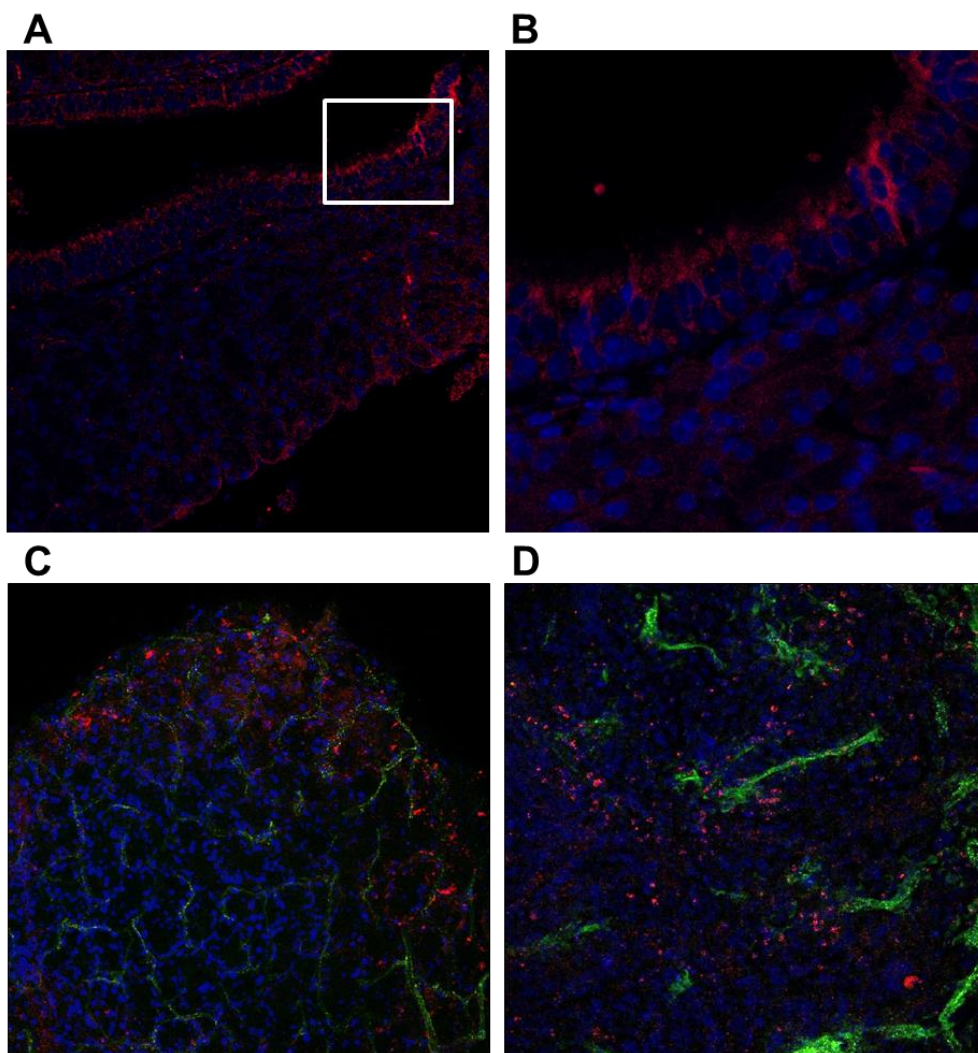


Figure 5. Assessment of nasal mucosa and TME after intranasal treatment. 4h after administration of Red dye – siRNA loaded PEGylated chitosan nanoparticles, nasal mucosa's were

isolated and processed for paraffin **(A and B)** and vibratome **(C)**; in both cases, a clear presence of red labeled siRNA was noted in the nasal mucosa (Red = siRNA, Blue = nuclei, green = vessels; only in vibratome sections). **(D)** Brains were also isolated at day 14 post tumor inoculation and 4 h after administration of Red labeled siRNA loaded PEGylated chitosan nanoparticles; and in the tumor area (as indicated by aberrant vasculature) red labeled siRNA was noted ; (Red = siRNA, Blue = nuclei, green = vessels; only in vibratome sections).

Discussion

In this work we have evaluated PEGylated chitosan nanoparticles to protect and transport siRNA molecules from the nasal cavity towards the TME. We found a rapid attachment to GL261 tumor cells and a consequent decrease in Gal-1 in vitro. Moreover, this formulation could modulate epithelial barriers, which in vivo results in a trans-mucosal transport. Furthermore also a diffuse distribution in the TME could be noticed.

PEGylation is considered as an optimization step for intranasal delivery since the inert PEG chains could decrease the reactivity of chitosan nanoparticles, and therefore rather promote a slip through the mucus layer, than sticking on it (223). By creating a co-polymer, the properties of chitosan are preserved, such as the transfection potential, and epithelial barrier modulation (245). In fact, we found a strong complexation of siRNA to PEGylated chitosan nanoparticles. Since the primary amines are partially covered by PEG, they are not accessible anymore for complexation with phosphates of TPP and siRNA. Since we chose a low Mw PEG polymer of 750 Da, and aimed for a low engraftment percentage under 5% (3.3 %), there is still interaction between the primary amines and the phosphate groups of TPP and siRNA, in order to form nanoparticles. Moreover, the siRNA was well protected as demonstrated by the gel retardation assay. This assay also demonstrated that SDS could still efficiently break the ionic interactions, and set siRNA free to migrate into the gel. Furthermore, in line with our previous findings, these nanocarriers can transfect GL261 tumor cells efficiently, and induce a knockdown for Gal-1 from day 4 to at least day 7 after transfection (243). With respect to Calu-3 epithelial monolayer modulation, we found no striking differences between the native formulation and this PEGylated formulation. Both are able to modulate the TEER, and promote permeation of macromolecules across the barrier. In contrary, some interesting findings were found on nasal biopsy monolayers. Here, we found that certain nasal epithelial cells do not respond to native chitosan, but do respond to PEGylated chitosan, although a substantial variance has been seen in two independent experiments, making this particular step of the transport prone for further research. This can indicate that PEGylation can promote the contact between the nanocarrier and the cells, due to an increased hydrophilicity (246). This was also reflected when we assessed the nasal mucosa of red dye labeled siRNA treated mice. Here we observed efficient transport through the columnar epithelium. To our opinion, this suggests a facilitated transport over this barrier. Furthermore, we also assessed the TME of an intracranially engrafted GBM model. Here we found a very quick and diffuse signal of red dye labeled siRNA. PEGylated chitosan nanoparticles seemed to spread more independent of vasculature than native chitosan nanoparticles, as demonstrated in our previous publication. Of note, the signal of red -dye labeled siRNA here, refers to an administered dose about 10 times lower than for native chitosan formulation, underlining a facilitated transport.

Conclusion

This work reflects a first step in the optimization of nose-to-brain transport, with respect to our prior publications. The intranasal transport in humans is predicted to be highly challenging in a clinical setting, with probably less smooth passage to the CNS as compared to in rodents. Therefore we are convinced that the optimization to the maximal extent in pre-clinical models can only positively influence the eventual outcome in a human setting. We demonstrated that PEGylated chitosan can modulate barriers that do not respond to native chitosan, and that they can easily induce a diffuse spread into GBM TME.

Materials and Methods

Materials

Chitosan (Heppe Medical Chitosan, Germany) was obtained that had a well-defined molecular weight of 50 kDa, giving a viscosity of 10 mPa.s for a 1% w/v solution in 1% acetic acid at 20°C. The degree of de-acetylation amounted to 85.2%. MeO-PEG-COOH was purchased from Iris Biotech (750 Da, PEG1161). 1-Ethyl-3-(3-dimethylaminopropyl)carbodiimide, N-hydroxysuccinimide, trifluoroacetic acid (TFA), sodium tripolyphosphate (TPP), sodium dodecyl sulfate (SDS) and Fluorescein Isothiocyanate-dextran (FITC-FD4) were purchased from Sigma-Aldrich. Anti-Gal-1 (5'ACCUGUGCCUACACUUCAdTdT3') and scrambled siRNA (5'GGAAAUCCCCAACAGUGAdTdT3') were purchased from GE Dharmacon, and if necessary, labeled with 5'-dye 547 (custom design, Lafayette, USA).

Methylcholanthrene-induced murine C57BL/6J syngeneic GL261 glioma cells were kindly provided by Dr. Eyupoglu (University of Erlangen, Germany) and were cultured as previously described (218). The *Calu-3* cell line was purchased from the American Type Culture Collection, ATCC HTB-55, and cultivated under the same conditions as described elsewhere (219). In case of primary nasal epithelium, cells were isolated and seeded as published in previous report (220).

Eight-to-ten week-old female C57BL/6J mice were purchased from Harlan (Horst, The Netherlands). The mice were maintained under conventional pathogen-free conditions. All experiments were approved by the bioethics committee of KU Leuven, which follows international guidelines.

Preparation of nanoparticles

PEGylated chitosan was prepared by carbodiimide crosslinker chemistry. As one chain of 50 kDa with 85% degree of deacetylation, contains about 265 primary amines, we aimed to graft 5% PEG, which is about 13 amines to target. Since the carbodiimide reaction is not perfect, we doubled this number to about 25 PEG to react. Excess of EDC and NHS was provided, and the reaction is 1 chitosan + 25 PEG + 50 EDC + 50 NHS. After reaction, the final product was washed over a 20 kDa membrane with at least 3 times the volume (Merck Millipore). The final product was freeze dried, and in case of ¹H NMR, dissolved in deuterium, and acidified with TFA. Nanoparticles were obtained by ionic gelation. Chitosan polymers were positively charged by dissolution in 0.1 M acetic acid buffer pH 4.5. TPP was

chosen as an ionic crosslinker to interconnect the chitosan polymers. Due to the negative charge of both TPP and the phosphates in siRNA, chitosan nanoparticles formed spontaneously (217). TPP (1 mg/ml) was added to chitosan (0.7 mg/ml) under constant stirring (1300 RPM, 25°C), with a chitosan to TPP weight ratio of 2.625/1. Per 6,3 mg of chitosan, 24 µg siRNA was administered. The final nanocarrier complex was filtered with 10 kDa (Merck Millipore Ultrafiltration), and the filter was washed with 0.075 M acetic acid buffer pH 4.5; so that in total 24 µl (i.e. in total 1 intranasal dose) contains about 3.5 µg siRNA.

Protection against siRNA degradation

Gel retardation assay was performed as described previously. In brief, the chitosan nanoparticles were incubated with 0.07% recombinant RNaseA (Life Technologies) at 37°C for different time periods. Then, the particles were loaded onto a 4% agarose gel that was prepared with Tris/borate/EDTA buffer (10 x Ultrapure TBE, Life Technologies). For better visualization, particles were dissociated using 0.1% SDS before loading them onto the gel. An equal amount of free siRNA was also incubated with RNaseA, and loaded onto the gel. Migration of siRNA was forced by applying 55 V for 2 h. Visualization was achieved by staining the gel with ethidium bromide for 30 min.

Interaction with glioma cells

Murine GL261 glioma cells were grown on a glass cover slip. Next, particles loaded with fluorescein-tagged siRNA were incubated with the cells. At regular time intervals, the glass cover slips were washed and fixed in 4% paraformaldehyde for 10 min. As background, brightfield pictures were taken, as described before. For protein analysis, 4 and 7 days after transfection, proteins were harvested and processed as described before.

Epithelial barrier integrity

As described before, Calu-3 cells were seeded on 12-well Transwell inserts at a density of 500 000 cells/ml (0.4 µm translucent polyester, Greiner). After 14 days, a confluent monolayer was formed that displayed a stable transepithelial electrical resistance (TEER), measured using an EVOM/Endohm (WPI Inc, Sarasota, USA). In case of primary nasal epithelium, cells were isolated and seeded as published in previous report (220) . In addition, macromolecular permeability was measured as an alternative parameter for evaluating the integrity of the epithelial barrier. Fluorescent Dextran 4kDa (FD4) was used as a hydrophilic model drug, a surrogate for the paracellular transport route (219).

In vivo experiments

As described before, nasal mucosa's were isolated and processed for paraffin and vibratome sectioning. In brief, for paraffin, samples were incubated in 70 % EtOH, and for vibratome in 4% PFA. Sections were prepared of 5 µm and 200 µm respectively, and visualized under Leica SP8 at 25x.

6. ADDENDUM – CARRIER DEVELOPMENT

To better understand the results of this thesis, we would like to explain why we chose the selected chitosan formulation. For this process, we have set-up a chain of targeted experiments, which could screen a potential 'ideal' candidate formulation, based on required/desired chemical characteristics to acquire necessary key features fit for intranasal transport, and silencing of Gal-1 expression in GL261 tumor cells. These results, and the previous publications, were also partially included in a patent application (GB1519841.9) is initiated by KU Leuven(LRD) and ULB(TTO) in agreement.

1. Selection procedure of carrier

In literature, many different carrier systems are developed that can protect siRNA. These carrier systems can prevent the degradation of siRNA by RNase enzymes, and promote the uptake in cells, thereby promoting the half-life and biological efficacy of siRNA molecules. For our purpose, delivering and protecting siRNA from the nasal cavity towards the brain, we will focus on the polymer **chitosan**. This polymer is able to transport molecules from the nasal cavity towards the brain, especially when they are prepared as nanoparticles. We will prioritize chitosan as first-choice carrier system, due to its GRAS status, wide use as pharmaceutical excipient, and low-toxicity profile. This linear polymer is an **ideal candidate in many aspects**. Chitosan is an extensively studied carrier system that is biodegradable and displays low toxicity and immunogenicity (135, 247). Moreover, chitosan can prolong its residence time in the nasal mucosa due to its mucoadhesive properties (178). The presence of chitosan on the nasal mucosa will also transiently open the tight junctions between the cells of the nasal epithelium (219). Chitosan can be formulated easily into nanoparticles by ionic gelation. In this process, nanoparticles are formed based on the crosslinking of the positively charged polymer chitosan, and a negative crosslinker e.g. tripolyphosphate. Many molecules can be loaded into these nanoparticles, and are thereby efficiently transported from the nasal cavity to the brain of mice and rats (147, 148). Due to the net positive charge of chitosan, it can also efficiently complexate with nucleic acids, such as DNA or siRNA (Fig1) (247). Both *in vitro* and *in vivo*, chitosan nanoparticles are able to complexate with siRNA and induce a specific knockdown in the targeted cell (217, 248).

However, in literature there is a huge variation in the properties of the chitosan polymer used for nanoparticle formulation. A literature overview for the different polymers that are used with a relation to A/ complexation with siRNA and *in vitro* knockdown assessment, and B/ intranasal delivery are depicted in Table 1.

Name	Mw	DD	DQ	Method	Size			Zetapotential			Encapsulation rate	N/P ratio	Chitosan/TPP	application	reference
					pH 7,4	pH 6,5	pH 4,5	pH 7,4	pH 6,5	pH 4,5					
CL113	50,000-150,000	84		simple complexation	108,7/20,8	130,1/4,9	235,2/36,6	6,1/3	11,6/6,8	24/2,1	>95%	30:1	6:1	in vitro silencing	20096725
CL213	150,000-400,000	86		simple complexation	186,6/34	203,2/30,9	244,3/50,9	5,6/0,5	16,9/2,9	24/1,6	>95%	30:1	6:1	in vitro silencing	20096725
L07293	67.400	84		simple complexation	122,7/43,6	119,6/18,3	248/27,3	9,7/7,9	16,5/2,3	22,2/2	>95%	30:1	6:1	in vitro silencing	20096725
TMC25	42.000	88,7	25,1	simple complexation	165,5/32,6	134,8/26,1	131,7/24,7	13,2/6,8	20,4/2,2	24,3/1,2	>95%	30:1	6:1	in vitro silencing	20096725
TMC30	50.000	86	27	simple complexation	161,6/14,5	120,1/21,1	172,5/41,8	13,3/2,7	13,8/7,1	20,4/4	>95%	30:1	6:1	in vitro silencing	20096725
TMC56	50.000	88,7	45,4	simple complexation	128,9/31	211,8/64	133,9/30,4	10,6/6,7	18/5,8	19,9/1	>95%	30:1	6:1	in vitro silencing	20096725
CL113	50,000-150,000	84		ionic gelation	108,2/14	155,6/46,3	167,6/24,3	6,7/3,4	16,1/2,4	21,5/1	>95%	30:1	6:1	in vitro silencing	20096725
CL213	150,000-400,000	86		ionic gelation	123,6/15,8	178,7/43,7	212,1/35,5	10,3/8,4	18,1/8,9	26,8/2,5	>95%	30:1	6:1	in vitro silencing	20096725
L07293	67.400	84		ionic gelation	114/25	154,6/49,1	169,8/26,9	7,1/6,2	17,2/4,2	20,9/1,7	>95%	30:1	6:1	in vitro silencing	20096725
TMC25	42.000	88,7	25,1	ionic gelation	168,6/20,8	234,7/33,1	165,5/39,8	15,1/4,2	22,5/4,1	23/2,3	>95%	30:1	6:1	in vitro silencing	20096725
TMC30	50.000	86	27	ionic gelation	193,7/7,6	232,1/41	211,1/42,1	10,5/3,5	21,1/5	25,9/1,5	>95%	30:1	6:1	in vitro silencing	20096725
TMC56	50.000	88,7	45,4	ionic gelation	144,6/10,8	183,6/23,9	181,9/26,5	10,8/7,8	17,6/5,5	17,8/0,7	>95%	30:1	6:1	in vitro silencing	20096725
chitosan	750.000	85		ionic gelation		185,4/8,4		38,4/2,85			no siRNA	-	2,19:1	intranasal delivery	22561106
LMW chitosan	20-300cps	>85		ionic gelation		167/6,5		23,83/1,76			no siRNA	-	2,19:2	intranasal delivery	S0144861712001889
MMW	200-800cps	85		ionic gelation		161,3/4,7		40,3/2,7			no siRNA	-	3,3:1	intranasal delivery	23266466
CL113 (chitosan chloride)	113.000	86		ionic gelation		415/44,6					59% ?	6:1	in vitro silencing	16959358	
CL213	270.000	86		ionic gelation		709/50,3					72% ?	6:1	in vitro silencing	16959358	
G113 (chitosan glutamate)	160.000	86		ionic gelation		276/17,9					90% ?	6:1	in vitro silencing	16959358	
G213	470.000	86		ionic gelation		510/22,9					84% ?	6:1	in vitro silencing	16959358	
92-10	11.800	92		simple complexation chitosan / siRNA		63/8		23/1			5:1		in vitro silencing	22457597	
80-10	14.500	80				91/7		18/2			10:1		in vitro silencing	22457597	
80-40	53.000	80				86/9		18/1			5:1		in vitro silencing	22457597	
80-80	110.000	80				100/8		16/1			5:1		in vitro silencing	22457597	

Table 1: available chitosan polymers in literature described.

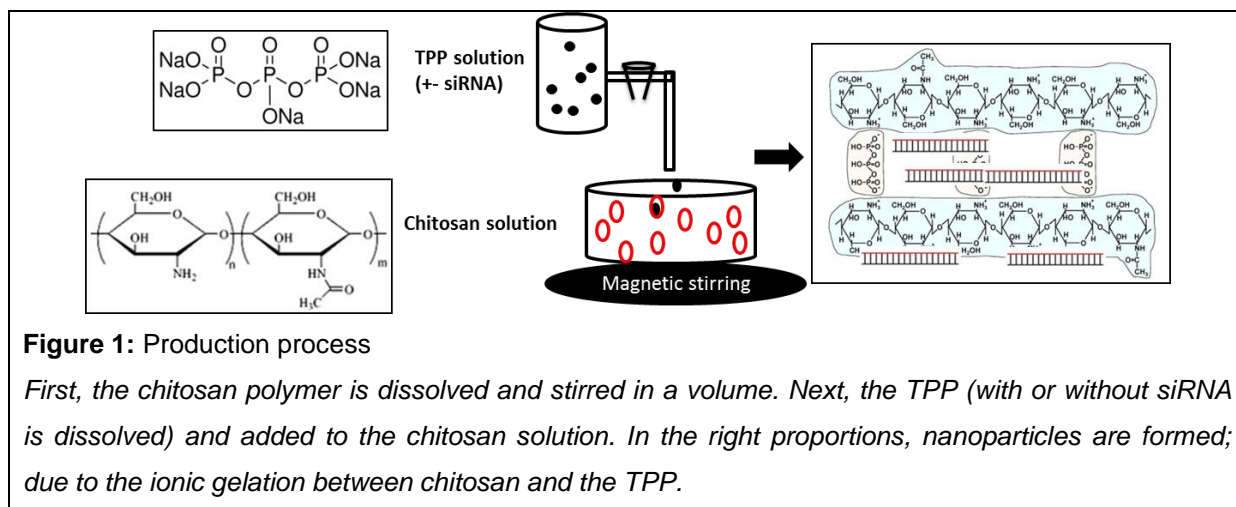
Abbreviations: Mw (Molecular Weight), DD (degree of deacetylation), DQ (degree of quaternization), nm (nanometer), stDEV (standard deviation), mV (millivolt), N/P ratio (primary amine to phosphate ratio), TPP (tripolyphosphate), Reference: PMID (pubmed ID), cps (centipoise)

As you can observe from this table, quite a few articles use chitosan polymer with a range of molecular weight, not a fixed number. To our knowledge, it would have been better to work with a well-defined exact molecular weight. Such a polymer will reduce inter- and intra- batch variability. Moreover, we postulated that a larger polymer, with a higher molecular weight, would result in larger particles. As for our perspective, small nanoparticles are probably desirable. Moreover, it is mentioned in literature that chitosan nanoparticles need to have a positive zeta-potential for many reasons: interactions with the cilia (muco-adhesive properties), interactions with cells (transfection properties), and stability in solutions (off-the-shelf availability). Therefore, we have ordered two polymers of chitosan with a well-defined low molecular weight: 50kDa, and 90kDa. Both polymers were ordered from Heppe Medical Chitosan (Saale, Germany), with product number 93000 (sample box, with 3 polymers (50, 90 and 150 kDa). Moreover, we demanded a degree of deacetylation of about 85%. Upon further investigation (see below) we opted to continue working with the 50kDa polymer.

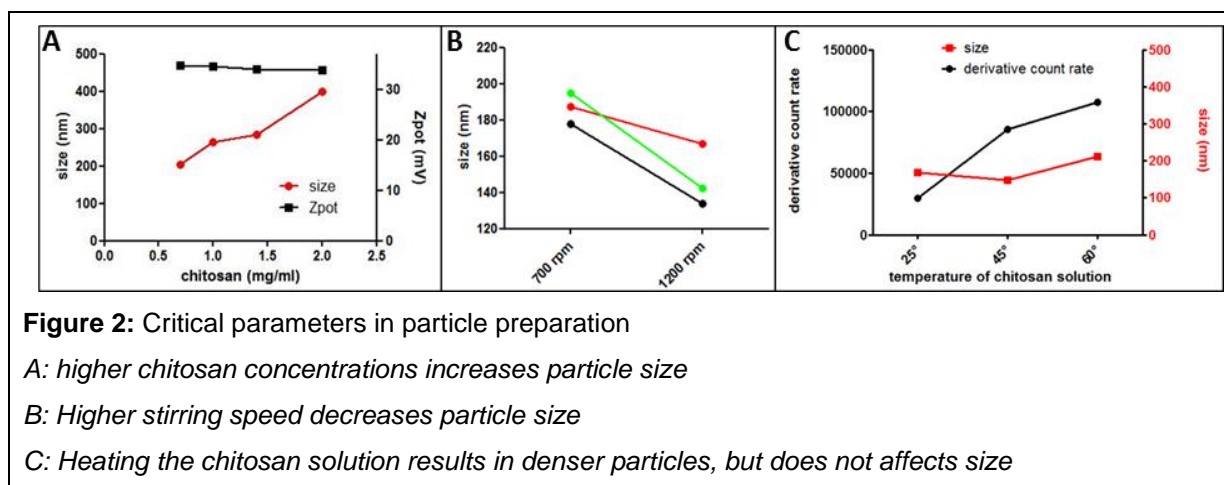
2. Selection of formulation

First of all, we started experimenting to make stable particles that have a size within the nano-range. To produce these particles we chose ionic gelation, as it is widely described in literature. It is a fairly easy process, with mild reagents, that will most likely not damage the active reagent (in casu: siRNA). For this ionic gelation, we needed to charge the chitosan polymer positively. This can be performed by dissolving the chitosan polymer in 0.1M acetic acid buffer. To be sure all primary amines are positively charged, the solution was dissolved for at least 16h. Now the positively charged chitosan can interact with negatively charged molecule, to act as a crosslinker, and promote the formation of particles (both nano and micro-particles). The anionic crosslinker that we used is sodium tripolyphosphate (TPP: CAS

Number 7758-29-4, Sigma 238503). We always used a volume ratio of $\frac{3}{4}$ chitosan and $\frac{1}{4}$ TPP. The experimental set-up is depicted in Fig1.



These pilot experiments were influenced by several parameters. We first tested different concentrations of chitosan polymer for a constant amount of TPP (0.8 ml of 1 mg/ml, adjusted to 1 ml with MilliQ water). We observed that at the lowest concentration (3 ml of 0.7 mg/ml), the smallest nanoparticles were achieved (Fig 2A). Lower concentrations did not result in nanoparticles, and higher concentrations result in larger particles: microparticles or even aggregates. Another parameter that we checked was the speed of magnetic stirring (Fig 2B). We observed that at higher stirring speed, smaller particles were obtained. Higher stirring speed prevents probably the aggregations, and promotes the formation of the strongest interactions between the chitosan and the TPP (and siRNA). Another parameter we checked was the temperature of the reaction. Heating the chitosan solution resulted in more dense particles (as reflected by the derivative count rate). Heating causes the chitosan polymer to be maximally unfolded, and maximally available for interaction with TPP. We wanted to obtain smallest possible particles with these excipients, and therefore we work at a chitosan concentration of 0.7 mg/ml, we stir the volume at 1200 RPM, and we work at room temperature.



With these settings, we prepared 4 different formulations. These four formulations were obtained via alterations in A/ chitosan to TPP ratio, and B/ molecular weight of chitosan. Chitosan to TPP ratio was either 2.625/1 or 6/1, and the molecular weight of chitosan was either 50 kDa or 90 kDa. The evaluation criteria for these four formulations were as follows: size, charge, density, complexation with siRNA, adherence to tumor cells *in vitro*, and galectin-1 suppressive capacity on murine glioblastoma GL261 cells (Table 2). As for the siRNA loading, we always included 0.4 ml of 50 μ M siRNA per 2.1 mg of chitosan (3 ml of 0.7 mg/ml chitosan).

Formulations:

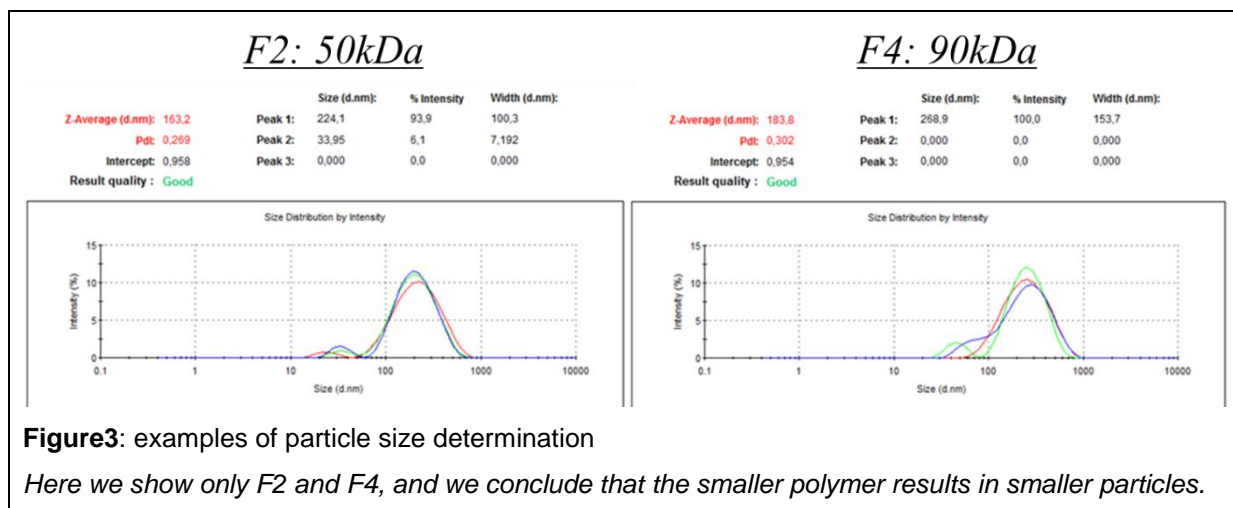
- 1) 50kDa, chitosan/TPP: 6/1
- 2) 50kDa, chitosan/TPP: 2.625/1
- 3) 90kDa, chitosan/TPP: 6/1
- 4) 90kDa, chitosan/TPP: 2.625/1

<i>Formulation</i>	<i>Size (nm)</i>	<i>Charge (mV)</i>	<i>siRNA complexation</i>	<i>siRNA encapsulation %</i>	<i>Adherence in vitro</i>	<i>Gal-1 suppression %</i>
1	165,9 \pm 3,9	+ 32.1	Yes	80	Ok, but aggregates	\pm 80
2	162,7 \pm 6,7	+ 30.1	Yes	79	Ok, less aggregates	\pm 80
3	189,1 \pm 5,9	+ 32.5	Yes, stronger than 50kDa	89,3	Ok, but aggregates	/
4	181,5 \pm 10,1	+ 28.9	Yes, stronger than 50kDa	84	Ok, less aggregates	\pm 50
Figure	3	/	4	5	6	7

Table 2: Summary formulations and parameters.

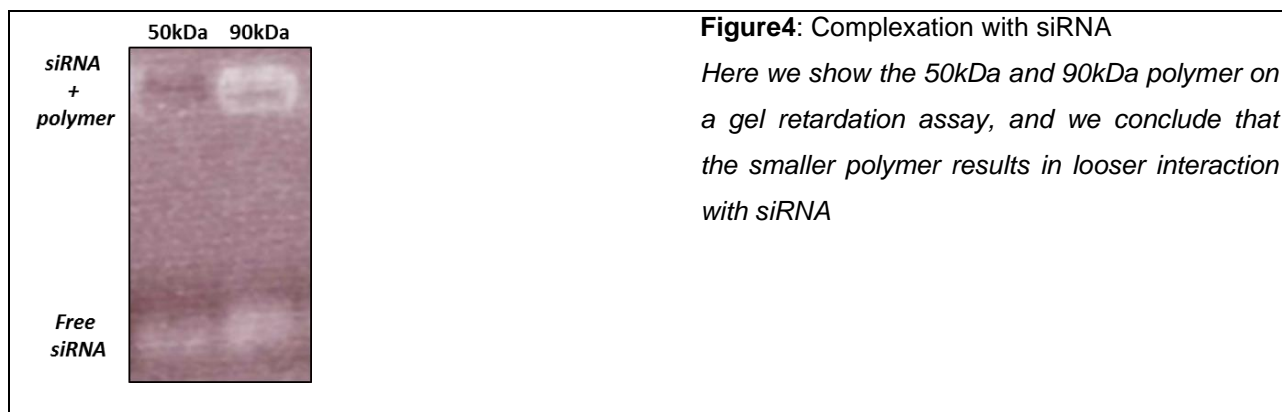
Here we provide a quick overview of the available formulations and different characteristics.

We will briefly show all the parameters step-by-step. The first parameter we evaluated is the (Z-average) size (Fig 3). This can be measured by using a Nano-series zetasizer (Malvern Instruments, UK). By means of light scattering, an indirect estimation of the size can be obtained. Moreover, we get information on the stability of the formulations, and also a quality report that calculates if the particles are in accordance with the standards for nanoparticle formulations. We continuously observed that the particles prepared with the smaller chitosan polymer, also results in smaller particles. This confirms the trend in literature as depicted in table 1. All formulations were stable in solution (no sedimentation/aggregation/dissolution of particles), and showed a good quality report.

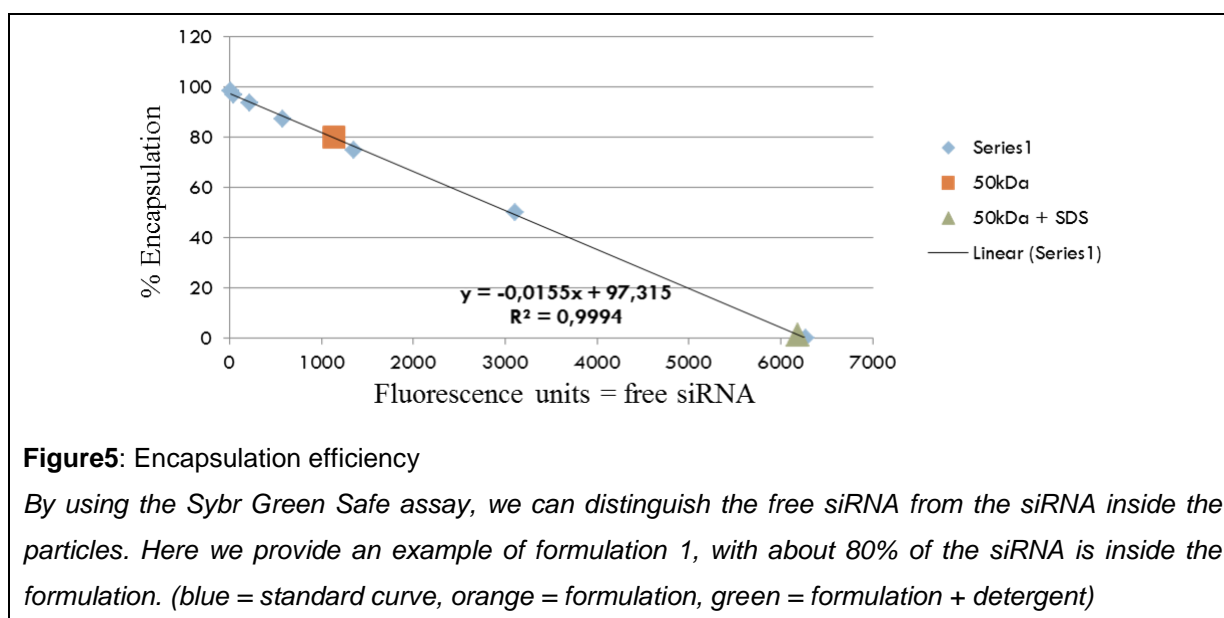


Next, we also analyzed the zeta potential. This is the netto charge of the prepared nanoparticle. This can be measured with same Zetasizer as used for the size measurement. We typically observed that the zeta potential was lower in the formulations with chitosan/TPP ratio of 2.625 as in formulations with chitosan/TPP of 6. By adding more TPP, we induce more crosslinking, and more dense particles; however TPP carries a netto negative charge at neutral pH. More TPP will therefore decrease the zeta potential (Table 2).

The main purpose of the project is to make nanoparticles, enloaded with siRNA. It has been widely described that chitosan polymer can complexate with siRNA molecules. In this test, we co-incubated the two chitosan polymers (50kDa and 90kDa) with the siRNA for 30min at room temperature. To examine how strong the interactions between the chitosan polymer and the siRNA are established we tried to break these interactions with SDS (detergent) + loading on a gel and applying a voltage of 55V for 2h (to pull the siRNA out of the complex) (Fig 4). To visualize the siRNA we treated the gel with Ethidium bromide. When we applied no SDS all signal remained on top of the gel (not shown), which means no siRNA is set free to migrate. When we apply SDS and a voltage, there is migration of the free siRNA. However, we observed that the 50kDa could more easily release the siRNA, while the 90kDa still retains fractions of the siRNA on top of the gel. A strong complexation of the siRNA with the chitosan polymer is wanted and necessary, but a too strong complexation might also impair the drug delivery capacity. SiRNA molecules need to be set free in the cytosol of cells to be biologically active.



To determine the encapsulation efficiency of the nanoparticles as described in table2, we needed to selectively detect the free siRNA. Via this way, we could calculate the percentage of siRNA that is inside the formulation. We found the sybr green safe reagent to be very helpful (Fig 5)(232). This is a dye that can only emit fluorescence if it is encapsulated inside the nucleotides (=free siRNA). Here we made a standard curve by exciting the dye + free siRNA at 480nm, and emission at 530nm. Here, F1 is depicted and results in about 80% encapsulation of the available siRNA. After treating the particles with SDS, all the siRNA is set free, and the sybr green can bind the 100 % of free siRNA = 0% encapsulation. (This result is confirming the gel retardation assay). In the overview table, we observe that the 50kDa seems to be less efficient to encapsulate the siRNA in comparison to the 90kDa, due to the strong binding.



Now that we knew the particles are conform size, charge, complexation and siRNA encapsulation, we started testing the adherence on tumor cells *in vitro*. For this set of experiments, we loaded fluorescent-labeled siRNA in chitosan particles. Next, we observed the adherence of the particles on the murine glioblastoma GL261 cells. Already after 30min, the particles adhered to the cells, and the

signal increased over time. Here in Fig 6, we show the 2h time point. We observed that there were more aggregates in F1 and F3 than in F2 and F4. Chitosan particles have been mentioned in literature to be not-serum compatible. Therefore we hypothesize that the formulation aggregates a bit with the serum present in the culture media. Reducing the reactivity of the chitosan particles, can be obtained with adding more TPP (F2 and F4). This not only results in a more decreased zeta potential, but also in a more dispersed distribution on the GL261 cells.

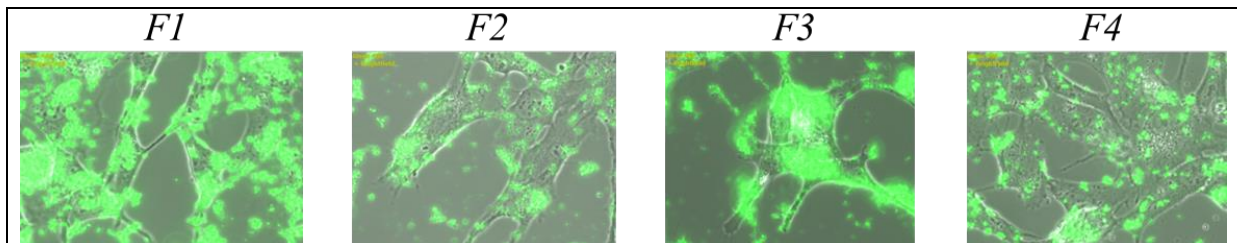


Figure6: Adherence to GL261 cells after 2h

All formulations can adhere rapidly to the GL261 tumor cells. F1 and F3 seem to be more aggregated than F2 and F4.

As we observed in figure 6 a rapid attachment to the cells, we wondered if the presence of the particles, enloaded with siRNA against Gal-1, would also result in a decrease of Gal-1 in the GL261 cells. To measure this phenomenon, we choose to measure the Gal-1 mRNA inside the GL261 cells as a primary outcome parameter of the formulation (Fig 7). Chitosan nanoparticles should be taken up by the cells, in an endo-lysosomal pathway, then released in the cytosol, and selectively destruct the mRNA encoding Gal-1. In the Y-axis, you can read the ratio of Gal-1 to GAPDH (housekeeping gene) in the anti-Gal-1 siRNA treated cells compared to the scrambled siRNA treated cells. In the X-axis you can read the days after transfection. We observe that all formulations can suppress Gal-1, with the strongest effect in the first days after transfection. We also observe that this is a transient effect, and that Gal-1 levels normalize after about 1 week.

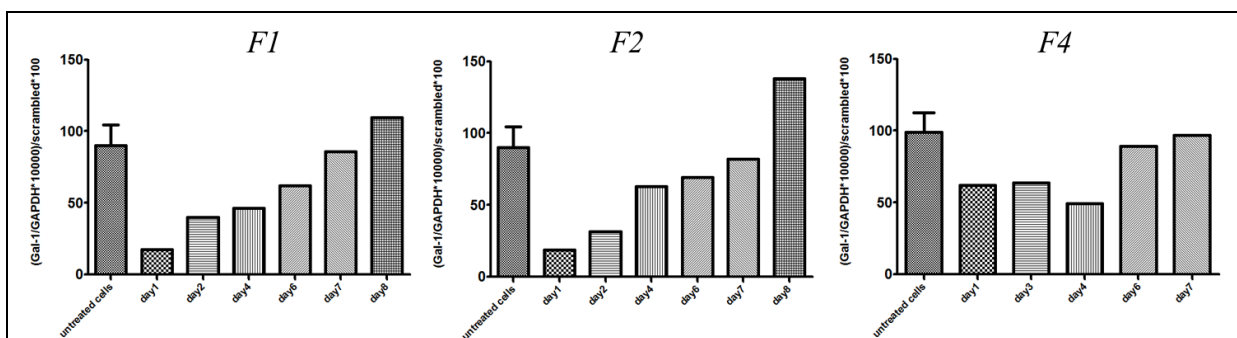


Figure7: *In vitro* suppression of Gal-1 in GL261 tumor cells

All formulations can induce a suppression of Gal-1. However, we noted that the particles that were prepared with the 50kDa chitosan polymer were more potent in delivering the siRNA inside the GL261 cells, despite having a lower encapsulation%.

After evaluating the different criteria described here above, we opted to continue working with F2. This formulation showed consistently the smallest particles (although it is only a small difference, nevertheless). Working at a chitosan/TPP ratio of 2.625 results in a decreased zeta potential, and thereby reducing the reactivity of the particles. Moreover, the 50kDa is shown to complexate the siRNA very well, but not as strong as the 90kDa. This reduced complexation might facilitate the release inside the cells. All formulations showed a very high encapsulation percentage. To this end, no big differences were observed. Nevertheless, we do observe that treating the siRNA loaded nanoparticles with a strong detergent, F2 released all his content. Next, we evaluated the adherence to the tumor cells. F2 and F4 showed a distinct behavior, and a more disperse distribution on the cells. As a primary outcome parameter for functionality, we checked Gal-1 mRNA after overnight incubation with the nanoparticles. As suggested from previous experiments, the 50kDa seemed to be more potent to induce Gal-1 suppression.

3. Concentration of particles

Selection of the most optimal formulation was a first crucial part of the project. As depicted in Fig 1, we need to have a certain amount of volume to stir the chitosan solution. Moreover, we show in Fig 2 that at a low concentration of chitosan the smallest particles are formed. These two aspects together, make that we have quite low numbers of particles in suspension. These diluted nanoparticles are no problem for the carrier characterization and early *in vitro* experiments as presented above. However, the goal of the project is to make a formulation that can be administered intranasally. The nasal cavity of mice, the major test animal we use, is very small (only 0.032 cm³, and a maximal volume of 24 μ l). The volume restriction and the low rate of transport are absolute crucial hurdles to overcome. Therefore, the concentration of the particles is just as important as selecting a good formulation.

In literature many techniques are described to concentrate nano-sized particles. The two most popular devices are ultrafiltration, and ultracentrifugation. We have tested the ultrafiltration device (Amicon). However, the F2 formulation blocked the membrane (10-30 kDa Ultrafiltration discs, Merck, Millipore) completely. Probably, the relative high reactivity of the chitosan particles is interacting with the membrane, and blocks the pores. Therefore, we were obliged to search for ultracentrifugation techniques. In literature, centrifugation is often mentioned for collecting chitosan nanoparticles. However, we did not find in literature a single study that analyses the concentration and quality of the particles after ultracentrifugation. Moreover, absolute *g*-forces are scarcely mentioned. For these reasons, we optimized the ultracentrifugation method for collecting the F2 formulation. We found that after overnight ultracentrifugation at 110 000 *xg*, still particles were in supernatant. These findings are conflicting with literature. Quite often, it is mentioned that the supernatants contain no nanoparticles. On the other hand, if we centrifuge overnight, we noticed the pellet was very difficult to dissolve. It seemed that particles were disrupted by the high *g* forces. To this end, we needed to make a compromise between **A/** having as much particles in the pellet as possible, and **B/** not centrifuging too long or too hard, as this will disrupt the particles. Therefore, we created a schedule to centrifuge the particles at 30 000 RPM (\pm 66 000 *xg*) during 20 min at 4°C. The obtained pellets we conserved, and the supernatant was centrifuged again. This 2nd pellet was combined with the first pellet. The

supernatant was centrifuged again, and the 3th and last pellet, was also combined with the two previous pellets. With this 3x centrifugation step, we typically concentrate the formulation from 25 ml to 1 ml. To measure the amount of concentrated particles, we loaded fluorescent siRNA into our particles. By measuring the fluorescent concentration in the pellet, we would not only know the factor of concentration, but also a confirmation of the encapsulation %. The combined centrifugation steps resulted in a concentration of the fluorescent siRNA of about 85.9%. This pellet was dissolved in the 0.1M acetic acid buffer. To our experience, the pellet was always easily resuspendable and no signs of aggregation were observed.

In order to further concentrate the particles, we optimized also the freeze drying conditions for our F2 formulation. Freeze drying will not only concentrate the formulation, but will also increase the stability over time. Moreover, it allows us to prepare big batches, with an off-the-shelf availability of the desired product, with a minimum of inter-experimental variability. The freezing and subsequent sublimation of the water will put a lot of stress on the nanoparticles. Therefore, we need to add a lyoprotectant. This is typically a sugar structure that will form a 3D matrix around the particles and preserve them throughout the lyophilisation process. Initially, we started with trehalose as a model sugar structure. In Fig 8, you can observe the result of such a freeze drying experiment. We lyophilised the ultracentrifuged F2 pellets, and added trehalose in different sugar/nanoparticles weight ratios. In Fig 8A, you can see the freeze dried products. We notice that if you add no lyoprotectant, the nanoparticles are destroyed during the freeze drying, as can be observed in the first tube. When suboptimal concentrations of trehalose are added, there is also destruction of the nanoparticles. We observed conservation of the nanoparticles, starting from a weight ratio of 11/1 (lyoprotectant/nanoparticles). These findings were also confirmed by zetasizer measurements (Fig 8B). Adding no lyoprotectant or suboptimal concentrations, failed to detect any nanoparticulated formulation. On the other hand, starting from tube 11/1, we observed a mild conservation of the particles, and from 14/1 a complete conservation of the particles. Therefore, we concluded that trehalose was an excellent lyoprotectant, when it is added in weight ratio lyoprotectant/nanoparticles of 14/1. We also depict here in Fig 8B, that there is no difference in particle morphology before or after ultracentrifugation.

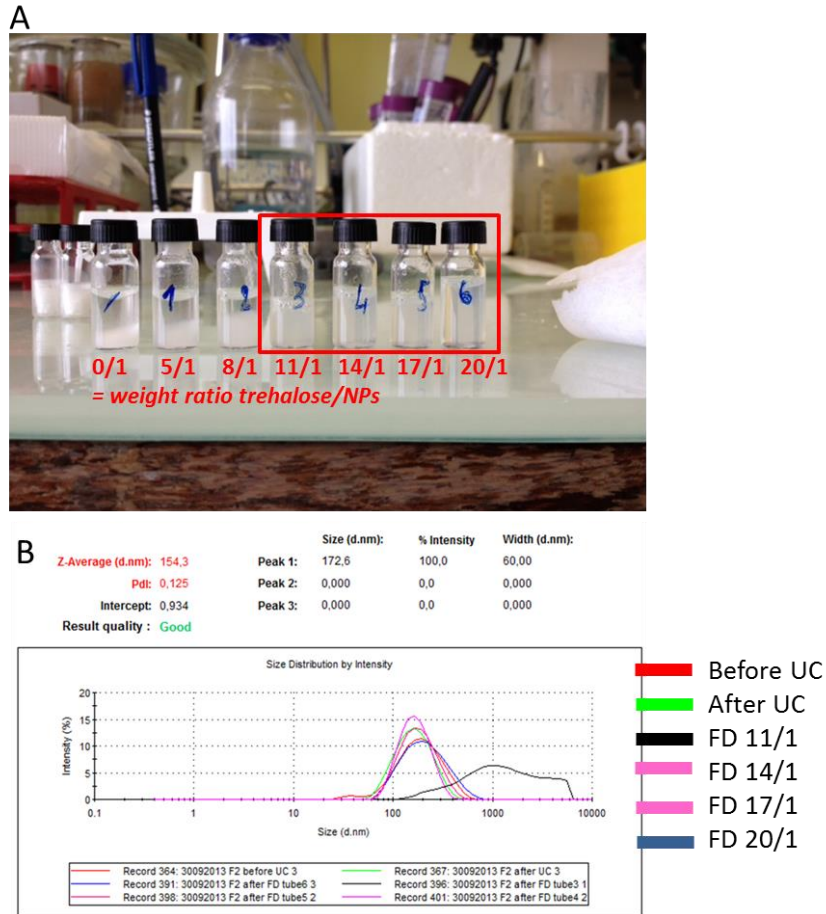


Figure8: Concentration process of F2 nanoparticles - trehalose

A: resuspended freeze dried products of F2 pellets

B: Zeta sizer read outs of the conditions mentioned in A

In conclusion, the optimized formulation was prepared with all the parameters as described above. The 50kDa polymer was dissolved in a 0.1M acetic acid buffer, and stirred for at least 16h. Next, we prepared F2 at the defined chitosan/TPP ratio, at room temperature, and with 1 200 RPM stirring. This formulation had an average size of well below 200 nm. Subsequently, we centrifuged the formulation for three times as described above, capturing 85.9% of siRNA (and formulation). Finally, this pellet was lyophilized with trehalose as a lyoprotectant, in the ratio as mentioned above. The volume, in which the freeze dried product is dissolved, is limited by the solubility of the trehalose (50 mg/ml).

With this construct our first *in vivo*-distribution experiments were performed. In parallel, we continued to optimize the freeze drying conditions. We found that sucrose is also a potent lyoprotectant for our F2 formulation (Fig 9). Here we show that sucrose can be used as a lyoprotectant in a weight ratio of 8/1 (or more). Adding no sucrose, or ratio 5/1, was not enough to preserve the particles. 8/1, 11/1, 14/1 and 17/1 seemed equally potent. Moreover, sucrose has a much higher solubility. Therefore, we can dissolve the F2 freeze dried pellets in a much smaller volume as before. In table3 we give an overview of the quantity of 1 formulation unit, which can be administered in 1 mouse for 1 intranasal

administration dose. Please note that now 1 dosis (freeze dried with sucrose) for 1 mouse is indeed 23-24 μ l, the total volume that can be administered in the nasal cavity of 1 mouse.

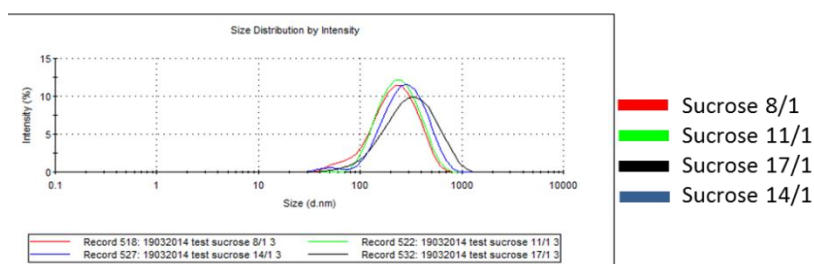
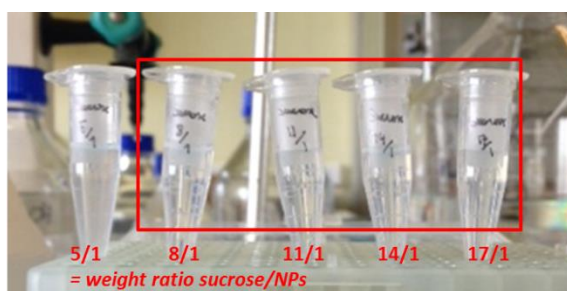


Figure9: Concentration process of F2 nanoparticles - sucrose

A: resuspended freeze dried products of F2 pellets

B: Zeta sizer read outs of the conditions mentioned in A

Product	Quantity
Chitosan (50kDa polymer)	1.5 ml of 0.7 mg/ml (1.05 mg)
TPP	0.1 ml of 4 mg/ml (0.4 mg)
Chitosan/TPP ratio	2.625
siRNA	0.2 ml of 20 μ M (\pm 48 μ g)
Trehalose	20.3 mg
	Dissolved in 406 μ l (50 mg/ml)
Sucrose	11.6 mg
	Dissolved in 23.2 μ l (500 mg/ml)

Table 3: Composition of 1 dose F2 formulation for 1 mouse.

7. Final discussion and Perspectives

7.1. Development of chitosan nanoparticles for nose-to-brain transport

Over the past years, it became clear that the TME of a GBM is a highly immune suppressive locus, with multiple mediators that can drive immune suppression and actively block immune activation. In this respect, Gal-1 is a key molecule which can fulfill both properties. Moreover, Gal-1 is demonstrated to have numerous GBM progression features. In this research project we evaluated the possibility that Gal-1 can be blocked via nose-to-brain transport of siRNA molecules. To achieve this goal, there is an immediate necessity to prevent degradation of siRNA molecules since there is an inherent risk of degradation by RNase enzymes present in the mucus layer. Therefore, nanoparticles were created that could protect siGal-1.

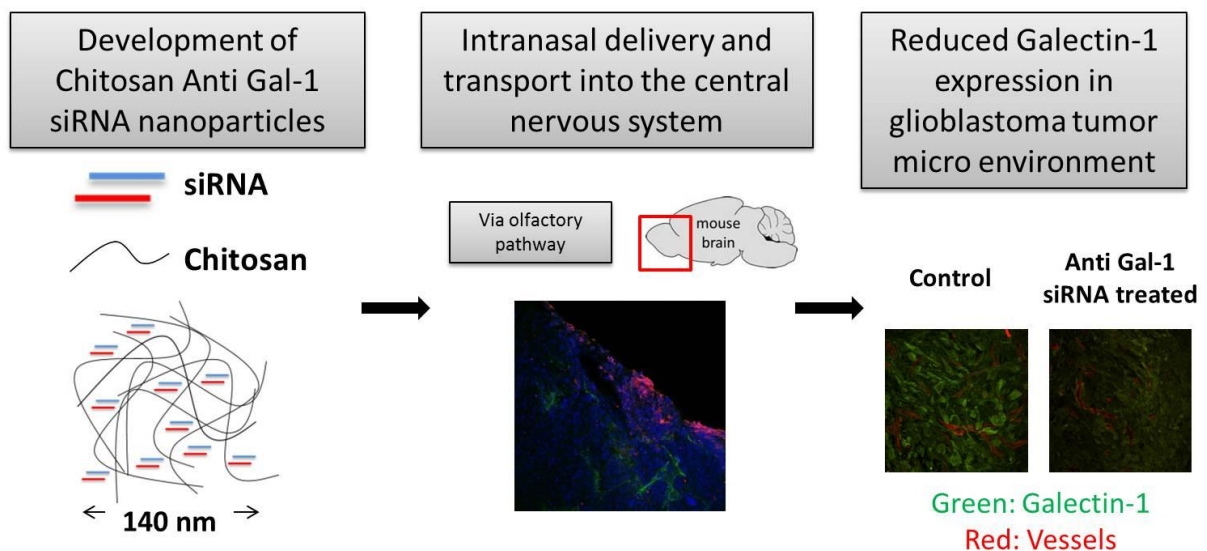
We selected the chitosan nanoparticle formulation on early-indicative and selective assays that could indicate the best candidate formulation fit for our purposes (see addendum). A first point of distinction was noticed in the polymer Mw, as higher Mw nanoparticles tend to complexate to larger nanoparticles. Multiple literature reports report similar results, and moreover indicate that smaller nanoparticles could also be more effectively delivered into cells (249, 250). We also observed a higher decrease of *gal-1* mRNA when incubated with 50 kDa chitosan in comparison with 90 kDa. Moreover, the amount of amines of chitosan and the amount of phosphates of TPP present in the mixture was another determinant for the final outcome. Remarkably, we found a ratio very similar to other literature reports (225). Adding higher quantity of negatively charged cross-linker to the mixture could induce more linkage, and even result in aggregates. Therefore, an optimized ratio of N:P, is important to obtain nanoparticles, and achieve stability in aqueous media. We also detected that higher amount of TPP, decrease the Zeta Potential (due to more negatively charged phosphates), which decreases the stability. Another major determinant was the concentration process of these nanoparticles. Since the nasal cavity of our murine GBM model is limited to about 24 μ l, the concentration process is of key importance (89). We tried several techniques, such as ultrafiltration, and Amicon centrifugal filter tubes, but ultracentrifugation was in our hands the best technique (147). By spinning the supernatant twice after initial centrifugation, an optimal concentration was achieved. To further decrease the volume per amount of particle, and to preserve the nanoparticles for longer time periods, we also optimized the freeze-drying process. Both sucrose and trehalose were found to be able to protect chitosan nanoparticles during lyophilization, when added in sufficient amounts. Mannitol was also tested, but failed to protect adequately. Interestingly, other reports that use chitosan nanoparticles to deliver therapeutics from the nasal cavity to the brain, also report lyophilization to concentrate particles, but do not use lyoprotectants (147).

Once the 'optimal' formulation could be selected, a thorough evaluation was performed elucidating the full potential of such chitosan formulation. As noticed by Katas et al, similar nanoparticles are capable to prevent degradation (217). We confirmed this feature via gel retardation assay, which revealed no degradation of siGal-1 even after 3 h co-incubation with RNase enzymes. Contrarily, free siRNA was

rapidly degraded, as it would be in contact with the mucus layer after intranasal administration. Furthermore, we assessed the formulation's potential to deliver siGal-1 *in vitro* to GBM cells. We started to evaluate in our murine GL261 cells, where we found a clear suppression of *gal-1* mRNA in the first days after transfection. This rapid knockdown is indicative for a rapid dissociation of siGal-1 from the nano-complex in the cytoplasm. Already after a few hours, we noticed nanoparticles adhering on the surface of GL261 cells. Consequently, these particles are taken up by clathrin/caveolin mediated mechanisms as reported in literature (251). After entry into the cell, endosomal/lysosomal degradation is likely to occur, potentially destroying the siGal-1 cargo. Interestingly, polymers as chitosan can function as a proton buffer sponge. By scavenging influx of H^+ during lysosomal degradation, disruption can occur, and the content is set free in the cytosol (252). Likely, protonation of primary amines on the chitosan reduces the charge and ionic gelation, thereby releasing siGal-1. Not only could we demonstrate the knockdown on mRNA level, but also on protein level. As such a rapid mRNA degradation would occur (within 48 h after transfection), then a rapid protein degradation can be expected (61). We observed a robust suppression of Gal-1 production from day 4 until at least day 7. Over time, cells will rapidly replicate and dilute siGal-1 until a certain threshold where RNAi is insufficient for protein decrease. Furthermore, we could also demonstrate the decrease of Gal-1 in several patient cell lines. This demonstrates the versatility of a nanoparticle platform, where solely by changing the siGal-1 from its murine sequence to the human sequence, could produce similar results. In brief, the functionality of decreasing Gal-1 in GL261 was evaluated by means of a scratch assay. We could identify the role of Gal-1 in migration and proliferation of GL261 cells. However, this assay could not distinguish between both, as each of them can explain the results of the scratch pattern.

Intranasal transport to reach the CNS is considered a harsh and challenging approach, with minimal passage. This was also indicated by the observation that free siRNA could not migrate into the CNS, but merely attach to the nasal mucosa. These results were very well in line with Kanazawa et al, who reported passage of siRNA exclusively if formulated into PEG-PCL nanoparticles (232). Moreover they could report a moderate entrapment of siRNA in the mucus layer, where it is most likely rapidly degraded. These data underline the necessity for nucleotides to be encapsulated in nanoparticles. To this end, chitosan is an interesting excipient as it does not merely passively protect siGal-1, but also actively modulates epithelial barriers. As mentioned before, chitosan can reduce mucus transport, and more importantly, transiently internalize tight-junction molecules (219). In an *in vitro* model for epithelial monolayers, we could confirm these data to most extent. Chitosan nanoparticles could transiently reduce the resistance, and promote transport of macromolecules across the monolayer. Since these effects had no permanent lifespan, chitosan was considered to have a transient effect on the tight-junctions, which normalizes after a few hours. This interesting feature is probably the main feature why chitosan nanoparticles could represent an optimal platform for nose-to-brain delivery. After intranasal instillation we did observe passage through the nasal mucosa, as demonstrated by multiple staining techniques. After passage through the nasal mucosa, the aforementioned pathways include an olfactory and trigeminal transport to the CNS. In our hands, we could identify multiple times the olfactory pathway. Stainings of treated olfactory bulb tissue revealed consistently the presence of siGal-1. Interestingly, we found highly similar pictures of previous reports, where particles were also

found in the glomerular layer of the olfactory bulb (232). These findings suggest an underlying common pathway used by both formulations, which results in similar distribution patterns in the CNS. Unfortunately, the trigeminal pathway was much more complex. We did not find clear evidence of this pathway, unless a preferential distribution in the hindbrain of treated mice. Other reports could measure transport along the trigeminal nerve with a variety of techniques (96, 232). More importantly, we found a vast presence of siGal-1 in the TME, suggesting the transport via the olfactory bulb is sufficient to reach the GBM. Via several experimental staining techniques, we could visualize siGal-1 in a controlled manner (where untreated controls were blank for autofluorescence). Furthermore, we could correlate the presence of siGal-1 with a strong decrease of Gal-1 in the TME. This feature was demonstrated via two parallel techniques (western blot and immunofluorescence). Thus far, this is the only report, to our knowledge, that shows a protein specific decrease via intranasal siRNA administration in the context of GBM. To make sure that we observed a sequence specific cleavage of *gal-1* mRNA we performed a GeneRace-PCR. This PCR has become the standard technique to demonstrate RNAi *in vivo* even in patients' tissue (222). With respect to the efficiency of delivery, we have not been able to determine to success rate of transported siRNA. We have demonstrated the presence of siGal-1 via fluorescence, which is rather a qualitative approach than a quantitative approach. To resolve this question, radiolabelling is probably the most informative technique. Successful labeling of phosphate groups of siRNA has been used track delivery efficiency in nose-to-brain research (180). Radioactive labeling is however unpractical in basic laboratory settings, to prepare nanoparticles, and to treat animals.



7.2. Sensitization of glioblastoma tumor micro-environment to chemo- and immunotherapy by Galectin-1 intranasal knock-down strategy

In this thesis, the evaluation of the nose-to-brain transport for siGal-1 molecules was performed. We demonstrated for the first time that Gal-1 could be efficiently reduced after intranasal administration. A logical next step included a detailed characterization of the TME when Gal-1 is reduced. As mentioned in the introduction, Gal-1 has a plethora of features in the TME. Given the primary focus of our

research group in tumor-immunology, we started by exploring the landscape on the myeloid and lymphoid parts. Whereas the effects of Gal-1 on T cells are well described, those on myeloid cells are much less well described. We found an overall reduction of myeloid cells, with in particular monocytic MDSCs. These results were in line with a previous report, which used shRNA targeting Gal-1 cell line. In contrast, we did not notice a decrease in granulocytic MDSCs (253). Monocytic MDSCs present more often the larger fraction (about 40%) of CD11b+ myeloid cells, whereas granulocytic MDSCs are typically < 10% of CD11b+ myeloid cells. To further explore, we also assessed the composition of the macrophages that infiltrate the TME. As mentioned in the introduction, reports have been describing how Gal-1 can motivate the arginase arm of macrophages, and drive immune suppression. With respect to our data, we found that the total pool of macrophages is not affected by Gal-1 reduction, but the polarization status is. This study indicated for the first time that Gal-1 can play a role in the polarization from M1 to M2 macrophages, contributing to the immune suppression. In an elegant recent paper, striking similarities have been reported: By supplying Gal-1 in a stroke model, the M1 phenotype was deliberately turned over to M2, providing immune suppression and preventing aggravated disease (59). For the lymphoid compartment we found a solid decrease of Treg, both on mRNA and cellular level and steady increase of Th1 and CTLs. This study reports for the first time a detailed analysis how the immunological compartment of TME in GBM can be modulated by intranasal administration.

Given the tremendous changes in immune contexture, we assessed the survival of treated mice. Upon four administrations, a significant survival benefit was noticed, especially in terms of long-term survival. The motivation for administering four times was based on the *in vitro* effects, and on preliminary intratumoral injections of the construct. Innovative treatment modalities are only rarely entering the clinical stage as a monotherapy, but rather are presented as an add-on therapy to state-of-the-art treatments. In this respect, intranasal siGal-1 treatment would be no exception. The true power of reducing Gal-1 is more likely to rely on its combinatorial effects with chemo- and immunotherapies. Previous reports already reported about synergy between targeting Gal-1 and TMZ in GBM context, mainly in human GBM cell lines (210). After experimenting with the dosing schedule, we found that prior siGal-1 treatment and later TMZ administration could drastically increase the survival of tumor bearing mice. To explain this synergy, we analyzed the complex vasculature in the TME. To this end, we found a thinner, healthier vasculature when Gal-1 was reduced, which might be explained by Gal-1 as an angiogenic factor, or by the fact that VEGF producing M2 macrophages were less abundantly present. This thinner vasculature was hypothesized to better perfuse the parenchyma and tumor environment, and allow a more beneficial distribution pattern of TMZ in the TME. Quantification of the TMZ attributed DNA damage revealed indeed that more tumor mass was affected by TMZ when siGal-1 was administered before. Of note, previous reports also indicate an inherent increased susceptibility of GBM cells to TMZ when Gal-1 is decreased and ER stress response is altered (210). Combination experiments with immunotherapies were initiated with DC vaccines and PD-1 blocking. In both cases, a synergistic survival benefit was noticed. This underlines that the immune stimulation by siGal-1 treatment, could be beneficial with both prophylactic strategies as with therapies for established tumor. There are only a limited amount of pre-clinical reports for PD-1

blocking in murine GBM models (254) and one small clinical report for GBM in the context of biallelic mismatch enzyme repair deficiency (255). This study revealed beneficial effects for both PD-1 and CTLA-4 blockade. In our study we demonstrate for the first time that the efficiency of checkpoint inhibition could be even further enhanced via siGal-1 therapy.

7.3. PEGylation of chitosan nanoparticles

The primary aims of this thesis were accomplished in a rather straight forward setting, where we tested one selected final formulation, in one murine GBM model. The positive results that were obtained in this project encouraged us to investigate whether further advances could be made. In essence, the chitosan nanoparticles are simple, easy to produce formulations (243). The most striking novelty, with respect to literature, is the thorough concentration process. In literature, we found several reports on PEGylated chitosan nanoparticles or other polymers that were PEGylated, for better nose-to-brain passage (256). We constructed these PEGylated chitosan nanoparticles ourselves, and could confirm most of our previous findings. The most notable differences were to be observed on the epithelial modulation capacity and in vivo distribution pattern. While some patient nasal mucosa monolayers could not respond to native chitosan nanoparticles, they could respond to PEGylated chitosan nanoparticles. Other cultures could respond to both. This underlines a crucial fact for further clinical advances, that the nasal epithelial barrier might be different from person to person. As recently demonstrated, striking differences can be found in the tight-junctions organization in subsets of patients with rhinitis (220). Furthermore, we could demonstrate an entry into the CNS, and at first glance, a more diffuse distribution in the TME. These results are still preliminary, and more research is needed to distinguish whether PEGylation is truly beneficial for nose-to-brain transport.

7.4. Perspectives

This thesis was initiated as a feasibility Proof-Of-Concept study to evaluate if we can modulate the TME during GBM progression. We started with chitosan nanoparticles as a platform to load siRNA molecules. After selection of the most promising chemical variant, we tested this single formulation to a full extent in one murine tumor model. In terms of perspectives, it is quite clear improvements can be made on both sides. For the optimization of chitosan nanoparticles, we already explored the feature of PEGylation. However, as described in the introduction, the design and decoration of nanoparticles is virtually unlimited. Multiple ligands, cell-penetrating peptides can be conjugated, in combination with liposomes, micelles, and the formation of gels. In recent years, the amount of papers describing such formulations is exponentially increasing, and the nose-to-brain transport is gaining momentum. We anticipate that in the coming years, innovative formulations will be described that can provide further enhancement on the complex route of delivery. For now, the construct was only tested in one validated murine GBM model. Given the robust and convincing data obtained, we hypothesize that different murine GBM models could produce similar results. Until now, no thorough toxicity testing of the construct has been performed, which is still a necessity before moving forward to the clinical stage. The real challenge would be to scale up to possibly larger animals but especially humans. Thus far, most research on nose-to-brain has been conducted on rodents (mice and rats) (214). Some reports

have been made on sheep nasal mucosa after intranasal administration, but no focus on brain targeting (257). Indirect evidence of nose-to-brain transport in GBM patients has been observed as mentioned in the introduction, for insulin in Alzheimers patients, and oxytocin (130, 189, 190). To accomplish the step from pre-clinical models to larger animals, and especially humans, the use of technologically enhanced devices will be indispensable. In recent years, multiple pharmaceutical device companies have gained interest in the nose-to-brain transport. Several devices are even specially designed to target the olfactory mucosa in the human nasal cavity, which is an extremely challenging task, given the complex airflow and anatomical structures of the nasal cavity. Leading development companies in the field are for example Aptar Pharma, Impel Neuropharma and Optinose. We hypothesize that one of these devices will evaluate the nose-to-brain transport on the clinical stage. In fact, in our facilities, we envision to launch a phase 0 study for the developed product.

Abstract

Glioblastoma multiforme (GBM) is until today, one of the most aggressive and lethal tumors. Recent advances in surgery, chemo-and radiotherapy were not able to induce a significant shift in prognosis for these patients, and therefore this clearly presents an unmet medical need. Galectin-1 (Gal-1) is a naturally occurring galactose-binding lectin, which is overexpressed in glioblastoma multiforme (GBM). Gal-1 is associated with tumor progression, and is a potent immune suppressor in the tumor micro-environment (TME). Gal-1 in the TME of GBM is known to drive chemo- and immunotherapy resistance. To inhibit Gal-1 in GBM, an effective therapy is required that (selectively) reaches the central nervous system tumor, with limited systemic effects. In this thesis, we report for the first time that concentrated chitosan nanoparticle suspensions can deliver small interfering RNA (siRNA) into the central nervous system tumor within hours after intranasal administration. These nanoparticles are able to complex siRNA targeting Gal-1 to a high percentage, and protect them from RNase degradation. Moreover, a successful intracellular delivery of anti-Gal-1 siRNA resulted in a decreased expression of Gal-1 in both murine and human GBM cells. Sequence specific RNA interference, resulted in more than 50 % Gal-1 reduction in tumor bearing mice.

This reduction induces a remarkable switch in the TME contexture where myeloid suppressor cells and regulatory T cells were reduced, while CD4+ helper and CD8+ cytotoxic T cells were increased. *gal-1* knock-down seems to reduce macrophages' polarization switch from M1 to M2 during GBM progression. These changes result in a tumor vasculature normalization and modest increase in survival for tumor bearing mice. The rational combination of intranasal siGal-1 treatment with temozolomide and immunotherapy such as dendritic cell vaccination or PD-1 blocking results in synergistic effects and drastically increases the survival of tumor bearing mice in a prophylactic and established intracranial tumor model respectively. In fact, we could demonstrate an aggravated DNA damage pattern when Gal-1 was reduced and TMZ was administered. Furthermore, we could document an increased infiltration of Th1 and CTL cells in the TME during siGal-1 treatment and PD-1 blocking.

In the presented thesis, we have also developed PEGylated chitosan nanoparticles intended for intranasal transport, to deliver Galectin-1 targeting siRNA molecules from the nasal cavity towards the central nervous system. We explored the potential of PEGylated chitosan nanoparticles in comparison to native chitosan nanoparticles as described before. Successful cytoplasmatic delivery was demonstrated by efficient Gal-1 reduction on GL261. Possible superior nasal epithelial barrier modulation was suggested in comparison to native chitosan. Moreover, we could demonstrate an efficient delivery into the tumor micro-environment of an orthotopic murine glioblastoma model.

This study indicates that the intranasal pathway is an underexplored transport route for delivering siRNA-based therapies targeting Gal-1 in the treatment of GBM. The current observations provide evidence that Gal-1 could be a valuable adjuvant clinical target to further increase the efficiency of checkpoint blockade and chemotherapy.

Summary

High grade gliomas remain a devastating disease, for which a curative therapy is virtually absent. The high medical need is unmet by novel treatment strategies and advances in chemo-and radiotherapy. Patients diagnosed for GBM face a median survival of 15 months after maximal standard-of-care therapy, and relapse is often observed due to micro-metastasis in the direct environment of resection. In part, current treatment modalities such as chemo-and immunotherapy are hampered in their efficacy due to the specialized TME. This area is adequately equipped to withstand the cytotoxic attack of chemo- and immunotherapy. Therefore, we hypothesized that modulation of the TME could decrease these defense mechanisms, and increase susceptibility to tumor lysis.

In this respect, we focused on Gal-1 as an ideal target to modulate the TME in the context of GBM. Gal-1 exerts multiple tumor promoting functions. From pre-clinical research, we have learned that Gal-1 is an important mediator for the proliferation and migration of tumor cells, moreover Gal-1 could also promote angiogenesis in the TME, providing nutrients and oxygen for GBM to grow. Gal-1 also maintains the inherent defense mechanisms to chemo and immunotherapy. Gal-1 is crucial for the resistance mechanisms to TMZ by altering the EPR stress response. Moreover, and most important for our purposes, Gal-1 is also a crucial immune suppressor in the TME, which can induce apoptosis in activated T cells, and recruit Tregs. To target Gal-1 in the TME would be clinically most relevant if this could be performed via a non-invasive treatment modality. Therefore, we developed a nanoparticle complex that could deliver siGal-1 from the nasal cavity directly to the CNS, and even the TME. This nose-to-brain delivery bypasses systemic routes, with a higher (and more selective) local bioavailability in the CNS.

The major pharmaceutical excipient in this nanoparticle complex consists of chitosan polymers. These polymers are highly interesting agents to promote nose-to-brain delivery due their muco-adhesive and epithelial barrier modulation properties. When applying these particles *in vitro* on GBM cells, a solid decrease of Gal-1 was noted, and the epithelial modulatory properties were confirmed. Furthermore, we observed a rapid transport from the nasal cavity to the brain upon intranasal administration of a highly-concentrated chitosan nanoparticle siGal-1 suspension and we could even observe the sequence-specific cleavage of Gal-1 mRNA, and a decrease of Gal-1 in the TME. This Gal-1 reduction could modulate the TME from immune suppression to immune activation, as demonstrated by decrease in suppressor cells, and increased stage of activation in rejective immune cells. Moreover, due to decreased Gal-1, also angiogenesis was alleviated, and a reduced size in vasculature was observed, mimicking a morphological vessel normalisation. Reversing the immune and vascular contexture of the TME by Gal-1 reduction seemed a prerequisite to increase the efficacy of TMZ, DC vaccination and PD-1 blocking. In combination experiments, we noticed that siGal-1 on top of these treatments, could further increase the efficiency of chemo and immunotherapy.

The findings presented in this thesis can serve as a proof of concept for the feasibility to modulate and re-orchestrate the TME of GBM via intranasal administration. The intranasal administration of siGal-1 could represent a valuable clinically translational treatment to increase the efficiency of chemo- and

immunotherapy for GBM patients. In our research facilities, a phase 0 as a first-in-human trial is actively pursued.

Nederlandse Samenvatting

Hooggradige gliomen zijn hersentumoren, die tot op heden behoren tot de meest dodelijke tumoren. In het geval van glioblastoma (GBM), het meest kwaadaardige glioom, bedraagt de prognose voor een patiënt ongeveer 15 maanden overleving na diagnose en standaard behandeling. De laatste jaren zijn de moderne technieken voor chirurgie, radio- en chemo therapie erg vernieuwd maar een drastische verlenging van de prognose voor de GBM patiënt bleef echter uit. Het wordt steeds duidelijker dat er een gespecialiseerde omgeving wordt gevormd rondom het GBM, die uitermate geschikt is om de tumor te laten groeien, en succesvol de aanvallen door chemo- en immuun therapie kan uitschakelen. In het bijzonder blijkt deze omgeving Galectine-1 (Gal-1) te gebruiken om de verdediging in stand te houden, en tumorgroei te promoten. De onderzoeksvraag in deze thesis richt zich op de mogelijkheid de omgeving rondom een GBM zodanig te beïnvloeden, door Gal-1 te onderdrukken, dat deze de sterke verdedigingsmechanismen niet meer kan gebruiken om chemo- en immuuntherapie af te wenden. In het bijzonder probeerden we de GBM omgeving te moduleren via een niet-invasieve toedieningsmodaliteit. In recente jaren is er evidentie dat we het transport van de nasale holte naar het centraal zenuwstelsel kunnen gebruiken om bv. een GBM tumor in de hersenen aan te vallen.

Om Gal-1 te inhiberen gebruiken we korte nucleotide sequenties die specifiek het boodschapper RNA van Gal-1 kunnen vernietigen via RNA interferentie. Het transport van deze naakte moleculen van de nasale holte naar het GBM is echter bijzonder inefficiënt, en bovendien kunnen deze korte nucleotide sequenties ook snel gedegradeerd worden in de slijmvlieslaag van de nasale holte. Om deze problemen te overwinnen, hebben de korte nucleotide sequenties verpakt in nanopartikels die bestaan uit chitosan polymeren. Uit onze in vitro testen blijkt dat deze nanopartikels de sequenties zeer goed beschermen en bovendien ook in het cytoplasma van GBM cellen kunnen afleveren, waardoor we een selectieve degradatie van het boodschapper RNA observeren. Voorts kunnen deze chitosan polymeren ook het rechtstreeks transport van de neus naar de hersenen bevorderen. We zien dan ook dat na intranasale toediening, er een snel transport over de mucus laag is, vervolgens in de olfactorische bulbus (reukzenuw) van de hersenen, en tenslotte ook in de omgeving van het GBM, in het gevalideerd GL261 GBM muis model. Dit is exact de plaats waar we onze nucleotiden willen krijgen om ze op de juiste locatie werkzaam te laten zijn. Eens ter plaatse, zien we dat de nanopartikels de sequenties afleveren, en dat er ook in vivo een efficiënte onderdrukking is van Gal-1 in de tumor omgeving. Ten gevolge van deze Gal-1 onderdrukking, blijkt er een sterke wijziging van de tumor omgeving waarbij de immuunactiviteit sterk verhoogt, door omkering van de immuunsuppressie. Zo zien we dat myeloïde cellen, regulatoire T cellen en type2 macrofagen onderdrukt worden, en dat T helper 1 cellen en cytotoxische T cellen gestimuleerd worden bij Gal-1 onderdrukking. Ten gevolge van deze shift in de balans immuun activatie/suppressie, hebben we de Gal-1 onderdrukking gecombineerd met dendritische cel vaccinatie of PD-1 blocking, beide opkomende immuuntherapieën die klinisch gebruikt kunnen worden om anti-tumor immuniteit aan te wakkeren. Deze combinatie experimenten leren ons dat intranasale anti-Gal-1 therapie, de werkzaamheid van beide immuuntherapieën sterk verhogen. De combinatie van Gal-1 onderdrukking en PD-1 blocking kan de T helper 1 cellen en de cytotoxische T cellen verder stimuleren. Voorts is er ook beschreven dat Gal-1

de resistentie tegen chemotherapie, in het geval van GBM is dit temozolomide (TMZ), in stand kan houden. Daartoe hebben we getest of het onderdrukken van Gal-1 de efficiëntie van TMZ kan verhogen. We observeerden een sterke stijging van de mediane overleving van de muizen die de combinatie therapie kregen, ten opzichte van de monotherapie anti Gal-1 , of monotherapie TMZ. Bovendien bemerkten we dat in deze muizen, éénzelfde dosis TMZ een sterkere beschadiging van het DNA van GBM tumor cellen kan teweeg brengen als Gal-1 werd onderdrukt.

In deze thesis onderzochten we of we de tumor omgeving kunnen moduleren door het toedienen van anti-Gal-1 sequenties via de nasale holte. De bevindingen ondersteunen dat het onderdrukken van Gal-1 via een niet-invasieve toedieningsmanier, de werkzaamheid van chemo- en immuuntherapie sterk kan verhogen. Het intranasale transport van de neus naar de hersenen, is een toedieningsweg die mogelijk een significante verbetering van de overleving voor GBM patiënten kan betekenen.

References

1. Lefranc F, Sadeghi N, Camby I, Metens T, Dewitte O, Kiss R. Present and potential future issues in glioblastoma treatment. Expert review of anticancer therapy. 2006;6(5):719-32. Epub 2006/06/09.
2. Louis DN, Perry A, Reifenberger G, von Deimling A, Figarella-Branger D, Cavenee WK, et al. The 2016 World Health Organization Classification of Tumors of the Central Nervous System: a summary. Acta neuropathologica. 2016;131(6):803-20. Epub 2016/05/10.
3. Louis DN, Ohgaki H, Wiestler OD, Cavenee WK, Burger PC, Jouvet A, et al. The 2007 WHO classification of tumours of the central nervous system. Acta neuropathologica. 2007;114(2):97-109. Epub 2007/07/10.
4. Hanahan D, Weinberg RA. Hallmarks of cancer: the next generation. Cell. 2011;144(5):646-74. Epub 2011/03/08.
5. Ohgaki H, Kleihues P. Genetic pathways to primary and secondary glioblastoma. The American journal of pathology. 2007;170(5):1445-53. Epub 2007/04/26.
6. Narita Y, Nagane M, Mishima K, Huang HJ, Furnari FB, Cavenee WK. Mutant epidermal growth factor receptor signaling down-regulates p27 through activation of the phosphatidylinositol 3-kinase/Akt pathway in glioblastomas. Cancer research. 2002;62(22):6764-9. Epub 2002/11/20.
7. Verhaak RG, Hoadley KA, Purdom E, Wang V, Qi Y, Wilkerson MD, et al. Integrated genomic analysis identifies clinically relevant subtypes of glioblastoma characterized by abnormalities in PDGFRA, IDH1, EGFR, and NF1. Cancer cell. 2010;17(1):98-110. Epub 2010/02/05.
8. Stupp R, Hegi ME, Mason WP, van den Bent MJ, Taphoorn MJ, Janzer RC, et al. Effects of radiotherapy with concomitant and adjuvant temozolomide versus radiotherapy alone on survival in glioblastoma in a randomised phase III study: 5-year analysis of the EORTC-NCIC trial. The lancet oncology. 2009;10(5):459-66. Epub 2009/03/10.
9. Stupp R, Mason WP, van den Bent MJ, Weller M, Fisher B, Taphoorn MJ, et al. Radiotherapy plus concomitant and adjuvant temozolomide for glioblastoma. The New England journal of medicine. 2005;352(10):987-96. Epub 2005/03/11.
10. Greenspoon JN, Shariieff W, Hirte H, Overholt A, Devillers R, Gunnarsson T, et al. Fractionated stereotactic radiosurgery with concurrent temozolomide chemotherapy for locally recurrent glioblastoma multiforme: a prospective cohort study. OncoTargets and therapy. 2014;7:485-90. Epub 2014/04/09.
11. Stummer W, Kamp MA. The importance of surgical resection in malignant glioma. Current opinion in neurology. 2009;22(6):645-9. Epub 2009/09/10.
12. Kristiansen K, Hagen S, Kollevold T, Torvik A, Holme I, Nesbakken R, et al. Combined modality therapy of operated astrocytomas grade III and IV. Confirmation of the value of postoperative irradiation and lack of potentiation of bleomycin on survival time: a prospective multicenter trial of the Scandinavian Glioblastoma Study Group. Cancer. 1981;47(4):649-52. Epub 1981/02/15.
13. Kanzawa T, Germano IM, Komata T, Ito H, Kondo Y, Kondo S. Role of autophagy in temozolomide-induced cytotoxicity for malignant glioma cells. Cell death and differentiation. 2004;11(4):448-57. Epub 2004/01/10.
14. Hegi ME, Diserens AC, Gorlia T, Hamou MF, de Tribolet N, Weller M, et al. MGMT gene silencing and benefit from temozolomide in glioblastoma. The New England journal of medicine. 2005;352(10):997-1003. Epub 2005/03/11.
15. Engelman JA, Settleman J. Acquired resistance to tyrosine kinase inhibitors during cancer therapy. Current opinion in genetics & development. 2008;18(1):73-9. Epub 2008/03/08.
16. Lu KV, Bergers G. Mechanisms of evasive resistance to anti-VEGF therapy in glioblastoma. CNS oncology. 2013;2(1):49-65. Epub 2013/06/12.
17. Kim R, Emi M, Tanabe K. Cancer immunoediting from immune surveillance to immune escape. Immunology. 2007;121(1):1-14. Epub 2007/03/28.

18. Dunn GP, Bruce AT, Ikeda H, Old LJ, Schreiber RD. Cancer immunoediting: from immunosurveillance to tumor escape. *Nature immunology*. 2002;3(11):991-8. Epub 2002/10/31.
19. Kmiecik J, Poli A, Brons NH, Waha A, Eide GE, Enger PO, et al. Elevated CD3+ and CD8+ tumor-infiltrating immune cells correlate with prolonged survival in glioblastoma patients despite integrated immunosuppressive mechanisms in the tumor microenvironment and at the systemic level. *Journal of neuroimmunology*. 2013;264(1-2):71-83. Epub 2013/09/21.
20. Cheng M, Chen Y, Xiao W, Sun R, Tian Z. NK cell-based immunotherapy for malignant diseases. *Cellular & molecular immunology*. 2013;10(3):230-52. Epub 2013/04/23.
21. Joffre OP, Segura E, Savina A, Amigorena S. Cross-presentation by dendritic cells. *Nature reviews Immunology*. 2012;12(8):557-69. Epub 2012/07/14.
22. Murray PJ, Allen JE, Biswas SK, Fisher EA, Gilroy DW, Goerdt S, et al. Macrophage activation and polarization: nomenclature and experimental guidelines. *Immunity*. 2014;41(1):14-20. Epub 2014/07/19.
23. Mantovani A. B cells and macrophages in cancer: yin and yang. *Nature medicine*. 2011;17(3):285-6. Epub 2011/03/09.
24. Martinez FO, Gordon S. The M1 and M2 paradigm of macrophage activation: time for reassessment. *F1000prime reports*. 2014;6:13. Epub 2014/03/29.
25. Gielen PR, Schulte BM, Kers-Rebel ED, Verrijp K, Petersen-Baltussen HM, ter Laan M, et al. Increase in both CD14-positive and CD15-positive myeloid-derived suppressor cell subpopulations in the blood of patients with glioma but predominance of CD15-positive myeloid-derived suppressor cells in glioma tissue. *Journal of neuropathology and experimental neurology*. 2015;74(5):390-400. Epub 2015/04/09.
26. Raychaudhuri B, Rayman P, Ireland J, Ko J, Rini B, Borden EC, et al. Myeloid-derived suppressor cell accumulation and function in patients with newly diagnosed glioblastoma. *Neuro-oncology*. 2011;13(6):591-9. Epub 2011/06/04.
27. El Andaloussi A, Lesniak MS. CD4+ CD25+ FoxP3+ T-cell infiltration and heme oxygenase-1 expression correlate with tumor grade in human gliomas. *Journal of neuro-oncology*. 2007;83(2):145-52. Epub 2007/01/12.
28. Jacobs JF, Idema AJ, Bol KF, Grotenhuis JA, de Vries IJ, Wesseling P, et al. Prognostic significance and mechanism of Treg infiltration in human brain tumors. *Journal of neuroimmunology*. 2010;225(1-2):195-9. Epub 2010/06/12.
29. Yue Q, Zhang X, Ye HX, Wang Y, Du ZG, Yao Y, et al. The prognostic value of Foxp3+ tumor-infiltrating lymphocytes in patients with glioblastoma. *Journal of neuro-oncology*. 2014;116(2):251-9. Epub 2013/11/28.
30. Fecci PE, Mitchell DA, Whitesides JF, Xie W, Friedman AH, Archer GE, et al. Increased regulatory T-cell fraction amidst a diminished CD4 compartment explains cellular immune defects in patients with malignant glioma. *Cancer research*. 2006;66(6):3294-302. Epub 2006/03/17.
31. Perng P, Lim M. Immunosuppressive Mechanisms of Malignant Gliomas: Parallels at Non-CNS Sites. *Frontiers in oncology*. 2015;5:153. Epub 2015/07/29.
32. Curiel TJ, Coukos G, Zou L, Alvarez X, Cheng P, Mottram P, et al. Specific recruitment of regulatory T cells in ovarian carcinoma fosters immune privilege and predicts reduced survival. *Nature medicine*. 2004;10(9):942-9. Epub 2004/08/24.
33. Zou W. Regulatory T cells, tumour immunity and immunotherapy. *Nature reviews Immunology*. 2006;6(4):295-307. Epub 2006/03/25.
34. Ostrand-Rosenberg S, Sinha P. Myeloid-derived suppressor cells: linking inflammation and cancer. *J Immunol*. 2009;182(8):4499-506. Epub 2009/04/04.
35. Couzin-Frankel J. Breakthrough of the year 2013. *Cancer immunotherapy*. *Science*. 2013;342(6165):1432-3. Epub 2013/12/21.
36. Van Gool SW. Brain Tumor Immunotherapy: What have We Learned so Far? *Frontiers in oncology*. 2015;5:98. Epub 2015/07/03.
37. Palucka K, Banchereau J. Cancer immunotherapy via dendritic cells. *Nature reviews Cancer*. 2012;12(4):265-77. Epub 2012/03/23.

38. Cheever MA, Higano CS. PROVENGE (Sipuleucel-T) in prostate cancer: the first FDA-approved therapeutic cancer vaccine. *Clinical cancer research : an official journal of the American Association for Cancer Research*. 2011;17(11):3520-6. Epub 2011/04/08.
39. Cao JX, Zhang XY, Liu JL, Li D, Li JL, Liu YS, et al. Clinical efficacy of tumor antigen-pulsed DC treatment for high-grade glioma patients: evidence from a meta-analysis. *PloS one*. 2014;9(9):e107173. Epub 2014/09/13.
40. Callahan MK, Postow MA, Wolchok JD. CTLA-4 and PD-1 Pathway Blockade: Combinations in the Clinic. *Frontiers in oncology*. 2014;4:385. Epub 2015/02/03.
41. Horvat TZ, Adel NG, Dang TO, Momtaz P, Postow MA, Callahan MK, et al. Immune-Related Adverse Events, Need for Systemic Immunosuppression, and Effects on Survival and Time to Treatment Failure in Patients With Melanoma Treated With Ipilimumab at Memorial Sloan Kettering Cancer Center. *Journal of clinical oncology : official journal of the American Society of Clinical Oncology*. 2015;33(28):3193-8. Epub 2015/08/19.
42. Teichberg VI, Silman I, Beitsch DD, Resheff G. A beta-D-galactoside binding protein from electric organ tissue of *Electrophorus electricus*. *Proceedings of the National Academy of Sciences of the United States of America*. 1975;72(4):1383-7. Epub 1975/04/01.
43. Nio-Kobayashi J, Abidin HB, Brown JK, Iwanaga T, Horne AW, Duncan WC. The Expression and Cellular Localization of Galectin-1 and Galectin-3 in the Fallopian Tube Are Altered in Women with Tubal Ectopic Pregnancy. *Cells, tissues, organs*. 2015;200(6):424-34. Epub 2015/09/12.
44. Camby I, Le Mercier M, Lefranc F, Kiss R. Galectin-1: a small protein with major functions. *Glycobiology*. 2006;16(11):137R-57R. Epub 2006/07/15.
45. Barondes SH, Castronovo V, Cooper DN, Cummings RD, Drickamer K, Feizi T, et al. Galectins: a family of animal beta-galactoside-binding lectins. *Cell*. 1994;76(4):597-8. Epub 1994/02/25.
46. Hughes RC. Secretion of the galectin family of mammalian carbohydrate-binding proteins. *Biochimica et biophysica acta*. 1999;1473(1):172-85. Epub 1999/12/02.
47. Yamaoka K, Mishima K, Nagashima Y, Asai A, Sanai Y, Kirino T. Expression of galectin-1 mRNA correlates with the malignant potential of human gliomas and expression of antisense galectin-1 inhibits the growth of 9 glioma cells. *Journal of neuroscience research*. 2000;59(6):722-30. Epub 2000/03/04.
48. Camby I, Belot N, Rorive S, Lefranc F, Maurage CA, Lahm H, et al. Galectins are differentially expressed in supratentorial pilocytic astrocytomas, astrocytomas, anaplastic astrocytomas and glioblastomas, and significantly modulate tumor astrocyte migration. *Brain Pathol*. 2001;11(1):12-26. Epub 2001/01/06.
49. Rorive S, Belot N, Decaestecker C, Lefranc F, Gordower L, Micik S, et al. Galectin-1 is highly expressed in human gliomas with relevance for modulation of invasion of tumor astrocytes into the brain parenchyma. *Glia*. 2001;33(3):241-55. Epub 2001/03/10.
50. Perillo NL, Pace KE, Seilhamer JJ, Baum LG. Apoptosis of T cells mediated by galectin-1. *Nature*. 1995;378(6558):736-9. Epub 1995/12/14.
51. Rubinstein N, Alvarez M, Zwirner NW, Toscano MA, Illarregui JM, Bravo A, et al. Targeted inhibition of galectin-1 gene expression in tumor cells results in heightened T cell-mediated rejection; A potential mechanism of tumor-immune privilege. *Cancer cell*. 2004;5(3):241-51. Epub 2004/03/31.
52. Rabinovich GA, Daly G, Dreja H, Tailor H, Riera CM, Hirabayashi J, et al. Recombinant galectin-1 and its genetic delivery suppress collagen-induced arthritis via T cell apoptosis. *The Journal of experimental medicine*. 1999;190(3):385-98. Epub 1999/08/03.
53. Blaser C, Kaufmann M, Muller C, Zimmermann C, Wells V, Mallucci L, et al. Beta-galactoside-binding protein secreted by activated T cells inhibits antigen-induced proliferation of T cells. *European journal of immunology*. 1998;28(8):2311-9. Epub 1998/08/26.
54. Rabinovich GA, Modesti NM, Castagna LF, Landa CA, Riera CM, Sotomayor CE. Specific inhibition of lymphocyte proliferation and induction of apoptosis by CLL-I, a beta-galactoside-binding lectin. *Journal of biochemistry*. 1997;122(2):365-73. Epub 1997/08/01.

55. Chung CD, Patel VP, Moran M, Lewis LA, Miceli MC. Galectin-1 induces partial TCR zeta-chain phosphorylation and antagonizes processive TCR signal transduction. *J Immunol.* 2000;165(7):3722-9. Epub 2000/10/18.
56. Norling LV, Sampaio AL, Cooper D, Perretti M. Inhibitory control of endothelial galectin-1 on in vitro and in vivo lymphocyte trafficking. *FASEB journal : official publication of the Federation of American Societies for Experimental Biology.* 2008;22(3):682-90. Epub 2007/10/30.
57. Garin MI, Chu CC, Golshayan D, Cernuda-Morollon E, Wait R, Lechler RI. Galectin-1: a key effector of regulation mediated by CD4+CD25+ T cells. *Blood.* 2007;109(5):2058-65. Epub 2006/11/18.
58. Correa SG, Sotomayor CE, Aoki MP, Maldonado CA, Rabinovich GA. Opposite effects of galectin-1 on alternative metabolic pathways of L-arginine in resident, inflammatory, and activated macrophages. *Glycobiology.* 2003;13(2):119-28. Epub 2003/03/11.
59. Wang J, Xia J, Zhang F, Shi Y, Wu Y, Pu H, et al. Galectin-1-secreting neural stem cells elicit long-term neuroprotection against ischemic brain injury. *Scientific reports.* 2015;5:9621. Epub 2015/04/11.
60. Tiligada E. Chemotherapy: induction of stress responses. *Endocrine-related cancer.* 2006;13 Suppl 1:S115-24. Epub 2007/01/30.
61. Le Mercier M, Mathieu V, Haibe-Kains B, Bontempi G, Mijatovic T, Decaestecker C, et al. Knocking down galectin 1 in human hs683 glioblastoma cells impairs both angiogenesis and endoplasmic reticulum stress responses. *Journal of neuropathology and experimental neurology.* 2008;67(5):456-69. Epub 2008/04/24.
62. Kuo P, Bratman SV, Shultz DB, von Eyben R, Chan C, Wang Z, et al. Galectin-1 mediates radiation-related lymphopenia and attenuates NSCLC radiation response. *Clinical cancer research : an official journal of the American Association for Cancer Research.* 2014;20(21):5558-69. Epub 2014/09/06.
63. Le Mercier M, Fortin S, Mathieu V, Kiss R, Lefranc F. Galectins and gliomas. *Brain Pathol.* 2010;20(1):17-27. Epub 2009/04/18.
64. Thijssen VL, Rabinovich GA, Griffioen AW. Vascular galectins: regulators of tumor progression and targets for cancer therapy. *Cytokine & growth factor reviews.* 2013;24(6):547-58. Epub 2013/08/15.
65. Croci DO, Cerliani JP, Dalotto-Moreno T, Mendez-Huergo SP, Mascanfroni ID, Dergan-Dylon S, et al. Glycosylation-dependent lectin-receptor interactions preserve angiogenesis in anti-VEGF refractory tumors. *Cell.* 2014;156(4):744-58. Epub 2014/02/18.
66. Ozawa K, Tsukamoto Y, Hori O, Kitao Y, Yanagi H, Stern DM, et al. Regulation of tumor angiogenesis by oxygen-regulated protein 150, an inducible endoplasmic reticulum chaperone. *Cancer research.* 2001;61(10):4206-13. Epub 2001/05/19.
67. Mathieu V, Le Mercier M, De Neve N, Sauvage S, Gras T, Roland I, et al. Galectin-1 knockdown increases sensitivity to temozolomide in a B16F10 mouse metastatic melanoma model. *The Journal of investigative dermatology.* 2007;127(10):2399-410. Epub 2007/05/15.
68. Paz A, Haklai R, Elad-Sfadia G, Ballan E, Kloog Y. Galectin-1 binds oncogenic H-Ras to mediate Ras membrane anchorage and cell transformation. *Oncogene.* 2001;20(51):7486-93. Epub 2001/12/26.
69. Miller MC, Klyosov A, Mayo KH. The alpha-galactomannan Davanat binds galectin-1 at a site different from the conventional galectin carbohydrate binding domain. *Glycobiology.* 2009;19(9):1034-45. Epub 2009/06/23.
70. Salomonsson E, Thijssen VL, Griffioen AW, Nilsson UJ, Leffler H. The anti-angiogenic peptide anginex greatly enhances galectin-1 binding affinity for glycoproteins. *The Journal of biological chemistry.* 2011;286(16):13801-4. Epub 2011/03/05.
71. Agrawal N, Dasaradhi PV, Mohammed A, Malhotra P, Bhatnagar RK, Mukherjee SK. RNA interference: biology, mechanism, and applications. *Microbiology and molecular biology reviews : MMBR.* 2003;67(4):657-85. Epub 2003/12/11.

72. van Woensel M, Wauthoz N, Rosière R, Amighi K, Mathieu V, Lefranc F, et al. Formulations for Intranasal Delivery of Pharmacological Agents to Combat Brain Disease: A New Opportunity to Tackle GBM? *Cancers*. 2013;5(3):1020-48.
73. Pardridge WM. Blood-brain barrier delivery. *Drug discovery today*. 2007;12(1-2):54-61. Epub 2007/01/03.
74. Varenika V, Dickinson P, Bringas J, LeCouteur R, Higgins R, Park J, et al. Detection of infusate leakage in the brain using real-time imaging of convection-enhanced delivery. *Journal of neurosurgery*. 2008;109(5):874-80. Epub 2008/11/04.
75. Debinski W. Local treatment of brain tumors with targeted chimera cytotoxic proteins. *Cancer investigation*. 2002;20(5-6):801-9. Epub 2002/08/29.
76. Laske DW, Youle RJ, Oldfield EH. Tumor regression with regional distribution of the targeted toxin TF-CRM107 in patients with malignant brain tumors. *Nature medicine*. 1997;3(12):1362-8. Epub 1997/12/13.
77. Kunwar S, Prados MD, Chang SM, Berger MS, Lang FF, Piepmeier JM, et al. Direct intracerebral delivery of cintredekin besudotox (IL13-PE38QQR) in recurrent malignant glioma: a report by the Cintredekin Besudotox Intraparenchymal Study Group. *Journal of clinical oncology : official journal of the American Society of Clinical Oncology*. 2007;25(7):837-44. Epub 2007/03/01.
78. Mardor Y, Roth Y, Lidar Z, Jonas T, Pfeffer R, Maier SE, et al. Monitoring response to convection-enhanced taxol delivery in brain tumor patients using diffusion-weighted magnetic resonance imaging. *Cancer research*. 2001;61(13):4971-3. Epub 2001/06/30.
79. Debinski W, Tatter SB. Convection-enhanced delivery for the treatment of brain tumors. *Expert review of neurotherapeutics*. 2009;9(10):1519-27. Epub 2009/10/17.
80. Bobo RH, Laske DW, Akbasak A, Morrison PF, Dedrick RL, Oldfield EH. Convection-enhanced delivery of macromolecules in the brain. *Proceedings of the National Academy of Sciences of the United States of America*. 1994;91(6):2076-80. Epub 1994/03/15.
81. Groothuis DR. The blood-brain and blood-tumor barriers: a review of strategies for increasing drug delivery. *Neuro-oncology*. 2000;2(1):45-59. Epub 2001/04/17.
82. Thorne RG, Emory CR, Ala TA, Frey WH, 2nd. Quantitative analysis of the olfactory pathway for drug delivery to the brain. *Brain research*. 1995;692(1-2):278-82. Epub 1995/09/18.
83. Shipley MT. Transport of molecules from nose to brain: transneuronal anterograde and retrograde labeling in the rat olfactory system by wheat germ agglutinin-horseradish peroxidase applied to the nasal epithelium. *Brain research bulletin*. 1985;15(2):129-42. Epub 1985/08/01.
84. Illum L. Transport of drugs from the nasal cavity to the central nervous system. *European journal of pharmaceutical sciences : official journal of the European Federation for Pharmaceutical Sciences*. 2000;11(1):1-18. Epub 2000/07/29.
85. Pajouhesh H, Lenz GR. Medicinal chemical properties of successful central nervous system drugs. *NeuroRx : the journal of the American Society for Experimental NeuroTherapeutics*. 2005;2(4):541-53. Epub 2006/02/21.
86. Reese TS, Karnovsky MJ. Fine structural localization of a blood-brain barrier to exogenous peroxidase. *The Journal of cell biology*. 1967;34(1):207-17. Epub 1967/07/01.
87. Miller DS. Regulation of P-glycoprotein and other ABC drug transporters at the blood-brain barrier. *Trends in pharmacological sciences*. 2010;31(6):246-54. Epub 2010/04/27.
88. Lochhead JJ, Thorne RG. Intranasal delivery of biologics to the central nervous system. *Advanced drug delivery reviews*. 2012;64(7):614-28. Epub 2011/11/29.
89. Dhuria SV, Hanson LR, Frey WH, 2nd. Intranasal delivery to the central nervous system: mechanisms and experimental considerations. *Journal of pharmaceutical sciences*. 2010;99(4):1654-73. Epub 2009/10/31.
90. Jansson B, Bjork E. Visualization of in vivo olfactory uptake and transfer using fluorescein dextran. *Journal of drug targeting*. 2002;10(5):379-86. Epub 2002/11/22.
91. Leopold DA. The relationship between nasal anatomy and human olfaction. *The Laryngoscope*. 1988;98(11):1232-8. Epub 1988/11/01.

92. Caggiano M, Kauer JS, Hunter DD. Globose basal cells are neuronal progenitors in the olfactory epithelium: a lineage analysis using a replication-incompetent retrovirus. *Neuron*. 1994;13(2):339-52. Epub 1994/08/01.
93. Carmichael ST, Clugnet MC, Price JL. Central olfactory connections in the macaque monkey. *The Journal of comparative neurology*. 1994;346(3):403-34. Epub 1994/08/15.
94. Lledo PM, Gheusi G, Vincent JD. Information processing in the mammalian olfactory system. *Physiological reviews*. 2005;85(1):281-317. Epub 2004/12/25.
95. Jafek BW. Ultrastructure of human nasal mucosa. *The Laryngoscope*. 1983;93(12):1576-99. Epub 1983/12/01.
96. Johnson NJ, Hanson LR, Frey WH. Trigeminal pathways deliver a low molecular weight drug from the nose to the brain and orofacial structures. *Molecular pharmaceuticals*. 2010;7(3):884-93. Epub 2010/04/28.
97. Bojsen-Moller F. Demonstration of terminalis, olfactory, trigeminal and perivascular nerves in the rat nasal septum. *The Journal of comparative neurology*. 1975;159(2):245-56. Epub 1975/01/15.
98. Fuss SH, Omura M, Mombaerts P. The Grueneberg ganglion of the mouse projects axons to glomeruli in the olfactory bulb. *The European journal of neuroscience*. 2005;22(10):2649-54. Epub 2005/11/26.
99. DeSesso JM. The relevance to humans of animal models for inhalation studies of cancer in the nose and upper airways. *Qual Assur*. 1993;2(3):213-31. Epub 1993/09/01.
100. Hadaczek P, Yamashita Y, Mirek H, Tamas L, Bohn MC, Noble C, et al. The "perivascular pump" driven by arterial pulsation is a powerful mechanism for the distribution of therapeutic molecules within the brain. *Molecular therapy : the journal of the American Society of Gene Therapy*. 2006;14(1):69-78. Epub 2006/05/03.
101. Johnston M, Zakharov A, Papaiconomou C, Salmasi G, Armstrong D. Evidence of connections between cerebrospinal fluid and nasal lymphatic vessels in humans, non-human primates and other mammalian species. *Cerebrospinal fluid research*. 2004;1(1):2. Epub 2005/02/01.
102. Walter BA, Valera VA, Takahashi S, Ushiki T. The olfactory route for cerebrospinal fluid drainage into the peripheral lymphatic system. *Neuropathology and applied neurobiology*. 2006;32(4):388-96. Epub 2006/07/27.
103. Yoffey JM, Drinker CK. The Lymphatic Pathway from the Nose and Pharynx : The Absorption of Dyes. *The Journal of experimental medicine*. 1938;68(4):629-40. Epub 1938/09/30.
104. Kaliner M, Shelhamer JH, Borson B, Nadel J, Patow C, Marom Z. Human respiratory mucus. *The American review of respiratory disease*. 1986;134(3):612-21. Epub 1986/09/01.
105. Khutoryanskiy VV. Advances in mucoadhesion and mucoadhesive polymers. *Macromolecular bioscience*. 2011;11(6):748-64. Epub 2010/12/29.
106. Moran DT, Rowley JC, 3rd, Jafek BW, Lovell MA. The fine structure of the olfactory mucosa in man. *Journal of neurocytology*. 1982;11(5):721-46. Epub 1982/10/01.
107. Schipper NG, Verhoef JC, Merkus FW. The nasal mucociliary clearance: relevance to nasal drug delivery. *Pharmaceutical research*. 1991;8(7):807-14. Epub 1991/07/01.
108. Van Itallie CM, Anderson JM. Claudins and epithelial paracellular transport. *Annual review of physiology*. 2006;68:403-29. Epub 2006/02/08.
109. Altner H, Altner-Kolnberger I. Freeze-fracture and tracer experiments on the permeability of the zonulae occludentes in the olfactory mucosa of vertebrates. *Cell and tissue research*. 1974;154(1):51-9. Epub 1974/01/01.
110. Conner SD, Schmid SL. Regulated portals of entry into the cell. *Nature*. 2003;422(6927):37-44. Epub 2003/03/07.
111. Baker H, Spencer RF. Transneuronal transport of peroxidase-conjugated wheat germ agglutinin (WGA-HRP) from the olfactory epithelium to the brain of the adult rat. *Experimental brain research Experimentelle Hirnforschung Experimentation cerebrale*. 1986;63(3):461-73. Epub 1986/01/01.

112. De Lorenzo AJ. Electron microscopy of the olfactory and gustatory pathways. Transactions of the annual meeting of the American Laryngological Association American Laryngological Association Meeting. 1960;81:39-49. Epub 1960/01/01.
113. Morrison EE, Costanzo RM. Morphology of olfactory epithelium in humans and other vertebrates. Microscopy research and technique. 1992;23(1):49-61. Epub 1992/10/01.
114. Mistry A, Stolnik S, Illum L. Nanoparticles for direct nose-to-brain delivery of drugs. International journal of pharmaceutics. 2009;379(1):146-57. Epub 2009/06/27.
115. Wang F, Jiang X, Lu W. Profiles of methotrexate in blood and CSF following intranasal and intravenous administration to rats. International journal of pharmaceutics. 2003;263(1-2):1-7. Epub 2003/09/05.
116. Rall DP. Conference on obstacles to the control of acute leukemia. Experimental studies of the blood-brain barrier. Cancer research. 1965;25(9):1572-7. Epub 1965/10/01.
117. Poortmans PM, Kluin-Nelemans HC, Haaxma-Reiche H, Van't Veer M, Hansen M, Soubeyran P, et al. High-dose methotrexate-based chemotherapy followed by consolidating radiotherapy in non-AIDS-related primary central nervous system lymphoma: European Organization for Research and Treatment of Cancer Lymphoma Group Phase II Trial 20962. Journal of clinical oncology : official journal of the American Society of Clinical Oncology. 2003;21(24):4483-8. Epub 2003/11/05.
118. Shingaki T, Inoue D, Furubayashi T, Sakane T, Katsumi H, Yamamoto A, et al. Transnasal delivery of methotrexate to brain tumors in rats: a new strategy for brain tumor chemotherapy. Molecular pharmaceutics. 2010;7(5):1561-8. Epub 2010/08/11.
119. Sakane T, Yamashita S, Yata N, Sezaki H. Transnasal delivery of 5-fluorouracil to the brain in the rat. Journal of drug targeting. 1999;7(3):233-40. Epub 2000/02/19.
120. Longley DB, Harkin DP, Johnston PG. 5-fluorouracil: mechanisms of action and clinical strategies. Nature reviews Cancer. 2003;3(5):330-8. Epub 2003/05/02.
121. Wang D, Gao Y, Yun L. Study on brain targeting of raltitrexed following intranasal administration in rats. Cancer chemotherapy and pharmacology. 2006;57(1):97-104. Epub 2005/07/20.
122. Hashizume R, Ozawa T, Gryaznov SM, Bollen AW, Lamborn KR, Frey WH, 2nd, et al. New therapeutic approach for brain tumors: Intranasal delivery of telomerase inhibitor GRN163. Neuro-oncology. 2008;10(2):112-20. Epub 2008/02/22.
123. Le S, Zhu JJ, Anthony DC, Greider CW, Black PM. Telomerase activity in human gliomas. Neurosurgery. 1998;42(5):1120-4; discussion 4-5. Epub 1998/05/20.
124. Ozawa T, Gryaznov SM, Hu LJ, Pongracz K, Santos RA, Bollen AW, et al. Antitumor effects of specific telomerase inhibitor GRN163 in human glioblastoma xenografts. Neuro-oncology. 2004;6(3):218-26. Epub 2004/07/29.
125. Rainov NG, Ren H. Oncolytic viruses for treatment of malignant brain tumours. Acta neurochirurgica Supplement. 2003;88:113-23. Epub 2003/10/09.
126. Ozduman K, Wollmann G, Piepmeyer JM, van den Pol AN. Systemic vesicular stomatitis virus selectively destroys multifocal glioma and metastatic carcinoma in brain. The Journal of neuroscience : the official journal of the Society for Neuroscience. 2008;28(8):1882-93. Epub 2008/02/22.
127. Reitz M, Demestre M, Sedlacik J, Meissner H, Fiehler J, Kim SU, et al. Intranasal delivery of neural stem/progenitor cells: a noninvasive passage to target intracerebral glioma. Stem cells translational medicine. 2012;1(12):866-73. Epub 2013/01/04.
128. Aboody KS, Najbauer J, Danks MK. Stem and progenitor cell-mediated tumor selective gene therapy. Gene therapy. 2008;15(10):739-52. Epub 2008/03/29.
129. da Fonseca CO, Schwartzmann G, Fischer J, Nagel J, Futuro D, Quirico-Santos T, et al. Preliminary results from a phase I/II study of perillyl alcohol intranasal administration in adults with recurrent malignant gliomas. Surgical neurology. 2008;70(3):259-66; discussion 66-7. Epub 2008/02/26.
130. da Fonseca CO, Simao M, Lins IR, Caetano RO, Futuro D, Quirico-Santos T. Efficacy of monoterpene perillyl alcohol upon survival rate of patients with recurrent glioblastoma. Journal of cancer research and clinical oncology. 2011;137(2):287-93. Epub 2010/04/20.

131. da Fonseca CO, Landeiro JA, Clark SS, Quirico-Santos T, da Costa Carvalho Mda G, Gattass CR. Recent advances in the molecular genetics of malignant gliomas disclose targets for antitumor agent perillyl alcohol. *Surgical neurology*. 2006;65 Suppl 1:S1:2-1:8; discussion S1:8-1:9. Epub 2006/01/24.
132. Shingaki T, Hidalgo IJ, Furubayashi T, Katsumi H, Sakane T, Yamamoto A, et al. The transnasal delivery of 5-fluorouracil to the rat brain is enhanced by acetazolamide (the inhibitor of the secretion of cerebrospinal fluid). *International journal of pharmaceuticals*. 2009;377(1-2):85-91. Epub 2009/05/19.
133. Sarkar MA. Drug metabolism in the nasal mucosa. *Pharmaceutical research*. 1992;9(1):1-9. Epub 1992/01/01.
134. Bernkop-Schnurch A, Dunnhaupt S. Chitosan-based drug delivery systems. *European journal of pharmaceuticals and biopharmaceuticals : official journal of Arbeitsgemeinschaft fur Pharmazeutische Verfahrenstechnik eV*. 2012;81(3):463-9. Epub 2012/05/09.
135. Garcia-Fuentes M, Alonso MJ. Chitosan-based drug nanocarriers: where do we stand? *Journal of controlled release : official journal of the Controlled Release Society*. 2012;161(2):496-504. Epub 2012/04/07.
136. Kang ML, Cho CS, Yoo HS. Application of chitosan microspheres for nasal delivery of vaccines. *Biotechnology advances*. 2009;27(6):857-65. Epub 2009/07/09.
137. Soane RJ, Hinchcliffe M, Davis SS, Illum L. Clearance characteristics of chitosan based formulations in the sheep nasal cavity. *International journal of pharmaceuticals*. 2001;217(1-2):183-91. Epub 2001/04/09.
138. Soane RJ, Frier M, Perkins AC, Jones NS, Davis SS, Illum L. Evaluation of the clearance characteristics of bioadhesive systems in humans. *International journal of pharmaceuticals*. 1999;178(1):55-65. Epub 1999/04/17.
139. Illum L. Chitosan and its use as a pharmaceutical excipient. *Pharmaceutical research*. 1998;15(9):1326-31. Epub 1998/10/02.
140. Amidi M, Mastrobattista E, Jiskoot W, Hennink WE. Chitosan-based delivery systems for protein therapeutics and antigens. *Advanced drug delivery reviews*. 2010;62(1):59-82. Epub 2009/11/21.
141. Agnihotri SA, Mallikarjuna NN, Aminabhavi TM. Recent advances on chitosan-based micro- and nanoparticles in drug delivery. *Journal of controlled release : official journal of the Controlled Release Society*. 2004;100(1):5-28. Epub 2004/10/20.
142. Wang X, Chi N, Tang X. Preparation of estradiol chitosan nanoparticles for improving nasal absorption and brain targeting. *European journal of pharmaceuticals and biopharmaceuticals : official journal of Arbeitsgemeinschaft fur Pharmazeutische Verfahrenstechnik eV*. 2008;70(3):735-40. Epub 2008/08/08.
143. Kolsch H, Rao ML. Neuroprotective effects of estradiol-17beta: implications for psychiatric disorders. *Archives of women's mental health*. 2002;5(3):105-10. Epub 2003/01/03.
144. Al-Ghananeem AM, Saeed H, Florence R, Yokel RA, Malkawi AH. Intranasal drug delivery of didanosine-loaded chitosan nanoparticles for brain targeting; an attractive route against infections caused by AIDS viruses. *Journal of drug targeting*. 2010;18(5):381-8. Epub 2009/12/17.
145. Alam S, Khan ZI, Mustafa G, Kumar M, Islam F, Bhatnagar A, et al. Development and evaluation of thymoquinone-encapsulated chitosan nanoparticles for nose-to-brain targeting: a pharmacoscintigraphic study. *International journal of nanomedicine*. 2012;7:5705-18. Epub 2012/11/28.
146. Mansour MA, Nagi MN, El-Khatib AS, Al-Bekairi AM. Effects of thymoquinone on antioxidant enzyme activities, lipid peroxidation and DT-diaphorase in different tissues of mice: a possible mechanism of action. *Cell biochemistry and function*. 2002;20(2):143-51. Epub 2002/04/30.
147. Fazil M, Md S, Haque S, Kumar M, Baboota S, Sahni JK, et al. Development and evaluation of rivastigmine loaded chitosan nanoparticles for brain targeting. *European journal of pharmaceutical sciences : official journal of the European Federation for Pharmaceutical Sciences*. 2012;47(1):6-15. Epub 2012/05/09.

148. Md S, Khan RA, Mustafa G, Chuttani K, Baboota S, Sahni JK, et al. Bromocriptine loaded chitosan nanoparticles intended for direct nose to brain delivery: Pharmacodynamic, Pharmacokinetic and Scintigraphy study in mice model. *European journal of pharmaceutical sciences* : official journal of the European Federation for Pharmaceutical Sciences. 2012;48(3):393-405. Epub 2012/12/26.
149. Lim JH, Kim SS, Boo DH, No H, Kang BY, Kim EM, et al. Protective effect of bromocriptine against BH4-induced Cath.a cell death involving up-regulation of antioxidant enzymes. *Neuroscience letters*. 2009;451(3):185-9. Epub 2009/01/17.
150. Mistry A, Glud SZ, Kjemis J, Randel J, Howard KA, Stolnik S, et al. Effect of physicochemical properties on intranasal nanoparticle transit into murine olfactory epithelium. *Journal of drug targeting*. 2009;17(7):543-52. Epub 2009/06/18.
151. Betbeder D, Sperandio S, Latapie JP, de Nadai J, Etienne A, Zajac JM, et al. Biovector nanoparticles improve antinociceptive efficacy of nasal morphine. *Pharmaceutical research*. 2000;17(6):743-8. Epub 2000/08/24.
152. Lai SK, O'Hanlon DE, Harrold S, Man ST, Wang YY, Cone R, et al. Rapid transport of large polymeric nanoparticles in fresh undiluted human mucus. *Proceedings of the National Academy of Sciences of the United States of America*. 2007;104(5):1482-7. Epub 2007/01/25.
153. Zhang QZ, Zha LS, Zhang Y, Jiang WM, Lu W, Shi ZQ, et al. The brain targeting efficiency following nasally applied MPEG-PLA nanoparticles in rats. *Journal of drug targeting*. 2006;14(5):281-90. Epub 2006/08/03.
154. Wang YY, Lai SK, Suk JS, Pace A, Cone R, Hanes J. Addressing the PEG mucoadhesivity paradox to engineer nanoparticles that "slip" through the human mucus barrier. *Angew Chem Int Ed Engl*. 2008;47(50):9726-9. Epub 2008/11/04.
155. Seju U, Kumar A, Sawant KK. Development and evaluation of olanzapine-loaded PLGA nanoparticles for nose-to-brain delivery: in vitro and in vivo studies. *Acta biomaterialia*. 2011;7(12):4169-76. Epub 2011/08/16.
156. Makadia HK, Siegel SJ. Poly Lactic-co-Glycolic Acid (PLGA) as Biodegradable Controlled Drug Delivery Carrier. *Polymers*. 2011;3(3):1377-97. Epub 2012/05/12.
157. Mattiuz E, Franklin R, Gillespie T, Murphy A, Bernstein J, Chiu A, et al. Disposition and metabolism of olanzapine in mice, dogs, and rhesus monkeys. *Drug metabolism and disposition: the biological fate of chemicals*. 1997;25(5):573-83. Epub 1997/05/01.
158. Kim ID, Shin JH, Kim SW, Choi S, Ahn J, Han PL, et al. Intranasal delivery of HMGB1 siRNA confers target gene knockdown and robust neuroprotection in the postischemic brain. *Molecular therapy : the journal of the American Society of Gene Therapy*. 2012;20(4):829-39. Epub 2012/01/19.
159. Kumar M, Misra A, Babbar AK, Mishra AK, Mishra P, Pathak K. Intranasal nanoemulsion based brain targeting drug delivery system of risperidone. *International journal of pharmaceutics*. 2008;358(1-2):285-91. Epub 2008/05/06.
160. Kumar M, Misra A, Mishra AK, Mishra P, Pathak K. Mucoadhesive nanoemulsion-based intranasal drug delivery system of olanzapine for brain targeting. *Journal of drug targeting*. 2008;16(10):806-14. Epub 2008/11/07.
161. Jogani VV, Shah PJ, Mishra P, Mishra AK, Misra AR. Intranasal mucoadhesive microemulsion of tacrine to improve brain targeting. *Alzheimer disease and associated disorders*. 2008;22(2):116-24. Epub 2008/06/06.
162. Eskandari S, Varshosaz J, Minaiyan M, Tabbakhian M. Brain delivery of valproic acid via intranasal administration of nanostructured lipid carriers: in vivo pharmacodynamic studies using rat electroshock model. *International journal of nanomedicine*. 2011;6:363-71. Epub 2011/04/19.
163. Joshi AS, Patel HS, Belgamwar VS, Agrawal A, Tekade AR. Solid lipid nanoparticles of ondansetron HCl for intranasal delivery: development, optimization and evaluation. *Journal of materials science Materials in medicine*. 2012;23(9):2163-75. Epub 2012/07/18.
164. Arumugam K, Subramanian GS, Mallayasamy SR, Averineni RK, Reddy MS, Udupa N. A study of rivastigmine liposomes for delivery into the brain through intranasal route. *Acta Pharm*. 2008;58(3):287-97. Epub 2008/12/24.

165. Migliore MM, Vyas TK, Campbell RB, Amiji MM, Waszczak BL. Brain delivery of proteins by the intranasal route of administration: a comparison of cationic liposomes versus aqueous solution formulations. *Journal of pharmaceutical sciences*. 2010;99(4):1745-61. Epub 2009/09/24.
166. Priprem A, Watanatorn J, Sutthiparinyanont S, Phachonpai W, Muchimapura S. Anxiety and cognitive effects of quercetin liposomes in rats. *Nanomedicine : nanotechnology, biology, and medicine*. 2008;4(1):70-8. Epub 2008/02/06.
167. Gao X, Tao W, Lu W, Zhang Q, Zhang Y, Jiang X, et al. Lectin-conjugated PEG-PLA nanoparticles: preparation and brain delivery after intranasal administration. *Biomaterials*. 2006;27(18):3482-90. Epub 2006/03/03.
168. Berger G, Kogan T, Skutelsky E, Ophir D. Glycoconjugate expression in normal human inferior turbinate mucosa: a lectin histochemical study. *American journal of rhinology*. 2005;19(1):97-103. Epub 2005/03/30.
169. Gao X, Wu B, Zhang Q, Chen J, Zhu J, Zhang W, et al. Brain delivery of vasoactive intestinal peptide enhanced with the nanoparticles conjugated with wheat germ agglutinin following intranasal administration. *Journal of controlled release : official journal of the Controlled Release Society*. 2007;121(3):156-67. Epub 2007/07/14.
170. Liu Q, Shen Y, Chen J, Gao X, Feng C, Wang L, et al. Nose-to-brain transport pathways of wheat germ agglutinin conjugated PEG-PLA nanoparticles. *Pharmaceutical research*. 2012;29(2):546-58. Epub 2011/12/15.
171. Gao X, Chen J, Tao W, Zhu J, Zhang Q, Chen H, et al. UEA I-bearing nanoparticles for brain delivery following intranasal administration. *International journal of pharmaceutics*. 2007;340(1-2):207-15. Epub 2007/05/15.
172. Park YJ, Chang LC, Liang JF, Moon C, Chung CP, Yang VC. Nontoxic membrane translocation peptide from protamine, low molecular weight protamine (LMWP), for enhanced intracellular protein delivery: in vitro and in vivo study. *FASEB journal : official publication of the Federation of American Societies for Experimental Biology*. 2005;19(11):1555-7. Epub 2005/07/22.
173. Elfinger M, Maucksch C, Rudolph C. Characterization of lactoferrin as a targeting ligand for nonviral gene delivery to airway epithelial cells. *Biomaterials*. 2007;28(23):3448-55. Epub 2007/05/04.
174. Liu Z, Jiang M, Kang T, Miao D, Gu G, Song Q, et al. Lactoferrin-modified PEG-co-PCL nanoparticles for enhanced brain delivery of NAP peptide following intranasal administration. *Biomaterials*. 2013;34(15):3870-81. Epub 2013/03/05.
175. Wan XM, Chen YP, Xu WR, Yang WJ, Wen LP. Identification of nose-to-brain homing peptide through phage display. *Peptides*. 2009;30(2):343-50. Epub 2008/11/15.
176. Yang ZZ, Zhang YQ, Wang ZZ, Wu K, Lou JN, Qi XR. Enhanced brain distribution and pharmacodynamics of rivastigmine by liposomes following intranasal administration. *International journal of pharmaceutics*. 2013. Epub 2013/05/18.
177. Kanazawa T, Morisaki K, Suzuki S, Takashima Y. Prolongation of life in rats with malignant glioma by intranasal siRNA/drug codelivery to the brain with cell-penetrating peptide-modified micelles. *Molecular pharmaceutics*. 2014;11(5):1471-8. Epub 2014/04/09.
178. Charlton ST, Davis SS, Illum L. Evaluation of bioadhesive polymers as delivery systems for nose to brain delivery: in vitro characterisation studies. *Journal of controlled release : official journal of the Controlled Release Society*. 2007;118(2):225-34. Epub 2007/01/31.
179. Charlton S, Jones NS, Davis SS, Illum L. Distribution and clearance of bioadhesive formulations from the olfactory region in man: effect of polymer type and nasal delivery device. *European journal of pharmaceutical sciences : official journal of the European Federation for Pharmaceutical Sciences*. 2007;30(3-4):295-302. Epub 2007/01/16.
180. Perez AP, Mundina-Weilenmann C, Romero EL, Morilla MJ. Increased brain radioactivity by intranasal P-labeled siRNA dendriplexes within in situ-forming mucoadhesive gels. *International journal of nanomedicine*. 2012;7:1373-85. Epub 2012/03/30.

181. Khan S, Patil K, Bobade N, Yeole P, Gaikwad R. Formulation of intranasal mucoadhesive temperature-mediated in situ gel containing ropinirole and evaluation of brain targeting efficiency in rats. *Journal of drug targeting*. 2010;18(3):223-34. Epub 2009/12/25.
182. Zaki NM, Awad GA, Mortada ND, Abd Elhady SS. Enhanced bioavailability of metoclopramide HCl by intranasal administration of a mucoadhesive in situ gel with modulated rheological and mucociliary transport properties. *European journal of pharmaceutical sciences : official journal of the European Federation for Pharmaceutical Sciences*. 2007;32(4-5):296-307. Epub 2007/10/09.
183. Jayachandra Babu R, Dayal PP, Pawar K, Singh M. Nose-to-brain transport of melatonin from polymer gel suspensions: a microdialysis study in rats. *Journal of drug targeting*. 2011;19(9):731-40. Epub 2011/03/25.
184. Graff CL, Pollack GM. P-Glycoprotein attenuates brain uptake of substrates after nasal instillation. *Pharmaceutical research*. 2003;20(8):1225-30. Epub 2003/09/02.
185. Charlton ST, Davis SS, Illum L. Evaluation of effect of ephedrine on the transport of drugs from the nasal cavity to the systemic circulation and the central nervous system. *Journal of drug targeting*. 2007;15(5):370-7. Epub 2007/06/02.
186. Dhuria SV, Hanson LR, Frey WH, 2nd. Intranasal drug targeting of hypocretin-1 (orexin-A) to the central nervous system. *Journal of pharmaceutical sciences*. 2009;98(7):2501-15. Epub 2008/11/26.
187. Dhuria SV, Hanson LR, Frey WH, 2nd. Novel vasoconstrictor formulation to enhance intranasal targeting of neuropeptide therapeutics to the central nervous system. *The Journal of pharmacology and experimental therapeutics*. 2009;328(1):312-20. Epub 2008/10/24.
188. Celebisoy N, Gokcay F, Sirin H, Akyurekli O. Treatment of idiopathic intracranial hypertension: topiramate vs acetazolamide, an open-label study. *Acta neurologica Scandinavica*. 2007;116(5):322-7. Epub 2007/10/10.
189. Kosfeld M, Heinrichs M, Zak PJ, Fischbacher U, Fehr E. Oxytocin increases trust in humans. *Nature*. 2005;435(7042):673-6. Epub 2005/06/03.
190. Craft S, Baker LD, Montine TJ, Minoshima S, Watson GS, Claxton A, et al. Intranasal insulin therapy for Alzheimer disease and amnesic mild cognitive impairment: a pilot clinical trial. *Archives of neurology*. 2012;69(1):29-38. Epub 2011/09/14.
191. Djupesland PG. Nasal drug delivery devices: characteristics and performance in a clinical perspective—a review. *Drug delivery and translational research*. 2013;3(1):42-62. Epub 2013/01/15.
192. Djupesland PG, Skretting A, Winderen M, Holand T. Breath actuated device improves delivery to target sites beyond the nasal valve. *The Laryngoscope*. 2006;116(3):466-72. Epub 2006/03/17.
193. Hardy JG, Lee SW, Wilson CG. Intranasal drug delivery by spray and drops. *The Journal of pharmacy and pharmacology*. 1985;37(5):294-7. Epub 1985/05/01.
194. van den Berg MP, Romeijn SG, Verhoef JC, Merkus FW. Serial cerebrospinal fluid sampling in a rat model to study drug uptake from the nasal cavity. *Journal of neuroscience methods*. 2002;116(1):99-107. Epub 2002/05/15.
195. Vogelbaum MA, Aghi MK. Convection-enhanced delivery for the treatment of glioblastoma. *Neuro-oncology*. 2015;17 Suppl 2:ii3-ii8. Epub 2015/03/10.
196. Frosina G. Limited advances in therapy of glioblastoma trigger re-consideration of research policy. *Critical reviews in oncology/hematology*. 2015. Epub 2015/06/09.
197. de Vleeschouwer S, Rapp M, Sorg RV, Steiger HJ, Stummer W, van Gool S, et al. Dendritic cell vaccination in patients with malignant gliomas: current status and future directions. *Neurosurgery*. 2006;59(5):988-99; discussion 99-1000. Epub 2006/12/05.
198. Van Gool S, Maes W, Ardon H, Verschuere T, Van Cauter S, De Vleeschouwer S. Dendritic cell therapy of high-grade gliomas. *Brain Pathol*. 2009;19(4):694-712. Epub 2009/09/12.
199. Blankenstein T, Coulie PG, Gilboa E, Jaffee EM. The determinants of tumour immunogenicity. *Nature reviews Cancer*. 2012;12(4):307-13. Epub 2012/03/02.
200. De Vleeschouwer S, Fieuws S, Rutkowski S, Van Calenbergh F, Van Loon J, Goffin J, et al. Postoperative adjuvant dendritic cell-based immunotherapy in patients with relapsed glioblastoma

- multiforme. *Clinical cancer research : an official journal of the American Association for Cancer Research*. 2008;14(10):3098-104. Epub 2008/05/17.
201. De Vleeschouwer S, Ardon H, Van Calenbergh F, Sciot R, Wilms G, van Loon J, et al. Stratification according to HGG-IMMUNO RPA model predicts outcome in a large group of patients with relapsed malignant glioma treated by adjuvant postoperative dendritic cell vaccination. *Cancer immunology, immunotherapy : CII*. 2012;61(11):2105-12. Epub 2012/05/09.
202. Ardon H, Van Gool SW, Verschuere T, Maes W, Fieuws S, Sciot R, et al. Integration of autologous dendritic cell-based immunotherapy in the standard of care treatment for patients with newly diagnosed glioblastoma: results of the HGG-2006 phase I/II trial. *Cancer immunology, immunotherapy : CII*. 2012;61(11):2033-44. Epub 2012/04/25.
203. Jackson C, Ruzevick J, Brem H, Lim M. Vaccine strategies for glioblastoma: progress and future directions. *Immunotherapy*. 2013;5(2):155-67. Epub 2013/02/19.
204. Weathers SP, Gilbert MR. Current challenges in designing GBM trials for immunotherapy. *Journal of neuro-oncology*. 2015. Epub 2015/01/13.
205. Grauer OM, Wesseling P, Adema GJ. Immunotherapy of diffuse gliomas: biological background, current status and future developments. *Brain Pathol*. 2009;19(4):674-93. Epub 2009/09/12.
206. Toussaint LG, 3rd, Nilson AE, Goble JM, Ballman KV, James CD, Lefranc F, et al. Galectin-1, a gene preferentially expressed at the tumor margin, promotes glioblastoma cell invasion. *Molecular cancer*. 2012;11:32. Epub 2012/05/16.
207. Verschuere T, Toelen J, Maes W, Poirier F, Boon L, Tousseyn T, et al. Glioma-derived galectin-1 regulates innate and adaptive antitumor immunity. *International journal of cancer Journal international du cancer*. 2013. Epub 2013/08/10.
208. Camby I, Belot N, Lefranc F, Sadeghi N, de Launoit Y, Kaltner H, et al. Galectin-1 modulates human glioblastoma cell migration into the brain through modifications to the actin cytoskeleton and levels of expression of small GTPases. *Journal of neuropathology and experimental neurology*. 2002;61(7):585-96. Epub 2002/07/20.
209. Thijssen VL, Postel R, Brandwijk RJ, Dings RP, Nesmelova I, Satijn S, et al. Galectin-1 is essential in tumor angiogenesis and is a target for antiangiogenesis therapy. *Proceedings of the National Academy of Sciences of the United States of America*. 2006;103(43):15975-80. Epub 2006/10/18.
210. Le Mercier M, Lefranc F, Mijatovic T, Debeir O, Haibe-Kains B, Bontempi G, et al. Evidence of galectin-1 involvement in glioma chemoresistance. *Toxicology and applied pharmacology*. 2008;229(2):172-83. Epub 2008/03/04.
211. Astorgues-Xerri L, Riveiro ME, Tijeras-Raballand A, Serova M, Rabinovich GA, Bieche I, et al. OTX008, a selective small-molecule inhibitor of galectin-1, downregulates cancer cell proliferation, invasion and tumour angiogenesis. *Eur J Cancer*. 2014;50(14):2463-77. Epub 2014/07/22.
212. Schutze N. siRNA technology. *Molecular and cellular endocrinology*. 2004;213(2):115-9. Epub 2004/04/06.
213. Thakker DR, Natt F, Husken D, Maier R, Muller M, van der Putten H, et al. Neurochemical and behavioral consequences of widespread gene knockdown in the adult mouse brain by using nonviral RNA interference. *Proceedings of the National Academy of Sciences of the United States of America*. 2004;101(49):17270-5. Epub 2004/12/01.
214. van Woensel M, Wauthoz N, Rosiere R, Amighi K, Mathieu V, Lefranc F, et al. Formulations for Intranasal Delivery of Pharmacological Agents to Combat Brain Disease: A New Opportunity to Tackle GBM? *Cancers (Basel)*. 2013;5(3):1020-48. Epub 2013/11/10.
215. Bonferoni MC, Sandri G, Rossi S, Ferrari F, Caramella C. Chitosan and its salts for mucosal and transmucosal delivery. *Expert opinion on drug delivery*. 2009;6(9):923-39. Epub 2009/07/30.
216. Davis SS, Illum L. Absorption enhancers for nasal drug delivery. *Clinical pharmacokinetics*. 2003;42(13):1107-28. Epub 2003/10/09.

217. Katas H, Alpar HO. Development and characterisation of chitosan nanoparticles for siRNA delivery. *Journal of controlled release : official journal of the Controlled Release Society*. 2006;115(2):216-25. Epub 2006/09/09.
218. Maes W, Verschuere T, Van Hoylandt A, Boon L, Van Gool S. Depletion of regulatory T cells in a mouse experimental glioma model through anti-CD25 treatment results in the infiltration of non-immunosuppressive myeloid cells in the brain. *Clinical & developmental immunology*. 2013;2013:952469. Epub 2013/05/28.
219. Vllasaliu D, Exposito-Harris R, Heras A, Casettari L, Garnett M, Illum L, et al. Tight junction modulation by chitosan nanoparticles: comparison with chitosan solution. *International journal of pharmaceutics*. 2010;400(1-2):183-93. Epub 2010/08/24.
220. Steelant B, Farre R, Wawrzyniak P, Belmans J, Dekimpe E, Vanheel H, et al. Impaired barrier function in patients with house dust mite-induced allergic rhinitis is accompanied by decreased occludin and zonula occludens-1 expression. *The Journal of allergy and clinical immunology*. 2016. Epub 2016/02/06.
221. Maes W, Rosas GG, Verbinnen B, Boon L, De Vleeschouwer S, Ceuppens JL, et al. DC vaccination with anti-CD25 treatment leads to long-term immunity against experimental glioma. *Neuro-oncology*. 2009;11(5):529-42. Epub 2009/04/02.
222. Davis ME, Zuckerman JE, Choi CH, Seligson D, Tolcher A, Alabi CA, et al. Evidence of RNAi in humans from systemically administered siRNA via targeted nanoparticles. *Nature*. 2010;464(7291):1067-70. Epub 2010/03/23.
223. Ragelle H, Riva R, Vandermeulen G, Naeye B, Pourcelle V, Le Duff CS, et al. Chitosan nanoparticles for siRNA delivery: optimizing formulation to increase stability and efficiency. *Journal of controlled release : official journal of the Controlled Release Society*. 2014;176:54-63. Epub 2014/01/07.
224. Hillaireau H, Couvreur P. Nanocarriers' entry into the cell: relevance to drug delivery. *Cellular and molecular life sciences : CMLS*. 2009;66(17):2873-96. Epub 2009/06/06.
225. Malhotra M, Tomaro-Duchesneau C, Saha S, Prakash S. Intranasal delivery of chitosan-siRNA nanoparticle formulation to the brain. *Methods Mol Biol*. 2014;1141:233-47. Epub 2014/02/26.
226. Ragelle H, Vandermeulen G, Preat V. Chitosan-based siRNA delivery systems. *Journal of controlled release : official journal of the Controlled Release Society*. 2013;172(1):207-18. Epub 2013/08/24.
227. Wiley DT, Webster P, Gale A, Davis ME. Transcytosis and brain uptake of transferrin-containing nanoparticles by tuning avidity to transferrin receptor. *Proceedings of the National Academy of Sciences of the United States of America*. 2013;110(21):8662-7. Epub 2013/05/08.
228. Nel AE, Madler L, Velegol D, Xia T, Hoek EM, Somasundaran P, et al. Understanding biophysicochemical interactions at the nano-bio interface. *Nature materials*. 2009;8(7):543-57. Epub 2009/06/16.
229. Marchiando AM, Graham WV, Turner JR. Epithelial barriers in homeostasis and disease. *Annual review of pathology*. 2010;5:119-44. Epub 2010/01/19.
230. Rezaee F, Georas SN. Breaking barriers. New insights into airway epithelial barrier function in health and disease. *American journal of respiratory cell and molecular biology*. 2014;50(5):857-69. Epub 2014/01/29.
231. Smith J, Wood E, Dornish M. Effect of chitosan on epithelial cell tight junctions. *Pharmaceutical research*. 2004;21(1):43-9. Epub 2004/02/27.
232. Kanazawa T, Akiyama F, Kakizaki S, Takashima Y, Seta Y. Delivery of siRNA to the brain using a combination of nose-to-brain delivery and cell-penetrating peptide-modified nano-micelles. *Biomaterials*. 2013;34(36):9220-6. Epub 2013/09/03.
233. Renner DB, Frey WH, 2nd, Hanson LR. Intranasal delivery of siRNA to the olfactory bulbs of mice via the olfactory nerve pathway. *Neuroscience letters*. 2012;513(2):193-7. Epub 2012/03/06.
234. Wolburg H, Wolburg-Buchholz K, Kraus J, Rascher-Eggstein G, Liebner S, Hamm S, et al. Localization of claudin-3 in tight junctions of the blood-brain barrier is selectively lost during

experimental autoimmune encephalomyelitis and human glioblastoma multiforme. *Acta neuropathologica*. 2003;105(6):586-92. Epub 2003/05/08.

235. Verschuere T, Van Woensel M, Fieuws S, Lefranc F, Mathieu V, Kiss R, et al. Altered galectin-1 serum levels in patients diagnosed with high-grade glioma. *Journal of neuro-oncology*. 2013. Epub 2013/07/05.

236. Van Woensel M, Wauthoz N, Rosiere R, Mathieu V, Kiss R, Lefranc F, et al. Development of siRNA-loaded chitosan nanoparticles targeting Galectin-1 for the treatment of glioblastoma multiforme via intranasal administration. *Journal of controlled release : official journal of the Controlled Release Society*. 2016;227:71-81. Epub 2016/02/24.

237. Melero I, Rouzaut A, Motz GT, Coukos G. T-cell and NK-cell infiltration into solid tumors: a key limiting factor for efficacious cancer immunotherapy. *Cancer discovery*. 2014;4(5):522-6. Epub 2014/05/06.

238. Rabinovich GA, Toscano MA. Turning 'sweet' on immunity: galectin-glycan interactions in immune tolerance and inflammation. *Nature reviews Immunology*. 2009;9(5):338-52. Epub 2009/04/15.

239. Garg AD, Vandenberg L, Koks C, Verschuere T, Boon L, Van Gool SW, et al. Dendritic cell vaccines based on immunogenic cell death elicit danger signals and T cell-driven rejection of high-grade glioma. *Science translational medicine*. 2016;8(328):328ra27. Epub 2016/03/05.

240. Thijssen VL, Barkan B, Shoji H, Aries IM, Mathieu V, Deltour L, et al. Tumor cells secrete galectin-1 to enhance endothelial cell activity. *Cancer research*. 2010;70(15):6216-24. Epub 2010/07/22.

241. Bonner WM, Redon CE, Dickey JS, Nakamura AJ, Sedelnikova OA, Solier S, et al. GammaH2AX and cancer. *Nature reviews Cancer*. 2008;8(12):957-67. Epub 2008/11/14.

242. Burnet NG, Jefferies SJ, Benson RJ, Hunt DP, Treasure FP. Years of life lost (YLL) from cancer is an important measure of population burden--and should be considered when allocating research funds. *British journal of cancer*. 2005;92(2):241-5. Epub 2005/01/19.

243. Van Woensel M, Wauthoz N, Rosiere R, Mathieu V, Kiss R, Lefranc F, et al. Development of siRNA-loaded chitosan nanoparticles targeting Galectin-1 for the treatment of glioblastoma multiforme via intranasal administration. *Journal of controlled release : official journal of the Controlled Release Society*. 2016. Epub 2016/02/24.

244. Fischer MJ. Amine coupling through EDC/NHS: a practical approach. *Methods Mol Biol*. 2010;627:55-73. Epub 2010/03/11.

245. Casettari L, Vllasaliu D, Mantovani G, Howdle SM, Stolnik S, Illum L. Effect of PEGylation on the toxicity and permeability enhancement of chitosan. *Biomacromolecules*. 2010;11(11):2854-65. Epub 2010/09/30.

246. Malhotra M, Lane C, Tomaro-Duchesneau C, Saha S, Prakash S. A novel method for synthesizing PEGylated chitosan nanoparticles: strategy, preparation, and in vitro analysis. *International journal of nanomedicine*. 2011;6:485-94. Epub 2011/05/13.

247. Bruno K. Using drug-excipient interactions for siRNA delivery. *Advanced drug delivery reviews*. 2011;63(13):1210-26. Epub 2011/09/29.

248. Howard KA, Paludan SR, Behlke MA, Besenbacher F, Deleuran B, Kjems J. Chitosan/siRNA nanoparticle-mediated TNF-alpha knockdown in peritoneal macrophages for anti-inflammatory treatment in a murine arthritis model. *Molecular therapy : the journal of the American Society of Gene Therapy*. 2009;17(1):162-8. Epub 2008/10/02.

249. Huang M, Khor E, Lim LY. Uptake and cytotoxicity of chitosan molecules and nanoparticles: effects of molecular weight and degree of deacetylation. *Pharmaceutical research*. 2004;21(2):344-53. Epub 2004/03/23.

250. Alameh M, Dejesus D, Jean M, Darras V, Thibault M, Lavertu M, et al. Low molecular weight chitosan nanoparticulate system at low N:P ratio for nontoxic polynucleotide delivery. *International journal of nanomedicine*. 2012;7:1399-414. Epub 2012/03/30.

251. Garaiova Z, Strand SP, Reitan NK, Lelu S, Storset SO, Berg K, et al. Cellular uptake of DNA-chitosan nanoparticles: the role of clathrin- and caveolae-mediated pathways. *International journal of biological macromolecules*. 2012;51(5):1043-51. Epub 2012/09/06.
252. Benjaminsen RV, Matthebjerg MA, Henriksen JR, Moghimi SM, Andresen TL. The possible "proton sponge " effect of polyethylenimine (PEI) does not include change in lysosomal pH. *Molecular therapy : the journal of the American Society of Gene Therapy*. 2013;21(1):149-57. Epub 2012/10/04.
253. Verschuere T, Toelen J, Maes W, Poirier F, Boon L, Tousseyn T, et al. Glioma-derived galectin-1 regulates innate and adaptive antitumor immunity. *International journal of cancer Journal international du cancer*. 2014;134(4):873-84. Epub 2013/08/10.
254. Reardon DA, Gokhale PC, Klein SR, Ligon KL, Rodig SJ, Ramkissoon SH, et al. Glioblastoma Eradication Following Immune Checkpoint Blockade in an Orthotopic, Immunocompetent Model. *Cancer immunology research*. 2016;4(2):124-35. Epub 2015/11/08.
255. Bouffet E, Larouche V, Campbell BB, Merico D, de Borja R, Aronson M, et al. Immune Checkpoint Inhibition for Hypermutant Glioblastoma Multiforme Resulting From Germline Biallelic Mismatch Repair Deficiency. *Journal of clinical oncology : official journal of the American Society of Clinical Oncology*. 2016;34(19):2206-11. Epub 2016/03/24.
256. Malhotra M, Tomaro-Duchesneau C, Prakash S. Synthesis of TAT peptide-tagged PEGylated chitosan nanoparticles for siRNA delivery targeting neurodegenerative diseases. *Biomaterials*. 2013;34(4):1270-80. Epub 2012/11/13.
257. Illum L, Hinchcliffe M, Davis SS. The effect of blood sampling site and physicochemical characteristics of drugs on bioavailability after nasal administration in the sheep model. *Pharmaceutical research*. 2003;20(9):1474-84. Epub 2003/10/22.

Curriculum Vitae

Matthias Van Woensel was born in Bonheiden (Belgium) on January 2th, in 1989. He graduated from secondary school in 2007 at Don Bosco in Haacht with a major in Latin and Mathematics. In 2007 he started his studies in Biomedical Sciences at the KU Leuven. During this study he performed an internship in the laboratory of Pediatric Immunology. In 2011 he started his master thesis work under supervision of Prof. Dr. Van Gool and Prof. Dr. De Vleeschouwer in the laboratory of Pediatric Immunology. In 2012 he graduated magna cum laude as Master in Biomedical Sciences with a major in Biomedical Research and a minor in Research in Biomedical Sciences. Subsequently, he started his PhD in the laboratory of Experimental neurosurgery and anatomy at KULeuven, and at the laboratory of Galenic pharmacy and biopharmacy at ULB, under guidance of Prof. Dr. De Vleeschouwer and Prof. Dr. Amighi.

Bibliography and awards

Verschuere T*, **Van Woensel M***, Fieuws S, Lefranc F, Mathieu V, Kiss R, et al. Altered galectin-1 serum levels in patients diagnosed with high-grade glioma. *Journal of neuro-oncology*. 2013;115(1):9-17. Epub 2013/07/05. * First shared authorship

Van Woensel M, Wauthoz N, Rosiere R, Amighi K, Mathieu V, Lefranc F, et al. Formulations for Intranasal Delivery of Pharmacological Agents to Combat Brain Disease: A New Opportunity to Tackle GBM? *Cancers (Basel)*. 2013;5(3):1020-48. Epub 2013/11/10.

Vandenberk L, Belmans J, **Van Woensel M**, Riva M, Van Gool SW. Exploiting the Immunogenic Potential of Cancer Cells for Improved Dendritic Cell Vaccines. *Frontiers in immunology*. 2015;6:663. Epub 2016/02/03.

Plessers J, Dekimpe E, **Van Woensel M**, Roobrouck VD, Bullens DM, Pinxteren J, et al. Clinical-Grade Human Multipotent Adult Progenitor Cells Block CD8+ Cytotoxic T Lymphocytes. *Stem cells translational medicine*. 2016. Epub 2016/07/29.

Rosiere R, **Van Woensel M**, Mathieu V, Langer I, Mathivet T, Vermeersch M, et al. Development and evaluation of well-tolerated and tumor-penetrating polymeric micelle-based dry powders for inhaled anti-cancer chemotherapy. *International journal of pharmaceutics*. 2016;501(1-2):148-59. Epub 2016/02/07.

Van Woensel M, Wauthoz N, Rosiere R, Mathieu V, Kiss R, Lefranc F, et al. Development of siRNA-loaded chitosan nanoparticles targeting Galectin-1 for the treatment of glioblastoma multiforme via intranasal administration. *Journal of controlled release : official journal of the Controlled Release Society*. 2016;227:71-81. Epub 2016/02/24.

Mathivet T.; Bouleti C.; **Van Woensel M.**; Verschuere T; Stanchi F.; Phng L.K.; Dejaegher J.; Balcer M.; Mazzone M.; De Vleeschouwer S.; Gerhardt H.; Dynamic stroma reorganization drives blood vessel abnormalization during glioma progression. *eLife*, 2016 (under revision)

Van Woensel, M.; Mathivet T.; Wauthoz, N.; Rosière, R.; Amighi, K.; Mathieu, V.; Lefranc, F.; van Gool, S.; Gerhardt, G.; de Vleeschouwer, S. Sensitization of glioblastoma tumor micro-environment to chemo- and immunotherapy by Galectin-1 intranasal knock-down strategy; *Oncolmmunology* 2016 (under revision)

Van Woensel, M.; Mathivet T.; Wauthoz, N.; Rosière, R.; Amighi, K.; Mathieu, V.; Lefranc, F.; van Gool, S.; Gerhardt, G.; de Vleeschouwer, S. PEGylated chitosan nanoparticles optimize nose-to-brain transport to target Galectin-1 in the treatment of glioblastoma; 2016 (in preparation)

Garg AD. ;Vandenberk L. ;, Fang S. ; Fasche T. ;Van Eygen S. ;Maes J.; **Van Woensel M.** et al. ; Pathogen response-like sensing of sterile dying cells by neutrophils drives residual cell-directed cytotoxicity, 2016 (in preparation)

Awards

Recipient of the Strategic Basic Research grant from the Agency for Innovation by Science and Technology in Flanders (121206 - IWT Vlaanderen) (2012-2016)

Belgian Brain Tumor Support (BBTS) prize for the results obtained in my PhD project (December 2015)

Best graduate award Peter Byron, Respiratory Drug Delivery congress, 2016, Arizona

Posters at scientific meetings

Annual Scientific Meeting of the Belgian Society of Neurosurgery. Gent, Belgium, 10 March, 2012.
Title: Altered galectin-1 serum levels in patients with high-grade glioma.

Oncoforum 2013, KULeuven, Belgium.

Title: Altered galectin-1 serum levels in patients diagnosed with high-grade glioma,

Immunology Summer School, Leuven (Belgium), September 2014.

Title: Direct transport of pharmacological agents from the nasal cavity to the brain might represent a new opportunity to tackle glioblastoma multiforme

Annual Scientific Meeting of the Belgian Society of Neurosurgery. Brussels, Belgium, 29 March, 2014.

Title: Direct transport of pharmacological agents from the nasal cavity to the brain might represent a new opportunity to tackle glioblastoma multiforme.

Annual Scientific Meeting of the Belgian Society of Neurosurgery. Brussels, Belgium, 21 March, 2015.

Intranasal delivery of anti-Galectin-1 formulation to increase the efficiency of chemo and immunotherapy for glioblastoma.

1st European congress on pharmaceuticals, 13-14/04/2015, Reims.

Title: Intranasal Delivery of Anti-Galectin-1 Formulation to Increase the Efficiency of Chemo - and Immunotherapy for Glioblastoma

Respiratory Drug Delivery, April 2016, Arizona, USA.

Title: Development of siRNA-loaded chitosan nanoparticles targeting Galectin-1 for the treatment of glioblastoma multiforme via intranasal administration

Oncoforum 2016, KULeuven, Belgium.

Title: Development of siRNA-loaded chitosan nanoparticles targeting Galectin-1 for the treatment of glioblastoma multiforme via intranasal administration

LKI symposium Tumor Immunology and Immunotherapy, Leuven, September 2016

Title: Sensitization of glioblastoma tumor micro-environment to chemo- and immunotherapy by Galectin-1 intranasal knock-down strategy

Presentations at scientific meetings

Rostock symposium for tumor immunology 2014, Rostock, Germany.

Title: Formulations for Intranasal Delivery of Pharmacological Agents to Combat Brain Disease: A New Opportunity to Tackle GBM?

Annual HGG-Immuno meeting, Würzburg (Germany), November 2014

Title: Intranasal Delivery of Anti-Galectin-1 Formulation to Increase the Efficiency of Chemo - and Immunotherapy for Glioblastoma

Nasal drug delivery, 16-17/04/2015, London.

Title: Intranasal Delivery of Anti-Galectin-1 Formulation to Increase the Efficiency of Chemo - and Immunotherapy for Glioblastoma

Respiratory Drug Delivery, April 2016, Arizona, USA.

Title: Development of siRNA-loaded chitosan nanoparticles targeting Galectin-1 for the treatment of glioblastoma multiforme via intranasal administration

ANOCEF, 17/18 June 2016, Brussels Belgium

Title: Development of siRNA-loaded chitosan nanoparticles targeting Galectin-1 for the treatment of glioblastoma multiforme via intranasal administration